2008-03-13

Error Sensor Strategies for Active Noise Control and Active Acoustic Equalization in a Free Field

Ryan T. Chester
Brigham Young University - Provo

ERROR SENSOR STRATEGIES FOR ACTIVE NOISE CONTROL AND ACTIVE ACOUSTIC EQUALIZATION IN A FREE FIELD

by

Ryan T. Chester

A thesis submitted to the faculty of

Brigham Young University

in partial fulfillment of the requirements for the degree of

Master of Science

Department of Physics and Astronomy

Brigham Young University

April 2008

BRIGHAM YOUNG UNIVERSITY

GRADUATE COMMITTEE APPROVAL

of a thesis submitted by

Ryan T. Chester

This thesis has been read by each member of the following graduate committee and by majority vote has been found to be satisfactory.

Date	Timothy W. Leishman, Chair
Date	Scott Sommerfeldt
Date	Craig C. Smith

BRIGHAM YOUNG UNIVERSITY

As chair of the candidate's graduate committee, I have read the thesis of Ryan T. Chester in its final form and have found that (1) its format, citations, and bibliographical style are consistent and acceptable and fulfill university and department style requirements; (2) its illustrative materials including figures, tables, and charts are in place; and (3) the final manuscript is satisfactory to the graduate committee and is ready for submission to the university library.

Date

Timothy W. Leishman
Chair, Graduate Committee

Accepted for the
Department

J. Ward Moody, Graduate Student Coordinator
Department of Physics and Astronomy

Accepted for the College

Thomas W. Sederberg, Associate Dean
College of Physical and Mathematical Sciences

ABSTRACT

ERROR SENSOR STRATEGIES FOR ACTIVE NOISE CONTROL AND ACTIVE ACOUSTIC EQUALIZATION IN A FREE FIELD

Ryan T. Chester

Department of Physics and Astronomy

Master of Science

Several measurements may be used as error signals to determine how to appropriately control a sound field. These include pressure, particle velocity, energy density and intensity. In this thesis, numerical models are used to show which signals perform best in two situations. The first is free-field active noise control (ANC) using error sensors located in the near field of the sound sources. The second is equalization in a free field and a semi-free field. Minimized energy density total power output (MEDToPO) plots are developed; these indicate the maximum achievable attenuation for a chosen error sensor as a function of location. A global listening area equalization coefficient (GLAEC) is found to evaluate the performance of the equalization methods. It is calculated by finding the average of the spectral standard deviation of several frequency response measurements in a specified listening area. For free-field ANC employing error sensors located in the near field,

pressure-based measurements perform the best. For free-field equalization over an extended listening region, total energy density performs best. Equalization of an extended listening region is more successful over a limited low-frequency bandwidth.

ACKNOWLEDGMENTS

I wish to express gratitude for help on this research. Without the help of these people I could not have accomplished this project.

- I would like to thank Dr. Timothy Leishman for his constant help and encouragement on the entire project. I would also like to thank the other two members on my research committee, Dr. Scott Sommerfeldt and Dr. Craig Smith, for making themselves available for help in research on this project.

- I would also like to thank other Brigham Young University faculty that helped in this research. Dr. Kent Gee for his help with acoustics-related questions. Dr. Brian Jeffs and Dr. David Long for fielding some DSP questions.

- I would like to thank others who worked with me: Chen Xi, Panu Puikkonen, Matt Morrise, and Trent Mouton for there assistance in concepts relating to this research. Their comments and questions were very important in the progression of this thesis.

- I would also like to thank other members of the acoustics research group at Brigham Young University. Special thanks to office mates Buye Xu, Matt Green, Micah Shepherd, and Ben Shafer for letting me bounce ideas off of them and for raising questions that resulted in progress in this research. I would also like to thank Derek Thomas, Daniel Tengelsen,

Connor Duke, Cole Duke and Brian Thornock for their comments and suggestions. I would also like to thank Gordon Dix, Sarah Rollins, and David Nutter for helping me as I started as a graduate student.

- I would like to thank my parents and family for their support in this endeavor.

- I would also like to thank the Brigham Young University Department of Physics and Astronomy for funding this research as well a providing the facilities and tools to do this research. I would also like to thank Diann Sorensen and Nan Ah You for all of their help with scheduling and other paperwork.

- I must also thank Heavenly Father for the opportunity to work on this project and for his help in this work.

Contents

Table of Contents **ix**

List of Figures **xiii**

List of Tables **xxi**

1 Introduction **1**
1.1 Objectives 4
1.2 Active Noise Control 5
1.3 Equalization 6
1.4 Plan of Development 9

2 Modeling Sound Fields **11**
2.1 Analytical Description of Sound Fields 12
2.1.1 Two Sources Acting Together 15
2.1.2 Radiation Patterns of a Source 16
2.1.3 Reflections, Ray Tracing and The Method of Images 18
2.2 Energetic Descriptions of Sound Fields 22
2.2.1 ED of a Sound Field 22
2.2.2 Sound Power 24
2.2.3 Acoustic Intensity 26
2.2.4 Relationship between ED and II 27
2.3 Sound Levels 30
2.4 Computational Model of the Sound Field 33

3 Active Sound Control Techniques **35**
3.1 Active Noise Control 35
3.1.1 Minimizing Sound Radiation 36
3.1.2 Minimized Energy Density Total Power Output 37
3.2 Equalization 38
3.2.1 Minimum Phase 43
3.2.2 Convolution 44
3.3 Evaluating Equalization 48
3.3.1 Auralization 48

3.3.2 Animations 51
3.3.3 Spectral Standard Deviation 51
3.3.4 Global Equalization Figure of Merit 53
3.3.5 Graphical Methods for Ranking Equalization Processes 54

4 Active Noise Control Results **63**
4.1 Models of the Sound Field 63
4.2 Active Noise Control 68
4.2.1 Control Using ED Quantities 70
4.2.2 Relationship Between ED and Π 75

5 Equalization Results **81**
5.1 Frequency-Domain Perspective of Equalization 81
5.1.1 Along a Line Above a Reflective Surface 84
5.1.2 Using a Reinforcing Source 91
5.2 Time-Domain Perspective of Equalization 97
5.2.1 Inverse Filters 98
5.3 Evaluating Equalization 100
5.3.1 Graphical Evaluation of Listening Areas 101
5.3.2 Development of a Global Listening Area Equalization Coefficient 105
5.3.3 Observations 114
5.3.4 Auralization 133
5.4 Toward Enclosures 141

6 Conclusions **143**
6.1 Near Field Sensor Active Noise Control 143
6.2 Equalization 145
6.3 Further Research 147

References **149**

A Explicit Derivation of Particle Velocity **159**

B Statistical Techniques **163**
B.1 Derivation of an Alternate Expression for Standard Deviation 163
B.2 Statistical Values of Energies 165

C Calculations for MEDToPO **169**
C.1 Minimizing PED for One Primary Source and One Control Source . . 169
C.1.1 Finding the Phase Difference of the Control Source 171
C.1.2 Finding the Magnitude of the Control Source 172
C.2 Minimizing KED for One Primary Source and One Control Source . . 173
C.2.1 Finding the Phase Difference of the Control Source 176
C.2.2 Finding the Magnitude of the Control Source 176

C.3 Minimizing TED for One Primary Source and One Control Source . . 178
C.3.1 Finding the Phase Difference of the Control Source 179
C.3.2 Finding the Magnitude of the Control Source 181
C.4 Minimizing PED 182
C.4.1 Finding the Phase Difference of the Control Source 183
C.4.2 Finding the Magnitude of the Control Source 184
C.5 Minimizing KED 184
C.5.1 Finding the Phase Difference of the Control Source 186
C.5.2 Finding the Magnitude of the Control Source 187
C.6 Minimizing TED 187
C.6.1 Finding the Phase Difference of the Control Source 189
C.6.2 Finding the Magnitude of the Control Source 189
C.7 Issues With Arctangents 190

D Finding an Impulse Response from a Frequency Response 191

E Animations 195
E.1 MEDToPO Animation 195
E.2 Relations Between ED and Power 197
E.3 Sound Fields 197

F Auralizations 203
F.1 Verification of Convolution 203
F.2 Example of Room Response 204
F.3 Examples of Equalization 204

G linearconv.m 213

H MEDToPO.m 215
H.1 Main File 215
H.2 Required Function: PowerFun.m 222

I STDofEQ.m 225
I.1 Main File: STDofEQ.m 225
I.2 Required Functions 239
I.2.1 Required Function: FundamentalAcoustics.m 239
I.2.2 Required Function: pressurefield.m 240
I.2.3 Required Function: pressure.m 242
I.3 Optional Controlling m-file: SpatialGLAEC.m 242

J EDfields.m 247

K HandS.m 253

List of Figures

2.1 Two point sources on a cartesian coordinate system. 14
2.2 This diagram indicates the angle that describes the size of a cap on a sphere. 17
2.3 In the law of reflections, as described in Eqs. (2.17) and (2.18), states that a vector incident on a surface will reflect from the surface with the same incident angle. This figure illustrates this law. 18
2.4 To use the method of images a virtual source is reflected to the other side of the reflecting plane. 19
2.5 The appropriate placements of image sources for two simple cases involving two reflecting surfaces. In both cases, the dark circle is the real source and the white circles represent the virtual sources. Solid lines represent reflective surfaces. 20

3.1 An example MEDToPO plot, at $kd = 2.473$, illustrates sound power output, at a given frequency, as a function of error sensor location and error signal type. The primary source is marked with an $\circ$ and the secondary source is marked by an $\times$. 39
3.2 The original signal is filtered by a correcting filter, the result is a frequency response that is flat over the entire frequency range. 40
3.3 Illustration of a discrete linear convolution of a four tap filter and a five term signal, both of which are found on the top row. The left middle shows the reversal and placement of the filter for the first iteration of the process. The remaining three illustrations show further steps of the shift process of the convolution. 46
3.4 In circular convolution, when the filter or sequence is shifted, the last tap or term is rotated to the beginning. 47
3.5 Abover are the resulting auralizations for convolutions using (a) GratisVolver™ and (b) the technique used in MATLAB®. Figure (c) shows the difference between the convolutions performed by both programs. It is important to note that the scale in the last figure is much smaller than the plots of the auralizations. The auralizations can be found on the digital version of this thesis in Appendix F.1. 50

3.6 An example of a curve comparing the standard deviation as a function of position in a one-dimensional listening area. 55
3.7 Above, surface plots of spectral standard deviation, from $kd = 0.3664$ to $kd = 366.4$, over a 2-D listening area The $\circ$ indicates the location of the error sensor while the + symbol indicates the locations of the sound sources. The frequency response of this plot is calculated over $|\hat{p}|^2$ to in crease the contrast in the plot. 56
3.8 The resulting ratio of the spectral standard deviation, from $kd = 0.3664$ to $kd = 366.4$, of an equalized field divided by the spectral standard deviation of the unequalized field. The portions that are indicated as being less than one indicate equalization improvement, while values greater than one show a decrease in equalization. The frequency response of this plot is calculated over $|\hat{p}|^2$ to increase the contrast in the plot. The sensor postion is marked by $\circ$. 57
3.9 This is a plot of the $\log_{10}$ of the standard deviations of frequency response, from $kd = 0.3664$ to $kd = 366.4$, normalized by their maximum value over a listening region. These are ordered from the best to worst, according to the plots, going from left to right, top to bottom. The Lagrangian density is off the scale for these plots, indicating superior equalization. The frequency response of this plot is calculated over $|\hat{p}|^2$ to in crease the contrast in the plot. 60
3.10 This is a plot of the standard deviations of frequency response, from $kd = 0.3664$ to $kd = 366.4$, normalized by their average value over frequency over a listening region. These are ordered from the best to worst going from left to right, top to bottom. The frequency response of this plot is calculated over $|\hat{p}|^2$ to in crease the contrast in the plot. 61

4.1 A sound field measured by PED, KED, and TED for (a) two sound sources acting in phase with one another with the same amplitude and (b) Two sound sources acting 180° out of phase from one another with the same amplitude at 1.9 kHz. The sources are marked by $\times$. 65
4.2 A sound field measured by PED, KED, and TED for (a) two sound sources acting in phase with one another with the same amplitude and (b) Two sound sources acting 180° out of phase from one another with the same amplitude at 5 kHz. The sources are marked by $\times$. 66
4.3 The sound field as it would be measured in PED, KED, and TED. Figure 4.3(a) is an arrangement of two linear arrays consisting of four point sources each, while Fig. 4.3(b) has five point sources laid out similarly to those used in a five source surround sound system. Each point source is marked in these figures by a $\times$. The axes are marked in meters and a $\circ$ indicates the center of the sources. These have corresponding animations over frequency in Appendix E of the digital version of this thesis. 67

4.4 Above are figures illustrating the radiation pattern of (a) a single sphere with a radiating cap, (b) a pair of monopole sound sources, (c) and (d) a pair of spheres with a radiating cap. Figures (a), (b) and (c) are shown at 1 kHz and (d) is shown at 250 Hz. 69
4.5 Measurements of the sound field when the control source acts to minimize the total radiated power. The color scale is in dB referenced to 3×10^{-15}J/m. The primary source is marked by $\circ$ and the control source is marked with $\times$. 70
4.6 Three MEDToPO plots illustrating the the amount of sound power produced by a system consisting of one primary source and one control source at $kd = 0.1832$ for (a), $kd = 1.832$ for (b) and $kd = 3.664$ for (c). 71
4.7 The maximum achievable sound power attenuation in dB using various coplanar sound source arrangements, also depicted here. 73
4.8 This shows the difference between the uncontrolled sound field and the optimally controlled sound field. Locations with the greatest reduction of the field measurement are traditionally considered the best locations for placing error sensors. 74
4.9 This is a MEDToPO for the situation given in Figure 4.8. 74
4.10 These figures show $10\log_{10}$ of the difference between the exact conversion and an approximation of the conversion from ED quantities to sound power for a pair of sources, where one source is driven to minimize sound power of the system. Figure (a) is for $kd = 0.128$, Fig. (b) is for $kd = 0.348$, and Fig. (c) is for $kd = 3.792$, where the source on the right leads the source on the left by $\pi/2$ radians. The $\times$ marks the locations of the sources. 77
4.11 Frequency dependence of the correction factors compared to their corresponding source if measured at $(0, 0.2)$ in units of the distance between the sources in (a) and at $(0.5, 0.2)$ in (b) where the coordinates correspond to those in Fig. 4.10. 78

5.1 Comparisons of L_p over space of the unequalized sound field (left column) to the sound field equalized by PED (right column) at the point marked by $\circ$. Frequency responses corresponding to this and the other markers are found in Fig. 5.2. Notice that the interference pattern of the sound field does not change when both sources are equalized with the same equalization filter. The whole field is busted or attenuated to equalize the response at the sensor location. 83
5.2 Frequency response magnitude curves that correspond, as marked in the legend, to the points mapped on the sound field in Fig. 5.1. The amplitude is in Decibels referenced to 20 μPa. 84

5.3 Example frequency responses as measured using pressure, the vector magnitude particle velocity and its components, PED, KED and TED. These are for a measurement with two point sources. The sensor was at (0.05,0.2) on the axis found in Fig. 5.1. 85
5.4 Example frequency response measurements using the vector magnitude of intensity and the spatially averaged pressure. These plots are for the same source arrangement and sensor location as found in Fig. 5.3. 85
5.5 The dark circle represents the position of the real source, the open circle represents the image source used to model the case where the solid horizontal line is a reflecting surface. The marker on the right is the sensor used to to determine the equalization. This is the setup used for producing Figs. 5.6 through 5.8. 86
5.6 The frequency response over space before any equalization occurs. Figure (a) is looking 10 cm above the surface, while Fig. (b) is 170 cm above the reflective surface. Below the a curve that indicates the $\log_{10}$ of the spectral standard deviation is plotted as a function of d_s. The source for these figures is 2 m above the reflective surface. 87
5.7 The frequency response after equalization with a listening region at $h_1 = 10$ cm above the reflecting plane. The source is at $h_2 = 2$ m. The left column is for the sensor placed with $d_s = 2$ m. while the right column is for a sensor placed with $d_s = 7$ m. The rows, listed from top to bottom, are separated into equalization performed by PED, KED and TED. Below are curves of the $\log_{10}$ of the spectral sandard deviation as a funciton of d_s. 89
5.8 The frequency response after equalization with the listening region at $h_1 = 170$ cm above the reflecting plane. The source is at $h_2 = 2$ m. The left column is for the sensor placed with $d_s = 2$ m. while the right column is for a sensor placed with $d_s = 7$ m. The rows, listed from top to bottom, are separated into equalization performed by PED, KED and TED. Below are curves of the $\log_{10}$ of the spectral sandard deviation as a funciton of d_s. 90
5.9 The dark circle represents a primary source, that is not equalized, the open circle represents a secondary reinforcement source that may be equalized in an attempt to equalize the overall sound field. The marker on the right indicates the sensor. The solid line at the bottom of the figure is a reflecting surface. This is the arrangement used for the initial model that represents a case where a sound source, in a semi-free field, is reinforced by a single secondary source. 92

5.10 The vertical axis indicates the relative amplification of a reinforcing sound source the system diagramed in Fig. 5.9, while the horizontal axis indicates the distance along the horizontal dashed line for the observed field in meters. The color in the plots indicate the $\log_{10}$ of spectral standard deviation of $|\hat{p}|^2$. This figure is the result with $d_s = 12$ m (marked by $\uparrow$), $h_1 = 1$ m, $h_2 = 3$ m and $h_3 = 1$ m. 93
5.11 This figure is very similar to Fig. 5.10, in this case the error sensor has been moved to $d_s = 2$ m (marked by $\uparrow$) with $h_1 = 1$ m, $h_2 = 3$ m and $h_3 = 1$ m. 94
5.12 These demonstrate the effect of sensor location on equalization of a sound field generated using a source pair where one is equalizes the compost field and the other is not. The secondary sound source produces a signal amplified by 6 dB compared to the unequalized source. The axes are marked off in meters. The horizontal axis indicates the observed position along the dashed line found in Fig. 5.9. 96
5.13 An example of a curve comparing the standard deviation as a function of position in a one-dimensional listening area. This figure is repeated from Fig. 3.6 102
5.14 The resulting ratio of the spectral standard deviation, from $kd = 0.3664$ to $kd = 366.4$, of an equalized field divided by the spectral standard deviation of the unequalized field. The portions that are indicated as being less than one indicate equalization improvement, while values greater than one show a decrease in equalization. The frequency response of this plot is calculated over $|\hat{p}|^2$ to increase the contrast in the plot. This figure is a repeat of Fig. 3.8. The sensor postion is marked by $\circ$. 103
5.15 The resulting ratio of the spectral standard deviation, from $kd = 0.3664$ to $kd = 366.4$, of an equalized field divided by the spectral standard deviation of the unequalized field. The portions that are indicated as being less than one indicate equalization improvement, while values greater than one show a decrease in equalization. The frequency response of this plot is calculated over $|\hat{p}|^2$ to increase the contrast in the plot. The sensor postion is marked by $\circ$. 104
5.16 Examples of ranking equalization performance using the GLAEC and plots of the spectral standard deviation. Here the sensor is located 1 cm from the center point of the five source arrangement of point sources and marked by a $\circ$. The axes are labeled in meters. 115
5.17 Examples of ranking equalization performance using the GLAEC and plots of the spectral standard deviation. The sensor is located at (1.7,2.6) and marked by a $\circ$. The axes are labeled in meters. 116

5.18 The standard deviation of the frequency response equalized using a spatially averaged squared pressure magnitude frequency response over a frequency range of (a) 20 Hz to 200 Hz, (b) 20 Hz to 2 kHz, (c) 20 Hz to 6 kHz, and (d) 20 Hz to 20 kHz. The sound sources are marked by +. The axes are labeled in meters. 118
5.19 The standard deviation of the frequency response equalized using a PED frequency response over a frequency range of (a) 20 Hz to 200 Hz, (b) 20 Hz to 2 kHz, (c) 20 Hz to 6 kHz, and (d) 20 Hz to 20 kHz. The sound sources are marked by + while the sensor is located at the point marked by ∘. The axes are labeled in meters. 119
5.20 The standard deviation of the frequency response equalized using a KED frequency response over a frequency range of (a) 20 Hz to 200 Hz, (b) 20 Hz to 2 kHz, (c) 20 Hz to 6 kHz, and (d) 20 Hz to 20 kHz. The sound sources are marked by + while the sensor is located at the point marked by ∘. The axes are labeled in meters. 120
5.21 The standard deviation of the frequency response equalized using a TED frequency response over a frequency range of (a) 20 Hz to 200 Hz, (b) 20 Hz to 2 kHz, (c) 20 Hz to 6 kHz, and (d) 20 Hz to 20 kHz. The sound sources are marked by + while the sensor is located at the point marked by ∘. The axes are labeled in meters. 121
5.22 The standard deviation of the frequency response equalized using the vector magnitude of intensity frequency response over a frequency range of (a) 20 Hz to 200 Hz, (b) 20 Hz to 2 kHz, (c) 20 Hz to 6 kHz, and (d) 20 Hz to 20 kHz. The sound sources are marked by + while the sensor is located at the point marked by ∘. The axes are labeled in meters. 122
5.23 Two sound sources equalized with a filter designed for the point marked by ∘ over the frequency range of 20 Hz to 2 kHz. 124
5.24 Five sound sources equalized with a filter designed for the point marked by ∘ over the frequency range of 20 Hz to 2 kHz. 125
5.25 Comparison of a sound field equalized for a position near the equalized sound source, (a) and (c), to a sound field equalized with a position near the unequalized sound source, (b) and (d). Figures (a) and (b) show fields equalized using PED, while Figs. (c) and (d) show sound fields equalized using KED. These sound field is equalized from 20 Hz to 2 kHz. The × indicates the unequalized sound source, + indicates the unequalized sound source and ∘ indicates the sensor location. . . 126

5.26 Comparison of a sound field equalized for a position near the equalized sound source, (a) and (c), to a sound field equalized with a position near the unequalized sound source, (b) and (d). Figures (a) and (b) show fields equalized using TED, while Figs. (c) and (d) show sound fields equalized using the vector magnitude of intensity. These sound field is equalized from 20 Hz to 2 kHz. The × indicates the unequalized sound source, + indicates the unequalized sound source and ∘ indicates the sensor location. 127
5.27 The GLAEC normalized by the GLAEC of the unequalized field as a function of sensor location for equalizing over a frequency range of 20 Hz to 200 Hz in 10 Hz increments. The sources are marked by +. . . 129
5.28 The GLAEC normalized by the GLAEC of the unequalized field as a function of sensor location for equalizing over a frequency range of 20 Hz to 800 Hz in 10 Hz increments. The sources are marked by +. . . 130
5.29 The GLAEC normalized by the GLAEC of the unequalized field as a function of sensor location for equalizing over a frequency range of 20 Hz to 2 kHz in 10 Hz increments. The sources are marked by +. . . . 131
5.30 The impulse and frequency responses for the unequalized case are presented here. 135
5.31 These are responses for a system equalized using (a) a filter designed for the listening position and (b) using a filter designed for a listening position several centimeters away. The equalization filters in this figure were designed using complex pressure. Plot (c) is a zoomed in version of (b). 136
5.32 These are responses for a system equalized using (a) a filter designed for the listening position and (b) using a filter designed for a listening position several centimeters away. The equalization filters in this figure were designed using the minimum phase portion of complex pressure. 137
5.33 These are responses for a system equalized using (a) a filter designed for the listening position and (b) using a filter designed for a listening position several centimeters away. The equalization filters in this figure were designed using PED. 138
5.34 These are responses for a system equalized using (a) a filter designed for the listening position and (b) using a filter designed for a listening position several centimeters away. The equalization filters in this figure were designed using KED. 139
5.35 These are responses for a system equalized using (a) a filter designed for the listening position and (b) using a filter designed for a listening position several centimeters away. The equalization filters in this figure were designed using TED. 140

5.36 These are responses for a system equalized using (a) a filter designed for the listening position and (b) using a filter designed for a listening position several centimeters away. The equalization filters in this figure were designed using complex pressure. This is similar to Fig. 5.31, the difference is that this model used significantly fewer terms to generate the responses for designing the filter an the model. 141

E.1 This is an animated MEDToPO plot for two sound sources where one source is minimizing the given ED quantity, while the other is putting out a predetermined signal. See also Figs. 3.1 and 4.6 and the accompanying discussions found in Secs. 3.1.2 and 4.2.1. The × indicates the control sources while the ∘ indicates the primary source. 196
E.2 This is an animated MEDToPO plot for five sound sources where four sources are minimizing the given ED quantity, while the other is putting out a predetermined signal. See also Fig. 4.9 and the accompanying discussions found in Secs. 3.1.2 and 4.2.1. The ×s indicate the control sources while the ∘ indicates the primary source. 196
E.3 This animation shows the conversion factor from ED to sound power, discussed in Secs. 2.2.4 and 4.2.2, animated over frequency. 197
E.4 This is a comparison of equalization using Lagrangian density, on the right and the sound field without equalization on the left. This shows how poorly Lagrangian density performs as a metric for equalizing a sound field. 198
E.5 This animation illustrates how the sound field changes when equalized at a point using PED. Note that the beam pattern is not altered by the equalization, while the sound level adjusts to keep the frequency response constant at the sensor location marked by ∘. This corresponds to Figs. 5.1 and 5.2. 199
E.6 These movies shows the effect of equalizing a reinforcing loudspeaker as a function of gain and is animated over error sensor location. See Figs. 5.10 and 5.11 200
E.7 The above animations demonstrate the flexibility of the methods used in this research. These animations correspond to Figs. 4.3 and 4.4. . . 201
E.8 These are some more animations that were generated to show the power of the computational approach to modeling a sound field. These do not correspond to other figures found in the text. 202

List of Tables

2.1 References used to calculate a given Sound Level measurement that is used with the computational models. 32

5.1 Summary of the values considered for use as a GLAEC and the statistical results. The row labeled pass indicates how many times out of 126 measurements that the value correctly ranked equalization performance. The row labeled fail indicates how many times the measurement failed to correctly rank equalization performance. The z-value indicates the result of the z-test of the performance of $\mu_s(\sigma_f)$ compared to the performance of the measurement of a given column. A larger z-value magnitude indicates a more discernible difference between the compared sampled populations. In this case, a positive value would indicate better performance at correctly ranking of the equalization methods. The confidence, labeled β, is a fractional comparison indicating the certainty that there is a difference between two populations. This data comes from the measurements made with the equalization filter designed for use near the the sound sources. 110

F.1 This table compares the results of using the MATLAB® function linearconv.m to produce auralizations to using GratisVolver^{tM} to generate auralizations. 204

F.2 This table compares an auralization of a reverberant room generated using a simulated impulse response 2^{12} terms long to one generated with an impulse response 2^{16} terms long. Both responses are too long for realistic measurements, but provide a proof of concept. 205

F.3 The impulse and frequency responses for the unequalized case are presented here. This is the same figure shown in Fig. 5.30. Below is an auralization of the unequalized case considered in Sec. 5.3.4. Compare with anechoic speech in Table F.2 206

F.4 These are responses for a system equalized using a filter designed for the listening position (a) and using a filter designed for a listening position several centimeters away (b). The equalization filters in this figure were designed using complex pressure. 207

F.5 These are responses for a system equalized using a filter designed for the listening position (a) and using a filter designed for a listening position several centimeters away (b). The equalization filters in this figure were designed using the minimum phase of complex pressure. . 208
F.6 These are responses for a system equalized using a filter designed for the listening position (a) and using a filter designed for a listening position several centimeters away (b). The equalization filters in this figure were designed using PED. 209
F.7 These are responses for a system equalized using a filter designed for the listening position (a) and using a filter designed for a listening position several centimeters away (b). The equalization filters in this figure were designed using KED. 210
F.8 These are responses for a system equalized using a filter designed for the listening position (a) and using a filter designed for a listening position several centimeters away (b). The equalization filters in this figure were designed using TED. 211
F.9 These are responses for a system equalized using a filter designed for the listening position (a) and using a filter designed for a listening position several centimeters away (b). The equalization filters in this figure were designed using complex pressure. This is similar to Table F.4, the difference is that this model used significantly fewer terms to generate the responses than the one used for Table F.4. 212

Chapter 1

Introduction

Two important objectives in the field of sound control are the elimination of excess noise and the improvement of the quality of sound reproduction. It is useful to examine sound fields generated by simple sources in free space to study techniques that may be beneficial in controlling sound. Mathematically describing sound fields in regions far from simple source configurations, such as a pair of point sources, requires little effort, given that appropriate approximations are made. Typically, many approximations are made to simplify the description of a sound field produced by multiple point sources with arbitrary source strengths. This restricts the results to the far field. Though useful for describing the far field, these approximations fail to properly describe sound near the sound sources. The math becomes more complicated when modeling the near field of sound sources. A good mathematical description of the near field of multiple sources may provide efficient ways to model, measure and control the sound field for many applications.

In the field of active noise control (ANC), an error sensor is used to characterize a sound field and adapt the control system to variations in the field. Because of spatially dependent variations in a sound field, it is critical that good locations are chosen for

the error sensors. Often, there are constraints that prohibit placing error sensors in the far field. Qiu et al. looked briefly at placing energy density (ED) sensors in the near field for use in ANC and analyzed the number of sensors necessary to achieve effective sound control [1]. In their research, they compared potential energy density (PED), kinetic energy density (KED), total energy density (TED) and intensity-based error sensors in their ability to control a source arrangement consisting of a single primary source and single control source. However, they mainly looked at the number of error sensors that should be used for ANC and did not move the error sensors closer than $\lambda/8$ from the sound sources. Better understanding of the nature of the near-field regions of sound sources allows one to find good locations for error sensors. Nevertheless, the work by Qiu et al. does show that there is a difference in the information given by the various metrics used to examine a sound field. Hansen and Snyder suggested methods for proper placement of error sensors. Their method involved determining regions where attenuation is greatest for a system that is operating optimally [2].

Often, noise control is the goal of active sound control. However, another interesting and useful application for active sound control is the equalization of a sound system. In this case, a filter is used to alter the signal provided to a set of loudspeakers to achieve an ideal frequency response at the receiver location. Using pressure-based measurements for designing equalization filters would be an intuitive first approach because human hearing is based on acoustic pressure. However, because pressure varies dramatically over listening areas, equalization using pressure-based filters can only be used for very isolated listening zones. There is a possibility that other measurements may be more useful for equalizing sound fields. A well-established method for evaluating equalization would provide a tool for determining the success of different equalization methods.

There are several measurements available to measure sound at a listening position. Each of these measurements describes different features of the sound field. In ANC and equalization, these measurements provide information concerning how the field may be altered as well as insight as to how well the sound is being controlled. It is often convenient to place error sensors in the (acoustic or geometric) near field of the sound sources. Which measurement will most effectively produce the appropriate information to accomplish the desired sound control? Though measurements such as pressure, TED and intensity have been used to a limited extent in ANC, pressure has almost exclusively been used for equalization. For the case of ANC, this question will be focused on effects of sensors in the near field of the sources involved. For the case of equalization, the question will be extended to sensors in many locations in the near field or far field.

The direct sound from a source or combination of sound sources is important for the entire sound field. In many ANC techniques, error sources are placed in close proximity to the primary source, in order to achieve the strong coupling that is necessary to control sound radiation. In some cases, the control sensors are placed in the near field of these sources. Placing the error sensors in the near field of the sources causes the direct sound to dominate the measured sound. To examine this situation, it is convenient to study the ANC system in the free field only, thus ignoring some issues involved with the reverberant field in enclosed cases.

The direct sound is also important for equalizing a sound field. This is clearly true for outdoor settings. While equalization is often performed in reverberant locations, the reverberation makes the situation more complicated than a free field situation. Starting with a free-field investigation, one can better understand the direct interaction of the sound sources. This in turn allows for better understanding of the effects of equalization on a sound field.

1.1 Objectives

The models developed in this research are used to answer two closely related questions. First, which measurement is most effective for global free-field ANC using error sensors located in the near field? Second, which measurement is most effective for global free-field sound equalization? In order to answer this, computational models of sound produced in a free field are developed, to accurately represent both the near and far field. Though in most listening environments there is at least some reverberation, the free-field model provides useful information because it also describes the direct sound field in an enclosure. The sources may be used to illustrate the results of performing sound control using various types of measurements (such as pressure, particle velocity, energy density and intensity to name a few). The model helps determine the control parameters and show the results of direct sound equalization.

There are several techniques that are useful for modeling sound fields. One convenient starting point is the use of computational models [1, 3–5]. Computational models show what may happen in an ideal situation, and serve to show what to expect in real experiments. This provides a good preliminary step for planning an experiment, because it indicates which methods should produce good results. More importantly, the computational experiments may also be used to efficiently find the limitations of a new approach to sound control. A good computer model may also be used as an experiment in its own right. Experiments using computer models can be used to look at many factors without having to change physical experimental setups repeatedly.

In this research, several computational models are developed using Maple™ and MATLAB®. Maple™ was mostly used to find symbolic solutions and descriptions of the sound field that verify the results calculated by hand. These results were coded

into MATLAB® to create computational models. The results from the MATLAB® computations are given in terms of plots and animations, as well as some that further describe the situations. Some of the more important portions of the MATLAB® code can be found in Appendices G throught K. Based on the results calculated from MATLAB®, the success or failure of ANC or equalization could be determined for several situations.

1.2 Active Noise Control

There are two basic classifications of methods used to control sound: active and passive. Some examples of passive sound control include placing a barrier to block sound transmission or resurfacing a room to alter its response. Control methods that produce sound to control noise and/or use electronics to alter a signal are considered active. Some examples of active sound control include the use of loudspeakers to cancel sound from another source or the use of an electronic filter to compensate for the response of a room.

Often, sound found in a given environment is undesired or even dangerous. In some cases, it is appropriate to use ANC to deal with the offending noise. In active sound control there are three basic components: the error sensors, the signal processing equipment and the actuators [6]. The error sensors detect the sound field and pass the information to the processing equipment. Commonly, a digital signal processor (DSP) is employed to analyze the sound field and determine how to drive the actuators to control the sound. The processing determines the ideal amplitude and phase for driving the actuators to cancel the sound for a given situation.

There are several error signal measurements available for use in ANC. The most familiar is acoustic pressure, which is the signal commonly detected by microphones

and sound level meters. Other measurements that may be used include particle velocity, PED, KED, TED, active intensity and reactive intensity [1,7]. Sound power may also be measured to describe a sound field. However, sound power is difficult to measure *in situ*, and therefore is not usually considered a viable measurement for performing ANC. On the other hand, it is often a very appropriate measure for judging the success of attempts at sound control, as well as for calculating the optimal sound control for a given source arrangement [8–10].

1.3 Equalization

Loudspeakers and listening environments tend to alter original audio signals. The process of equalization may be used to compensate for the resulting inaccuracies including [11,12]. Some situations call for filters to compensate for known acoustical problems in a system, while others may be post processed to deal with inaccuracies due to distortions of an audio signal [13].

The frequency response between the audio signal and listener is altered by the transducers used to produce sound, transducer interactions, and the environment in which the sound is generated. In many cases, the loudspeakers are equalized under anechoic conditions [14]. The process of equalization involves adjusting a sound system so that the source to listener frequency response matches some desired frequency response. It is not limited to adapting only the loudspeakers in the system. Three things cause the system to be unequalized: nonuniform frequency response of the loudspeakers, superposition of reflected sound and the sound from other loudspeakers, and frequency-dependent air absorption [15]. An equalization filter boosts or cuts the signal sent to the loudspeaker as a function of frequency in order to obtain the desired frequency response of the system. User-adjustable filters are commonly referred

to as equalizers [15]. Often, certain spectral curves are desired that can be easily implemented using a equalizer. However, there is considerable difficulty in applying a given spectral response to a large listening area because of the spatial dependence of the sound field [16]. In this research, an equalized system will be one in which the frequency response is as close to uniform over frequency as possible. The primary concern will be to achieve a frequency response that is uniform both over frequency and over space.

Equalization is a filtering process. A room acts as a filter that introduces delay and spectral coloration. One goal of equalization is to reduce the spectral variation of the room response. The delayed reflections in the room interact constructively and destructively causing the response at a specified position to vary over frequency. Filters in series commute, so an electronic filter designed to correct for the response of a room does not need to be implemented after the room has changed the signal. This means that the correction filter may be implemented before it is used to drive a loudspeaker in the room. In a sense, the correction filter corrupts the signal and the room response restores the signal. However, it is important to note that a filter cannot replace a portion of the signal that has been removed. This means that there is a limit to how much correction is possible with a filtering technique.

Determining an appropriate equalization filter requires measuring the transfer function between some input signal and the output signal. Once this has been done, the inverse of the response is found, and a filter is created by inverting the response function. If the goal is to equalize the sound at one well-defined listening location, pressure equalization will provide the best equalization because our hearing is based on pressure. However, use of one or only a few pressure measurements will likely degrade the average equalization for a large listening area [11, 17, 18]. This raises an important question: which measured value would provide an optimal equalization

filter for an expanded listening area?

All equalization methods fail to remove the extreme dips caused by destructive interference due to reflections or multiple sound sources. The spatial dips depend on the geometry of the listening area as well as source location and strength. Using the filtering methods discussed here, it is impossible to completely replace a frequency that has been removed from the frequency response. However, the spectral peaks that occur in the field may be attenuated using the filters designed from the error sensors.

In a listening environment, frequency response varies as a function of space. This means that a listener at one point will hear something different than a listener at another point. Ideally, each listener in a given listening area would hear the same thing [16]. However, because of interference effects, this is rarely the case. Because of the relationship between frequency response and impulse response, unequalized sound fields are also subject to reverberation problems, which can degrade speech intelligibility.

In addition to the variation in magnitude response of acoustic systems, there are frequency-dependent variations in the phase response of any acoustic system [19]. There are methods available to compensate for variation in the phase distortion of an acoustic system. At the same time, phase is much more sensitive to delay and other conditions of an acoustic system. It is also questionable whether there is value in trying to equalize phase—especially over extended listening areas. Examination of phase equalization is outside of the scope of this research, but it is worth noting as an important part of all acoustic systems.

1.4 Plan of Development

The topics discussed in the chapters of this thesis will precede as described here. Chapter 2 discusses mathematical approaches for modeling sound fields. Both analytical and computational methods are discussed. The discussion of modeling sound fields continues in Ch. 3, with a focus on techniques for modeling equalization methods. Chapter 4 discusses the effects of ANC techniques and the benefits and limitations of using the different methods. Chapter 5 focuses on examination of the changes in sound fields due to equalization. This chapter also discusses a procedure for judging the success of equalization methods. Chapter 6 provides a brief summary and conclusions of this research followed by some suggestions for future research.

Chapter 2

Modeling Sound Fields

Often, it is useful to derive mathematical descriptions of sound fields produced by a combination of sources when trying to alter the field produced by them. Before choosing a metric for controlling a sound field, it is important to decide which measurement is best for the given application. In order to determine the best measurement to use for active sound control, several computational setups were devised. Initially, closed form solutions were calculated to describe the sound field in terms of PED (proportional to squared pressure), KED (proportional to the magnitude of squared particle velocity), and TED (the sum of PED and KED). Plots of these quantities were used to determine whether KED or TED offered a significant advantage over squared pressure.

In most situations, far field-approximations are made to model a field produced by a combination of sound sources. These approximations simplify the mathematics required to arrive at a good description of the sound field. However, in this case we are interested in error sensors located in the near field. Since far-field approximations cannot be used in performing the calculations to describe the near field, these approximations will not be used in this research. Using a more exact model for the

sound field allows for a better description of how applying active sound control using near-field sensors will affect the sound field.

Analytical and computational methods both have advantages in modeling a sound field. An analytic expression can often describe the field in a way that yields both a qualitative and quantitative understanding of the sound field. In order to interpret the analytical expression easily, some simplification is necessary. Even for simple situations, this is a cumbersome process. This complicates the study of different sound-source arrangements. Computational calculations of complicated analytic expressions can be quickly and easily altered to accurately represent different sound source configurations. The results of these calculations can be used to produce detailed plots that describe the sound field in a way that can be readily interpreted, thus showing the qualitative characteristics of the sound field. However, with a computational approach, it is difficult to interpret computer code to make qualitative predictions of the sound field. A combination of computational and analytical methods for describing sound fields can illustrate which acoustic measurement performs the best for a given sound control application.

2.1 Analytical Description of Sound Fields

Pressure is one of the fundamental and most common variables used when measuring sound. As a starting point, the field is described using analytical methods. Later, similar methods are developed for computational models used for predicting the nature of the sound field. For simplicity, cases involving two sources will serve as a starting point for this discussion. To calculate the pressure field, the principle of superposition is used [20]. The pressure field for an arbitrary number, N, of sources

is found by the sum [21–23]

$$\hat{p} = \sum_{n=1}^{N} \frac{\hat{A}_n e^{-jkR_n}}{R_n}, \tag{2.1}$$

where $\hat{A}_n$ is the monopole amplitude of the n^{th} source,

$$\hat{A}_n = \frac{j\rho_0 ck\hat{q}_n}{4\pi}, \tag{2.2}$$

R_n is the distance between the n^{th} source and the field point P in question, and $\hat{q}_n$ is the source strength of the n^{th} source. Throughout this research, ρ_0 is the fluid density, c is the speed of sound, k is the wave number and $\hat{q}$ is the complex source strength. One of the simplest ways to calculate R_n is the Pythagorean theorem,

$$R_n = \sqrt{(x - x_n)^2 + (y - y_n)^2 + (z - z_n)^2}, \tag{2.3}$$

where $\vec{r} = (x, y, z)$ indicates the field point and the subscript n indicates which sound source produces the sound for that iteration of the sum. The sum in Eq. (2.1) describes, in the frequency domain, the complex sound pressure amplitude produced by multiple point sources, at the field point (See Fig. 2.1 for an example of two sources). This expression leads to other acoustic quantities that describe the resulting sound field around the sources.

Another fundamental measurement of sound is particle velocity. Pressure is related to particle velocity through the linearized Euler's equation [24],

$$-\nabla\hat{p} = \rho_0 \frac{\partial\hat{\vec{u}}}{\partial t}. \tag{2.4}$$

By assuming time harmonicity, Euler's equation can be simplified to

$$-\nabla\hat{p} = j\omega\rho_0\hat{\vec{u}} = jck\rho_0\hat{\vec{u}}. \tag{2.5}$$

If we apply Euler's equation to Eq. (2.1), and solve for $\hat{\vec{u}}$, we obtain a vector expression that describes the particle velocity. After some simplification, in cartesian coordinates

the result becomes[1] [23, 25–27]

$$\hat{\vec{u}} = \sum_{n=1}^{N} \frac{\hat{q}_n e^{-jkR_n}}{4\pi R_n^3}(jkR_n + 1)\vec{R}_n \tag{2.6}$$

where

$$\vec{R}_n = \begin{pmatrix} x - x_n \\ y - y_n \\ z - z_n \end{pmatrix}, \tag{2.7}$$

and x, y, and z are the coordinates of the field point, and x_n, y_n, and z_n are the coordinates of the n^{th} sound source.

ED can be calculated from the pressure and particle velocity terms. The time averaged frequency-dependent expression for TED is the sum of the PED and the

[1]This expression agrees with work by Beranek, Morse and Ingard, Kinsler *et al.*, and Pierce [23, 25–27]. The derivation of particle velocity from acoustic pressure is explicitly shown in Appendix A, along with a brief explanation of how the result agrees with Beranek, Morse and Ingard, Kinsler *et al.*, and Pierce.

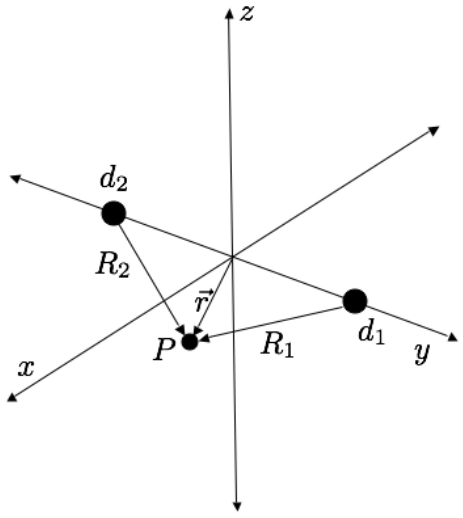

Figure 2.1 Two point sources on a cartesian coordinate system.

KED. These expressions are [28–32],

$$\langle w_p \rangle_t = \frac{|\hat{p}|^2}{4\rho_0 c^2}, \qquad \langle w_\mathrm{k} \rangle_t = \frac{\rho_0}{4}(\hat{\vec{u}} \cdot \hat{\vec{u}}^*), \qquad \langle w_\mathrm{t} \rangle_t = \langle w_\mathrm{k} \rangle_t + \langle w_p \rangle_t. \tag{2.8}$$

The ED values can be calculated to describe the sound field. Because the KED and TED values include particle velocity, they contain more information than pressure alone, which may facilitate better control. The vector nature of particle velocity also means that it contains more information than pressure based-quantities alone.

Equations (2.8) may also be used to calculate the Lagrangian density (LD). The Lagrangian, commonly found in physics textbooks, is the difference of the kinetic and potential energy. Mathematically, the Lagrangian is defined by [33]

$$\mathcal{L} = T - V \tag{2.9}$$

where $\mathcal{L}$ is the Lagrangian, T is the kinetic energy and V is the potential energy. The LD may than be defined as

$$\langle w_\mathcal{L} \rangle_t = \langle w_\mathrm{k} \rangle_t - \langle w_p \rangle_t. \tag{2.10}$$

Again, this is a time-averaged quantity. This quantity does have a few drawbacks. Specifically, when the PED and the KED are equal, the LD goes to zero. Furthermore, when the PED is larger than the KED, the LD becomes negative, which complicates the design of an equalization filter.

2.1.1 Two Sources Acting Together

One of the simplest cases to explore is two sources acting in phase with one another with equal source strengths. This brings $\hat{A}_n$ out of the sum for pressure in Eq. (2.1), and $\hat{q}_n$ out of the sum for particle velocity in Eq. (2.6). The expression for the pressure field for this simple situation is the same as Eq. (2.1) with $N = 2$ and $\hat{A}_1 = \hat{A}_2$.

Another simple case is two sources with equal magnitude, but 180° out of phase. Equation (2.1) again describes the pressure field with $N = 2$ and $\hat{A}_1 = -\hat{A}_2$. Setting the pressure amplitude of the two sources to have opposite signs is equivalent to changing the phase by π. Aside from factoring the source strengths from the sum, there is little simplification that may be performed.

2.1.2 Radiation Patterns of a Source

A physical loudspeaker has a directivity pattern. In order to model this analytically, it is useful to approximate a loudspeaker as a vibrating cap in a sphere. Though this does not result in a closed-form solution, it does result in a sum that converges. The pressure produced by a vibrating cap on a sphere can be expressed by [34]

$$\hat{p}(r,\theta) = \rho_0 c \sum_{m=0}^{\infty} \frac{U_m}{C_m(kr)} \mathrm{P}_m(\cos\theta) \mathrm{h}_m^{(2)}(kr), \tag{2.11}$$

where P_m indicates the Legendre polynomial, $\mathrm{h}_m^{(2)}$ represents the spherical Hankel function of the second kind, which will be defined shortly. The term C_m is a function defined as

$$C_m(\chi) = \frac{j}{2m+1}\left\{ m\mathrm{j}_{m-1}(\chi) - (m+1)\mathrm{j}_{m+1}(\chi) - j\left[m\eta_{m-1}(\chi) - (m+1)\eta_{m+1}(\chi) \right] \right\}, \tag{2.12}$$

where $\mathrm{j}_m(\chi)$ and $\eta_m(\chi)$ are the spherical Bessel functions of the first and second kinds which are in turn related to the cylindrical Bessel functions of the first and second kinds by [34, 35]

$$\mathrm{j}_m(\chi) = \sqrt{\frac{\pi}{2\chi}} \mathrm{J}_{m+\frac{1}{2}}(\chi) \qquad \eta_m(\chi) = \sqrt{\frac{\pi}{2\chi}} \mathrm{N}_{m+\frac{1}{2}}(\chi). \tag{2.13}$$

The aforementioned spherical Hankel function of the second kind is defined as [34,35]

$$\mathrm{h}_m^{(2)}(\chi) = \mathrm{j}_m(\chi) - j\eta_m(\chi). \tag{2.14}$$

The final term in Eq. (2.11), U_m, depends on how the cap on the sphere is vibrating. In this research the model for a radially vibrating cap is used, rather than an axially vibrating cap, so the model in this research may model a simple horn better than a loudspeaker. In this case, the term representing the velocity of the vibrating surface becomes

$$U_m = \begin{cases} \frac{\hat{u}_0}{2}(1 - \cos\theta_0) & m = 0 \\ \frac{\hat{u}_0}{2}[\mathrm{P}_{m-1}(\cos\theta_0) - \mathrm{P}_{m+1}(\cos\theta_0)] & m = 1, 2, 3, \ldots \end{cases} \tag{2.15}$$

The term θ_0 describes the polar angle which defines the edge of the cap, see Fig. 2.2. This value for a given cap on a sphere may be found using the relation

$$\sin\theta_0 = \frac{a_c}{a}, \tag{2.16}$$

where a_c is the radius of the cap and a is the radius of the sphere. The sum in Eq. (2.11) is an infinite sum. In the computational model, it is only necessary to use enough terms that the pressure expression converges at the frequencies of interest. This process may be repeated for multiple sources and summed in order to model the interactions in the pressure field.

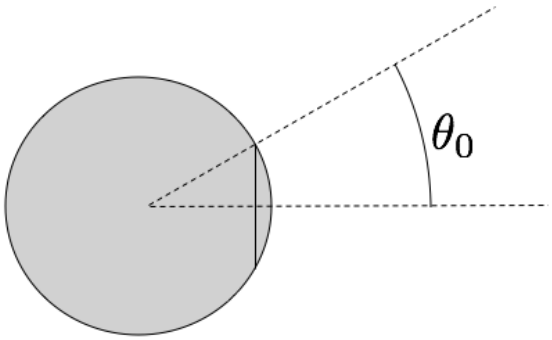

Figure 2.2 This diagram indicates the angle that describes the size of a cap on a sphere.

2.1.3 Reflections, Ray Tracing and The Method of Images

Another interesting case is one in which reflecting surfaces are present. To deal with reflections, geometric acoustic techniques may be used. In acoustics, the law of reflections works the same way that it does in optics, as long as the assumption that the wavelengths are much smaller than the dimensions of the reflective surfaces is valid. Expressing a reflection as a function of angles, the angle of incidence is equal to the angle of reflection [36, 37],

$$\theta_i = \theta_r. \tag{2.17}$$

This may also be expressed using vector notation,

$$\mathbf{v}_r = \mathbf{v}_i - 2(\mathbf{v}_i \cdot \mathbf{n})\mathbf{n}. \tag{2.18}$$

where $\mathbf{v}_r$ is the reflected vector while $\mathbf{v}_i$ is the incident vector as in Fig. 2.3.

There are two common methods for modeling reflections in a sound field, ray tracing and image sources. The method of ray tracing uses the law of reflections to determine the path that sound travels from the source to the receiver. This provides a visual method to describe how the sound propagates for a given source and surface arrangement. The path length can be determined from this method, along with the sound attenuation due to absorption. This may be taken into account to arrive at a reasonable description of the sound field [36]. The method of images is an alternate

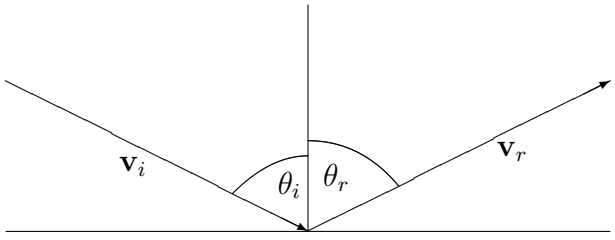

Figure 2.3 In the law of reflections, as described in Eqs. (2.17) and (2.18), states that a vector incident on a surface will reflect from the surface with the same incident angle. This figure illustrates this law.

method that uses virtual sources to model a sound field. Modeling an acoustic field using the method of images works the same as it does when used for electromagnetic fields. A reflecting surface and a sound source can be modeled using two sound sources in free space such that they are equidistant from the original reflecting plane, as illustrated in Fig. 2.4. The path length is naturally taken into account in this model by the placement of the virtual source [36, 37]. This system works well in computer simulations because it simply requires the use of additional image sound sources to represent more reflections. However, modeling a system with multiple reflecting surfaces quickly become difficult for complicated geometries. For example, situations where the geometry causes an acoustic shadow would need more complicated methods to correctly describe the sound field.

The first step for modeling sound reflected from a plane is to determine the location of the virtual source. With just one source and one reflecting surface, a virtual source should simply be placed opposite the real source. The directivity of the source as well as its orientation should be reversed front to back, like a mirror, as it is placed on the opposite side of the of the source. When this technique is used correctly, a mirror image of the entire sound field is created on the side of the virtual image. This is illustrated in Figs. 2.4 and 2.5. This process may be repeated for each reflective

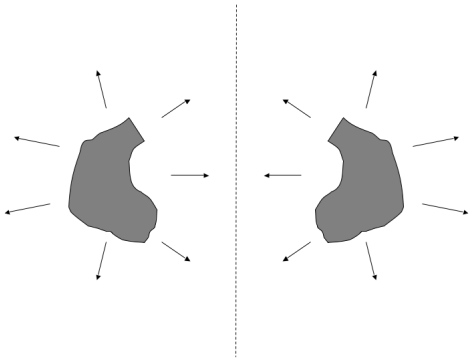

Figure 2.4 To use the method of images a virtual source is reflected to the other side of the reflecting plane.

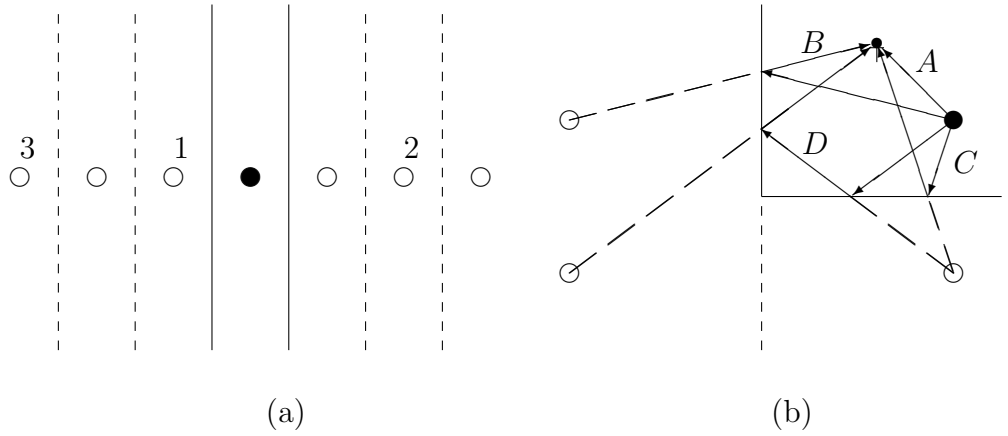

Figure 2.5 The appropriate placements of image sources for two simple cases involving two reflecting surfaces. In both cases, the dark circle is the real source and the white circles represent the virtual sources. Solid lines represent reflective surfaces.

surface encountered along a sound path. In the case of multiple reflections, the previous virtual source becomes the new primary source, and a corresponding image source is placed opposite the new reflecting surface. An example involving two parallel reflective surfaces, indicated by solid lines, is shown in Fig. 2.5(a). The numbers indicate a chain of image sources; the image source marked with 1 is the first image source, the 2 indicates the secondary image source, which simulates the reflection of the first image source, and the 3 indicates the tertiary image source, which is the image of the secondary image source. The unmarked image sources are based on another set of reflections. In theory, the process would be repeated infinitely, though real cases are limited by absorption. In a practical computational model, the number of virtual sources is limited by the desired time duration of the impulse response.

The additional path length for the image sources is taken into account regardless of the number of reflections. This occurs because the image source from one reflection is placed farther from the next reflecting surface, as shown in Fig. 2.5. The resulting source array may be used to model the sound field in computational models [29,36,37].

Figure 2.5(b) shows two perpendicular reflecting surfaces with a single source and a receiver. The direct sound path is marked by A. A pair of sound paths, marked by B and C, have single reflections. The sound path marked as D has two reflections. All of these contribute to the spectral and temporal response for this arrangement.

The method of images is useful in the development of a computer model. In order to produce an accurate computer model using this method, the techniques discussed in Sec. 2.4 can be directly applied. The greatest difficulty comes from determining the image source locations; however, these positions may be found by ray tracing and geometry. The result is a model of the sound field that shows variations due to reflections and can produce either the impulse response or frequency response of the source-receiver pair.

The method of images can extend the model described in Sec. 2.1 and discussed in Sec. 2.4 to model an enclosed sound field, a partial free field or a free field. In the case of a free field, only the direct sound from the sources is calculated. In an enclosed field, the reverberation is modeled by the use of many virtual sources. In theory, an infinite number of sources would be required. In practice, this is not possible nor necessary. Sound arriving from higher-order reflections is modeled by virtual sources located farther away. This can be seen in Fig. 2.5(b) by comparing the the distance from the virtual source used to model path C or B to the listening position, and the distance from the virtual source to the listening position used to model path D. The extra distance that the sound must travel inherently attenuates the sound produced by the virtual source. Classical absorption may also be easily included in the model by introducing a complex-valued wave number. There are difficulties with appropriately representing the absorption due to the reflections of obliquely incident waves. This absorption is outside of the scope of this research, so models will only be used here to represent perfectly reflecting surfaces.

2.2 Energetic Descriptions of Sound Fields

Commonly in physics it is useful to look at systems in terms of their energy. Acoustics is no different. It is useful to look at the sound power, acoustic intensity and energy density of sound. Energetic descriptors provide another view point for examining sound fields and have useful properties for sound control.

2.2.1 ED of a Sound Field

A simplified expression for ED of two point sources in phase and 180° out of phase can be found. Equations (2.1) and (2.6) are sums that account for several sound sources to describe the pressure and particle velocity, respectively. Combining these equations with Eqs. (2.8) results in descriptions of the sound field due to a set of sources. For time-averaged PED the expression is

$$\langle w_p \rangle_t = \frac{1}{4\rho_0 c^2} \left| \sum_{n=1}^{N} \frac{\hat{A}_n e^{-jkR_n}}{R_n} \right|^2 \tag{2.19}$$

while the time-averaged KED is

$$\langle w_{\mathrm{k}} \rangle_t = \frac{\rho_0}{4} \left| \sum_{n=1}^{N} \frac{-\hat{q}_n e^{-jkR_n}}{R_n^3} (jkR_n + 1)\vec{R}_n \right|^2, \tag{2.20}$$

where $\vec{R}_n$ was previously defined as

$$\vec{R}_n = \begin{pmatrix} x - x_n \\ y - y_n \\ z - z_n \end{pmatrix}. \tag{2.7}$$

Equation (2.2) defines $\hat{A}_n$ as

$$\hat{A}_n = \frac{j\rho_0 ck\hat{q}_n}{4\pi}. \tag{2.2}$$

For a sound field produced by only two sound sources, the specific expressions can be determined using analytical methods. The PED for a pair of sound sources is

described by[2]

$$\langle w_p \rangle_t = \frac{\rho_0 k^2}{64\pi^2} \left(\frac{|\hat{q}_p|^2}{R_p^2} + \frac{|\hat{q}_s|^2}{R_s^2} + \frac{2|\hat{q}_p||\hat{q}_s|\Theta}{R_p R_s} \right) \tag{2.21}$$

where

$$\Theta = \cos(k(R_p - R_s)) \cos\gamma - \sin(k(R_p - R_s)) \sin\gamma \tag{2.22}$$

$\gamma = \phi_p - \phi_s$ describes the phase difference of the sound sources, $\hat{q}_p$ and $\hat{q}_s$ are the complex source strengths of the sources, and R_p and R_s are the distances from the sound sources to the field point of interest. The KED is[3]

$$\langle w_\mathrm{k} \rangle_t = \frac{\rho_0}{64\pi^2} \left(\frac{|\hat{q}_p|^2[k^2 R_p^2 + 1]}{R_p^4} + \frac{|\hat{q}_s|^2[k^2 R_s^2 + 1]}{R_s^4} + \frac{2|\hat{q}_p||\hat{q}_s|\Delta}{R_p^3 R_s^3} \zeta \right), \tag{2.23}$$

where

$$\Delta = (x - x_p)(x - x_s) + (y - y_p)(y - y_s) + (z - z_p)(z - z_s), \tag{2.24}$$

and

$$\zeta = (\xi \cos(\chi) + \chi \sin(\chi)) \cos\gamma + (\chi \cos(\chi) - \xi \sin(\chi)) \sin\gamma \tag{2.25}$$

where $k(R_p - R_s) = \chi$ and $k^2 R_p R_s + 1 = \xi$. TED is described by[4]

$$\langle w \rangle_t = \frac{|\hat{q}_p|^2 \rho_0}{64\pi^2 R_p^4 R_s^4} \left(\begin{array}{l} 2k^2 R_s^4 R_p^2 + R_s^4 + B^2(2k^2 R_p^4 R_s^2 + R_p^4) + \\ +2k^2 R_p^3 R_s^3 B \left[\begin{array}{l} \cos\gamma \cos(\chi)) + \\ -\sin\gamma \sin(\chi)) \end{array} \right] + \\ +2BR_p R_s \Delta \left(\left(\begin{array}{l} \xi \cos(\chi) + \\ \chi \sin(\chi) \end{array} \right) \cos\gamma + \right. \\ \left. \left(\begin{array}{l} \chi \cos(\chi) - \\ \xi \sin(\chi) \end{array} \right) \sin\gamma \right) \end{array} \right). \tag{2.26}$$

[2]Squared pressure is calculated in Appendix C.1.

[3]The vector magnitude of particle velocity is calculated in Appendix C.2.

[4]TED is found in Appendix C.3.

again $k(R_p - R_s) = \chi$, $k^2 R_p R_s + 1 = \xi$, and Δ is defined in Eq. (2.24). These expressions will be used to determine a relationship between ED quantities and total radiated sound power.

In the special case where the two sources have the same source strength and act in phase, the expressions for ED can be further reduced. For the case of PED the expression simplifies to

$$\langle w_p \rangle_t = \frac{\rho_0 k^2}{64\pi^2} |\hat{q}|^2 \left(\frac{1}{R_p^2} + \frac{1}{R_s^2} + \frac{2}{R_p R_s} \cos\left(k(R_s - R_p)\right) \right). \tag{2.27}$$

The ζ in the expression for KED simplifies to

$$\zeta = (k^2 R_p R_s + 1)\cos(k(R_p - R_s)) + (k(R_p - R_s))\sin(k(R_p - R_s)) \tag{2.28}$$

This simplification shows little significance at this point; however, it yields a relationship between ED and sound power that is independent of source strength. This solution also provides a first approximation to the relationship between ED and sound power. This relationship will be discussed later.

2.2.2 Sound Power

In sound control, one important measurement of the system is the sound power. Sound power describes the energy flux radiated per unit time from a system of sound sources. Sound power can then be thought of as the sound energy that leaves or enters a closed surface per amount of time. This is a Gaussian surface, similar to those used in electromagnetism. Sound power can be divided into two types of power: active and reactive. The active power is the power that is radiated from the system, passing through the enclosing surface, while the reactive power describes the energy that remains in the system.

The method for calculation of sound power illustrates the concept of reactive and active sound power. For a single point source the power radiated, or self power, can

be expressed by [9, 32]

$$\Pi = \frac{1}{2}\Re\{\hat{p}^*\hat{q}\}. \tag{2.29}$$

If a second sound source is introduced to the system, the contribution of the first sound source to the total radiated power is affected by the second source. There are complications because the second source introduces an impedance into the system. The result may be an increase or a decrease in the radiated power of the whole system. The change in radiated power is due to the impedance of the other sources in the space. The acoustic power calculations must include both self power and mutual power from the other sources in the system. The sound power produced by just one of the two sources in the sound field is expressed as

$$\Pi = \frac{1}{2}\Re\{(\hat{p}_{11} + \hat{p}_{12})^*\hat{q}_p\}. \tag{2.30}$$

The power radiated, taking into account the impedances of the other sources, can be added together to arrive at the total sound power radiated by the sound sources. The resulting expression describing the total sound power for two point sources is [9]

$$\Pi = \frac{1}{2}\Re\{(\hat{p}_{11} + \hat{p}_{12})^*\hat{q}_p\} + \frac{1}{2}\Re\{(\hat{p}_{21} + \hat{p}_{22})^*\hat{q}_s\}. \tag{2.31}$$

The total resulting power is different than summing the self power produced by the two sources independent. Introducing a new sound source to the system changes the impedance of all of the sources already in the system.

A similar process may be used to calculate the sound power of much more complicated systems, relying mainly on computational methods. To simplify the calculations it is useful to use the relationship of pressure to the source strength and impedance. This can be expressed as [10]

$$\hat{\mathbf{p}} = \hat{\mathbf{Z}}\hat{\mathbf{q}}. \tag{2.32}$$

In this case, we let $\hat{\mathbf{p}}$ and $\hat{\mathbf{q}}$ be vectors representing the pressures and source strengths in the system, and let $\hat{\mathbf{Z}}$ be a matrix that represents the impedance of each source's

relationship with the other sources. We thus arrive at a description of the power of the system. It is important to note that the conjugation on the pressure is Hermitian, meaning that the vector is conjugated and transposed. The resulting expression for the sound power of an arbitrary set of point sources becomes [10]

$$\Pi = \frac{1}{2}\Re\{\hat{\mathbf{p}}^{\mathbf{H}}\hat{\mathbf{q}}\} = \frac{1}{2}\Re\{\hat{\mathbf{q}}^{\mathbf{H}}\hat{\mathbf{Z}}^{\mathbf{H}}\hat{\mathbf{q}}\}. \tag{2.33}$$

Because of reciprocity, the matrix $\hat{\mathbf{Z}}$ is Hermitian [8, 10, 38]. This expression is convenient for determining the sound power of many arbitrarily positioned sources.

For the special case of two point sources, a simple analytical expression is well defined. For a pair of point sources, with source strengths $\hat{q}_p$ and $\hat{q}_s$ and separation distance d, the sound power is [39]

$$\Pi = \frac{k^2\rho_0 c}{8\pi}|\hat{q}_p|^2\left(1 + \frac{|\hat{q}_s|^2}{|\hat{q}_p|^2} + 2\frac{|\hat{q}_s|}{|q_p|}\text{sinc}(kd)\cos(\gamma)\right), \tag{2.34}$$

where γ is the phase difference $\phi_p - \phi_s$. This expression for sound power will be used to explore control achieved when source coupling is used in ANC.

2.2.3 Acoustic Intensity

Another useful measurement in acoustics is the acoustic intensity. The instantaneous intensity describes the energy per unit area transferred from one element of fluid to another element of fluid, and may be expressed as [30]

$$\hat{\vec{I}} = \hat{p}\hat{\vec{u}}. \tag{2.35}$$

It is important to note that intensity is a vector quantity. The time averaged-acoustic intensity, which is often more useful, may be expressed by [30, 31]

$$\langle\hat{\vec{I}}(t)\rangle_T = \frac{1}{T}\int_0^T \hat{p}\hat{\vec{u}}\, dt, \tag{2.36}$$

where T is the period of a single frequency wave. For time-harmonic conditions, it may also be expressed using the complex frequency domain values of pressure and particle velocity:

$$\langle \vec{I}(t) \rangle_T = \frac{1}{2} \Re\{\hat{p}^* \hat{\vec{u}}\} = \frac{1}{2} \Re\{\hat{p} \hat{\vec{u}}^*\}. \tag{2.37}$$

Intensity is a point measurement that varies as a function of spatial location, while sound power is a global measurement, which does not vary over space. This can be see by noting that sound power depends on the source strength of the sources in the system, while the intensity depends on pressure and particle velocity measured at a single point. Because of this, acoustic intensity may measure sources that are not in the system of interest. As previously mentioned, the sound power expresses how much energy exits or enters a complete closed surface containing the system of sound sources. Intensity, however, is the acoustic energy per area that is transferred through a cross section.

The acoustic intensity is also more convenient for making measurements in the lab than sound power. Measuring acoustic intensity requires the same information necessary to find ED. Both are dependent upon the acoustic particle velocity and acoustic pressure. Because of these similarities, most instruments used to measure ED may also be used to measure acoustic intensity [1, 7, 40, 41]. Measuring sound power, however, requires measurements at several locations around the system of sound sources. This makes the sound power a less convenient quantity in many practical situations, where both the number of sensors and available time are limited.

2.2.4 Relationship between ED and Π

Kestell *et al.* showed in their work that a measurement taken by an error sensor at one location may be used to minimize sound at a different location, which indicates that one measurement may be used to predict another measurement [42]. This raises

an interesting question: could a given localized measurement such as ED be used to predict or approximate a global measurement such as Sound Power? If a relationship of some kind can be found between two different measurements, then it should be possible to use that relationship to predict the value of one measurement from the other.

Sound power describes the sound energy radiated from a system of sound sources so, it is a quantity that is important for active nose control (ANC) [43, 44]. Because of the inherent difficulty in measuring sound power directly, it would be convenient and potentially useful to use an ED measurement to approximate sound power.

Using Eq. (2.21), (2.23), (2.26), and (2.34) can yield a relationship between ED quantities and total sound power. This relationship becomes complicated for even simple sound source arrangements. A ratio of ED to sound power can be used as a tool for approximating sound power, like a units conversion factor. Putting PED and KED in the numerator provides a convenient simplification for calculating the ratio relating TED to power. Defining the ratio of TED and sound power by

$$\frac{\langle w_{\mathrm{t}}\rangle_t}{\Pi} = \frac{\langle w_{\mathrm{p}}\rangle_t + \langle w_{\mathrm{k}}\rangle_t}{\Pi} = \frac{\langle w_{\mathrm{p}}\rangle_t}{\Pi} + \frac{\langle w_{\mathrm{k}}\rangle_t}{\Pi} \tag{2.38}$$

allows it to be easily split into two parts, which can be conveniently added together after calculating the two ratios. One characteristic of the above equation is that all of the terms involve the source strengths. In practical situations, approximating the source strength involves the knowledge of the signal used to drive the sound source as well as the frequency response of the source along with any components used to drive it.

For the simple case of two point sources acting in phase with the same magnitude in a free field, the ratio of ED to sound power can be found in a straightforward maner. With this source arrangement, the source strengths conveniently cancel in

the ratio. It can be shown that the ratio of PED to sound power can be expressed by dividing Eq. (2.27) by Eq. (2.34), resulting in the ratio

$$\frac{\langle w_{\mathrm{p}}\rangle_t}{\Pi} = \frac{1}{4\pi c}\frac{\frac{1}{R_p}+\frac{1}{R_s}+\frac{2}{R_pR_s}\cos\left(k[R_p-R_s]\right)}{1+\mathrm{sinc}(kd)}, \tag{2.39}$$

where R_p and R_s indicate the distance from sources one and two to the field point, respectively. The relationship for the KED can be found by dividing Eq. (2.23) by Eq. (2.34), which yields

$$\frac{\langle w_{\mathrm{k}}\rangle_t}{\Pi} = \frac{\frac{k^2R^1+1}{R_p^4}+\frac{k^2R^2+1}{R_s^4}+\frac{2\Delta}{R_p^3R_s^3}\zeta}{16\pi ck^2(1+\mathrm{sinc}(kd))}, \tag{2.40}$$

where ζ is defined in Eq. (2.28) as

$$\zeta = (k^2R_pR_s+1)\cos(k(R_p-R_s)) + (k(R_p-R_s))\sin(k(R_p-R_s)) \tag{2.28}$$

and Δ is defined by Eq (2.24). To get the relationship between TED and total sound power for a system, it is only necessary to use Eqs. (2.39) and (2.40) in Eq. (2.38).

For slightly more complicated situations, Eqs. (2.39) and (2.40) become much more involved. Equations (2.21) and (2.25) may be used instead of Eqs. (2.27) and (2.28) to arrive at a more general description of a sound field produced by two sound sources. The resulting expression for the relationship between PED and sound power becomes

$$\frac{\langle w_p\rangle_t}{\Pi} = \frac{1}{8\pi c}\left\{\frac{\frac{|\hat{q}_p|^2}{R_p^2}+\frac{|\hat{q}_s|^2}{R_s^2}+2\frac{|\hat{q}_p||\hat{q}_s|}{R_pR_s}\Theta}{|\hat{q}_p|^2+|\hat{q}_s|^2+2|\hat{q}_p||\hat{q}_s|\mathrm{sinc}(kd)\cos(\gamma)}\right\}. \tag{2.41}$$

where Θ was defined in Eq. (2.22). For the case of KED, the relationship becomes

$$\frac{\langle w_{\mathrm{k}}\rangle_t}{\Pi} = \frac{1}{8\pi k^2c}\left\{\frac{\frac{|\hat{q}_p|^2[k^2R_p^2+1]}{R_p^4}+\frac{|\hat{q}_s|^2[k^2R_s^2+1]}{R_s^4}+\frac{2|\hat{q}_p||\hat{q}_s|\Delta}{R_p^3R_s^3}\zeta}{|\hat{q}_p|^2+|\hat{q}_s|^2+2|\hat{q}_p||\hat{q}_s|\mathrm{sinc}(kd)\cos(\gamma)}\right\}, \tag{2.42}$$

where ζ is defined as

$$\zeta = (\xi\cos(\chi)+\chi\sin(\chi))\cos\gamma + (\chi\cos(\chi)-\xi\sin(\chi))\sin\gamma \tag{2.25}$$

in Eq. (2.25), $\chi = k(R_p - R_s)$, $\xi = k^2 R_p R_s + 1$ and Δ is defined by Eq. (2.24). Adding these two expressions together yields an expression relating TED to sound power for two sound sources. These equations require knowledge of both source strengths and locations of the sources where the simpler expressions found in Eqs. (2.39) and (2.40) do not require knowledge of the source strength. In an enclosed field, boundary conditions would also be required to fully specify the system.

It is also interesting to look at the situation of approximating the formulations with the sensor at a mathematically simple location. To do this, one may assume that the two sources are equidistant from the error sensor, thus setting R_p equal to R_s. Applying this simplification to Eqs. (2.41), and (2.42) does simplify the expressions for the relationship. The relationship becomes

$$\frac{\langle w_p \rangle_t}{\Pi} = \frac{1}{8\pi c R^2} \left\{ \frac{|\hat{q}_p|^2 + |\hat{q}_s|^2 + 2|\hat{q}_p||\hat{q}_s| \cos(\gamma)}{|\hat{q}_p|^2 + |\hat{q}_s|^2 + 2|\hat{q}_p||\hat{q}_s| \text{sinc}(kd) \cos(\gamma)} \right\}. \tag{2.43}$$

For the case of KED,

$$\frac{\langle w_\text{k} \rangle_t}{\Pi} = \frac{k^2 R^2 + 1}{8\pi c k^2 R^4} \left\{ \frac{|\hat{q}_p|^2 + |\hat{q}_s|^2 + 2|\hat{q}_p||\hat{q}_s| \cos(\gamma)}{|\hat{q}_p|^2 + |\hat{q}_s|^2 + 2|\hat{q}_p||\hat{q}_s| \text{sinc}(kd) \cos(\gamma)} \right\} \tag{2.44}$$

where Δ is again defined by Eq. (2.24). Equations (2.41) and (2.42) may be compared to Eqs. (2.43) and (2.44) to assess what regions would be good candidates for placing an error sensor for calculating the sound power of the system. However, it is important to remember that these relationships are dependent on frequency and source strength.

2.3 Sound Levels

In acoustics it is often convenient to express measurements of sound on a decibel scale. In the case of pressure, this is referred to as the Sound Pressure Level (L_p) and may be defined as [45]

$$L_P = 20 \log_{10} \left(\frac{p_\text{rms}}{p_\text{ref}} \right) = 10 \log_{10} \left(\frac{p_\text{rms}^2}{|\hat{p}|_\text{ref}^2} \right), \tag{2.45}$$

where

$$p_{\text{rms}} = \frac{p}{\sqrt{2}}$$

and the reference pressure, p_{ref} is commonly set to 20μPa for measurements in air. The Sound Intensity Level (L_I) is likewise well known and defined as [45]

$$L_I = 10 \log_{10} \left(\frac{|\vec{I}|}{I_{\text{ref}}} \right), \tag{2.46}$$

where the reference intensity, I_{ref}, is chosen to be 10^{-12} W/m^2 in air. These reference values result in nearly equivalent decibel values for either method of measuring sound [45, 46]. However, at this point it is apparent that there are other measurements of interest in acoustics, such as particle velocity and ED. For particle velocity and ED different reference values would be appropriate for decibel representations.

In order to put the particle velocity on a similar scale, the relationship for a plane wave may be exploited to calculate a reference value for particle velocity from the reference value used for pressure [47, 48]. The resulting expression is [45, 47, 48]

$$u_{\text{ref}} = \frac{p_{\text{ref}}}{\rho_0 c}. \tag{2.47}$$

It is apparent that the value for particle velocity will vary with the ambient conditions of the measurement [47, 48]. For the computational models, ρ_0 is set to 1.21 kg/m^3 and c is assumed to be 343 m/s. Using this method, the resulting reference particle velocity is 48.2 nm/s, which may be approximated as 50 nm/s [48]. This leads to a Sound Velocity Level (L_v) that is defined as

$$L_v = 20 \log_{10} \left(\frac{u_{\text{rms}}}{u_{\text{ref}}} \right) = 10 \log_{10} \left(\frac{u_{\text{rms}}^2}{u_{\text{ref}}^2} \right) \tag{2.48}$$

where

$$u_{\text{rms}} = \frac{|\hat{u}|}{\sqrt{2}}$$

and where $u_{\text{ref}} = 50$ nm/s.

A similar method may be used for finding TED level. Instantaneous ED is used to appropriately find the ED reference level and is expressed [47, 48]

$$w_{p,\text{ref}} = \frac{p_{\text{ref}}^2}{2\rho_0 c^2}, \qquad w_{k,\text{ref}} = \frac{\rho_0}{2}|\vec{u}|_{\text{ref}}^2, \qquad w_{\text{ref}} = w_{k,\text{ref}} + w_{p,\text{ref}}. \tag{2.49}$$

The calculation of the reference value may be further simplified by substituting in the expression for the particle velocity reference value found in Eq. (2.47). The substitution allows the reference values to simplify to

$$w_{p,\text{ref}} = w_{k,\text{ref}} = \frac{p_{\text{ref}}}{2\rho_0 c^2}, \qquad w_{\text{ref}} = \frac{p_{\text{ref}}}{\rho_0 c^2}. \tag{2.50}$$

Equation (2.49) results in reference values of $w_{\text{p,ref}} = 1.41 \times 10^{-15}$ J/m^3, $w_{\text{k,ref}} = 1.51 \times 10^{-15}$ J/m^3, and $w_{\text{ref}} = 2.92 \times 10^{-15}$ J/m^3 using $p_{\text{ref}} = 20\mu$Pa and $u_{\text{ref}} = 50$nm. Equation (2.50) results in $w_{\text{p,ref}}$ and $w_{\text{k,ref}}$ having the same value of 1.41×10^{-15} J/m^3 and $w_{\text{ref}} = 2.81 \times 10^{-15}$ J/m^3. It is reasonable to round the results for w_{ref} to 3×10^{-15} J/m^3. However, a more precise calculation of L_v and ED Level (L_w) in Eqs. (2.47) and (2.50) should be used because the density, ρ_0, and speed of sound, c, may vary significantly. If these variations are significant enough, it may not be appropriate to use an approximate value for the references in calculating level values. However, because PED, KED, and TED are related and have the same units, it is *convenient* to use the same reference value. Table 2.1 includes a list of the reference values used for for the computational models in this work.

Table 2.1 References used to calculate a given Sound Level measurement that is used with the computational models.

Nominal Sound Level Reference Values			
p_{ref}	u_{ref}	I_{ref}	w_{ref}
20μPa	50nm	$10^{-12}\frac{\text{W}}{\text{m}^2}$	$3 \times 10^{-15}\frac{\text{J}}{\text{m}^3}$

2.4 Computational Model of the Sound Field

MATLAB® was used to computationally model the sound fields explored in this thesis. In order to make the computational models useful for many situations, the computer code was written to calculate the fundamental acoustic measurements by summing the pressure and vector components of the particle velocity of the sound sources. This process is performed by initializing the variables representing total pressure and particle velocity components to zero. The program cycles through a loop. In each iteration the contribution to one source is added to the variables. This process calculates the results for Eqs. (2.1) and (2.6).

The pressure and particle velocity is then used to calculate other acoustic quantities. Because TED depends on the magnitude of pressure squared and the magnitude of particle velocity squared, these quantities are calculated next. The magnitude of squared pressure is

$$|\hat{p}|^2 = \hat{p}^* \hat{p}. \tag{2.51}$$

Since particle velocity is a vector, the magnitude squared of the particle velocity is calculated by finding the dot product of the particle velocity with its complex conjugate,

$$|\hat{\vec{u}}|^2 = \hat{\vec{u}} \cdot \hat{\vec{u}}^* = \hat{\vec{u}}^* \cdot \hat{\vec{u}} = \hat{u}_x^* \hat{u}_x + \hat{u}_y^* \hat{u}_y + \hat{u}_z^* \hat{u}_z. \tag{2.52}$$

These results can be applied to Eqs. (2.8) to calculate the PED, KED and TED fields. Other combinations of the fundamental acoustic variables, acoustic pressure and acoustic particle velocity, may be used to produce alternate measurements of sound fields.

These computational sound field models may be expanded to represent enclosed sound fields. Section 2.1.3 mentioned that this would require many virtual sources. The primary difficulty results from determining the locations of the virtual sources.

For simple room geometries, basic algorithms may be used to determine the locations of the virtual sound sources. However, a large number of image sources requires long computation times for code executed in MATLAB®. The time required to calculate the sound field using this method prohibited the generation of surface plots for enclosures; however, some auralizations were generated.

Animations

Often, visual methods aid understanding of a physical system; animating a plot allows for visualization of up to four dimensions in a single plot. In order to better understand control of a system of sound sources, MATLAB® was used to create visual illustrations of the sound field. In order to see the pertinent effects, the visualizations were often animated over frequency. These animations show how the sound field changes as a function of frequency, providing insight into the effects of control methods.

The animations were generated using the methods previously described. The data for a surface plot is calculated at a frequency and saved to a file. The process is repeated with the frequency increasing until the data for several surface plots has been stored on the computer. The data for the surface plots at each frequency is retrieved one data set at a time. This data is used to generate a plot that is added to the animation. The end result is an animation that can be shown in a short period of time.

Chapter 3

Active Sound Control Techniques

Active sound control includes both active noise control and equalization of sound. Acoustic coupling may be used to globally control sound radiated from combinations of sound sources located near one another. Electronic filters may be designed, using measured field quantities, to equalize a sound system. It is also important to know how well the techniques used accomplish their intended goals.

3.1 Active Noise Control

For active noise control, the objective is to reduce the sound of a given source configuration as effectively as possible. To do this, it is important to find the optimal control solution. For a free-field situation, the sound power provides a useful measure of the global radiation. For successful global active noise control (ANC), the sound power radiated from the system of sources will be reduced.

3.1.1 Minimizing Sound Radiation

The simplest situation for looking at active noise control is to minimize a sound quantity using one secondary (control) point source to reduce the sound from one primary point source in free space. For a reference, the minimization of the sound power output of the source pair will be used. Later, this setup will serve to compare the effectiveness of using different types and locations of error sensors. For this section, we will focus on the sound power output of a pair of point sources. The sound power is a global measurement that is independent of the locations of the sensors used to detect it. As previously mentioned, for a pair of point sources, with source strengths $\hat{q}_p$ and $\hat{q}_s$ and separation distance d, the sound power is [39]

$$\Pi = \frac{k^2\rho_0 c}{8\pi}|\hat{q}_p|^2\left(1 + \frac{|\hat{q}_s|^2}{|\hat{q}_p|^2} + 2\frac{|\hat{q}_s|}{|q_p|}\text{sinc}(kd)\cos(\gamma)\right), \tag{2.34}$$

where γ is the phase difference $\phi_p - \phi_s$. Here, and throughout this thesis, the $\text{sinc}(x)$ function is defined as

$$\text{sinc}(x) = \frac{\sin(x)}{x}, \tag{3.1}$$

for notational convenience.

To model a field acting in this setup, the source strength for the control source needs to be calculated. The expression [49],

$$\hat{q}_s = -\hat{q}_p\text{sinc}(kd), \tag{3.2}$$

describes the ideal relationship between the primary source strength, $\hat{q}_p$, and the control source strength, $\hat{q}_s$, to minimize the total power output of the source pair, where d is the distance between sources. This results in a minimum sound power of [49]

$$\Pi = \frac{k^2\rho_0 c}{8\pi}|\hat{q}_p|^2\left(1 - \text{sinc}^2(kd)\right). \tag{3.3}$$

It is important to remember that sound power is independent of the location where the sound field is measured; it is a global quantity [31, 43]. Because of this global nature, minimizing sound power makes a good reference for judging the ability to control sound in a free field [9]. The global nature of sound power also helps judge how much global sound control has been achieved using different measurement quantities, especially for the cases in which sound sources are placed in a free field.

Equation (2.34) can also be simplified for the case where there are two sound sources with the same source strength magnitude. The sound power than simplifies to

$$\Pi = \frac{k^2 \rho_0 c}{4\pi} |\hat{q}|^2 \big(1 + \operatorname{sinc}(kd)\cos(\gamma)\big). \tag{3.4}$$

Again, the value γ describes the phase difference between the sound sources.

3.1.2 Minimized Energy Density Total Power Output

An important question in active sound control is, where should the error sensor be placed? How much attenuation can be achieved using a given measurement method and sensor location? This thesis will demonstrate that in the near field of sound sources, TED has less spatial and spectral variations than squared pressure or squared particle velocity. Because of the increased uniformity of TED in the near field, it stands to reason that placing an ED-based error sensor in the near field would relieve some of the difficulties in carefully choosing a location of an error sensor, as well as reduce the problems that result from the frequency dependence of the optimal location of an error sensor. In order to assess this claim, Minimized Energy Density Total Power Output (MEDToPO) plots have been developed to illustrate the power output of a controlled source pair as a function of the location of a single error sensor. Here the MEDToPO plots are generated for the cases where PED, KED, and TED are used for error sensors.

Making a MEDToPO plot requires several steps. First, an error sensor location is chosen, then the ED that would be detected by that error sensor is calculated. Next, appropriate adjustments to the control sound source are made to minimize ED at the error sensor. At that point, the total sound power output of the system is calculated. This value is recorded for the location of the error sensor. This process is repeated for each location where an error sensor may be placed. The resulting set of data is used to produce a plot that shows the total power output of the system when a given error quantity is minimized at a number of points in the sound field. Figure 3.1 shows examples of these types of plots for a single primary sound source, marked with an $\times$, and a single secondary source, marked with an $\circ$, at $kd = 2.473$. Plots of PED, KED, and TED schemes are generated.

Often, it is useful to know how the optimal sensor locations vary as a function of frequency. This may be seen by creating a MEDToPO plot for each frequency of interest. The process leads to an array of MEDToPO plots, that may be used individually to look at each frequency, as in Fig. 3.1. The plots may also be used as frames in an animation to examine how changes in frequency alter the controlled sound field.[1] Unfortunately, the MEDToPO plot is limited to cases involving only one error.

3.2 Equalization

For some systems it is desirable to equalize a frequency response in order to match some ideal response curve. The dashed curve in Fig. 3.2 represents the frequency response measured at a point a short distance from the center of two point sources

[1] An example of this animation can be seen on the digital version of this thesis in Appendix E Fig. E.1. The MATLAB® code used to generate MEDToPO plots and animations is found in Appendix H.

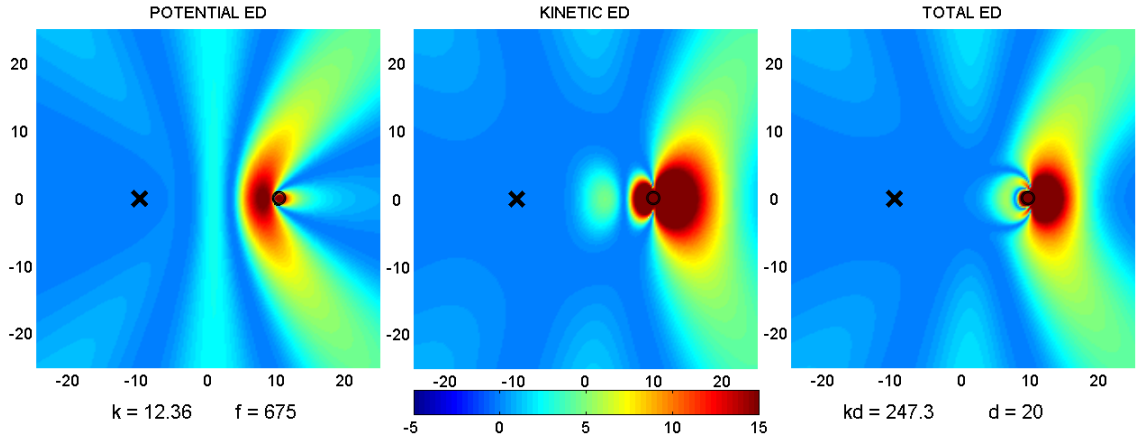

Figure 3.1 An example MEDToPO plot, at $kd = 2.473$, illustrates sound power output, at a given frequency, as a function of error sensor location and error signal type. The primary source is marked with an $\circ$ and the secondary source is marked by an $\times$.

radiating in a free field. To equalize this, the signal used to drive the sources would be filtered with a response similar to the dot-dash curve in Fig. 3.2. The result wold be a measured frequency response that is perfectly flat, like the solid line in the figure.

In equalization a method of dereverberation is used to correct the sound system to minimize the effects due to the listening environment. In this case, deconvolution is used. Several methods have been applied to find an appropriate correction filter, including the development of a cost function and use of least-squares methods to arrive at an appropriate solution [13,50–52]. Another method of equalization requires measuring the transfer function between some input signal and a measured output signal. Once this has been done, the inverse filter is found by inverting the frequency response such that

$$g[n] = h[n] \otimes h_{eq}[n] \quad \text{or} \quad H_{eq}(f) = \frac{1}{H(f)}, \tag{3.5}$$

where $\otimes$ indicates convolution, $g[n]$ is a delta function whose Fourier transform is unity across the spectrum of interest, and the corresponding transform relationships

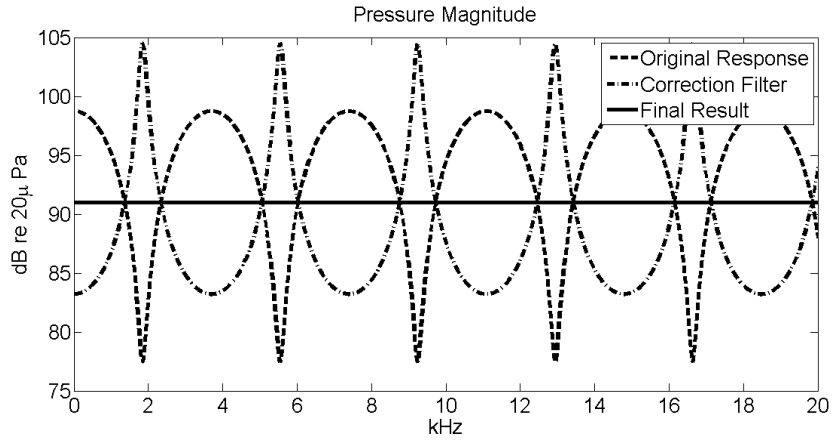

Figure 3.2 The original signal is filtered by a correcting filter, the result is a frequency response that is flat over the entire frequency range.

are defined

$$h[n] \leftrightarrow H(f), \quad h_{eq}[n] \leftrightarrow H_{eq}(f), \tag{3.6}$$

where $\leftrightarrow$ indicates a transform relationship.[2] The variable n indicates time and f indicates frequency. A time domain filter may be created from the resulting inverse frequency response function, $H_{eq}(f)$ [13, 53, 54]. To arrive at a usable filter, the inverted response must be transformed from the frequency domain to the time domain. The inverse of the response filter is then convolved with the recorded signal using a linear convolution, a process that will be discussed later [53, 55, 56].

Inverting the frequency response in the frequency domain and using the inverse Fourier transform to arrive at a time domain filter inherently creates a circular filter. This is because performing a discrete Fourier transform assumes that a circular system is being modeled. One interesting result of this inversion process is that the inverting filter is only causal in certain special cases [54]. If this filter is used in the compu-

[2] Though this inverse relationship is defined for a transfer function in the Laplace domain, it applies to the frequency, or Fourier, domain. This is because the Fourier domain is a special case of the Laplace domain.

tational model, it will produce a very notable anomaly in the auralization: an echo will begin before the direct sound. This may be dealt with by shifting the inverted impulse response in a circular fashion. A circular shift is performed by bringing the first section of an array representing the discrete impulse response to the end while maintaining the order of the elements in the array [57]. Under certain circumstances this minor adjustment allows the inverted impulse response to be corrected for the response of the room, even in cases when the room is not a minimum phase system. This is because a circular shift in the time domain is equivalent to multiplying by a linear phase factor in the frequency domain [57].

In practice, an inverse response found by simply inverting the function is not necessarily useful [54]. If the system has nonminimum phase, the filter found by inverting the response will be noncausal [12, 13, 53, 54]. For a minimum phase system, both the system and its inverse will be causal and stable [58]. This can be seen by noting that a minimum phase system will have all of its poles and zeros inside of the unit circle in the z-plane, wich implies that the system is stable and causal. After the system is inverted, the zeros in the z-plane are replaced by poles, and the poles are replaced by zeros. Thus, for the inverse to be causal and stable, the original system must have all of its zeros inside of the unit circle in the z-plane [59]. Another option for dealing with nonminimum phase involves approximating the appropriate inverse filter; however, this method is outside of the scope of this research.

Any nonminimum phase filter can be separated into a minimum phase portion and an all-pass portion [58]. In the frequency domain, the signal may be separated such that

$$H(z) = H_{min}(z)H_{ap}(z). \tag{3.7}$$

This expression may also be written in the time domain as

$$h[n] = h_{min}[n] \otimes h_{ap}[n]. \tag{3.8}$$

The filter, $H_{min}(z)$, will have the same magnitude as $H(z)$, while $H_{ap}(z)$ will have a uniform magnitude [53, 58].

In practice, a stable causal filter is required when performing filtering operations. Because the minimum phase portion of a response has the same magnitude as the full response, it may be used to design an equalization filter to equalize the magnitude response. An equalizing filter may be found by inverting the minimum phase portion of the frequency response. This changes Eq. (3.5) slightly to

$$H_{eq}(z) = \frac{1}{H_{min}(z)}. \tag{3.9}$$

Using a minimum phase filter will assure that the resulting filter inverse will be both causal and stable [12, 13, 54, 58, 60]. The resulting filter is capable of equalizing the magnitude response of the system. Though the phase is altered by a minimum phase filter, it does not always correct the phase issues. A minimum phase inverse filter will perfectly restore an acoustic signal that was reverberated by an impulse response that is minimum phase [12].

For each set of systems with a given magnitude frequency response there is one common minimum phase frequency response [58]. This means that magnitude equalization of a system may be performed using the minimum phase portion of the system, though this still alters the phase of the system. In theory, a correction filter defined using this method will inherently be causal and stable. However, a minimum phase filter may not correctly correct phase and can introduce phase issues. This can be seen by noting that the response of a minimum phase system has less delay than all of the other possible responses with the same magnitude frequency response. Research has previously shown that if the impulse response of the listening environment is nonminimum phase, there will be a residual reverberation in the result described in the literature as a "metallic tone" like a "bell chime" [12, 53].

3.2.1 Minimum Phase

The Hilbert transform may be used to find the minimum phase portion of a signal. A minimum phase signal is related to the log magnitude and phase of the frequency response. The complex cepstrum, as it is commonly called, is stated mathematically as [12, 58, 60]

$$C(f) = \ln[H(f)] = \ln\left[|H(f)|\right] + j\arg[H(f)] \tag{3.10}$$

where

$$h[n] \leftrightarrow H(f), \quad c[n] \leftrightarrow C(f). \tag{3.11}$$

If the filter length N is very long, the minimum phase portion of $H(f)$ may be found by noting that $c[n]$ is a periodic function, and that the second half of the array may be zeroed such that [12, 61]

$$m[n] = \begin{cases} c[n], & n = 0, N/2 \\ 2c[n], & 1 \leq n < N/2 \\ 0, & N/2 < n \leq N-1. \end{cases}$$

where the cepstrum, $C(f)$, is expressed in quefrency and $c[n]$ is its transform. Letting

$$M(f) \leftrightarrow m[n], \tag{3.12}$$

finishes out the Hilbert transform. The minimum phase portion of the signal $H(f)$ is expressed by [12]

$$H_{min}(f) = e^{M(f)}. \tag{3.13}$$

This process can be described as taking the log of the Fourier transform of the input signal, than inverse transforming the result and raising it to the power of the base of the logarithm taken in the initial step. In this example the natural log was used, though any convenient base may be chosen. It is important to remember that any

modeled filter is implemented using linear convolution in order to represent how the filter would perform.

Another option for building a time-domain equalization filter from a frequency response function is to shift the filter in the time domain. After a filter is designed in the frequency domain, it can be expressed in the time domain. The process of transforming the filter from one domain to another assumes a circular symmetry, which may be used to change the phase of the filter. In the time domain, the filter may be circularly shifted so that the terms pushed out one end of the filter are moved in to the other end. The magnitude frequency response of the filter is maintained through this process, but can be made causal if appropriately shifted. This method does not result in a minimum phase filter, but can be made to work well consistently. Effectively, this technique is introducing a pure delay to compensate for non minimum phase.

3.2.2 Convolution

Calculating a convolution involves four major steps: reversal or folding, shifting, multiplying, and integrating or summing [62, 63]. Considering filters or signals as curves helps understand the concept of convolution. First one of the curves is reversed left to right, and moved to the start of the other array. The first array is moved, or shifted, along the other while the area under both of the curves is integrated resulting in a new curve. The new curve represents the area under both curves as a function of the location of the curve that is moved along the other. This can be expressed mathematically as [62, 64]

$$h(t) = \int_{-\infty}^{\infty} f(\tau)k(t-\tau)\mathrm{d}\tau. \tag{3.14}$$

In some situations, it may also be convenient to assume that the system is at

rest before the signal is used by starting the integral at an initial point. In this research, the convolution is performed mostly using arrays of numbers representing signals or filters. The process is essentially the same, and is illustrated in Fig. 3.3. The reversal step is performed by reversing the order of the terms in the filter and placing the filter to the left of the signal array. The shifting is performed by shifting one term at time instead of integrating the area, the aligned taps are multiplied, and the results are summed. This produces the first value in the resulting convolution. The shifting, multiplying, and summing steps are repeated, resulting in the next term in the final series. The process is repeated until the last term of both the filter and the signal line up, producing the last term of the series. This results in a series that is $L+P-1$ long where L is the length of the signal and P is the length of the filter [63]. Mathematically this is stated

$$h[n] = \sum_{\eta=-\infty}^{\infty} f[\eta]k[n-\eta] \tag{3.15}$$

and is commonly referred to as linear discrete-time convolution. For a practical situation this is further limited to having a finite set of data which further simplifies the sum to [63]

$$h[n] = \sum_{\eta=0}^{N} f[\eta]k[n-\eta], \tag{3.16}$$

This process is straight forward and has the convenience of performing the computations in the time domain, but the process is computationally inefficient.

Up to this point, only linear convolution has been discussed; another type of convolution known as circular convolution also exists. In linear convolution, when the two data sets have terms that do not overlap, the unpaired terms are multiplied by zero. In the case of circular convolution, the terms wrap around so that all of the terms of the shorter array aligns with terms on the longer data set. This is illustrated in Fig. 3.4 by showing the change from one iteration to the next of the

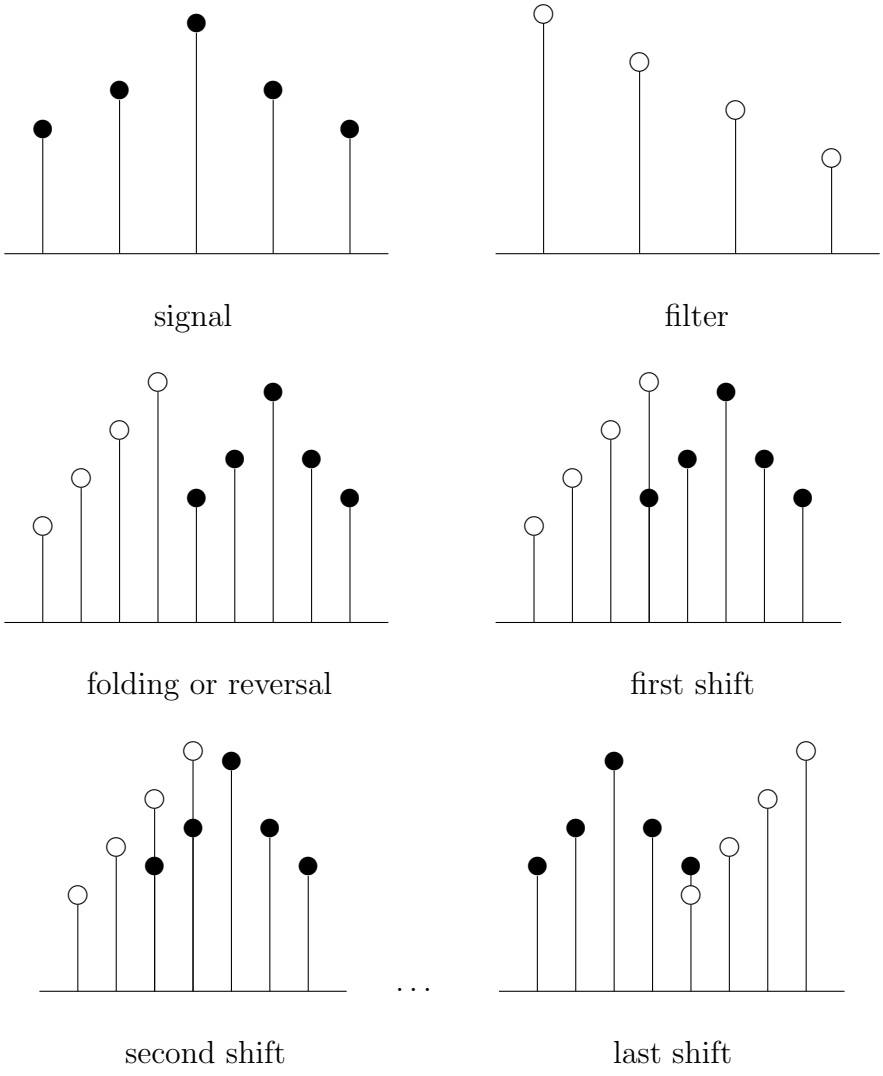

Figure 3.3 Illustration of a discrete linear convolution of a four tap filter and a five term signal, both of which are found on the top row. The left middle shows the reversal and placement of the filter for the first iteration of the process. The remaining three illustrations show further steps of the shift process of the convolution.

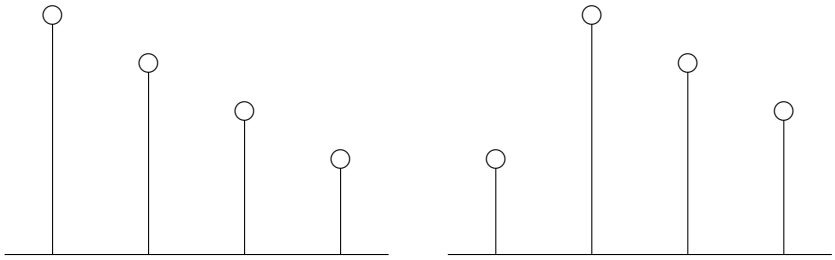

Figure 3.4 In circular convolution, when the filter or sequence is shifted, the last tap or term is rotated to the beginning.

shifted filter. Circular convolution does not model the response of an acoustic signal in a room or any other listening environment, but it matches the results of some more computationally efficient methods of performing the convolution.

A more computationally efficient method for calculating the convolution relies on the convolution theorem of the Fourier transform, which states that multiplication in one domain is related to convolution in the other domain. Stating this in mathematical terms, letting [63]

$$y[n] = x[n] \otimes h[n] \leftrightarrow X(f)H(f) = Y(f) \tag{3.17}$$

where

$$x[n] \leftrightarrow X(f), \quad y[n] \leftrightarrow Y(f), \quad h[n] \leftrightarrow H(f), \tag{3.18}$$

On a computer, convolution is often computed by first using a fast Fourier transform (fft) on the arrays to transform them to the frequency domain. The arrays are then multiplied term by term, producing a new array. The new array is then inverse transformed using the inverse fast Fourier transform (ifft). The result is the convolution of the two arrays. However, this is a circular convolution, not a linear convolution. It assumes that the arrays represent periodic signals or filters. To compensate for this issue, the arrays may be zero padded before the initial Fourier transform, the

result will have extra zeros at one end which may be removed after the convolution is computed [56, 63, 65, 66]. This process results in a linear convolution.

In order to model an acoustic system, a linear convolution between a signal and a filter should be used [56, 65, 66]. The circular convolution assumes that the signal or filter repeats itself. In a real acoustic system, the room, which is modeled by the filter, does not repeat; under common circumstances the signal does not repeat either. This means that a linear convolution will produce a realistic representation of the acoustic system, while a circular convolution will introduce an error due to its periodic nature. This process may be used to produce an auralization to determine how a given sound will act in a given acoustic environment. A function was written for this research to perform the convolutions, the MATLAB® code used can be found in Appendix G.

3.3 Evaluating Equalization

There are several techniques that might be used to judge the success of methods of equalization. These methods include modeling what would be heard at a given listening position with an auralization, plotting information about the sound field, and calculating an equalization coefficient to rank the effectiveness of the equalization.

3.3.1 Auralization

In order to simulate and demonstrate what would happen when a sound system in an environment is equalized, computer simulations were created in MATLAB®. To better understand the effects of multiple sources in a free field, or sound sources in the presence of a reflecting plane, a computer model was used to generate auralizations of the situations of interest. Creation of these auralizations requires an impulse response that represents the relationship between the sound sources, reflective surfaces, and

the listening position for a given listening environment. The impulse response is then convolved with an anechoic recording to produce an auralization [64].

The techniques described in Sec. 2.1, are used to find the pressure frequency response for a listening position in a defined environment. The pressure frequency response, convolved with a given signal describes the pressure function at a listening position, thus modeling the sound that would be heard at that given point. This frequency response is used to find the impulse response for the listening position, which is used to make the auralization. The auralization made to model the listening position can then be convolved with any equalization filter to produce an auralization that demonstrates the effect of a given equalization filter at a specific listening position.

To validate the convolution used in this research, its results were compared to the results found using GratisVolver$^{\text{TM}}$, a free executable file produced by CATT Acoustic$^{\text{TM}}$ [67]. The resulting auralizations sounded identical. To further substantiate the similarities between the two auralizations, the auralizations were both read into MATLAB® and plotted (See Figs. 3.5(a) and (b)). The difference between the results of the MATLAB® convolution and the GratisVolver$^{\text{TM}}$ convolution is on the order of 10^{-3}, as shown in Fig. 3.5(c). This result is an example of the typical results of the convolutions from these two programs.

Frequency responses based on other acoustical measurements, such as particle velocity, TED, and sound power, were also used to equalize the systems. These filters were calculated using developments found in Ch. 2. The resulting filters are convolved with the previously found pressure based auralization using the previously described methods. The new set of auralizations exhibited what a listener would hear if the given filter were used to equalize the sound produced by a source. A similar process could be used to model situations where the sound from a primary source is reinforced

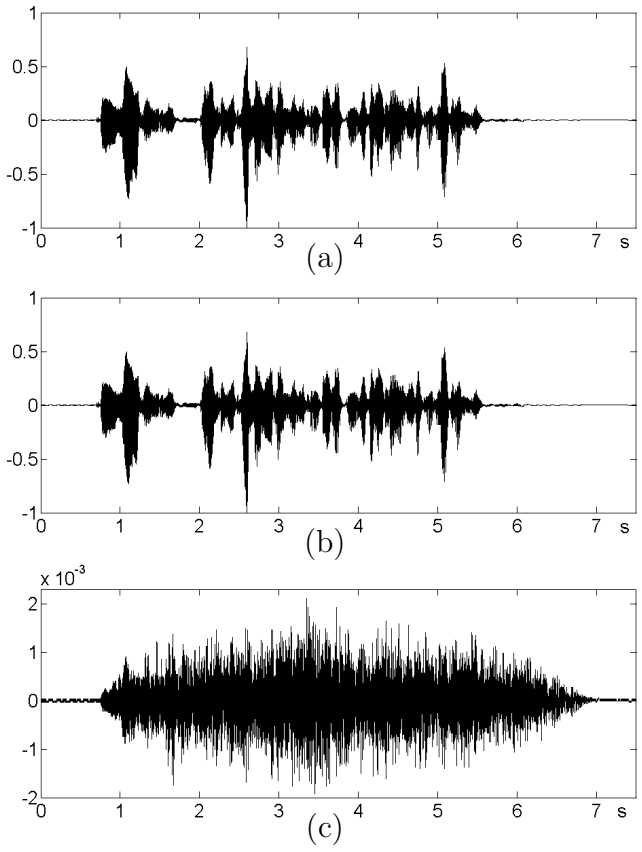

Figure 3.5 Abover are the resulting auralizations for convolutions using (a) GratisVolver^{TM} and (b) the technique used in MATLAB®. Figure (c) shows the difference between the convolutions performed by both programs. It is important to note that the scale in the last figure is much smaller than the plots of the auralizations. The auralizations can be found on the digital version of this thesis in Appendix F.1.

by an equalized secondary source.

3.3.2 Animations

The techniques mentioned in Sec. 2.4 were used to generate animations to illustrate the effects of equalization on the sound field. A frequency response for a listening position is obtained computationally to design an equalizing filter. A spatial plot of the equalized sound field is generated at each frequency. These plots are then used to generate an animation that shows the spectral fluctuations of the given listening region and helps determine if the equalization process is beneficial over a large area.[3]

The animations in this research show how the field changes as frequency increases. A circle is marked on these animations indicating the position of the error sensor in order to demonstrate that the response at that position maintains a constant response over frequency while showing that the field changes over frequency at other locations. It quickly becomes apparent that the entire field increases or decreases due to the gain and attenuation used to equalize the sensor at its fixed location. Animations give a general idea of how the field changes, but it is still often difficult to see where the field is equalized and where the performance is degraded.

3.3.3 Spectral Standard Deviation

Standard deviation of the frequency response may be used to indicate the level of equalization of a listening area. The standard deviation may be calculated for many listening positions, such that a map of the equalized space may be generated. If the

[3]Some of these animations can be viewed in the digital version of this thesis in Appendix E

entire sample is available concurrently, the variance may be calculated by,[4]

$$s^2 = \frac{\sum_{i=1}^{N} (x_i - \bar{x})^2}{N-1}, \tag{3.19}$$

where $\bar{x}$ is the mean of x [68]. In many cases only some of the data is available at one time, as in this research. This requires another form of the equation for standard deviation. The standard deviation can be found using

$$s^2 = \frac{\sum_{i=1}^{N} x_i^2 - \frac{\left(\sum_{i=1}^{N} x_i\right)^2}{N}}{(N-1)}, \tag{3.20}$$

by calculating the standard deviation as the data becomes available [68]. A verification that Eqs. (3.19) and (3.20) are equal is given in Appendix B.1. This method of calculating the standard deviation becomes useful for finding spectral standard deviations at many points in a sound field while generating animations of a sound field. The method of calculation using Eq. (3.20) does not require knowledge of the mean while performing the summations. In the computation process, this allows the data to be overwritten for each computation cycle, which reduces memory usage. Though both equations are equivalent, Eq. (3.20) is subject to numerical errors, which can become noticeable when the standard deviation is nearly zero. These special cases have been known to result in negative valued standard deviations on the order of 10^{-6} for small sample sizes.

[4]In practice, this process is performed using only a discrete data set. The only feasible way to get a true population for analysis is to use analytical expressions to model the frequency response and calculate the variance σ^2 using an integral representation. Because of this, it is not useful to calculate the population standard deviation. Note: It is common practice to use letters from the roman alphabet to indicate statistical quantities based on a sample and use greek letters for statistical quantities based on an entire population.

3.3.4 Global Equalization Figure of Merit

A reliable figure of merit is important for appropriately judging the success, or lack thereof, of an equalization system. A list of desirable attributes of the desired qualities of the figure of merit for sound equalization has been proposed by Morrise [69], who recognized that the figure of merit should:

i. have a physical basis.

ii. have a clear and unambiguous definition.

iii. have a clear explanation.

iv. apply universally to all methods of equalization (both practical and theoretical).

v. apply universally to all listening areas.

vi. be found in a straightforward manner.

vii. be contained in a single figure.

These results are similar to the requirements proposed by Hargreaves et. al. in their work for a coefficient describing diffusers [70]. The goals of diffusion and equalization are similar. The objective of a diffuser is to uniformly distribute sound regardless of frequency; the goal in equalization is to achieve a uniformity in frequency response in a large area. It is also important to note that a perfect definition for diffusion is impossible [70]. In a like manner, a perfect global equalization coefficient would be difficult.

There are two additional items that should also be considered for selecting a figure of merit. The figure of merit should also:

viii. work well in real world applications.

ix. consistently predict which methods perform best.

A computer model can generate very large sample sizes that would be ridiculous to acquire in practical applications. Practicality introduces the difficulty of making the equalization factor work in a real environment where only a limited number of measurements may be taken for a sample. The global equalization factor should also consistently predict which method of equalization has the most success. This last requirement is obvious and perhaps is not worth explicitly including in the list; however, it is probably the most important factor.

3.3.5 Graphical Methods for Ranking Equalization Processes

In order to develop this global equalization figure of merit, techniques were developed to verify that it appropriately ranked the equalization methods. Initially, it is useful to inspect a one-dimensional listening area, either by examining equalization in a one dimensional system such as a tube, or a line chosen in a three dimensional listening area. In these cases, a surface plot may be used to show the frequency response along one axis and the position along a line used to define a listening position. Though this type of plot reveals detailed information, it is difficult to judge directly from these plots which method provides better equalization. To simplify this, spectral standard deviations for each point may be plotted as a function of the listening position (see Fig. 3.6 for an example). These frequency responses may also be used to generate animations of the sound field over frequency. These tools can help determine where to place error sensors to control the sound field.

Typical listening areas are spread over two-dimensional surfaces. Because of this, it is useful to have a technique to judge the equalization of a two-dimensional field. Following the method used in the one-dimensional case, a surface plot representing the spectral standard deviations of squared pressure for each listening position can

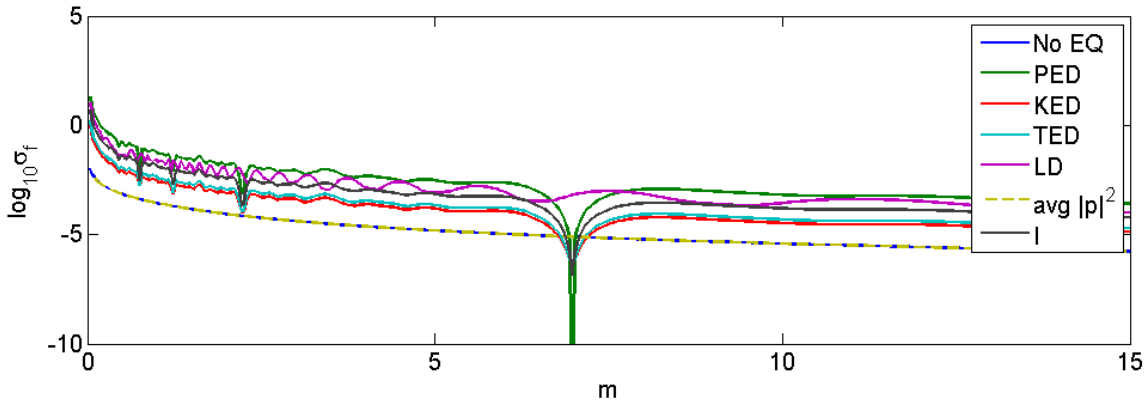

Figure 3.6 An example of a curve comparing the standard deviation as a function of position in a one-dimensional listening area.

be generated to show how standard deviation changes as a function of space. One example of these plots is shown in Fig. 3.7. The standard deviations in Figs. 3.7 and 3.8 are calculated from $kd = 0.3664$ to $kd = 366.4$ in steps of 0.1832; this plot is equivalent to spacing the sound sources $d = 4$ m apart and calculating the standard deviation over a range of 20Hz to 20kHz in 10Hz increments. Figure 3.7 shows the spectral standard deviation on a logarithmic scale. Figure 3.8 is normalized by dividing the spectral standard deviation of the equalized field by the spectral standard deviation of the unequalized field, showing a relative improvement in equalization.[5] It is readily apparent from Fig. 3.7, that as the listening position gets farther from the sound sources the standard deviation decreases. In free space, as the sound level gets smaller with increasing distance from the sources, so does the change in the magnitude of the response from one frequency to another, which in turn decreases the calculated standard deviation value. This decrease can be seen by remembering

[5] Appendix I contains a MATLAB® script that can be used to generate plots like those found in Figs. 3.8.

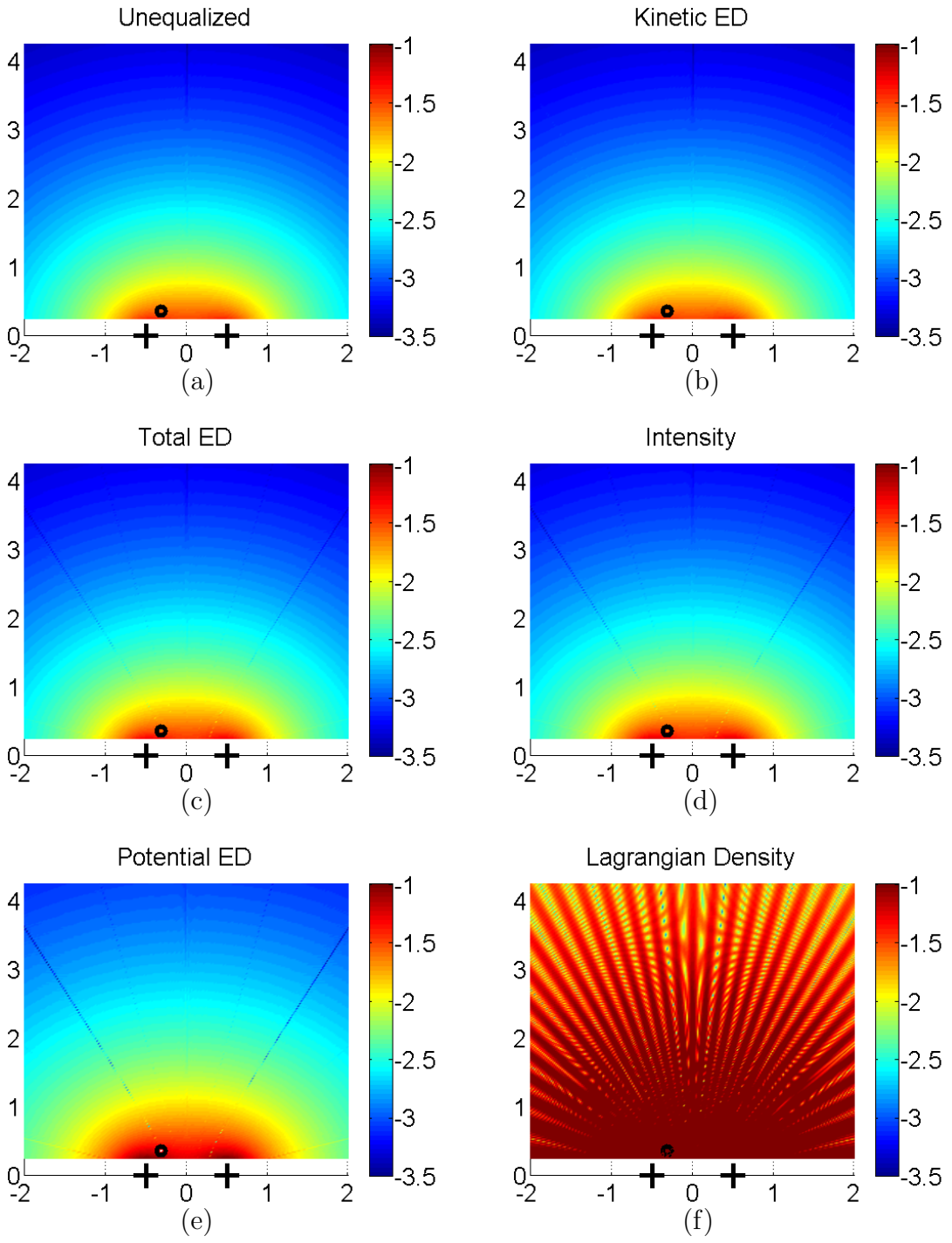

Figure 3.7 Above, surface plots of spectral standard deviation, from $kd = 0.3664$ to $kd = 366.4$, over a 2-D listening area The $\circ$ indicates the location of the error sensor while the $+$ symbol indicates the locations of the sound sources. The frequency response of this plot is calculated over $|\hat{p}|^2$ to in crease the contrast in the plot.

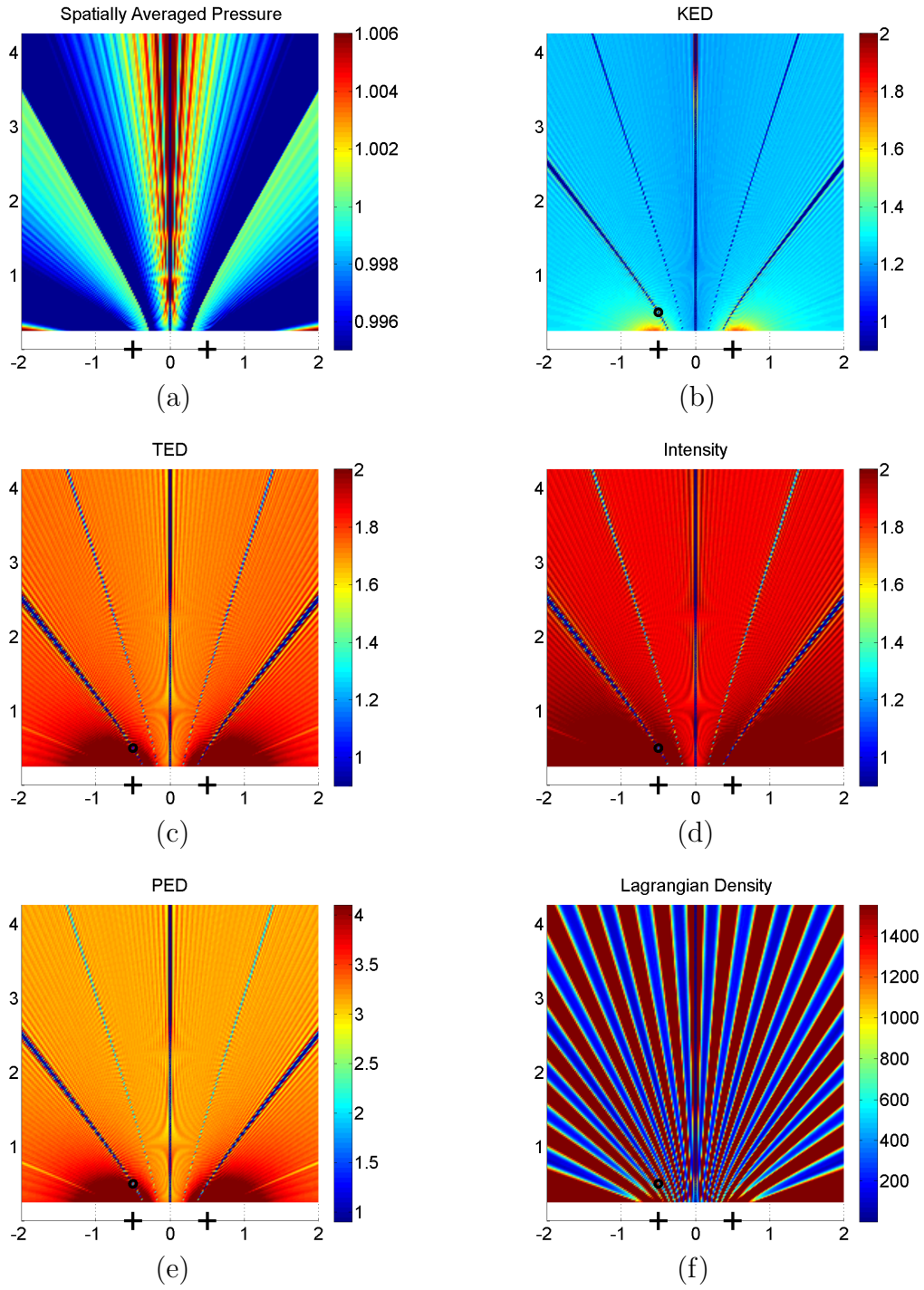

Figure 3.8 The resulting ratio of the spectral standard deviation, from $kd = 0.3664$ to $kd = 366.4$, of an equalized field divided by the spectral standard deviation of the unequalized field. The portions that are indicated as being less than one indicate equalization improvement, while values greater than one show a decrease in equalization. The frequency response of this plot is calculated over $|\hat{p}|^2$ to increase the contrast in the plot. The sensor postion is marked by $\circ$.

that the variation may be expressed by,

$$s^2 = \frac{\sum_{i=1}^{N} (x_i - \bar{x})^2}{n-1}. \tag{3.19}$$

This expression shows that the standard deviation is dependent on the mean difference from the mean value of the data set, which inherently decreases as the sound level decreases far from the source. Dividing the spectral standard deviation of the equalized case by the spectral standard deviation removes the extraneous effect of the attenuation due to the proximity of the listening position to the sound source, while leaving the variation due to interference. In this case the normalization is performed on the spectral standard deviations.

A normalization may be used in order to deal with the spatial dependence of the standard deviation apparent in Fig. 3.7. Three methods for this normalization of the unprocessed data were considered:

i. normalizing by dividing each frequency response by its maximum value before calculating the spectral standard deviation.

ii. normalizing by dividing each frequency response by its average value before calculating the standard deviation.

iii. dividing the spectral standard deviations of the equalized sound field by their corresponding spectral standard deviations in the unequalized field.

Normalizing the standard deviations of the sound field by either the maximum values or average values of the frequency response first requires calculating the frequency response at each position of the sound field. From these responses, the normalizing values are calculated. The frequency response values are then divided by their own normalization factor. At this point the standard deviations are calculated for each

normalized frequency response. This yields an array of standard deviations that may be used to illustrate the normalized spectral standard deviation field.

Normalizing the spectral responses before calculating the standard deviations causes some problems. When the frequency responses are normalized by their maximum values, the plots of the spectral standard deviation improperly rank the performance of equalization techniques. According to plots generated using this normalization, the Lagrangian density (LD) worked best to equalize, but it was readily apparent in the animations that this was not the case.[6] Some plots generated using these normalization methods are shown in Fig. 3.9; they are ordered from left to right, then top to bottom, according to the ranking suggested by the plots.

Normalizing the frequency response using a spectral average has problems as well. One difficulty with using the average to normalize the frequency response produces results that look very similar regardless of the equalization technique used, causing difficulty in determining which method functions best. This phenomenon is demonstrated in Fig. 3.10, which again is sorted according to the way these plots rank equalization from best to worst, going from left to right and top to bottom.

The final method of normalization compares the changes due to the different equalization routines. The spectral variance is calculated for each listening position of the sound field before and after equalization. The spectral variances of the equalized field are then divided by the corresponding spectral variances of the unequalized field. These results show comparative improvement or degradation of the equalizing method over space. Since this expression is a ratio, positions with values between zero and unity indicate improvement with the smaller values indicating more improvement, values above unity indicate degradation of equalization. Expressed on a logarithmic

[6] An animation of the L_p of the field equalized using LD as well as an unequalized sound field can be seen in Appendix E in Fig. E.4.

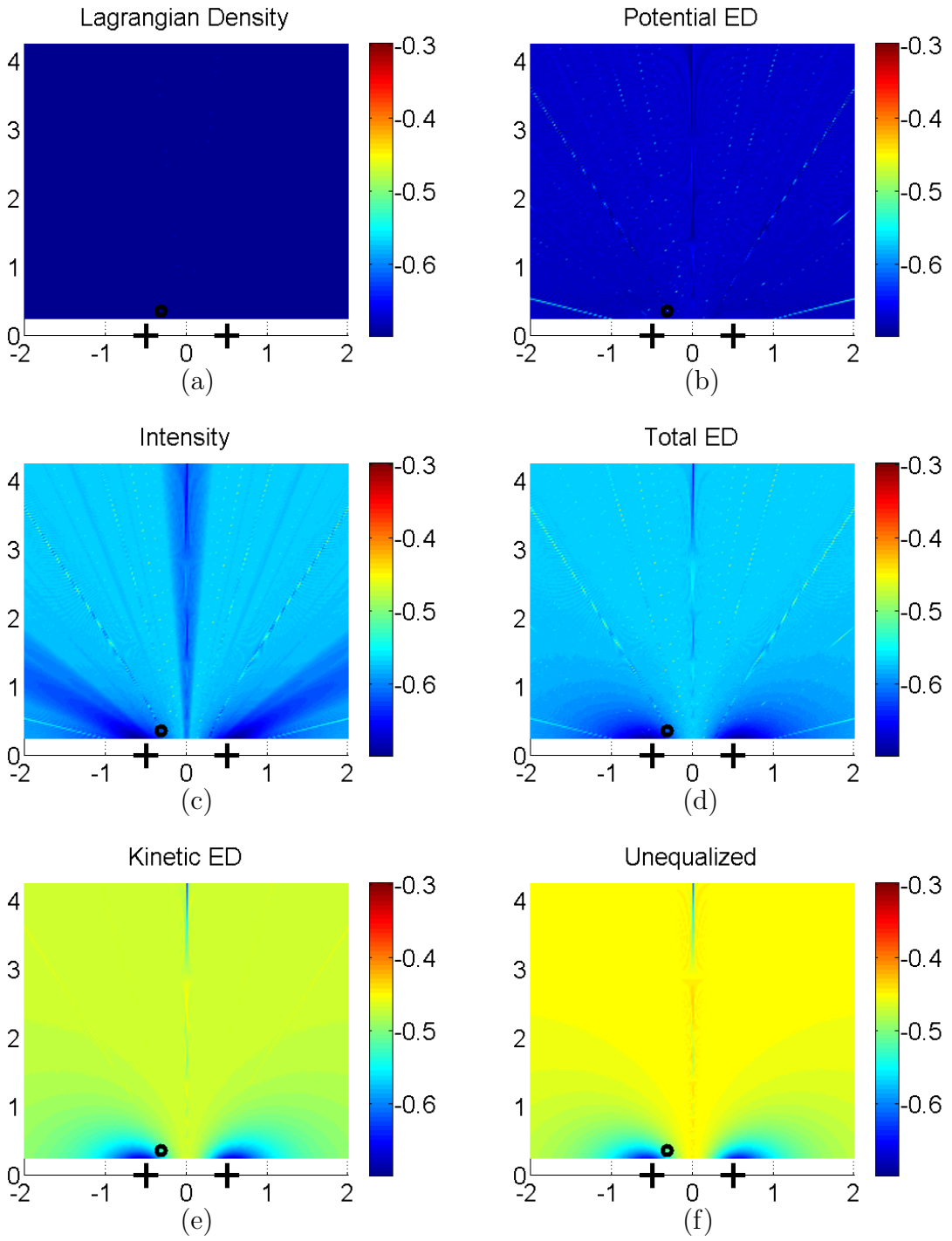

Figure 3.9 This is a plot of the $\log_{10}$ of the standard deviations of frequency response, from $kd = 0.3664$ to $kd = 366.4$, normalized by their maximum value over a listening region. These are ordered from the best to worst, according to the plots, going from left to right, top to bottom. The Lagrangian density is off the scale for these plots, indicating superior equalization. The frequency response of this plot is calculated over $|\hat{p}|^2$ to in crease the contrast in the plot.

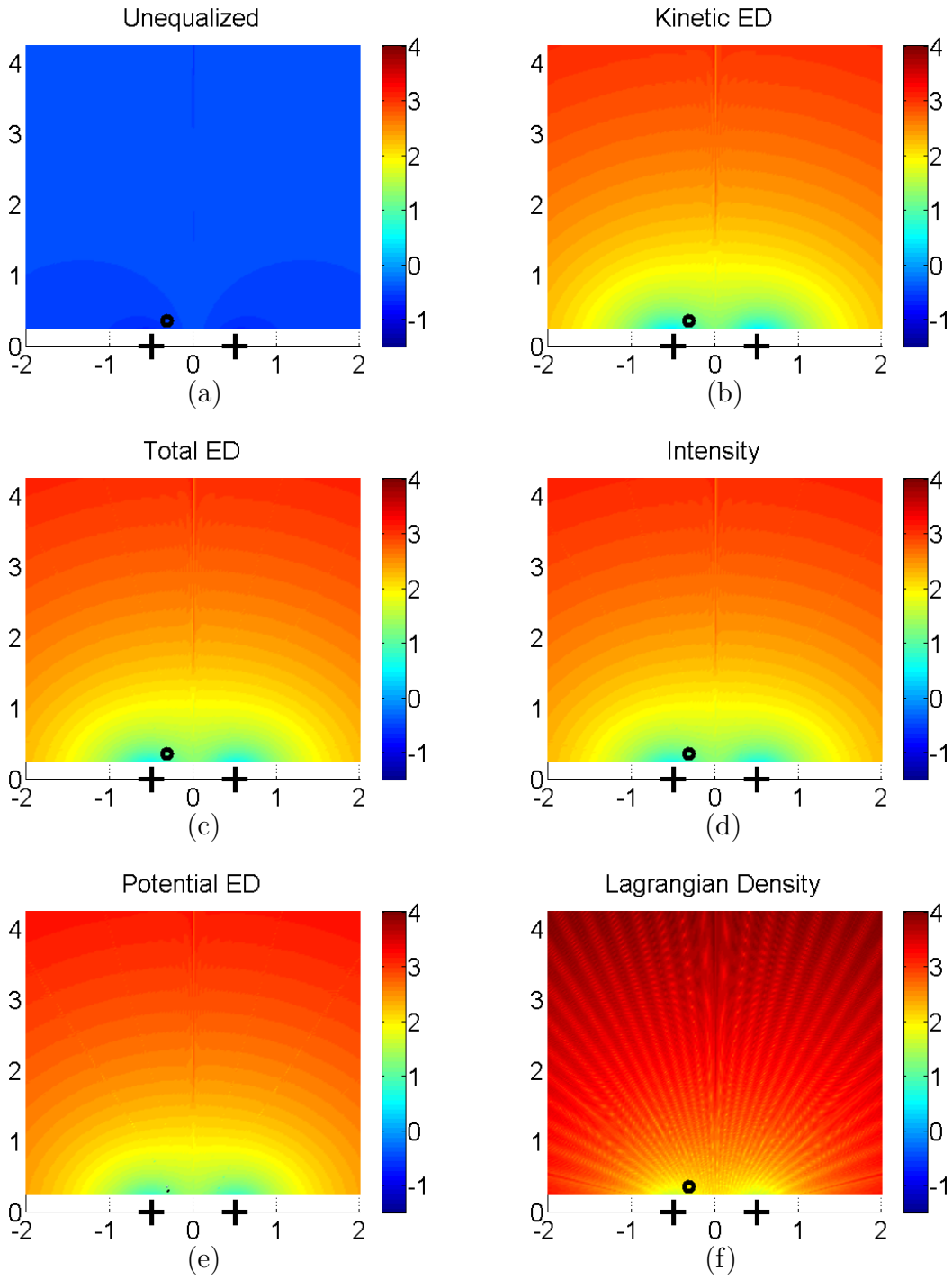

Figure 3.10 This is a plot of the standard deviations of frequency response, from $kd = 0.3664$ to $kd = 366.4$, normalized by their average value over frequency over a listening region. These are ordered from the best to worst going from left to right, top to bottom. The frequency response of this plot is calculated over $|\hat{p}|^2$ to in crease the contrast in the plot.

scale, values less than zero indicate improvement in equalization, while values greater than zero indicate degradation. This type of plot provides a tool for comparing one method against another to judge which equalization works better. The plots for the different methods of equalization may be compared to one another to show which one equalizes best. Some examples of these plots can be seen in Fig. 3.8 for one case.

The ratio method is very similar to the F-test found in statistics. This test compares the difference between the variance of two samples by calculating their ratio [71], just as in the difference plot method just mentioned. At this point the F-test could be used to check to see which regions do or do not improve significantly with equalization.

Another way to judge the equalization is to look at the size of the region in the spectral standard deviation plots that the method successfully equalizes. This is measured by looking at the size of the area inside the listening region in which the variation of the frequency response is smaller than a given value. In many cases, this results in well-equalized regions that are long and narrow. The shape of these curves are determined by surfaces in and around the listening area as well as source arrangements and error sensor locations. This could be given as a percentage of the listening area meeting a given frequency response variation. The limits could also be given based on the F-test. A global equalization factor could be generated from this by looking at the size of regions where equalization is improved. This process would require many measurements to approximate the size of the region where equalization improves. Because of this, determining a global equalization factor using this technique is not practical in a nontheoretical situation.

Chapter 4

Active Noise Control Results

The previously discussed tools produce data that help understand how to better control the sound field produced by sources in free space. The methods also serve to illustrate how the sound fields change for given situations and success or failure of different techniques used to control sound fields. This chapter discusses the results found using these tools for active noise control problems. It examines different metrics for use as error sensors in the near field of sound sources as well as tools for evaluation of the success of active noise control (ANC).

4.1 Models of the Sound Field

Chapter 2 demonstrated methods for inspecting sound fields using mathematical models and graphical representations of the acoustic fields. The graphical representations are capable of illustrating what can be measured using various instruments. These measurements are referred to as a reference signal and are used to determine how to control a sound field. These measurements provide the data used to determine the correct control settings. In addition to determining how to alter the sound

field, measurements of an unaltered sound field also provide a comparison to show the success or failure of the control system.

The situations with two sources reveal many of the features expected for pressure and particle velocity. With two equal amplitude sources in phase, we see a pressure maximum running along a line equidistant from the two sources. At the point halfway between the two sources is a particle velocity minimum. This is because the particle velocity due to one source is canceled by the contribution of the other source at that point. In contrast, the situation where the two sources are 180° out of phase, a pressure minimum exists along a line equidistant from the two sources and the particle velocity has a maximum at the point half way between the two sources. Figure 4.1 shows these characteristics for a kd value of 6.961. However, the stated observations hold for a wide range of frequencies. For either arrangement, TED is more spatially uniform than PED or KED in a region between the two sources over a large frequency range in the region between the sources. The relative spatial uniformity is easer to see at higher frequencies like Fig. 4.2 or with arrays of sources with more sources like those in Fig. 4.3. This uniformity suggests that placement of an error sensor that measures TED will work equally well for controlling a sound field for these near field error sensor locations. This uniformity also persists for more complicated situations with more sound sources.

The processes of visualization and analysis may be easily used to explore more complicated sound fields. Acoustic pressure and acoustic particle velocity are calculated by summing the contributions from each source. The method is limited by the number of sources, not the frequency range, as is the case with modal modeling. This means that the sound field may be quickly modeled over a wide frequency range for systems with a limited number of sound sources. Some examples of the sound field models may be found in Fig. 4.3. The frequency response is calculated over the space

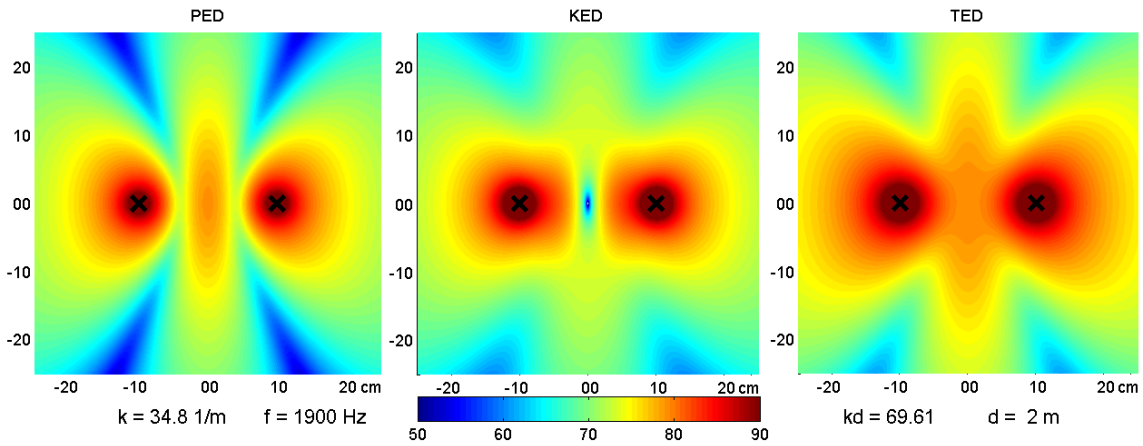

(a)

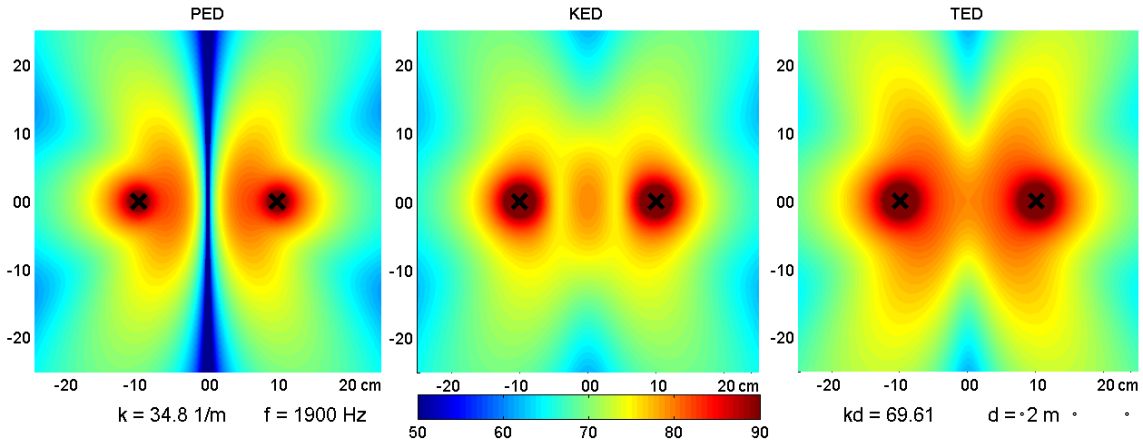

(b)

Figure 4.1 A sound field measured by PED, KED, and TED for (a) two sound sources acting in phase with one another with the same amplitude and (b) Two sound sources acting 180° out of phase from one another with the same amplitude at 1.9 kHz. The sources are marked by ×.

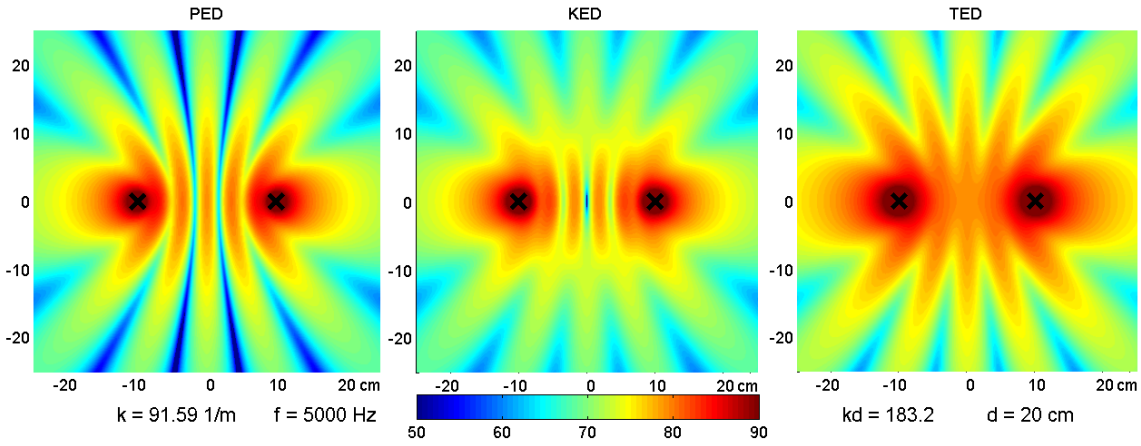

(a)

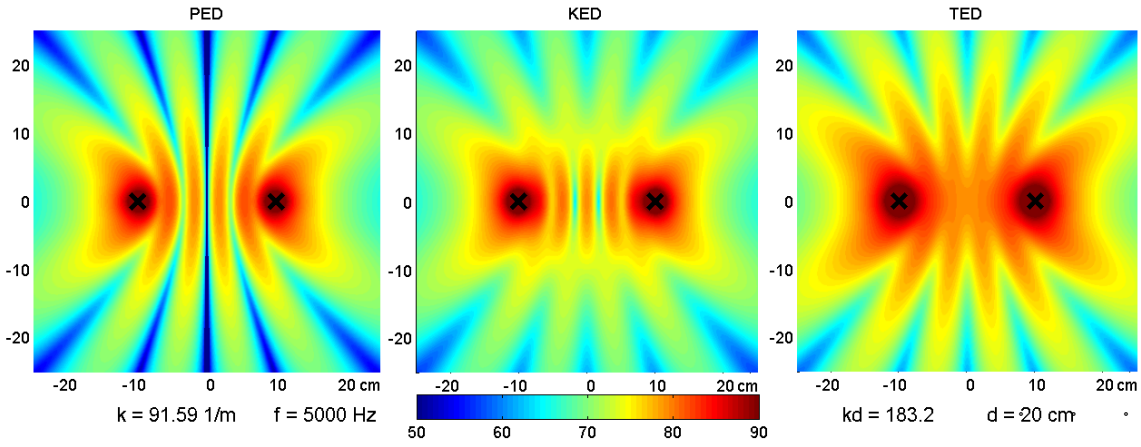

(b)

Figure 4.2 A sound field measured by PED, KED, and TED for (a) two sound sources acting in phase with one another with the same amplitude and (b) Two sound sources acting 180° out of phase from one another with the same amplitude at 5 kHz. The sources are marked by ×.

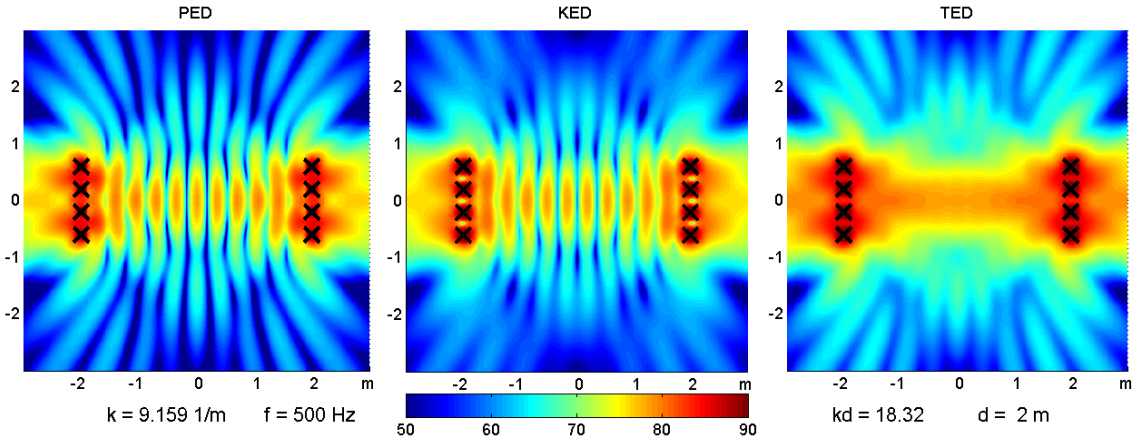

(a)

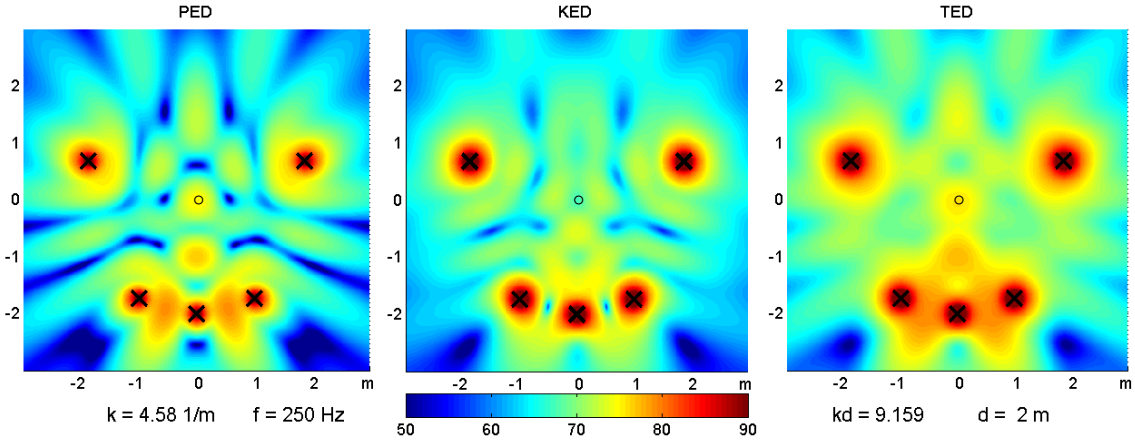

(b)

Figure 4.3 The sound field as it would be measured in PED, KED, and TED. Figure 4.3(a) is an arrangement of two linear arrays consisting of four point sources each, while Fig. 4.3(b) has five point sources laid out similarly to those used in a five source surround sound system. Each point source is marked in these figures by a $\times$. The axes are marked in meters and a $\circ$ indicates the center of the sources. These have corresponding animations over frequency in Appendix E of the digital version of this thesis.

shown and may be used to generate animations of the sound field over frequency.[1] This tool can help determine ideal locations for error sensors.

To make the situation more interesting, the models may be further refined to include the radiation patterns of directional sound sources in free space. The model of an axially vibrating cap in a sphere is well suited for these situations. This produces a radiation pattern similar to that of a dynamic loudspeaker in an enclosure or a horn type driver. The equations describing these sources are described in Sec. 2.1.2. Figure 4.4(a) shows the pressure field produced at 1 kHz for a sphere of radius 15 cm and a cap of radius 3 cm. The radiation pattern of a pair of equal strength point sources, separated by 4 m, radiating together is shown in Fig. 4.4(b). The directivity patterns for a pair of caps in spheres can be seen in Figs. 4.4(c) and (d). As the frequency decrease the spacing between nulls decreases, as shown in Fig. 4.4 (d) at a frequency of 250 Hz.

4.2 Active Noise Control

A basic case for ANC consists of one control point source minimizing sound from one primary point source. This situation, with a kd value of 0.476, for minimized sound power can be seen in Fig. 4.5. In the case of a free field, when the control sources minimize total sound power it is often referred to as the optimal case. A closed form solution can be found to minimize the total power output from the combination of sources [9, 10]. The appropriate control source strengths may also be found for minimizing sound power [49, 72]. It is not practical to measure the sound power directly for active sound control, thus other acoustic quantities are used for minimizing

[1] Some animations of sound fields may be found in Appendix E in the electronic version of this thesis.

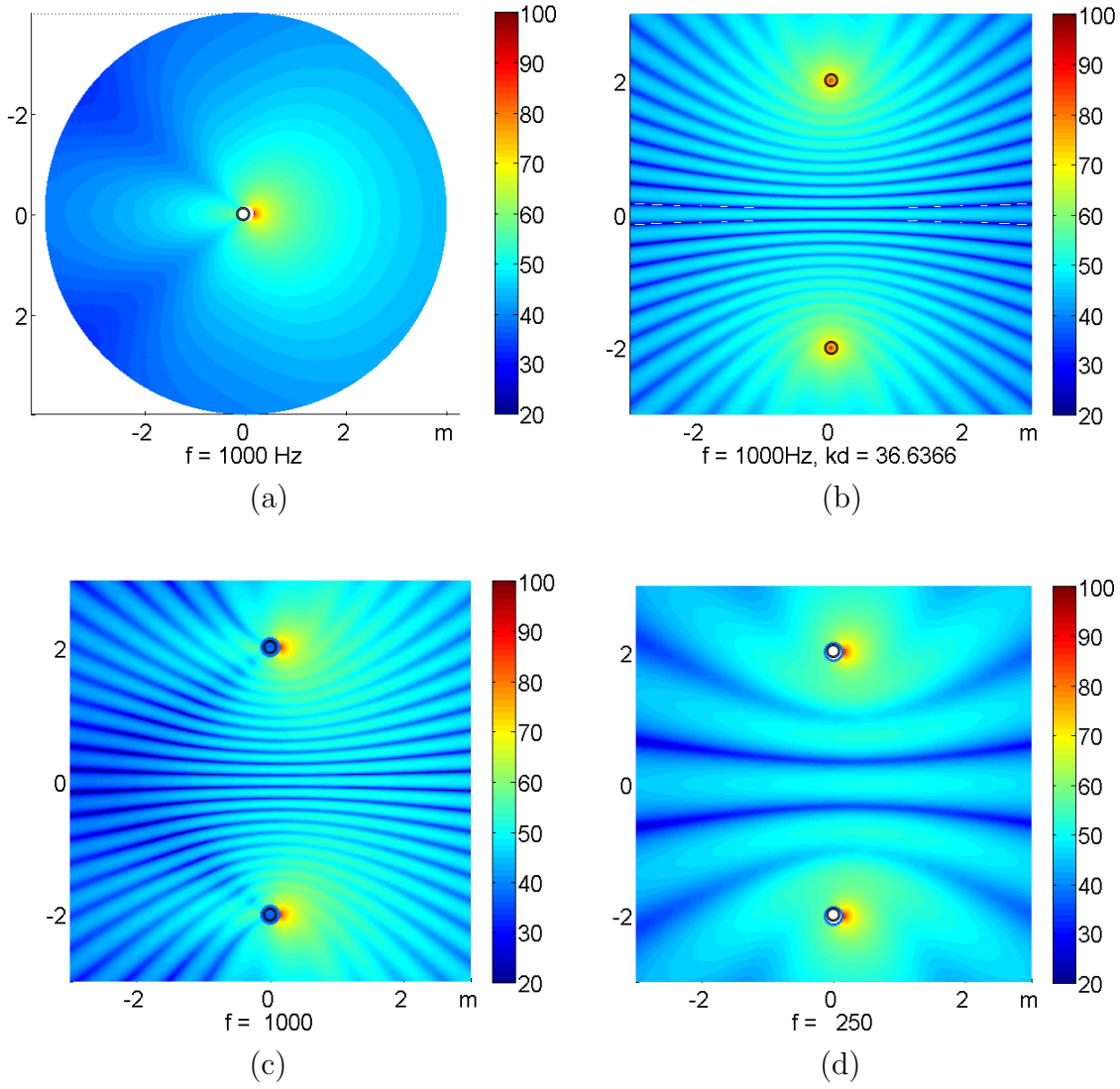

Figure 4.4 Above are figures illustrating the radiation pattern of (a) a single sphere with a radiating cap, (b) a pair of monopole sound sources, (c) and (d) a pair of spheres with a radiating cap. Figures (a), (b) and (c) are shown at 1 kHz and (d) is shown at 250 Hz.

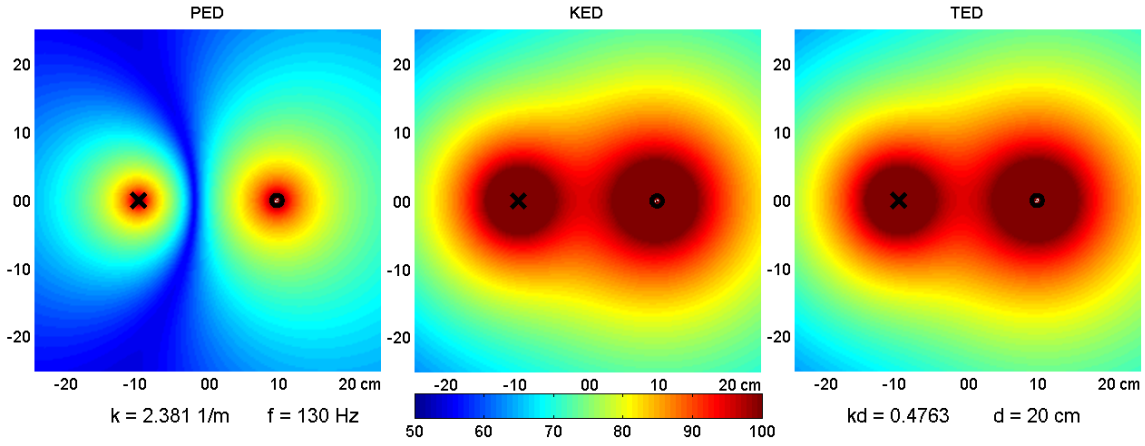

Figure 4.5 Measurements of the sound field when the control source acts to minimize the total radiated power. The color scale is in dB referenced to 3×10^{-15}J/m. The primary source is marked by $\circ$ and the control source is marked with $\times$.

sound fields. Techniques discussed in Sec. 3.1 are used here to examine the prospect of active sound control in a free field using ED quantities.

4.2.1 Control Using ED Quantities

Measuring total radiated power as an error signal in ANC is impractical due to the many inherent difficulties. Other quantities, such as ED, are much more practical. To help determine how well some of the other quantities work as error signals, we look at the MEDToPO plots described in Sec. 3.1.2. Figure 4.6 shows MEDToPO plots for two point sources, where $kd = 0.1832$, $kd = 1.823$, and $kd = 3.664$. These plots show the total radiated power for cases where control is performed at each point using PED, KED, and TED. These results predict that TED provides sound control that is more independent of error sensor location than PED or KED alone. This *would* suggest that using TED would provide more freedom in the placement of a control sensor than PED or KED. Upon closer examination, little or no control is achieved

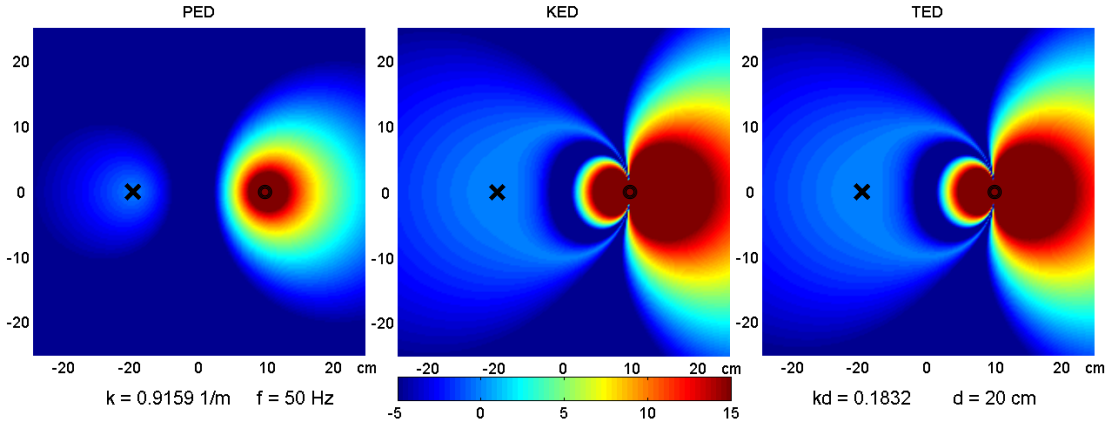

(a)

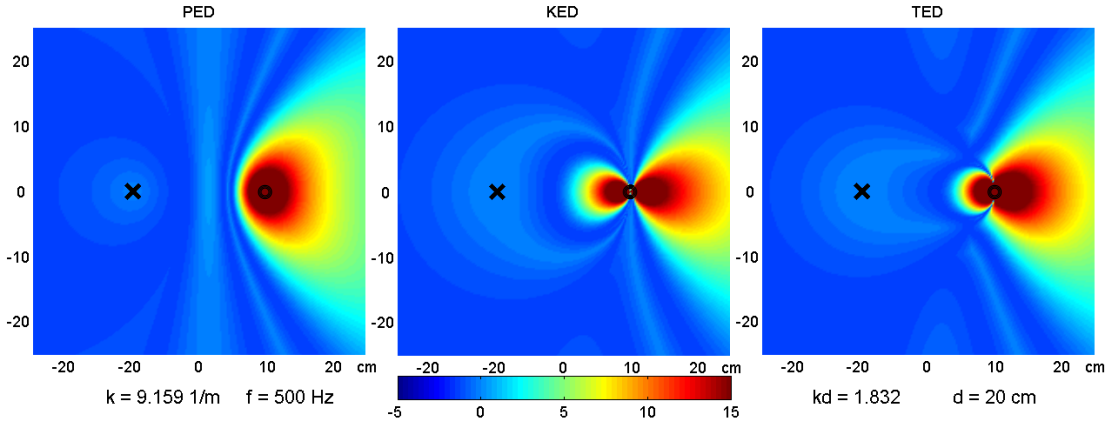

(b)

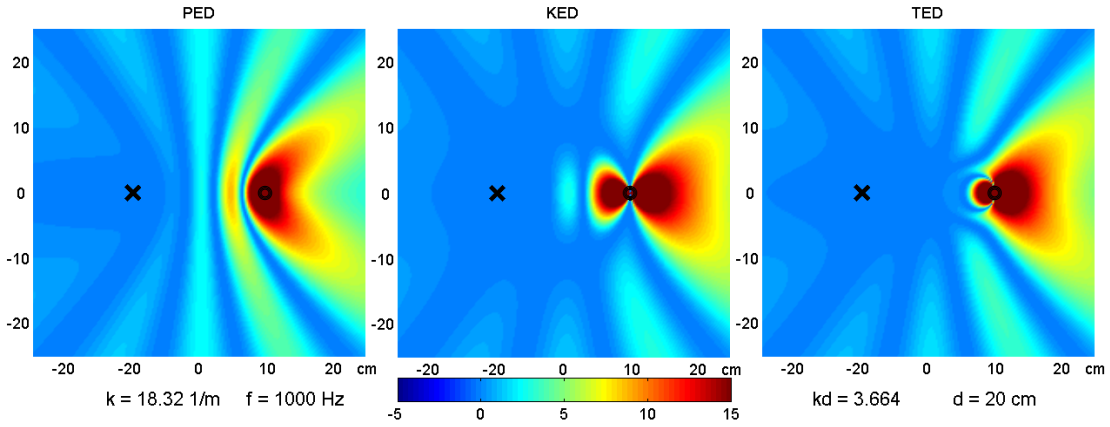

(c)

Figure 4.6 Three MEDToPO plots illustrating the the amount of sound power produced by a system consisting of one primary source and one control source at $kd = 0.1832$ for (a), $kd = 1.832$ for (b) and $kd = 3.664$ for (c).

at in these regions where performance is spatially uniform for the placement of TED. These regions are just better than the surrounding areas.

Control using TED benefits from spatial uniformity in the geometric near field of the sound sources. However, it is important to note that the uniformity only occurs above a certain kd value. The uniformity usually starts at frequencies where kd is greater than about π. Other researchers have shown that global ANC is limited to frequencies *below* this range [72]. Figure 4.7 is similar to a figure found in the work by Nelson and Elliott that illustrates the maximum possible attenuation of sound power for various source arrangements as a function of kd [72]. All of the source arrangements modeled in Figs. 4.7 are coplanar arrays. In the work by Nelson and Elliot the arraignment with four control sources was arranged in a tetrahedral arrangement. These plots shows that even in the ideal case, active control in a free field environment is only reasonable when kd is noticeably less than π. It is important to note that for kd values at or above π, ANC does not significantly reduce the sound power and other methods of noise control should be employed.

Returning to Fig. 4.6, it is important to note that at the lowest kd value shown, there is a large region where a sensor measuring PED performs better than KED or TED. In fact, in the lower frequency range, where kd is somewhat lower than π, the PED error signal has greater spatial uniformity than either the KED or TED. Since the uniformity for TED only exists at kd values that are too high for ANC to function effectively, this uniformity is of little benefit in ANC applications.

It is also important to note that in ANC applications, error sensors should be placed where the improvement from the uncontrolled case to the optimally controlled case is the greatest [2, 73]. Hansen and Snyder state that "the optimum error sensor location(s) are always at the locations of greatest acoustic pressure attenuation when the control source is generating the optimum volume-velocity relationship" [2]. Often

the regions where the improvement is greatest are found in very narrow nulls in the pressured fields. Figure 4.8 shows an example of this for a single primary source surrounded by four control sources with a kd value of 0.36 [2, 73]. The scale on this plot is

$$10 \log_{10} \frac{\nu_o}{\nu_u} \tag{4.1}$$

where ν_o indicates the field quantity for the optimally controlled case, and ν_u indicates the filed quantity for the uncontrolled case.[2] For PED their is a path that follows a

[2]Appendix K contains the MATLAB® code used to generate figures like those found in Fig. 4.8.

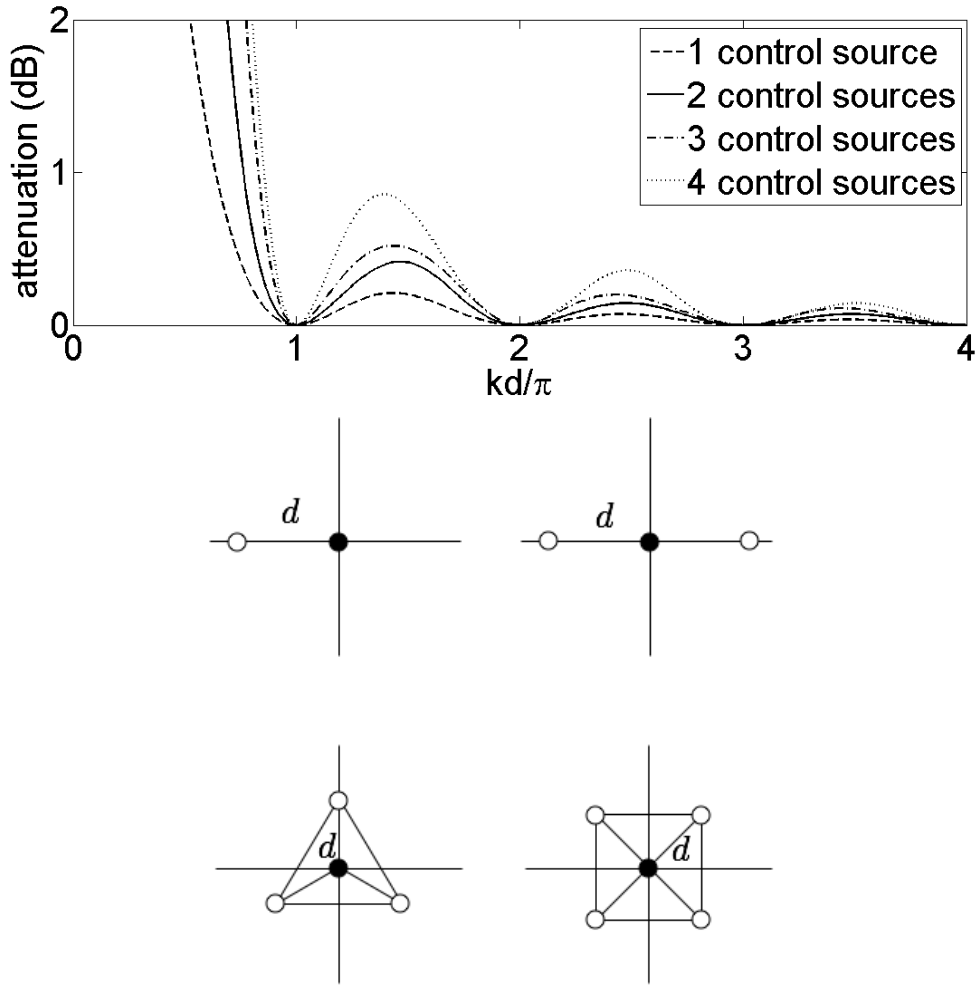

Figure 4.7 The maximum achievable sound power attenuation in dB using various coplanar sound source arrangements, also depicted here.

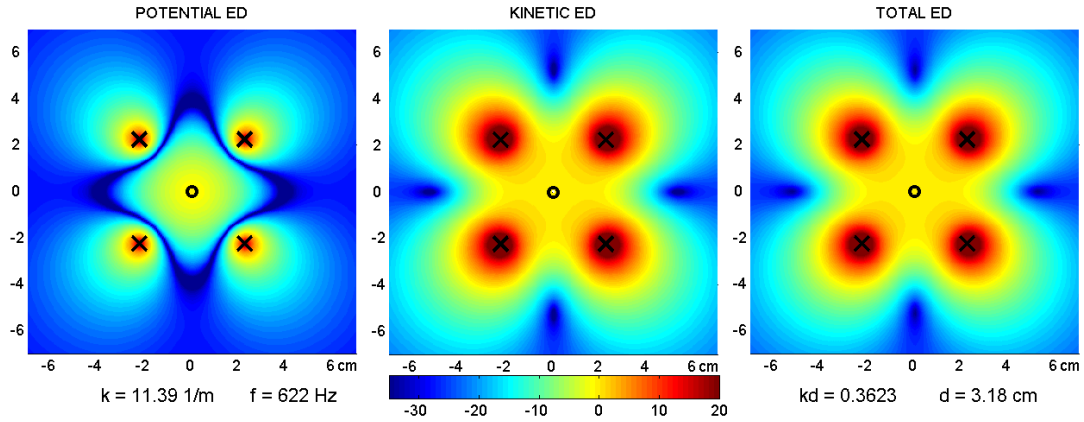

Figure 4.8 This shows the difference between the uncontrolled sound field and the optimally controlled sound field. Locations with the greatest reduction of the field measurement are traditionally considered the best locations for placing error sensors.

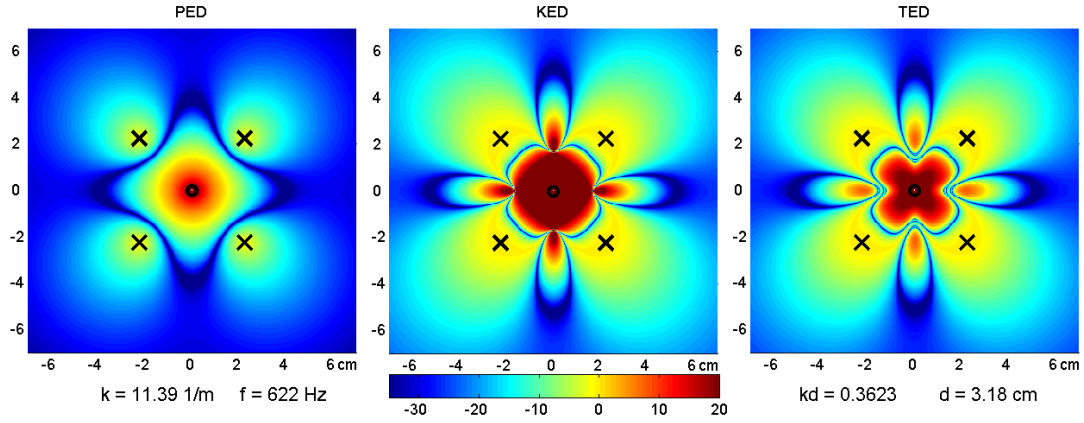

Figure 4.9 This is a MEDToPO for the situation given in Figure 4.8.

curve that indicates the recommended placement for a pressure based error sensor. The PED results for the MEDToPO plot in Fig. 4.9 agree. This verifies that the traditional method for finding optimal sensor locations does show optimal locations for error sensors.

In addition to describing where the error sensors should be placed, the MEDToPO shows necessary accuracy for the placement of an error sensor for producing acceptable performance. For KED and TED, the MEDToPO plots indicate that there are larger

regions that produce good sound control performance than are indicated by the plots of the sound field under optimal control. This verifies that the traditional method for choosing error sensor locations works but has some limitations. Comparing Fig. 4.8 with Fig. 4.9 reveals that there are some good locations for error sensor placement not predicted by examining the optimally controlled sound field. The MEDToPO plots also indicate how sensitive to location the error sensors are. A wider region where good control is achieved indicates less sensitivity to error sensor placement.

From this analysis, it is apparent that PED produces a better error signal than KED or TED for ANC. The frequency range where TED has a potential to have more freedom in choosing an error sensor location only occurs at frequency that are too high for source coupling to perform well. At low frequencies, the location for PED error sensor tends to have a more regular optimal location, one example of this was shown in Fig. 4.9. This figure also indicates that sensitivity to position for PED is also more regular than KED or TED.

4.2.2 Relationship Between ED and Π

The relations found in Sec. 2.2.4 describe how the ED relates to sound power. However, these relationships are very dependent on the source arrangements that they correspond to. To simulate ANC using the expressions, the source arrangement and its surrounding environment must be very well defined. Even for the case of two sources in a free field, the expressions quickly became rather complicated in the simple case of two sources in a free field. Adding just one additional source would significantly complicate the situation. Making certain assumptions about the source strengths significantly simplifies this process, at the cost of losing generality of the results.

In Sec. 2.2.4, the calculations were simplified by assuming that the sensor is located

half way between two sources. To check the accuracy of the approximation, a few numerical computations were performed. Figure 4.10 shows the difference between the exact conversion factor and one approximated by assuming the sensor is at the origin. The colors represent the difference between the approximate conversion factor and the exact conversion factor, expressed by

$$\beta = 10 \log_{10} \frac{C_{ex}}{C_{ap}} \tag{4.2}$$

where C_{ex} indicates the exact relationship between ED and sound power and C_{ap} is the approximated value. This figure shows how the correction factor changes as a function of location for three frequencies. Figure 4.10(a) shows that there are curved regions where the correction factor is valid. These are regions that have the same measured ED values. These regions change their shape with frequency. However, because these regions vary over frequency and are very narrow, they are not a convenient or practical method for approximating sound power.[3]

To better understand the frequency dependence of the correction factor, Fig. 4.11 shows the correction factors and their corresponding approximations for two positions. Figure 4.11(a) shows the frequency dependence of the correction factor at the point $0.2d$ from the sensor, corresponding to $(0, 0.2)$ on Fig. 4.10. At $(0, 0.2)$ the approximate and the exact values of the measurement may work well for PED, KED, and TED. When the error sensor is moved to $(0.5, 0.2)$, as shown in Fig. 4.11(b), the approximation and the exact relationship intersect at a few positions. However, they do not stay relatively close to one another as frequency changes.

One significant problem still exists with using the conversion factors: calculating this approximation requires the source strength of both sources. If the source strength

[3]An animation over frequency showing the difference in the conversion factor relating ED to sound power to its approximated version is available in the electronic version of this thesis in Appendix E in Fig. E.3. The images found in Fig. 4.10 were produced by the same MATLAB® script.

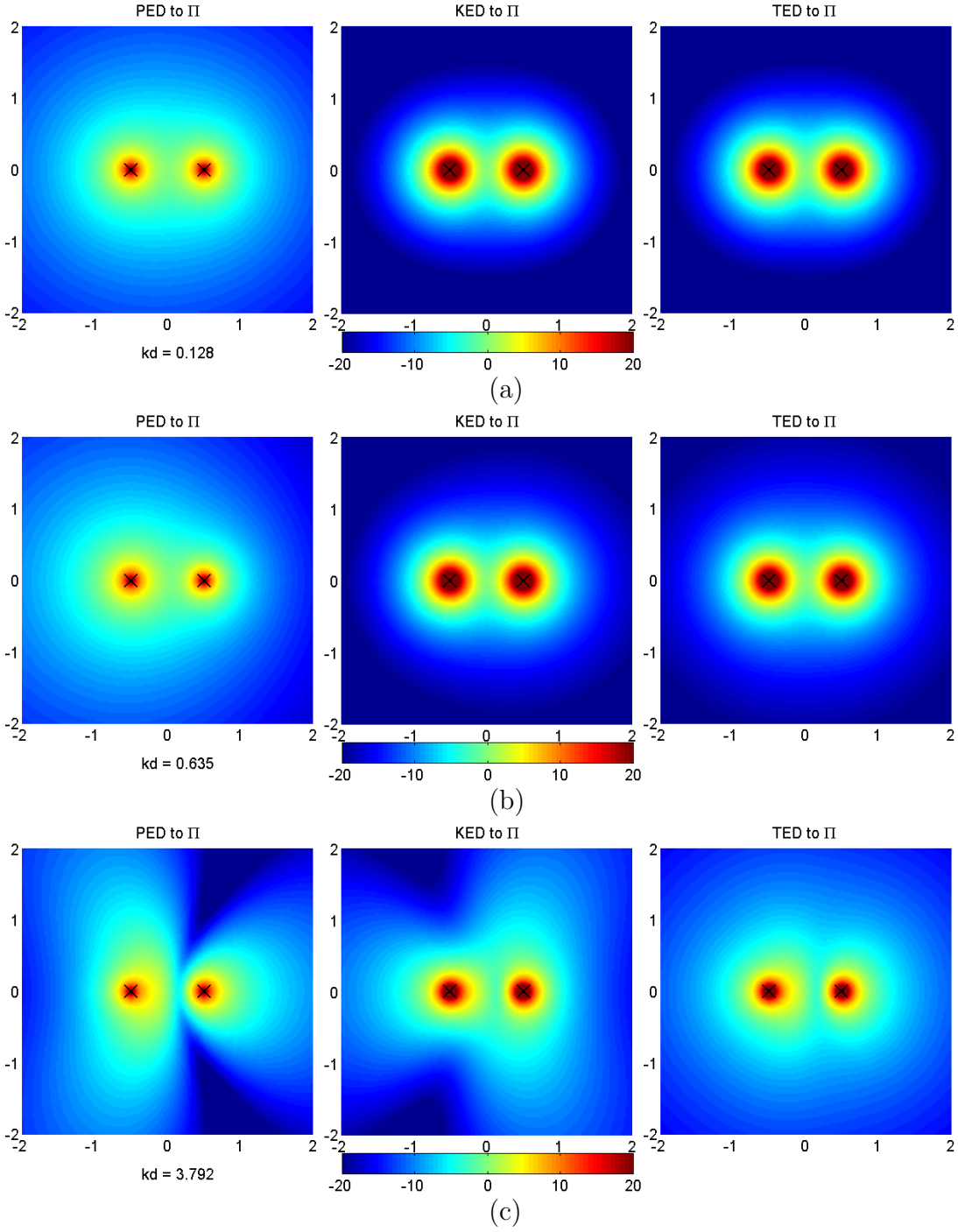

Figure 4.10 These figures show $10\log_{10}$ of the difference between the exact conversion and an approximation of the conversion from ED quantities to sound power for a pair of sources, where one source is driven to minimize sound power of the system. Figure (a) is for $kd = 0.128$, Fig. (b) is for $kd = 0.348$, and Fig. (c) is for $kd = 3.792$, where the source on the right leads the source on the left by $\pi/2$ radians. The $\times$ marks the locations of the sources.

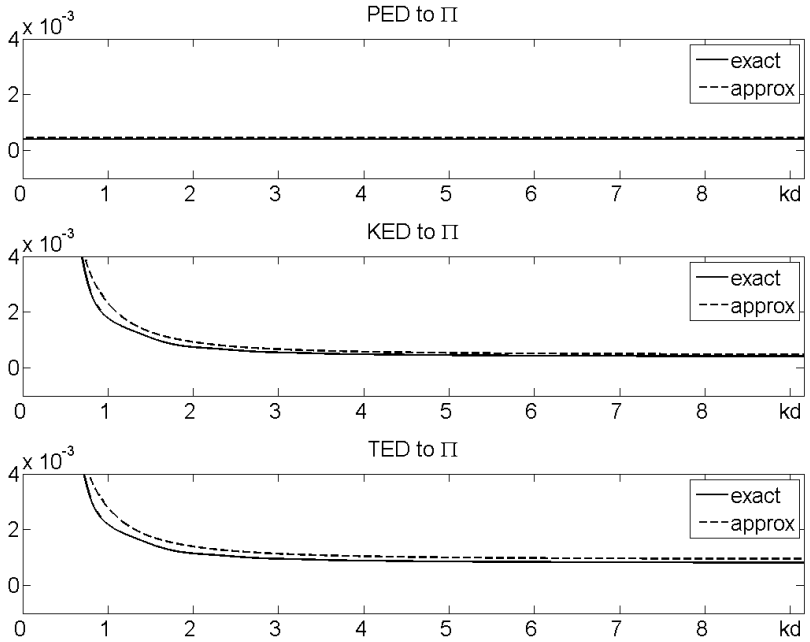

(a)

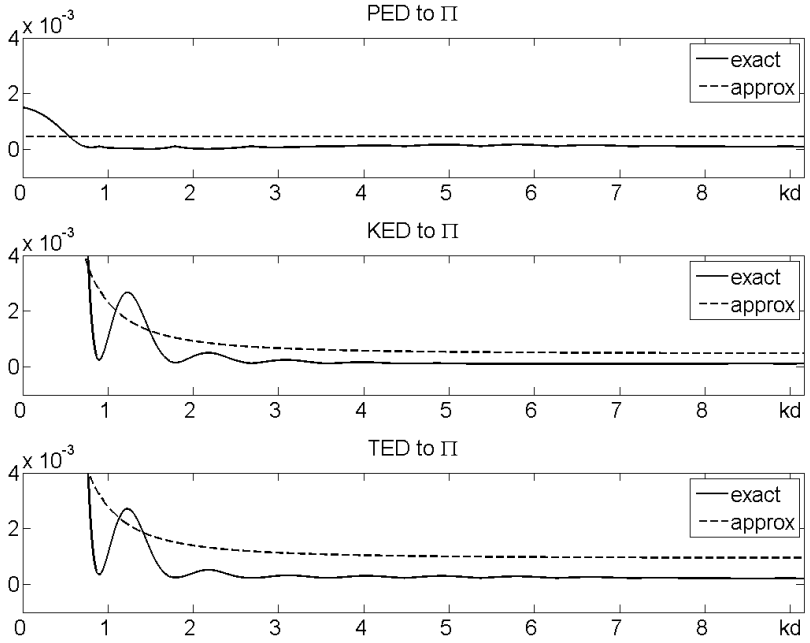

(b)

Figure 4.11 Frequency dependence of the correction factors compared to their corresponding source if measured at $(0, 0.2)$ in units of the distance between the sources in (a) and at $(0.5, 0.2)$ in (b) where the coordinates correspond to those in Fig. 4.10.

is known, there are numerical methods to calculate the sound power directly [10]. The relationship between ED and sound power are less useful for theoretical study because the known numerical methods are more direct and well established. Assuming that both sources act in phase can reduce the relationship to one that is independent of the source strengths; this produces difficulty due to the sensitivity of phase inherent in acoustic systems. If the two sources are acting even slightly out of phase the conversion factors change, invalidating these approximations. This is not a practical approach for finding sound power because of the many complications that arise in developing a ratio that could serve as a conversion factor that relates ED to sound power.

Chapter 5

Equalization Results

The models previously discussed have been used to compare the effects of different equalization methods to one another and to unequalized sound fields. This chapter will discuss equalization from the point of view of the frequency domain and the time domain, and discuss tactics for correctly evaluating the performance of equalization methods. At the end of the chapter, a short discussion is given to show how these techniques could be used to expand this study to enclosures.

5.1 Frequency-Domain Perspective of Equalization

The radiation beam patterns formed by multiple sources with equal amplitude are well known and readily described [9, 74, 75]. It is important to remember that these radiation beam patterns do not change when the sources are all equalized the same way. At a point of equalization in the field, the frequency response should become uniform over frequency. The frequency responses at all other locations are heard such that the frequency dependent beam pattern does not change. This is expected, as consistant equalization of a group of sources only attempts to alter the spectral

nature of the sound field; it does nothing to alter the spatial characteristics of the sound field.

The effects of equalization can be easily seen by looking at how the sound field varies as a function of frequency, as shown in Fig. 5.1. Figure 5.1 displays unequalized sound fields in the left column, and sound fields equalized using PED in the right column. Comparing Fig. 5.1(a) to Figs. 5.1(b) and 5.1(c), shows that equalization changes the strength as a function of frequency. In each pair of figures, the same radiation pattern is visible but the sound level is modified depending on the frequency for the equalized case. This can be noted by comparing the overall changes in sound pressure level in parts (a), (b) and (c) of Fig. 5.1.[1] Figure 5.2 shows the frequency response magnitude at three locations for the same pair of monopole sources. The dashed curve indicates the effect of equalization at the error sensor. The equalized response becomes perfectly flat over frequency at the error sensor position. The other two curves vary more drastically than they did without equalization as a function of frequency, further illustrating how the sound field changes. Equalization using other metrics has a similar effect on the sound field.

It is useful to get a sense of the frequency response measured by different quantities. Figures 5.3 and 5.4 display frequency responses of a sound field measured at the point (0.05,0.2) on the surface plots found in Fig. 5.1 if the axes are marked off in meters. The quantities measured are pressure magnitude, particle velocity magnitude, PED, KED, TED, the vector magnitude of intensity and spatially averaged pressure magnitude. Pressure magnitude, particle velocity magnitude, PED and KED follow the curve of a comb filter. Pressure magnitude and PED have minima and maxima, as does the vector magnitude of particle velocity and KED. The TED has less variation

[1]These figures come from the animation found in Appendix E, Fig. E.5, in the digital version of this work. The variation as a function of frequency is perhaps most easily noted in the animation.

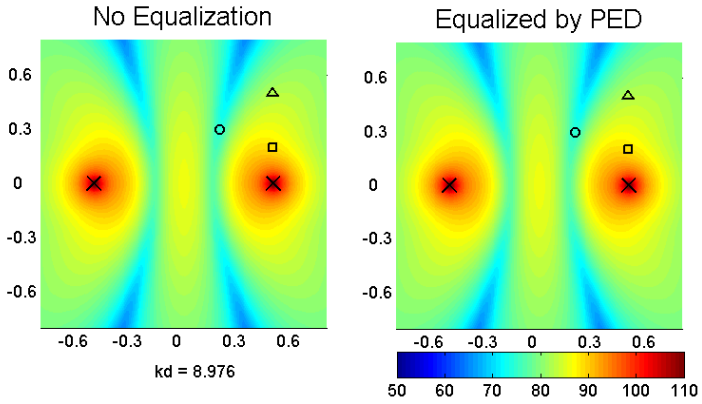

(a)

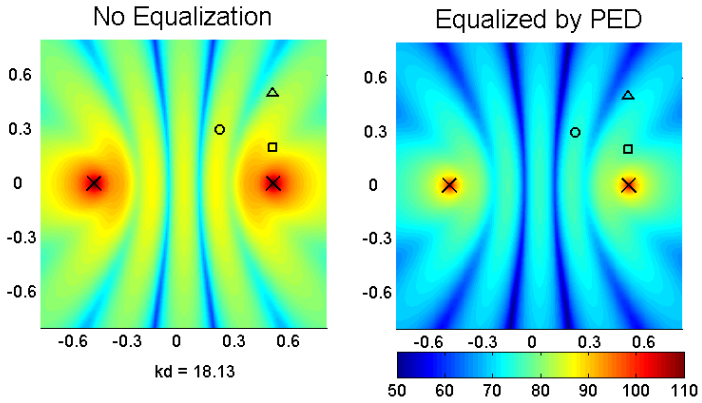

(b)

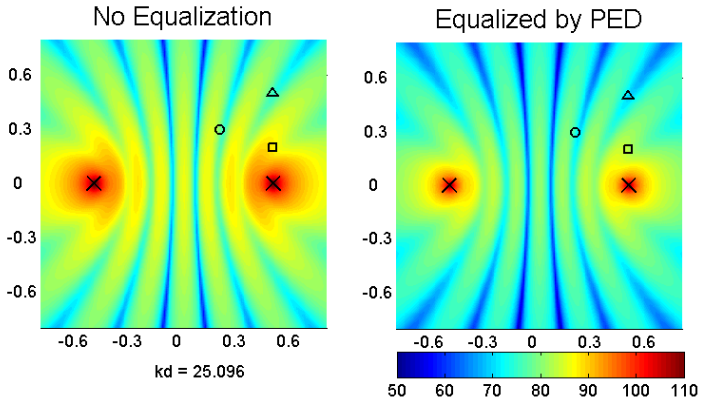

(c)

Figure 5.1 Comparisons of L_p over space of the unequalized sound field (left column) to the sound field equalized by PED (right column) at the point marked by ∘. Frequency responses corresponding to this and the other markers are found in Fig. 5.2. Notice that the interference pattern of the sound field does not change when both sources are equalized with the same equalization filter. The whole field is busted or attenuated to equalize the response at the sensor location.

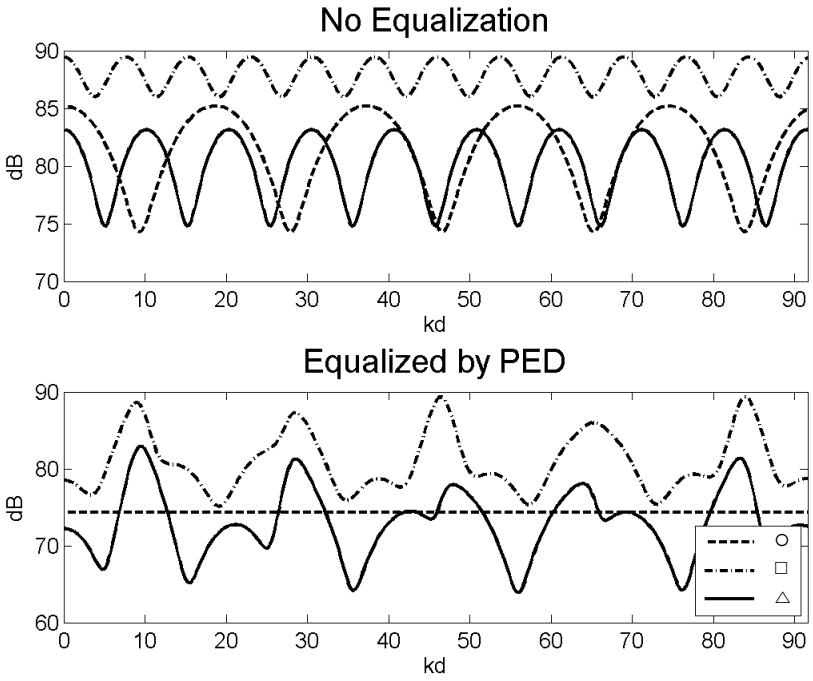

Figure 5.2 Frequency response magnitude curves that correspond, as marked in the legend, to the points mapped on the sound field in Fig. 5.1. The amplitude is in Decibels referenced to 20 μPa.

over frequency than the other measurements, because it is the sum of PED and KED, which alternate with one another in the near field. The frequency response of the vector magnitude of intensity contains information from complex pressure and complex particle velocity, incorporating the information carried in both measurements. The spatially squared pressure magnitude has a ragged looking frequency response that contains information from the entire listening area.

5.1.1 Along a Line Above a Reflective Surface

A simple case for equalization of a listening area is to restrict the region to a line. A set of frequency responses were generated along a line running perpendicular to an axis that runs between two sources. The boservation line is shown as the horizontal dashed line in Fig. 5.5. Surface plots were generated for this source receiver arrangement with

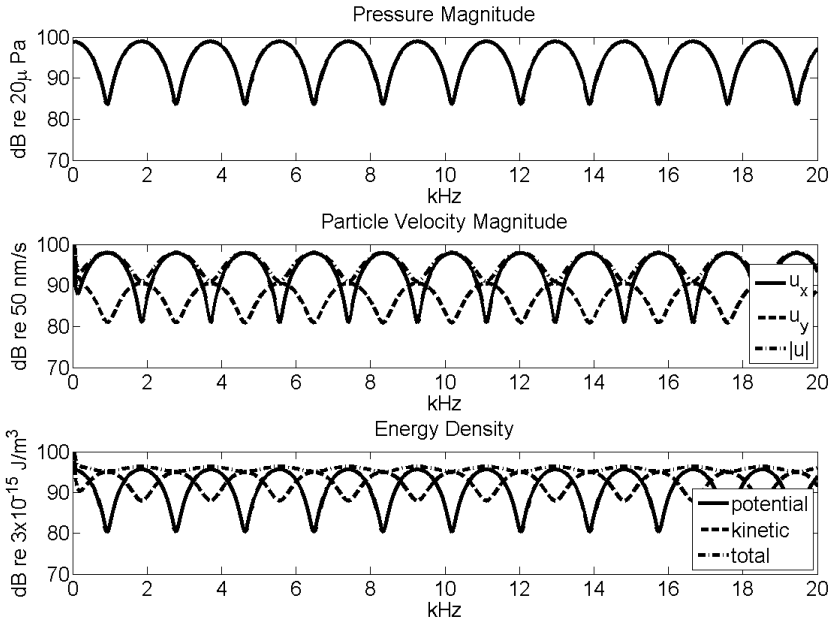

Figure 5.3 Example frequency responses as measured using pressure, the vector magnitude particle velocity and its components, PED, KED and TED. These are for a measurement with two point sources. The sensor was at (0.05,0.2) on the axis found in Fig. 5.1.

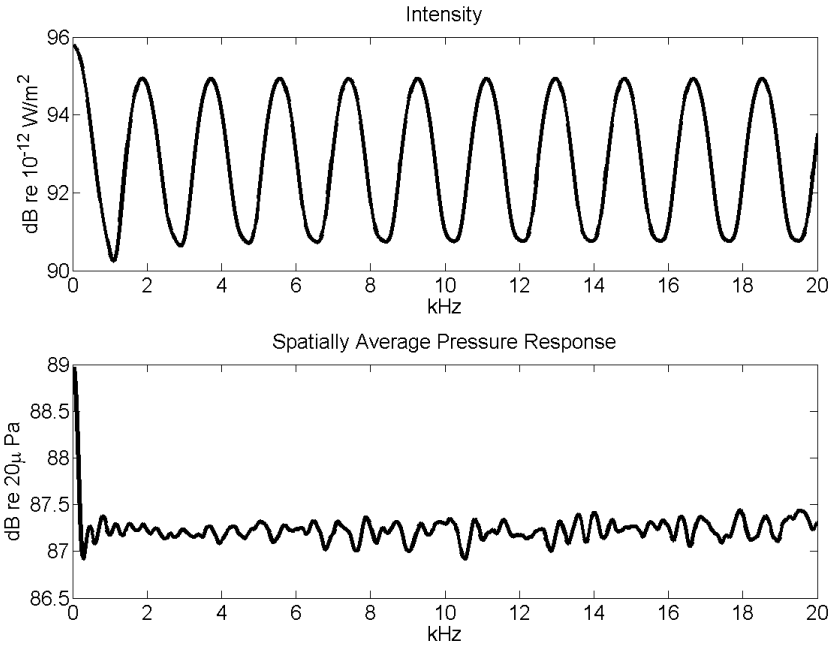

Figure 5.4 Example frequency response measurements using the vector magnitude of intensity and the spatially averaged pressure. These plots are for the same source arrangement and sensor location as found in Fig. 5.3.

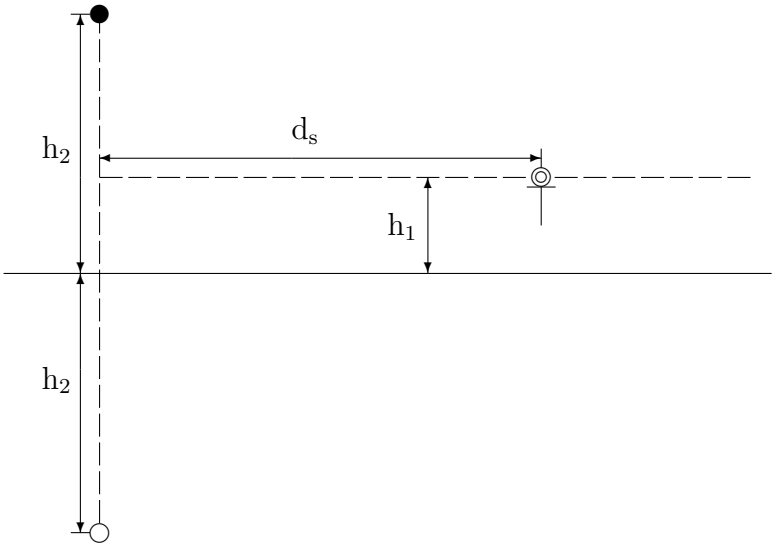

Figure 5.5 The dark circle represents the position of the real source, the open circle represents the image source used to model the case where the solid horizontal line is a reflecting surface. The marker on the right is the sensor used to to determine the equalization. This is the setup used for producing Figs. 5.6 through 5.8.

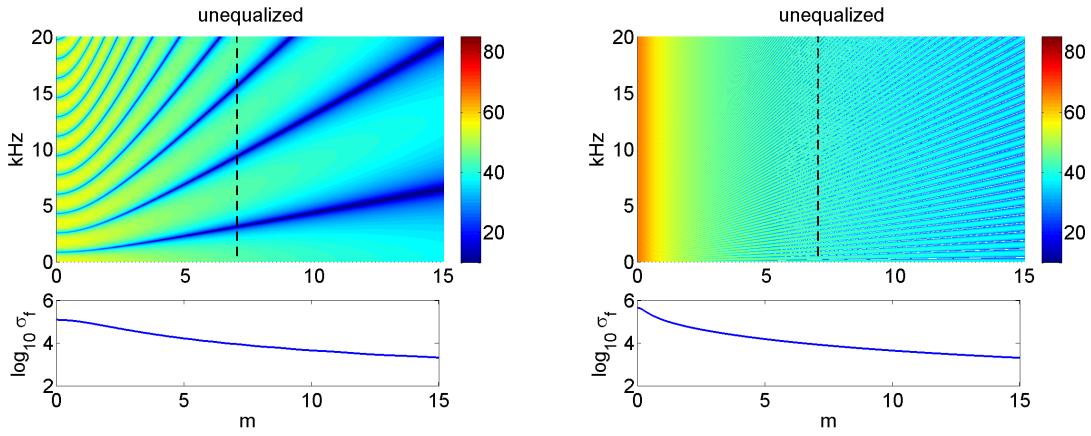

(a) (b)

Figure 5.6 The frequency response over space before any equalization occurs. Figure (a) is looking 10 cm above the surface, while Fig. (b) is 170 cm above the reflective surface. Below the a curve that indicates the $\log_{10}$ of the spectral standard deviation is plotted as a function of d_s. The source for these figures is 2 m above the reflective surface.

the distance from the axis running between the two sources represented the horizontal axis, while the frequency is represented along the vertical axis with colors assigned to represent the sound levels in dB referenced to 20 μPa. There are several examples of these plots in Figs. 5.6 through 5.8. Figure 5.6 shows the unequalized case observed near the reflective surface, where h_1 is 10 cm, in (a) of Fig. 5.5, and $h_1$is 170 cm in (b). The vertical dashed line in Figs. 5.6 through 5.8 indicates the sensor position, labeled d_s in Fig. 5.5. For the cases shown here, the source is placed 2 m above the reflecting plane ($h_2 = 2$ m). The plots in Figs. 5.7 represent the equalized cases where the listening height is near the reflecting surface ($h_1 = 10$ cm) to demonstrate the nature of the sound field. Figure 5.8 contains plots of a more realistic situations where the listening height ($h_1 = 170$ cm) is farther from the floor. To help assess the quality of the equalization, a plot of the spectral standard deviation is shown below each of the surface plots in the various figures. For the arrangements of plots in Figs. 5.7 and

5.8, the equalization was performed at $d_s = 2$ m and $d_s = 7$ m.

In Figs. 5.7(a), 5.7(b), 5.8(a) and 5.8(b), as seen from equalization at the point marked by the dotted line, PED works very well. There is a cost for this equalization; it is apparent that at other locations equalization is much less successful. At each of the unequalized spectral nulls, the sound source is boosted, causing spectral maxima for listeners located at other points on the line. A comparable process happens with the peaks at the measurement locations; dips appear in the frequency response at positions away from the equalization sensor. These dips can be very deep and wide, causing important information to be removed from the signal.

For situations where KED sensors are used, the equalization is less dramatic than when PED is used. For the cases shown in Figs. 5.7 and 5.8, the equalization does not become ideal at the position of the sensor used to measure the sound field, though it is improved slightly. This is most visible for equalization performed with $d_s = 7$ m with $h_1 = 10$ cm as shown in Fig. 5.7. This can be seen by noting the dip in the curve indicating $\log_{10}$ of the spectral standard deviation. Another sign of the improved equalization near the sensor location is that along the dotted line marking the point of equalization, the sound field varies less over frequency than for other values of d_s. It is also interesting to note that the spectral peaks are not as sharp as those from PED (or pressure) based equalization, this is only noticeable when h_1 is short as in Fig. 5.7.

TED takes into account both the pressure and the particle velocity to determine the equalization filter. The equalization performed using TED has several similarities with that performed using KED. Like KED, TED does not result in perfect equalization at a single point. The sharpness of the spectral peaks lies between that of the KED and the PED methods. Again, this can be seen by noting the dip in the $\log_{10}$ or by looking at the uniformity along the dashed line indicating the equalization

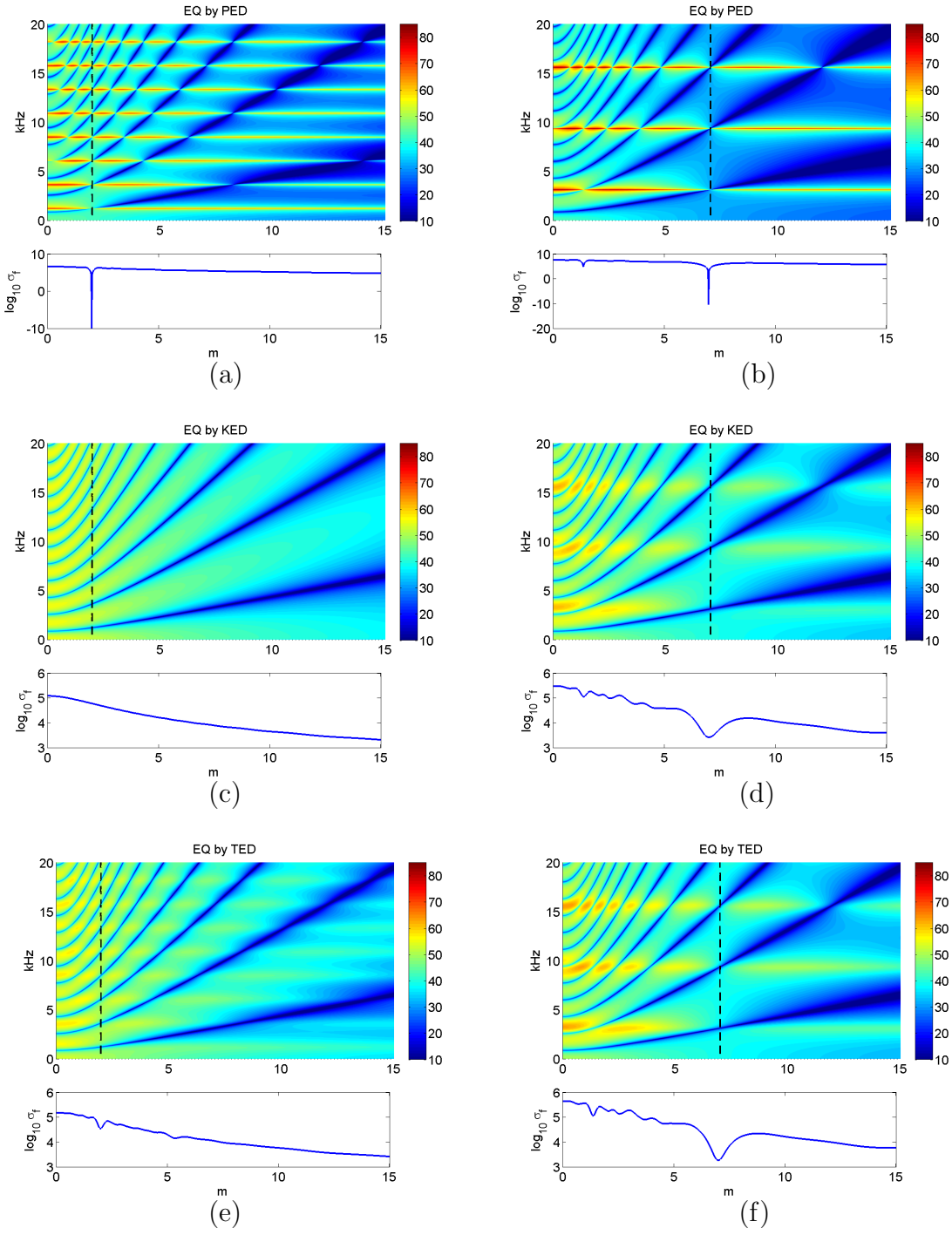

Figure 5.7 The frequency response after equalization with a listening region at $h_1 = 10$ cm above the reflecting plane. The source is at $h_2 = 2$ m. The left column is for the sensor placed with $d_s = 2$ m. while the right column is for a sensor placed with $d_s = 7$ m. The rows, listed from top to bottom, are separated into equalization performed by PED, KED and TED. Below are curves of the $\log_{10}$ of the spectral sandard deviation as a funciton of d_s.

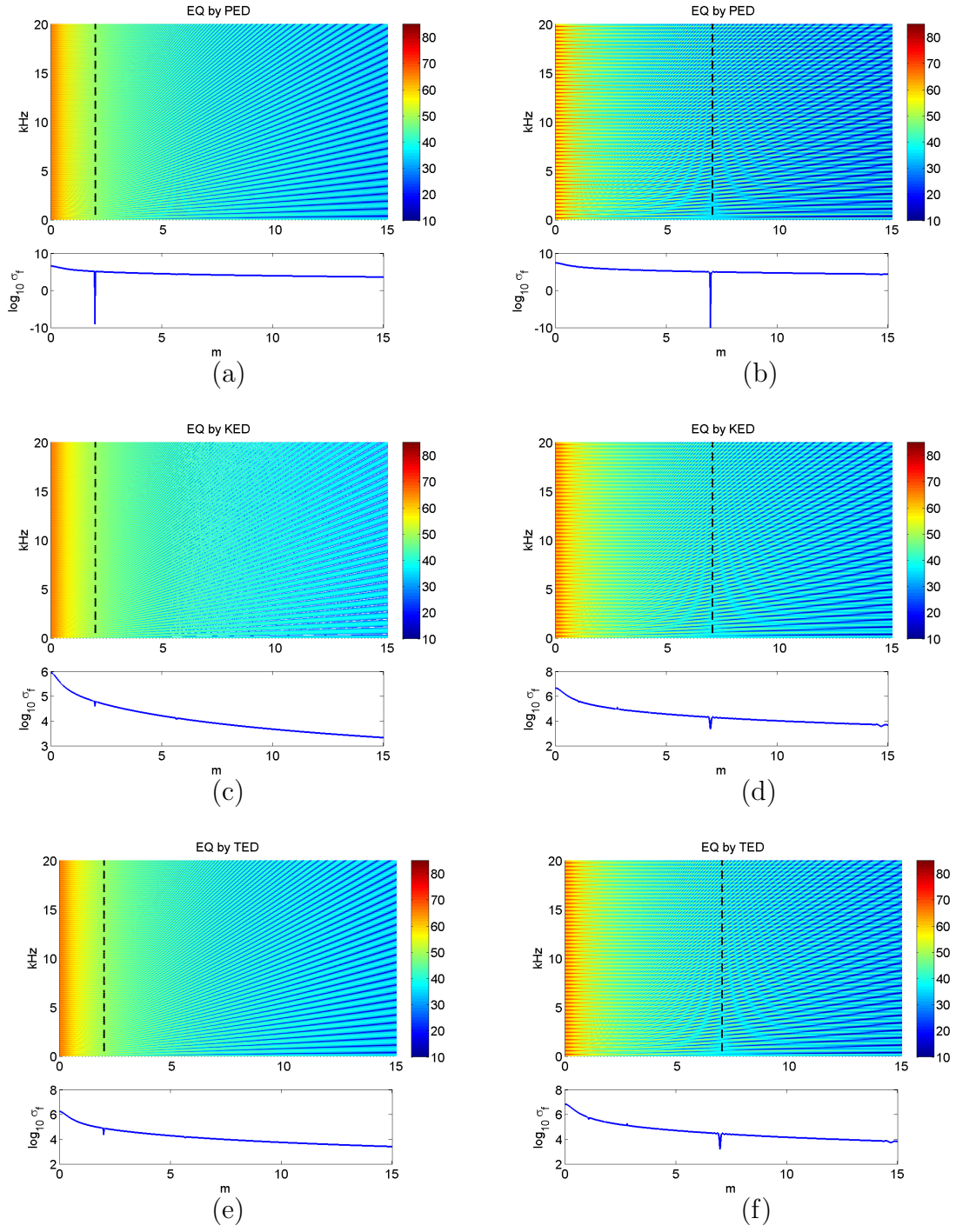

Figure 5.8 The frequency response after equalization with the listening region at $h_1 = 170$ cm above the reflecting plane. The source is at $h_2 = 2$ m. The left column is for the sensor placed with $d_s = 2$ m. while the right column is for a sensor placed with $d_s = 7$ m. The rows, listed from top to bottom, are separated into equalization performed by PED, KED and TED. Below are curves of the $\log_{10}$ of the spectral sandard deviation as a funciton of d_s.

location.

Similar processes may be noted in Figs. 5.7 and 5.8, which may be compared to the corresponding unequalized situation in Fig. 5.6. There are positions where the equalization is improved for the three equalization methods. For the cases shown in Fig. 5.8, the distance from the image source to the points on the measurement line is significantly longer than the distance from the primary source to the measurement line. This difference in path length introduces more notches in the frequency response. This is normal for a system consisting of two sound sources. This means that locations away from the error sensor will have more peaks in the equalized response. These peaks are due to compensation for notches determined using the equalizing error sensor. The resultant plots suggest that the spectral response of the system is more erratic as the path length from each source to the field point becomes significantly different. This is not at all surprising because it is expected in situations where two sound sources interact. This also illustrates that equalization only compensates for some of the frequency dependence of a listening area.

5.1.2 Using a Reinforcing Source

The computational model used to describe a single source above a reflecting plane, as described in Sec. 5.1.1, may be used to model a situation where a single primary sound source is reinforced by a secondary source (or combination of secondary sources). In this case, the first source produces a signal, while the reinforcing source generates a copy of that signal. The reinforcing source signal may be altered to equalize the composite sound system, while the primary source is not altered. This situation is a good model for representing the direct field produced by a person speaking with a reinforcement sound source. Figure 5.9 shows the source arrangement that is used to model a reinforced sound source in a simi-free field.

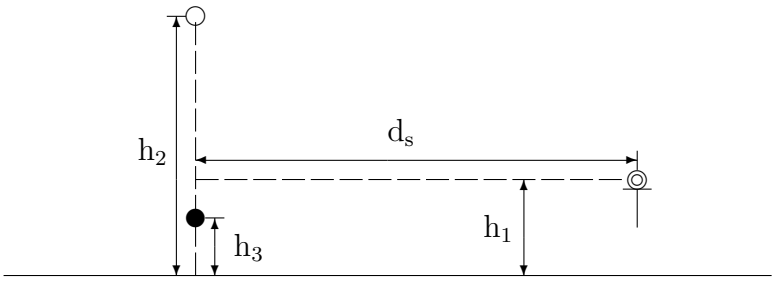

Figure 5.9 The dark circle represents a primary source, that is not equalized, the open circle represents a secondary reinforcement source that may be equalized in an attempt to equalize the overall sound field. The marker on the right indicates the sensor. The solid line at the bottom of the figure is a reflecting surface. This is the arrangement used for the initial model that represents a case where a sound source, in a semi-free field, is reinforced by a single secondary source.

In the case of a reinforcing sound source, the gain or amplification of the additional source comes into play. Here the gain is defined in decibels as

$$G = 10 \log_{10} \frac{|\hat{A}_r|^2}{|\hat{A}_p|^2}, \tag{5.1}$$

where $\hat{A}_r$ is the complex pressure amplitude of the reinforcing sound source at a set distance r and $\hat{A}_p$ is the complex pressure amplitude of the primary source at the same distance r. Figures 5.10 and 5.11 illustrate the effects on a sound field generated by a primary source and an equalized reinforcement source.[2] The vertical axis indicates the amplification, while the horizontal axis is the distance marked $\mathrm{d_s}$ Fig. 5.9. The coloration of the plot indicates the $\log_{10}$ of the spectral standard deviation of squared pressure magnitude, $|\hat{p}|^2$, as a function of the amplification and the listening position along the horizontal dashed line on Fig. 5.9. The spatially averaged frequency response in Figs. 5.10(b) and 5.11(b) were equalized using an average of the frequency responses along the horizontal dashed line in Fig. 5.9.

Figures 5.10 and 5.11 demonstrate several expected characteristics of equalization.

[2]Some animations of Figs. 5.10 and 5.11 are shown in Appendix E, Fig. E.6.

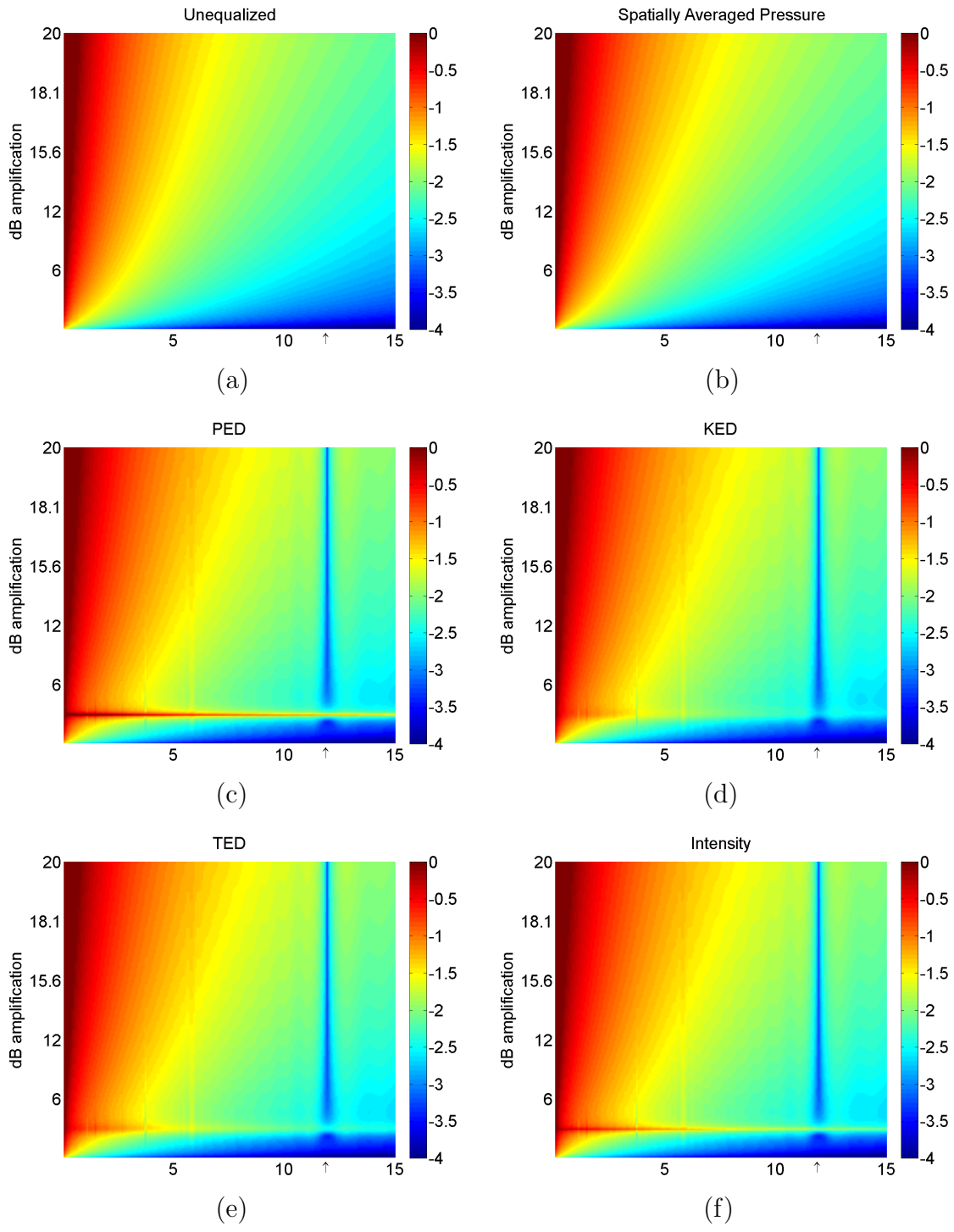

Figure 5.10 The vertical axis indicates the relative amplification of a reinforcing sound source the system diagramed in Fig. 5.9, while the horizontal axis indicates the distance along the horizontal dashed line for the observed field in meters. The color in the plots indicate the $\log_{10}$ of spectral standard deviation of $|\hat{p}|^2$. This figure is the result with $d_s = 12$ m (marked by $\uparrow$), $h_1 = 1$ m, $h_2 = 3$ m and $h_3 = 1$ m.

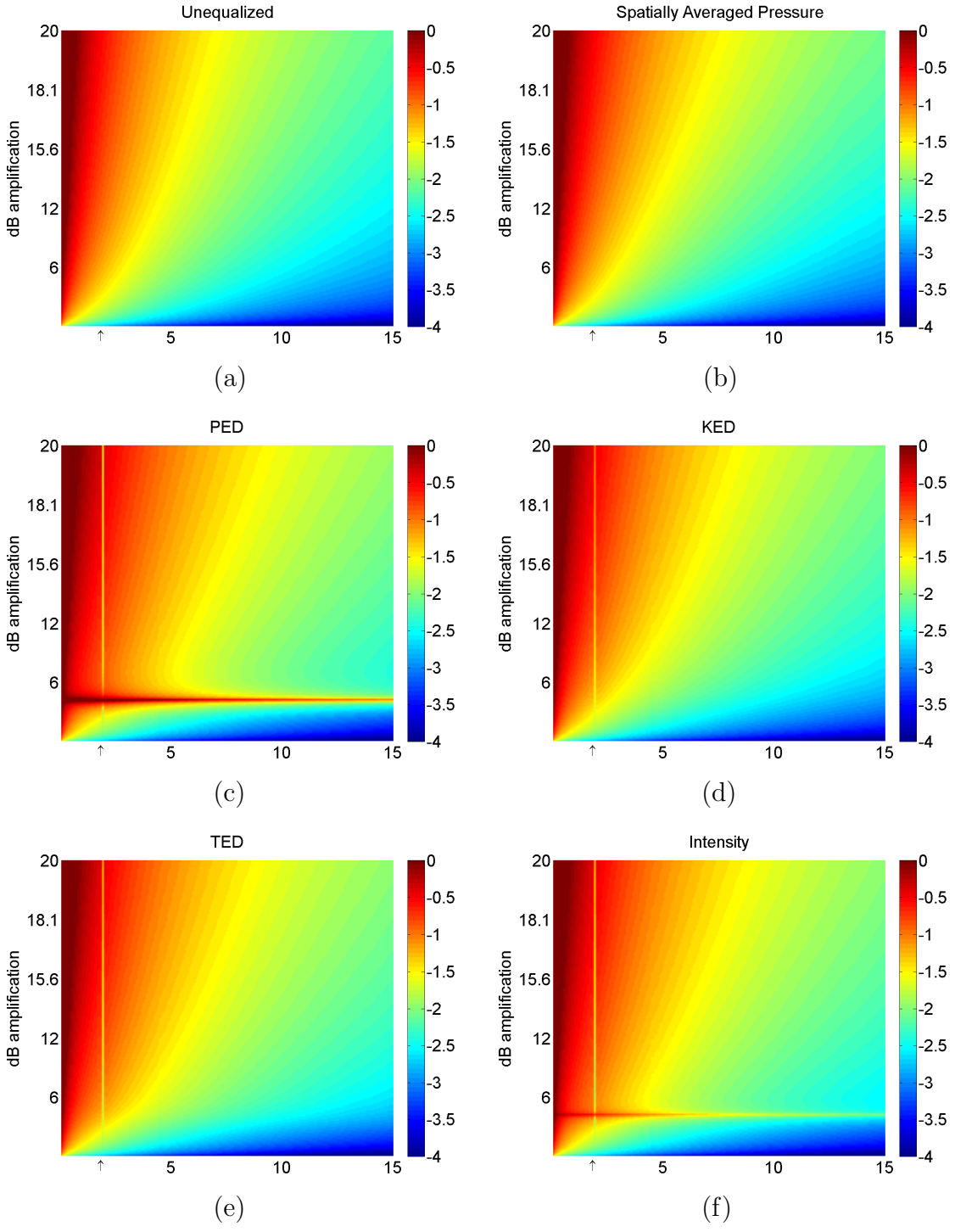

Figure 5.11 This figure is very similar to Fig. 5.10, in this case the error sensor has been moved to $d_s = 2$ m (marked by ↑) with $h_1 = 1$ m, $h_2 = 3$ m and $h_3 = 1$ m.

As the listener gets farther from the sources, the standard deviation decreases, especially for low amounts of amplification. This feature is more pronounced with less amplification. This is because the measurable signal decreases as the sensor is moved further from the source, thus producing smaller numerical values in the measured frequency response. The smaller values of the frequency response limit the amount of variation found in a signal. For the equalization methods that depend on single point measurements, a long narrow blue vertical strip, indicating a region of good equalization, occurs near the error sensor location. The color in Figs. 5.10 and 5.11 indicates the $\log_{10}$ of the spectral standard deviation, thus the blue regions indicate a more negative value of the spectral standard deviation. These point-measurement equalizations inherently produce good results at or near the sensor location, but perform poorly at many other locations.

Another experiment may be conducted where the sensor location is varied and the boost applied to the amplification of a reinforcing signal is held constant as shown in Fig. 5.12. The vertical axis in the plot for this case changes to represent the sensor location, marked by d_s in Fig. 5.9. The horizontal axis still represents the listening position, and the colors assigned to the plot still indicate the $\log_{10}$ of the spectral standard deviation. In this case, the blue line rises diagonally to the right for the point-source based equalization methods. This indicates that the region of best equalization is located near the sensor location. It is also interesting to note that the blue line widens as the sensor is moved farther away from the sound sources. Part of the reason for this is that the response decreases in overall magnitude and thus the spectral standard deviation decreases because of a decreased amplitude rather than a more uniform frequency response. This can also be seen by comparing Fig. 5.10 to 5.11 and noting the region of good equalization is much narrower in Fig 5.11 (closer sensor location) than in Fig 5.11 (farther sensor locations).

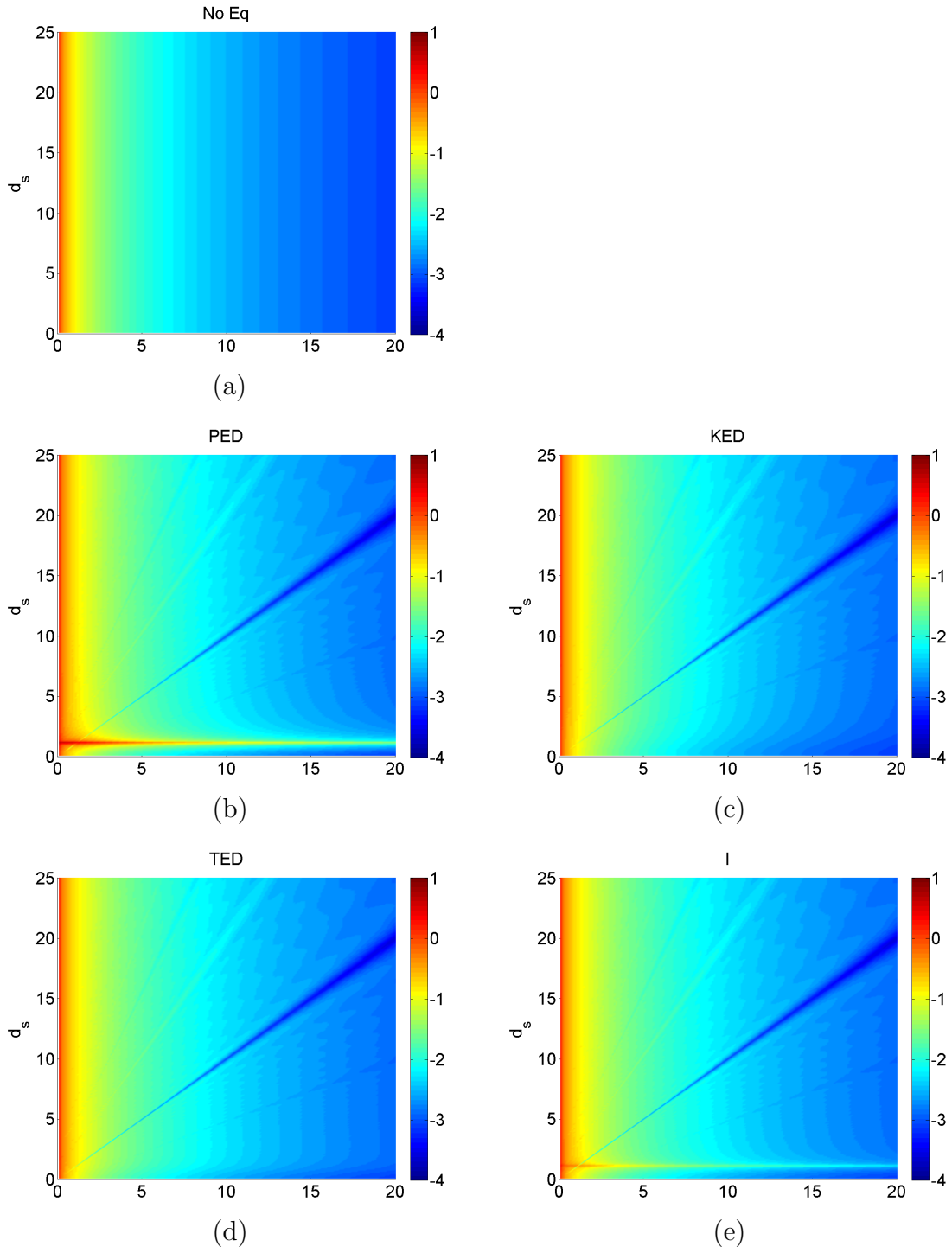

Figure 5.12 These demonstrate the effect of sensor location on equalization of a sound field generated using a source pair where one is equalizes the compost field and the other is not. The secondary sound source produces a signal amplified by 6 dB compared to the unequalized source. The axes are marked off in meters. The horizontal axis indicates the observed position along the dashed line found in Fig. 5.9.

It is also good to note that equalization does not work as well if the sensor is moved closer to the unequalized sound source. This is because the sound field becomes dominated by the unequalized sound source. In Fig. 5.12, there is a region of very poor equalization indicated in red horizontal strip. This is a special case where the pressure sensor in the model detects very quiet signal, which in turn leads to very large gains at some frequencies for the equalization process. The filter values in this region are large enough (approaching infinity in the numerical models) that equalization is adversely affected. Setting $h_1 = h_2$ yields results where equalization works very well as the sensor is moved closer to the equalized sound source, and the region of poor equalization does not appear.

5.2 Time-Domain Perspective of Equalization

Equalization is usually done in the time domain by using a filter that has an impulse response which compensates for the frequency response of the system. Because of this, equalization in the time domain is sometimes referred to by the term *dereverberation*, though equalization usually refers to the adjustment of sources while dereverberation usually refers to adjustments done for a listening environment [76]. This process of equalizing can result in both spectral corrections and reduction of reverberation at the sensor location. For many situations, equalization using a time-domain filter is more efficient because it does not require transforming a signal from the time domain, altering the response in the frequency domain, then returning to the time domain. While a correction filter may be defined in the frequency domain, it must be implemented in the time domain.

5.2.1 Inverse Filters

Equalization filters are referred to as inverse filters because they are designed by inverting the frequency response between a source and receiver in a listening environment. This filter is intended to negate the effects of the response of the listening environment. The filter is an inverse filter in the frequency domain, though it may not be practical to equalize in the frequency domain. The filter can be transformed from the frequency domain to the time domain in order to equalize the system.

Processing in the frequency domain is performed by multiplying the frequency-dependent version of the filter by a signal transformed into the frequency domain. In this case, the signal is transformed in blocks that are the same size as the equalizing filter. This allows for the multiplication of corresponding terms in the filter and the signal to occur correctly. In the time domain, the processing is performed using a convolution. The convolution is performed with a time-domain version of the filter, which acts on the time-domain representation of the signal. The time-domain filter may be designed in two ways. First, the filter may be designed by inverting the measured frequency response, then finding the corresponding impulse response for use as the equalization filter. The second method is to design a n^{th} order filter that has frequency response that approximates the inverse of the measured frequency response.

Because filters are commutative, a recorded signal may be preprocessed in order to demonstrate equalization in the listening environment. In this case, the signal may be either transformed to the frequency domain for the equalization or may be processed in the time domain. An equalizing filter may be tested using a recorded signal played back through the measured sound system. A recorded signal may be preprocessed, producing an equalized signal that may be introduced to the listening environment. This will demonstrate how well the equalization worked.

In equalization, many frequency-domain measurements may be used to determine the ideal frequency response of an equalizing filter. Complex measurements, such as pressure and particle velocity, include phase information. Thus, filters designed using these measurements inherently address the phase response of a system in addition to the magnitude response. The result is often a nonminimum phase condition. This means, as previously mentioned in Sec. 3.2, that the inverse of that filter will not usually be stable and causal. Care must be taken in this case to verify that the correction filter will be viable. For simplicity, the pressure magnitude is useful for equalizing the sound field. This is also acceptable because, as mentioned in Sec. 1.3, phase equalization is outside of the scope of this research. It may also be impractical because of the immense phase variation over a large listening area.

Because our hearing is based on pressure, it would intuitively appear that pressure measurements would be the ideal measurements for equalization. However, pressure measurements result in very spatially dependent equalization. Because of the limited size of regions where equalization is effective, it may be more beneficial to use a measurement that may not equalize as effectively at one point, but provides a larger region with improved equalization. For this reason it is interesting to look at alternative measurements such as particle velocity, TED and others as potential candidates for use with equalization.

Though particle velocity may be complex valued in the frequency domain, it is a vector quantity, which introduces difficulty in its implementation. Considering global equalization to be the primary interest, and phase equalization to be of secondary interest, the vector magnitude and modulus of the particle velocity may be found and used in place of the complex vector-valued measurements. This removes the phase information, resulting in equalization identical to equalization based on KED.

Filters designed using ED quantities are zero phase, which in turn result in zero-

phase filters that do not introduce A zero-phase filter is a situation in which there is no phase introduced to the system. new phase to the equalized system. A zero-phase system does not have imaginary components in the frequency domain, so inverting the frequency response of a zero-phase system results in another zero-phase system. The ED quantities do not introduce phase because these measurements retain no phase in their frequency-domain expressions. The vector magnitude of acoustic intensity also results in a zero phase system. In each of these cases, the filters neglect phase conditions in the system

Filters may also be designed using the minimum phase portion of a measurement of the system. A Hilbert transform may be performed to separate the measurement into two parts, a minimum-phase portion and an all-pass portion. The minimum-phase portion of the measurement has the same frequency response magnitude, but has a different phase. The inverse of the minimum phase portion of a measurement can be used as a filter. This filter is inherently causal and stable, however it introduces phase to the system.

5.3 Evaluating Equalization

In this section, several graphical and computational methods are considered for evaluating the success of different equalization procedures. These approaches are used to evaluate how successful different equalization methods are for achieving a desired response in a given listening area. Each has advantages and drawbacks.

The listening areas are square in the investigation and point sources are used to model the systems. Radiation patterns of the sound sources could also be included, but use of these advanced sources only complicates the sound fields. Including these advanced models to arrive at a method for evaluating the equalization of a system is

likely to contribute very little.

5.3.1 Graphical Evaluation of Listening Areas

The graphical tools mentioned previously describe the sound field and may be appropriately used to evaluate sound control systems. These range from simple curves representing frequency responses and impulse responses to complicated surface plots that display the ratio of two standard deviations. Together, they provide information that is useful for analyzing a sound field.

For convenience, plots involving listening regions that are spread over a line are considered first in this discussion. Each plot indicating the frequency dependence over a line in space, found in Figs. 5.6, 5.7, and 5.8, has a corresponding plot below it. The corresponding plot is a curve representing the spectral standard deviation of $|\hat{p}|^2$. These standard deviation curves may be overlaid on the same plot to show the differences in the different methods for determining an equalization filter. While the curves illustrate the relative performance of different methods of equalization, they also indicate which equalization tactic performs best overall. Figure 3.6, repeated in Fig. 5.13 contains a plot indicating the curves over space for seven situations for equalization. These provide an example of how equalization may be gauged from the plots; the curve that is lowest is the best while the curve that is highest is the worst.

While these curves help when the listening region is a line, these types of illustrations become more difficult to read and interpret when the listening regions become two dimensional areas, like those in most listening venus. Instead of plotting the standard deviations as curves, one must plot them as surface plots or color maps. Overlaying these standard deviation surface plots does not help to distinguish which method performs best. Surface plots like these may be seen in Figs. 5.14 and 5.15 and in Sec. 5.3.3. It is also difficult to compare the surface plots side by side. Of-

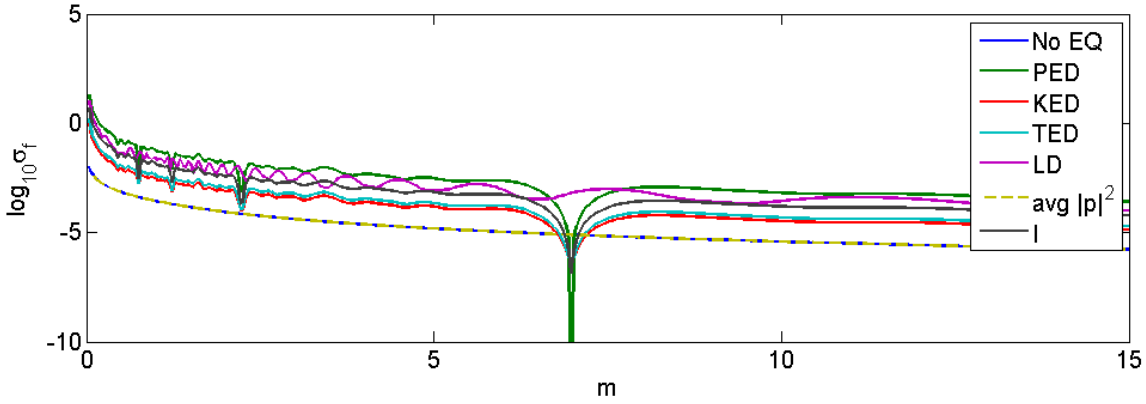

Figure 5.13 An example of a curve comparing the standard deviation as a function of position in a one-dimensional listening area. This figure is repeated from Fig. 3.6

ten, it is useful to plot the ratio of the standard deviation of the equalized sound field to the standard deviation of the unequalized sound field. This normalizes the equalization, providing easier comparison of equalization techniques as well as indicating where equalization has improved. This normalization scheme also removes the proximity dependance of the spectral standard deviation in a free field. As discussed in Sec. 3.3.5, this proximity dependance comes from the variation in the sound field because sound is farther from the sources, while we are primarily interested in the interference pattern. Plots generated in this manner are found in Figs. 5.14 and 5.15. This final technique can be used to see where equalization improves or deteriorates for different equalization methods, which in turn can be used to judge which method provides better equalization.

Comparing plots like those in Figs. 5.14 and 5.15 reveals some features of equalization methods and sensor placement. It demonstrates a greater disparity among the performance of the different equalization methods for the case where the sensor is located farther from the sources. To notice this it is useful to note that the color scale was adjusted from plot to plot in an attempt to reveal some detail of the variation

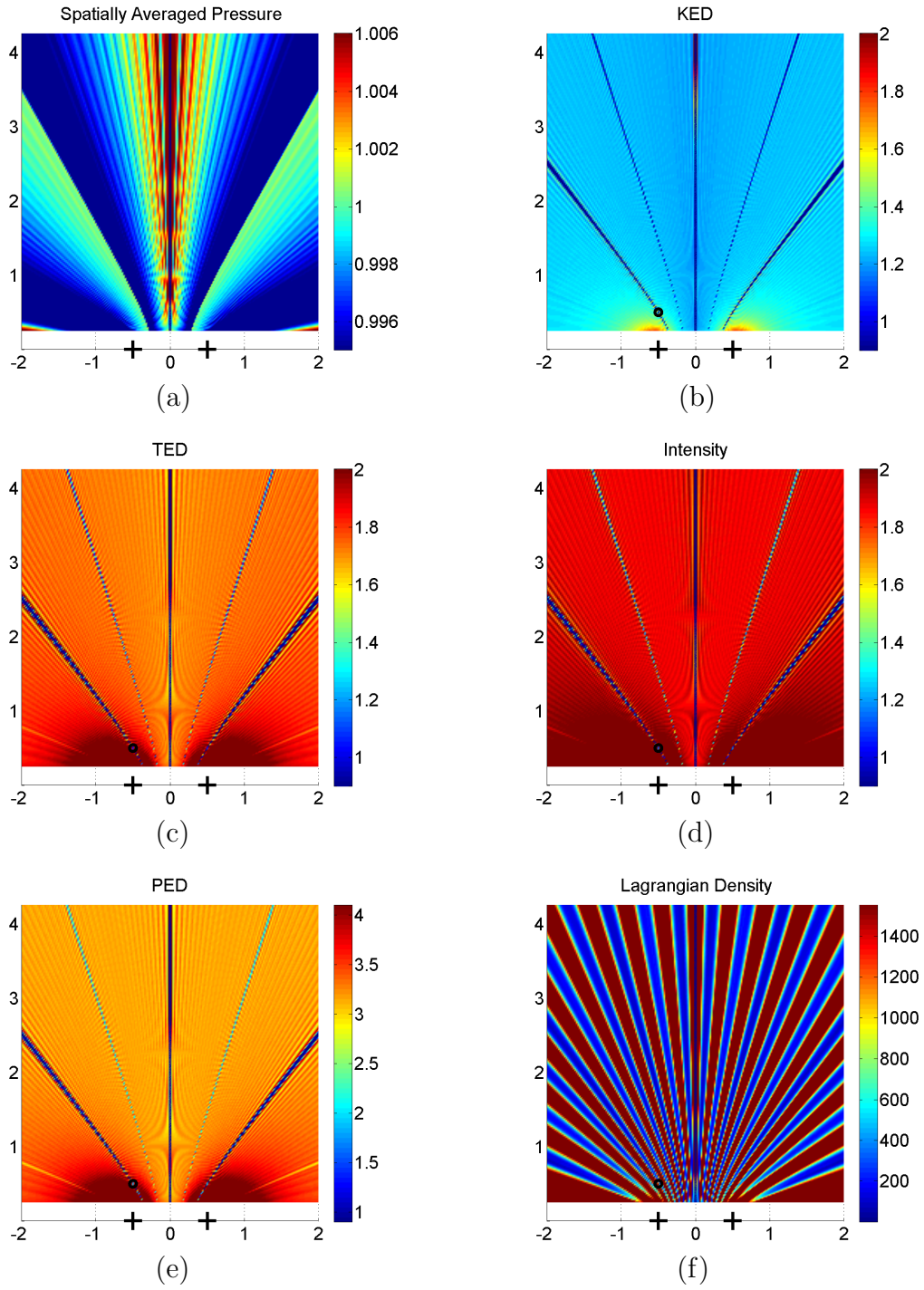

Figure 5.14 The resulting ratio of the spectral standard deviation, from $kd = 0.3664$ to $kd = 366.4$, of an equalized field divided by the spectral standard deviation of the unequalized field. The portions that are indicated as being less than one indicate equalization improvement, while values greater than one show a decrease in equalization. The frequency response of this plot is calculated over $|\hat{p}|^2$ to increase the contrast in the plot. This figure is a repeat of Fig. 3.8. The sensor postion is marked by $\circ$.

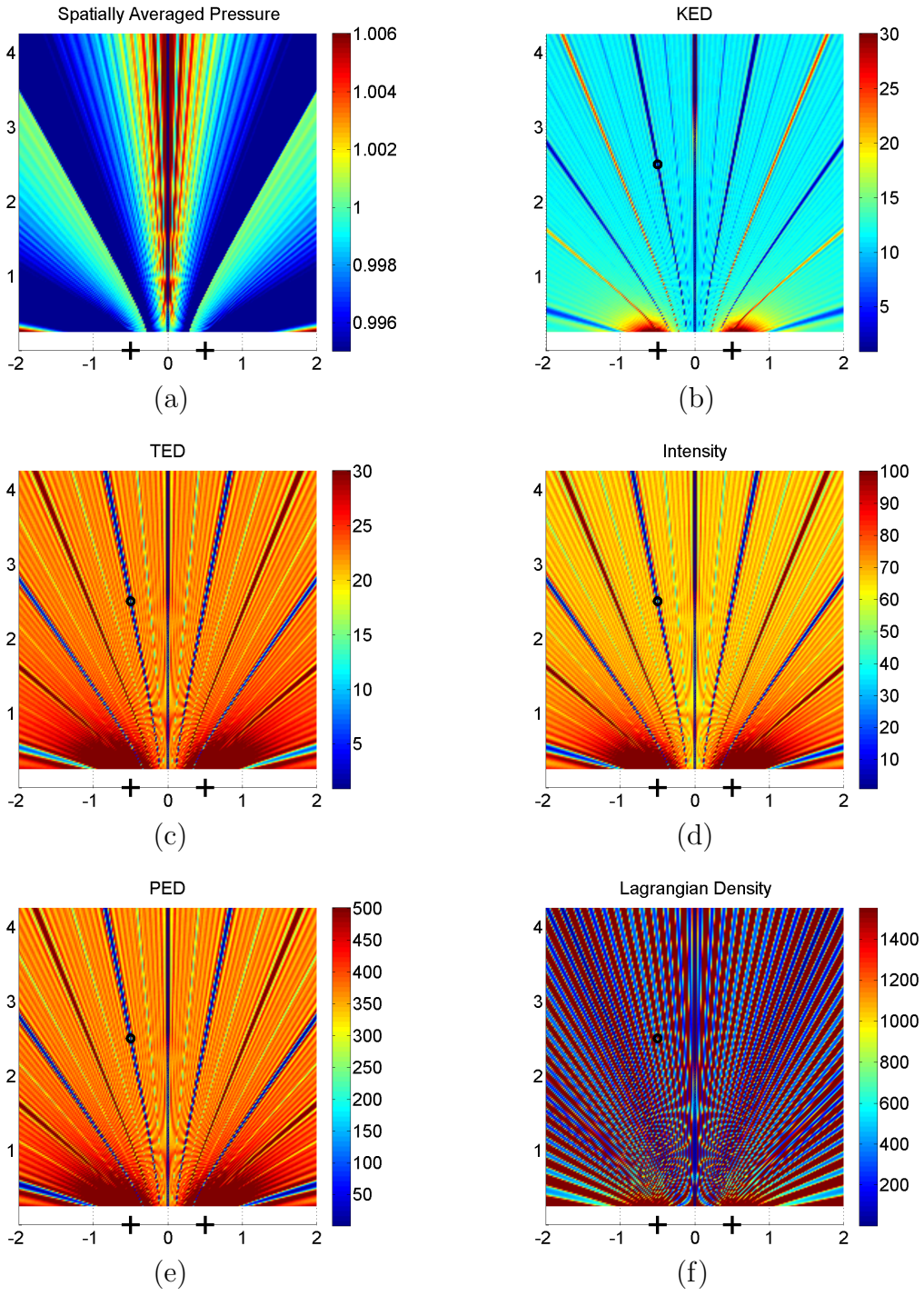

Figure 5.15 The resulting ratio of the spectral standard deviation, from $kd = 0.3664$ to $kd = 366.4$, of an equalized field divided by the spectral standard deviation of the unequalized field. The portions that are indicated as being less than one indicate equalization improvement, while values greater than one show a decrease in equalization. The frequency response of this plot is calculated over $|\hat{p}|^2$ to increase the contrast in the plot. The sensor postion is marked by $\circ$.

of the spectral standard deviation in the plots. These plots also show which methods perform the best. They are arranged from the best global equalization within the listening area to the worst.

5.3.2 Development of a Global Listening Area Equalization Coefficient

It is often convenient to have a single value to describe a control scheme, even if it means overlooking some of the details. In equalization, it is common to just say that equalization worked at the error sensor location and mention that it did not succeed in other locations. In order to determine a best method for equalization, it would be useful to have a coefficient or figure of merit to decide which procedure works best over an extended listening area. The computational models developed in this work provide a convenient set of tools for testing such a global listening area equalization coefficient (GLAEC).

Several procedures were proposed to determine a single number for rating the success of equalization techniques. Each included a set of error sensor locations, along with an identical arrangement of unequalized and equalized sources. For each setup, the possible values of the figure of merit were calculated using the full set of data used to generate surface plots of the sound field. Each potential equalization metric was also calculated using randomly located sensors. Groups of 4, 6, 8, and 10 sensors placed randomly in the listening area were used to calculate the coefficients. (Area-weighting was not used in the process of computing the coefficients this might have improved the the reliability of the coefficients. The random positioning of the sensors used to compute the coefficents was repeated five times for each error sensor position. The results were judged by visual inspection of the ratio surface plots.

The success of equalization coefficients was judged using the χ^2 test of contingency and the z-test as an estimator of difference techniques to see which method correctly ranked equalization methods with the most consistency according to subjective visual inspections of the corresponding plots.

Eleven quantities were compared for use as global listening area equalization coefficients (GLAECs), many of which are similar with those used for acoustic diffuser evaluation [70]. These were calculated using non-normalized squared pressure data, squared pressure measurements that were normalized by the maximum value of the frequency responses, and squared pressure data that were normalized by the average of the frequency responses for each sample position in the listening field.

The first and most striking difference among the different equalization variables was the catastrophic failure of the potential GLAEC coefficients to correctly rank the equalization methods when using normalized data. The equalization factors failed nearly every time when normalized by the maximum value or the average value of the frequency responses. In these cases the normalization was performed on the unprocessed data. These methods for computing the GLAEC were considered for cases where the error sensor was placed in the listening area far from the sound sources. In these same situations, all of the equalization methods that were not normalized worked nearly every time. The difference was so significant that the normalized methods were thrown out right away. Proper normalization only scales data, it does not fundamentally alter data. There may have been problems with the techniques used to normalize the data prior to calculating the GLAEC—problems that altered the data in the process. One possible reason for this would be the method for obtaining the normalization factors. The normalization factors were found from the unequalized sound field, which does take into account the interference patterns of the sound field.

Other methods for normalizing the measurements may produce better results. The plots used as a reference to find the GLAEC were of the equalized spectral standard deviation divided by the unequalized spectral standard deviation at each point. For the coefficients where the spectral standard deviation is computed first, the coefficients could be normalized by dividing the equalized spectral standard deviations by the unequalized spectral standard deviations. It stands to reason that this method would produce a coefficient that would perform most like visual inspection of the plots; however, this requires further research for verification.

It is also important to note that the frequency response used for calculating the candidates for the GLAEC were calculated using $|\hat{p}|^2$ rather than $|\hat{p}|$. The effect of this change is to adjust the contrast on the surface plots used to judge the equalization, and perhaps increase the sensitivity of candidates for the GLAEC.

The first measurement considered for use as the GLAEC is similar to one used by Hargreaves and D'Antonio for their acoustic diffuser characterizations [70, 77]. First, the spectral standard deviation σ_f of the frequency response is measured at several locations. The spatial average of the standard deviations μ_s is then used as a number to evaluate the overall performance of the equalization in the designated listening area. This method can be described mathematically as $\mu_s(\sigma_f)$. This measurement provides an average of the standard deviation of the listening area.

The next two values considered for use as GLAECs are also calculated using spectral standard deviations. One examines how much the spectra change over space and is determined by calculating the spatial standard deviation σ_s of the spectral standard deviation σ_f and is represented by $\sigma_s(\sigma_f)$. This factor shows how much the variation of the spectral standard deviation changes over space. Another is the sum of the first two, $\mu_s(\sigma_f) + \sigma_s(\sigma_f)$. The idea behind this value is that by summing these two variables, the expression would prohibits the factor from producing ratings that

predict equalization better than it actually is. That is, *if* $\mu_s(\sigma_f)$ and $\sigma_s(\sigma_f)$ both correctly rank equalization, but erroneously rank some an equalization factor too well, summing the values would limit that mistake. However, this correction would come at the cost of increasing the likelihood of erroneously detecting degradation of equalization.

Because human hearing is based on variations of pressure, the best measurement for equalizing a sound field is a spatially averaged pressure frequency response. Another potential equalization coefficent takes advantage of this concept. This equalization factor is calculated by taking the squared pressure magnitude values over space in the frequency domain to get a spatially averaged pressure response μ_s, then finding its spectral standard deviation σ_f, and may be expressed as $\sigma_f(\mu_s)$. As this value gets lower, it indicates that the system is closer to being equalized. In an attempt to keep the units consistent with the actual measured data, a slight variation of the last measurement was also tested, the standard deviation of the square root of the spatially averaged pressure, $\sigma_f(\sqrt{\mu_s})$.

In the process of gathering the data, it was noted that most of the potential GLAEC calculations worked well when each of the different methods of equalization produces very obvious differences in the ratio-style equalization plots. However, there are situations where it is less obvious from visual evaluations witch equalization method performs best. Some of the methods considered for calculating the GLAEC began to incorrectly rank the equalization methods for these cases. Placing the sensor in the near field of the sound sources tended to produce results where the diagnosed equalization performances were more similar, regardless of the equalization method. This provided useful cases for finding a reliable GLAEC, as can be seen by comparing Figs. 5.14 to 5.14, and noting that the difference in the equalization performance is greater in Fig. 5.15, where the sensor is placed farther from the sources. In order to

find the GLAEC that performed best, the performance of the GLAEC was evaluated for cases where the error sensor was restricted to a region near the sources. This produced results where all of the potential GLAEC values would occasionally fail to predict which method equalized best. Some methods for computing the GLAEC failed to correctly rank equalization performance more than others, this was used to find which method had better resolving power. With these results, the χ^2 value was 122.25 with a critical value of 18.3. This means that there was a very significant detectable difference among the different values considered for the GLAEC.

The χ^2 test is good for comparing the several variables at the same time, but it does not mean that every variable performs significantly different from other variables. Because of the nature of the χ^2 test, there is not a guarantee that every equalization coefficient performs differently, just that some of them do. The z-test can check to see if the best two or three coefficients perform differently. To compute the χ^2 and z-test information a count of passes and fails were used. If a run of the equalization test GLAEC ranked the performance in the same order that a visual inspection of the ratio style surface plots did, it was counted a pass, other wise it was counted as a fail.

The latter of the statistical tests used is the z-test and estimator of difference between two proportions [78]. This was specifically used to compare the difference between the best and second best methods according to the χ^2 test. For this test, a success rate for two variables is calculated, then a z-value is calculated from this data. The z-value indicates the confidence level, which tells how certain we can be that the best tested factor really was better than the second factor. Again a large value of the test statistic indicates a significant difference between the two variables [78]. A summary of the statistical data is found in Table 5.1.

The three best functioning values for the GLAEC according to the χ^2 contingency

Table 5.1 Summary of the values considered for use as a GLAEC and the statistical results. The row labeled pass indicates how many times out of 126 measurements that the value correctly ranked equalization performance. The row labeled fail indicates how many times the measurement failed to correctly rank equalization performance. The z-value indicates the result of the z-test of the performance of $\mu_s(\sigma_f)$ compared to the performance of the measurement of a given column. A larger z-value magnitude indicates a more discernible difference between the compared sampled populations. In this case, a positive value would indicate better performance at correctly ranking of the equalization methods. The confidence, labeled β, is a fractional comparison indicating the certainty that there is a difference between two populations. This data comes from the measurements made with the equalization filter designed for use near the the sound sources.

	Tested GLAEC values										
	$\mu_s(\sigma_f)$	$\sigma_s(\sigma_f)$	$\mu_s(\sigma_f)+\sigma_s(\sigma_f)$	$\mu_s(\mu_f)$	$\sigma_s(\mu_f)$	$\mu_f(\sigma_s)$	$\sigma_f(\sigma_s)$	$\mu_f(\sigma_s)+\sigma_f(\sigma_s)$	$\sigma_f(\mu_s)$	$\mu_f(\mu_s)$	$\sigma_f(\sqrt{\mu_s})$
Pass	106	80	91	62	38	70	86	84	97	79	95
Fail	20	46	35	64	88	56	40	42	29	47	31
z-value	0	-3.73	-2.29	-5.88	-8.66	-4.94	-2.96	-3.22	-1.43	-3.85	-1.72
β	0.5	1.00	0.98	1.00	1.00	1.00	1.00	1.00	0.92	1.00	0.96

$\chi^2 = 122.25$ $\chi^2_{critical} = 18.31$

table were, listed starting with the best, the spatial mean of the spectral standard deviation ($\mu_s(\sigma_f)$), the spectral standard deviation of the spatial mean ($\sigma_f(\mu_s)$), which was closely followed by the standard deviation of the square root of the spatial mean ($\sigma_f(\sqrt{\mu_s})$). According to the z-test of differences, we can claim with a 92% certainty that $\mu_s(\sigma_f)$ is better than $\sigma_f(\mu_s)$. Likewise, there is a 96% certainty that $\mu_s(\sigma_f)$ is better than $\sigma_f(\sqrt{\mu_s})$. At the same time, there was not sufficient evidence to say that $\sigma_f(\mu_s)$ was better than $\sigma_f(\sqrt{\mu_s})$. For the sake of simplifying the calculation of the GLAEC, we may eliminate the method that requires the square root, since there is no significant advantage to taking the square root.

Because Hargreaves and D'Antonio use the $\log_{10}$ of the data for their diffusion coefficient, a new sample of measurements was taken using both the $\log_{10}$ of the data and the raw data to see if this produced a significant benefit [70,77]. This comparison was only performed using the best performing GLAEC from the previous tests. Again the results were very statistically significant, for nearly every case the ranking used was different from one another. This result should not be a surprise, calculating the average of a sample and then taking the $\log_{10}$ of the data is different than taking the $\log_{10}$ of the data and then averaging. The version of the GLAEC calculated without taking the $\log_{10}$ of the data consistently worked better. A z-test of difference verified that the performance was significantly better.

Recommended GLAEC

The coefficient that performed best at ranking the equalization was the spatial average of the spectral standard deviation $\mu_s(\sigma_f)$. Because of this, it is used in the calculation of the recommended GLAEC. To compute the recommended GLAEC value, compute the spatial averages of both the spectral standard deviation of the unequalized sound field and the equalized sound field. The latter may be divided by

the former

$$GLAEC = \frac{\mu_s(\sigma_f)_{equalized}}{\mu_s(\sigma_f)_{unequalized}}. \tag{5.2}$$

This produces a value that contains the same data as the best coefficient tested for the GLAEC, but also has a value that can be interpreted in a straight forward manner. If this ratio is grater than unity, than the overall equalization in the listening area is degraded. If it is less than unity than overall equalization in the listening area is improved. Equation 5.2 could potentially be improved by an appropriate normalization during the spatial average, similar to that used in Figs. 5.14 and 5.15. This would result in

$$\mu_s \left(\frac{(\sigma_f)_{equalized}}{(\sigma_f)_{unequalized}} \right), \tag{5.3}$$

but this coefficient *has not yet* been tested to check its validity. As mentioned previously, an area weighted mean may also have some benefits.

Though most of the different coefficents considered for rating equalization succeeded when the success of the different methods was very different, few of them had the power to distinguish the equalization when different equalization methods performed almost equally well. None of the potential equalization factors worked in every case; however, some performed better than others. The difference in performance quickly becomes more notable when there is a limitation on the number of measurements that may be practically taken to assess the equalization of the listening area. The difference in the performance of the coefficients considered for use as a GLAEC was greater when the sensor is moved closer to the sources, as mentioned previously.

Evaluating the equalization of a given listening area requires several frequency response measurements. The maximum number of pressure responses that may be reasonably taken should be used. These measurements should be taken at randomly distributed positions within the listening area. For the statistical tests in this research,

combinations of sensor locations and sensor arrangements, ranging from four to thirty sensors in, were used in an attempt to determine a minimum number of sensors. However, the data collected were insufficient to determine a minimum number of sensor locations to ensure success. A larger sample size is necessary to to arrive at a clear conclusion of how many error sensors are required to make a valid calculation of the GLAEC.

These frequency response measurements may then be used to calculate a recommended coefficient for judging the equalization of the sound field. The spectral standard deviations of the frequency responses may be calculated and the spatial average of that value may then be found. Ideally, these measurements would be made with and without equalization at the same microphone positions. The equalization coefficient for the equalized field may be divided by the coefficient for the unequalized field. The resultant factor is normalized and may be interpreted without comparing other factors. If the ratio is less than one, the equalization method was successful; if it is greater than one, equalization has introduced new problems in the field. This normalized factor may potentially assist in judging equalizations in different listening spaces. However, this would require more measurements to arrive at a valid comparison. For most applications normalizing an GLAEC by an unequalized GLAEC of the same listening environment is the most useful form.

As a demonstration, Figs. 5.16 and 5.17 show the resulting equalization from four different measurements used to equalize a system of five equal-strength point sources over a frequency range from 20 Hz to 200 Hz. The center of the system is at the point $(0, 2)$ in the figures, with the sound sources marked by $+$ and the sensor location marked by $\circ$. To the left of each plot is the ratio of the proposed GLAEC of the equalized field divided by the GLAEC of the unequalized system. The plots are ordered from left to right, top to bottom starting from the best. Notice that the

ordering is consistent with both the GLAEC value and the surface plot. These results show the best quantities for equalizing for the given source arrangement and, except of the case of the spatially averaged equalization, sensor location.

Perhaps some restrictions on sensor number and locations could be made to improve the reliability of the calculated GLAEC value. Further experimental work could be performed to judge a minimum number of microphones that should be used to ensure similar constant values of the GLAEC. Another improvement could be a recommendation on the minimum spacing of the sensors, as would be required to qualify a reverberation chamber, a process which is described in Nutter's work as well as in an ISO standard [48, 79].

5.3.3 Observations

The surface plots and the recommended GLAEC allows simple evaluation of the performed equalization of a sound field. In the process of developing the GLAEC, several features became apparent. Changing frequency range, source arrangement, or the sensor location alters the success of attempts to equalize a sound field. The effects of these changes are discussed here.

Frequency Range

Changing the frequency range over which equalization is performed changes the size of the regions where equalization is successful. Equalizing a narrow frequency range can help the performance, especially for low frequencies. At low frequencies the wavelength is longer, which in turn extends the region where an equalization filter successfully improves the frequency response of a sound field. Figures 5.18 through 5.22 show equalization over several frequency ranges using spatially averaged pressure, PED, KED, TED, and the vector magnitude of intensity to design an equalization

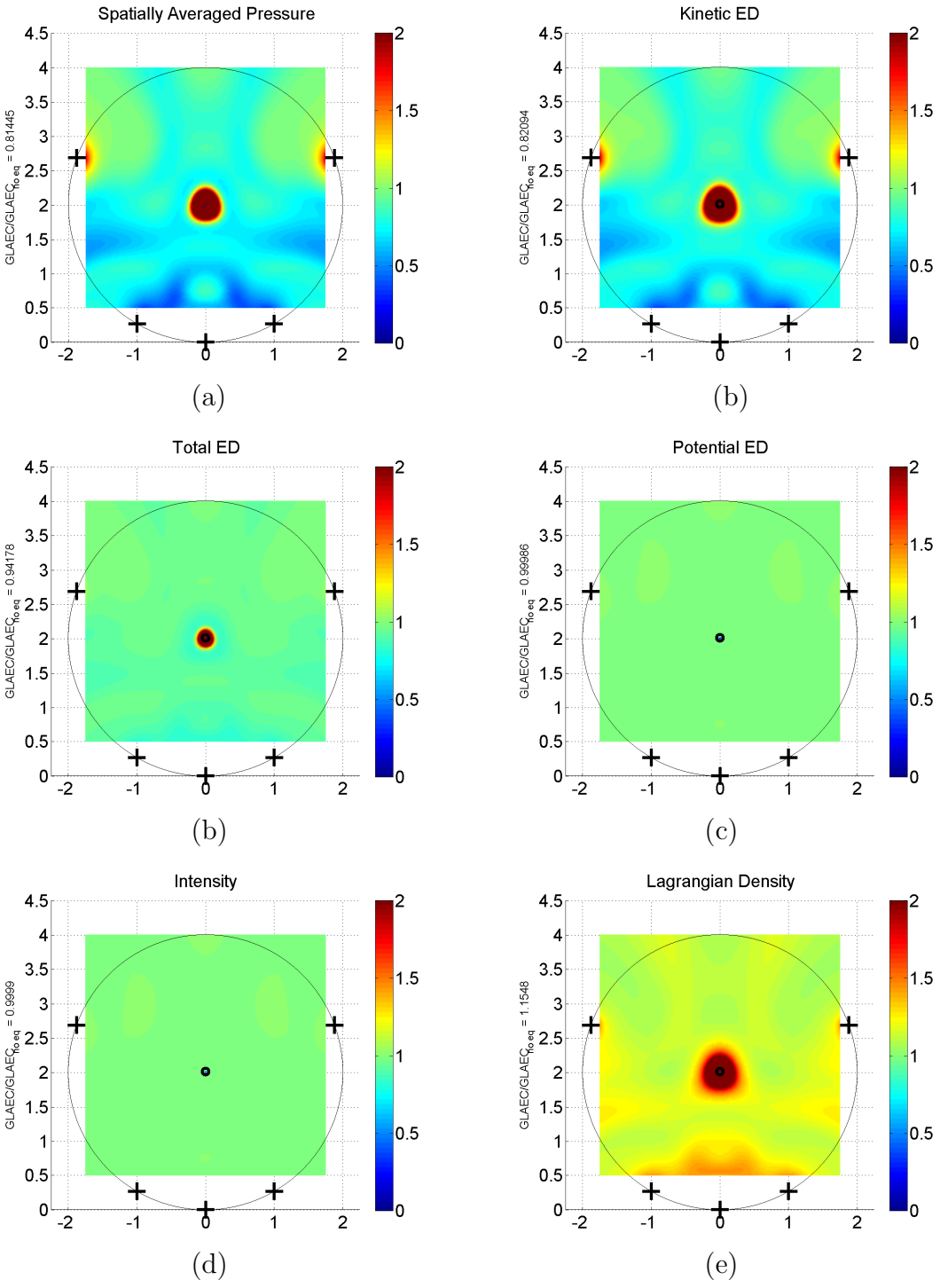

Figure 5.16 Examples of ranking equalization performance using the GLAEC and plots of the spectral standard deviation. Here the sensor is located 1 cm from the center point of the five source arrangement of point sources and marked by a ∘. The axes are labeled in meters.

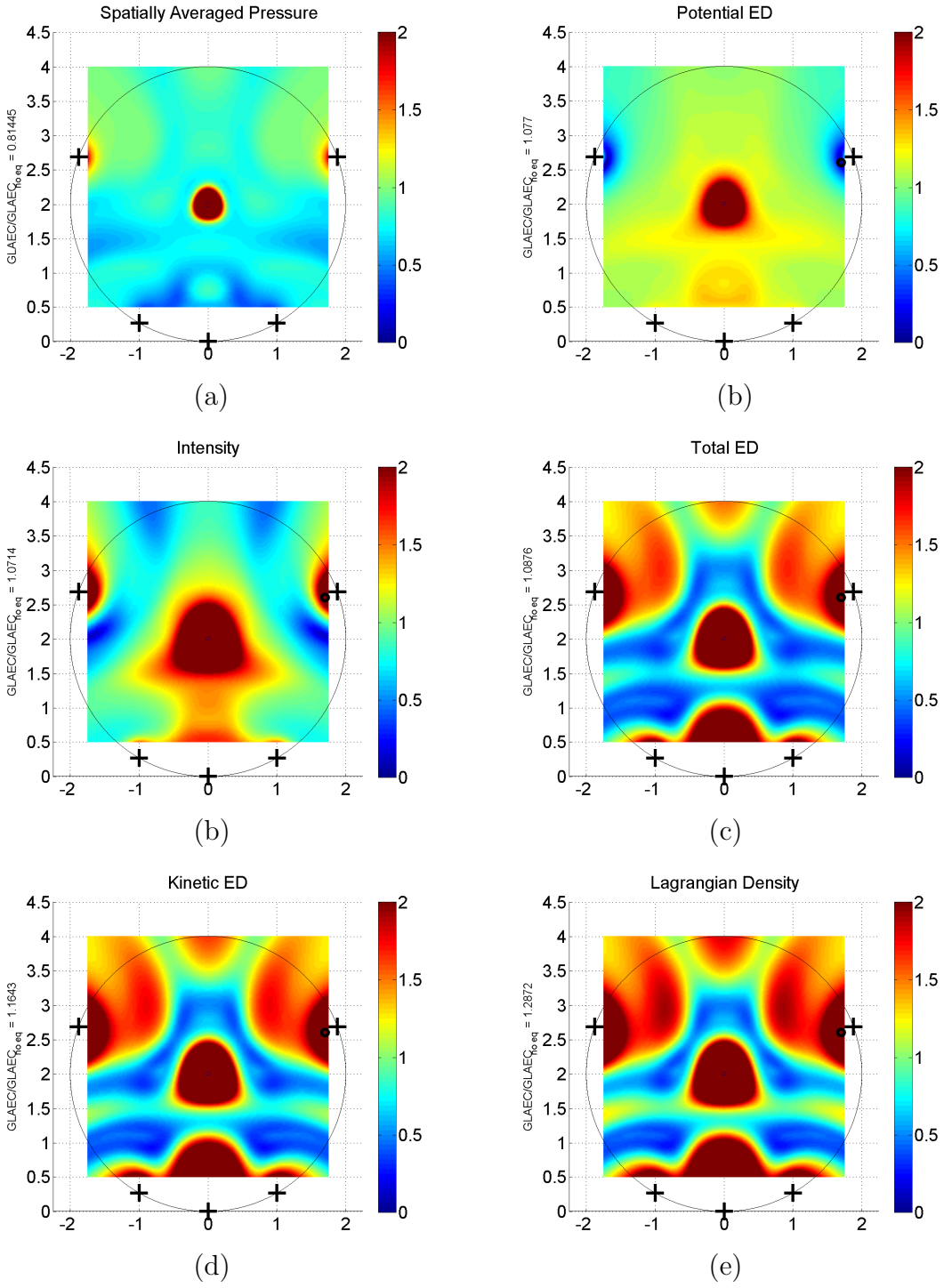

Figure 5.17 Examples of ranking equalization performance using the GLAEC and plots of the spectral standard deviation. The sensor is located at (1.7,2.6) and marked by a ∘. The axes are labeled in meters.

filter respectively. These plots show the spectral standard deviation of pressure magnitude over space.[3] These figures show that equalization over a large region is more likely for narrower frequency ranges. One item to note in these plots is that the position of the equalization sensor did not line up with the grid of the positions used to compute the spectral standard deviations on the sound field. Because of this, the color inside of the circle a combination of the points around the sensor. This is apparent in Fig. 5.19 and Fig. 5.23(d), especially at wider frequency ranges where the spectral standard deviation has more spatial variation due to the shorter wavelengths considered in the calculations.

Source Arraignment

Two source arrangements were principally used in this research; one consisted of a pair of point sources, the other consisted of five equal-strength point sources arranged like a five point surround sound system. Figure 5.23 shows plots of the spectral standard deviation of the equalized sound field produced by two equal-strength sound sources equalized over a frequency range of 20 Hz to 2 kHz divided by the spectral standard deviation over the same range of the unequalized sound field. Comparing Fig. 5.23 to Fig. 5.24, where the only difference is the source arrangement, shows the difference in the size of the region where equalization improves. Equalization of the two point source sound field produces a region with a curve where equalization is successful. This leads to a very limited region where equalizing the frequency response improves the sound field. However, equalization performed with five sources surrounding the listening region tended to have larger regions within the listening area with improved equalization. Remembering from Sec. 2.1.3 that a sound field in

[3]Using the pressure magnitude instead of the squared pressure magnitude adjusts the color scale but not the meaning of the results.

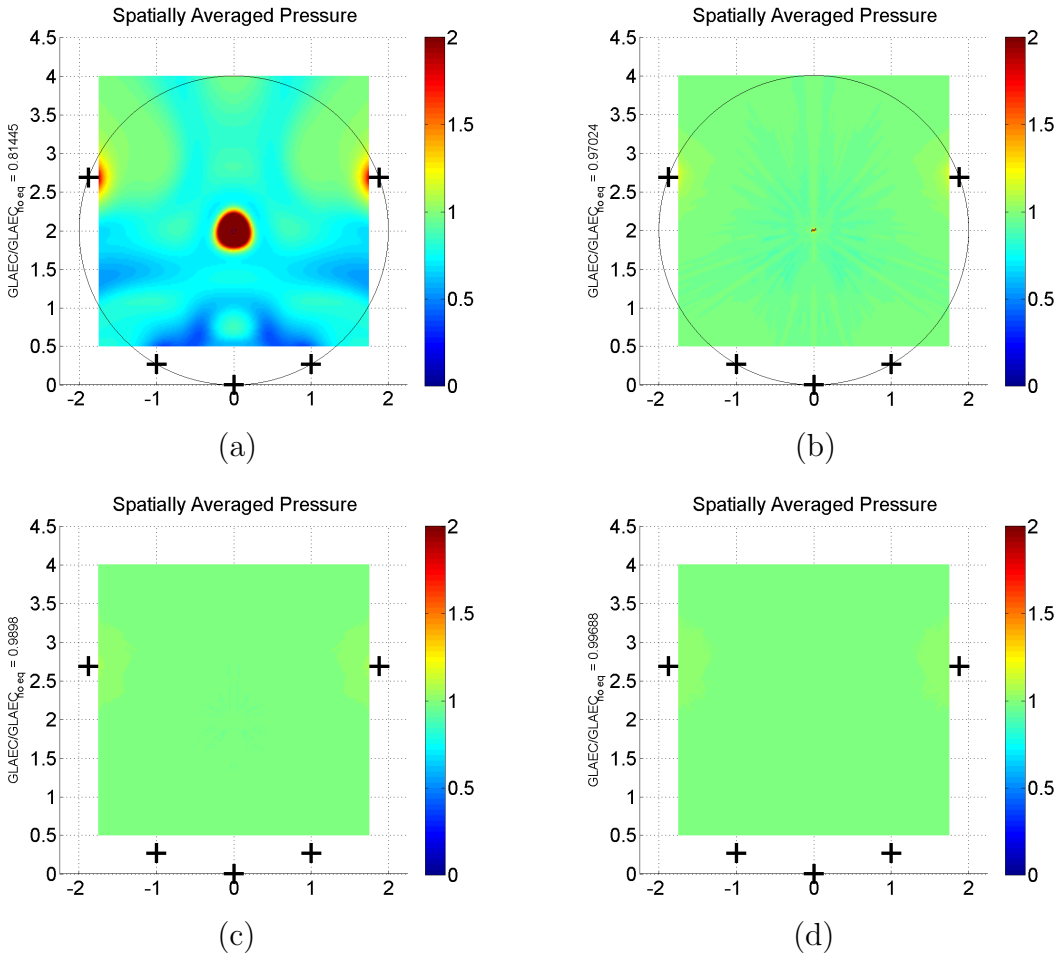

Figure 5.18 The standard deviation of the frequency response equalized using a spatially averaged squared pressure magnitude frequency response over a frequency range of (a) 20 Hz to 200 Hz, (b) 20 Hz to 2 kHz, (c) 20 Hz to 6 kHz, and (d) 20 Hz to 20 kHz. The sound sources are marked by +. The axes are labeled in meters.

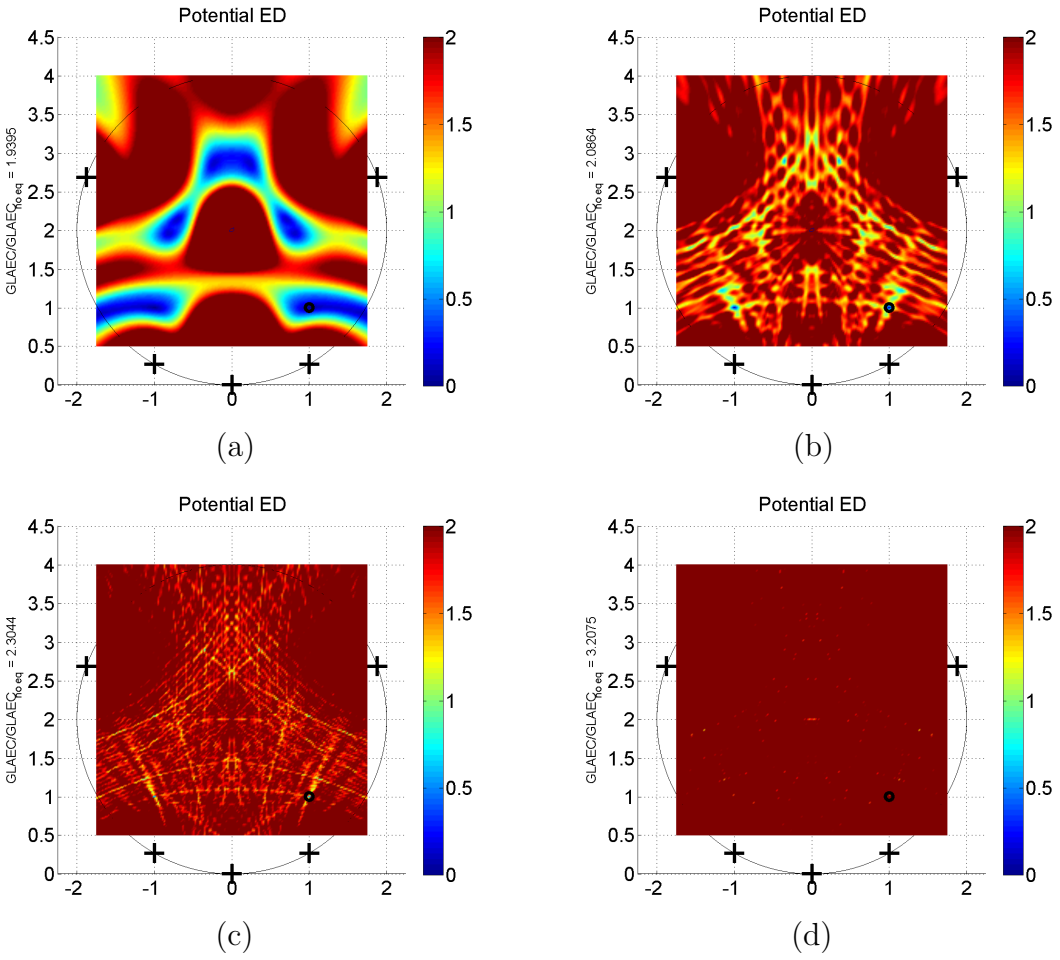

Figure 5.19 The standard deviation of the frequency response equalized using a PED frequency response over a frequency range of (a) 20 Hz to 200 Hz, (b) 20 Hz to 2 kHz, (c) 20 Hz to 6 kHz, and (d) 20 Hz to 20 kHz. The sound sources are marked by + while the sensor is located at the point marked by ∘. The axes are labeled in meters.

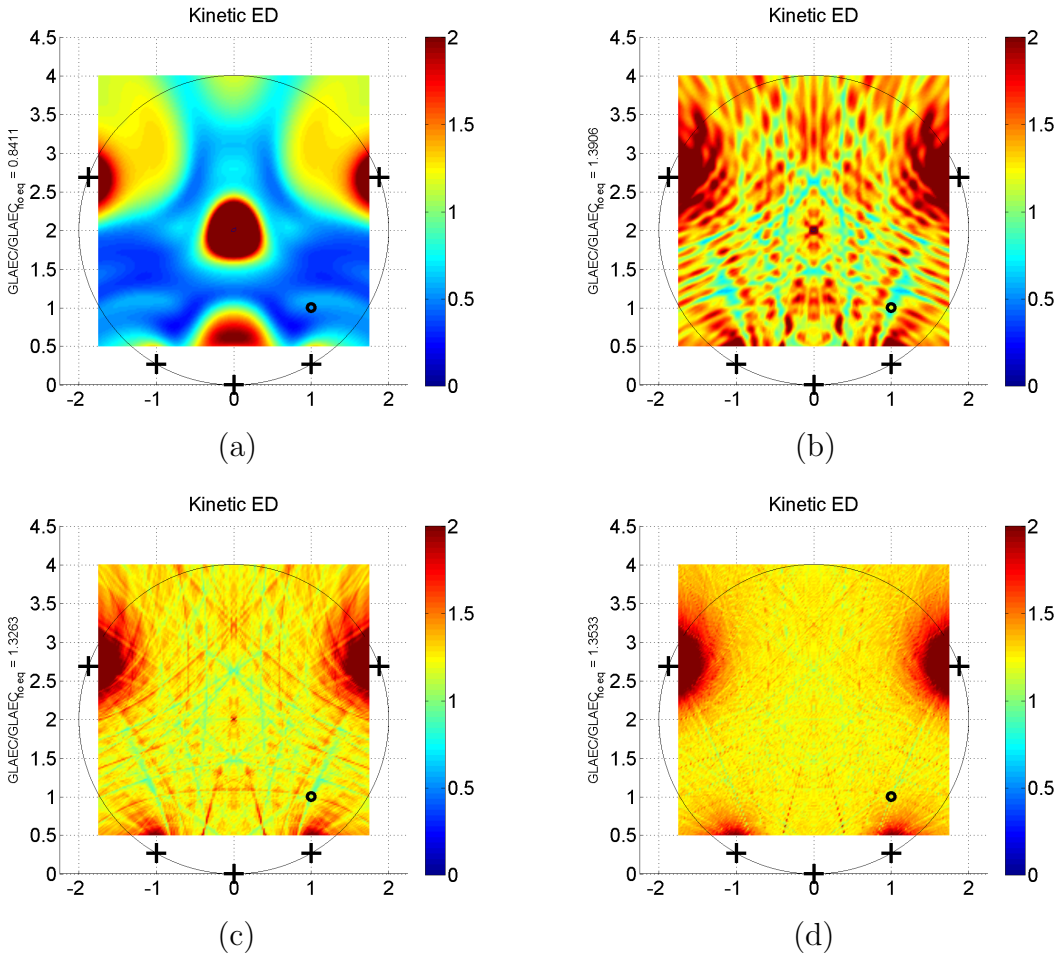

Figure 5.20 The standard deviation of the frequency response equalized using a KED frequency response over a frequency range of (a) 20 Hz to 200 Hz, (b) 20 Hz to 2 kHz, (c) 20 Hz to 6 kHz, and (d) 20 Hz to 20 kHz. The sound sources are marked by + while the sensor is located at the point marked by ∘. The axes are labeled in meters.

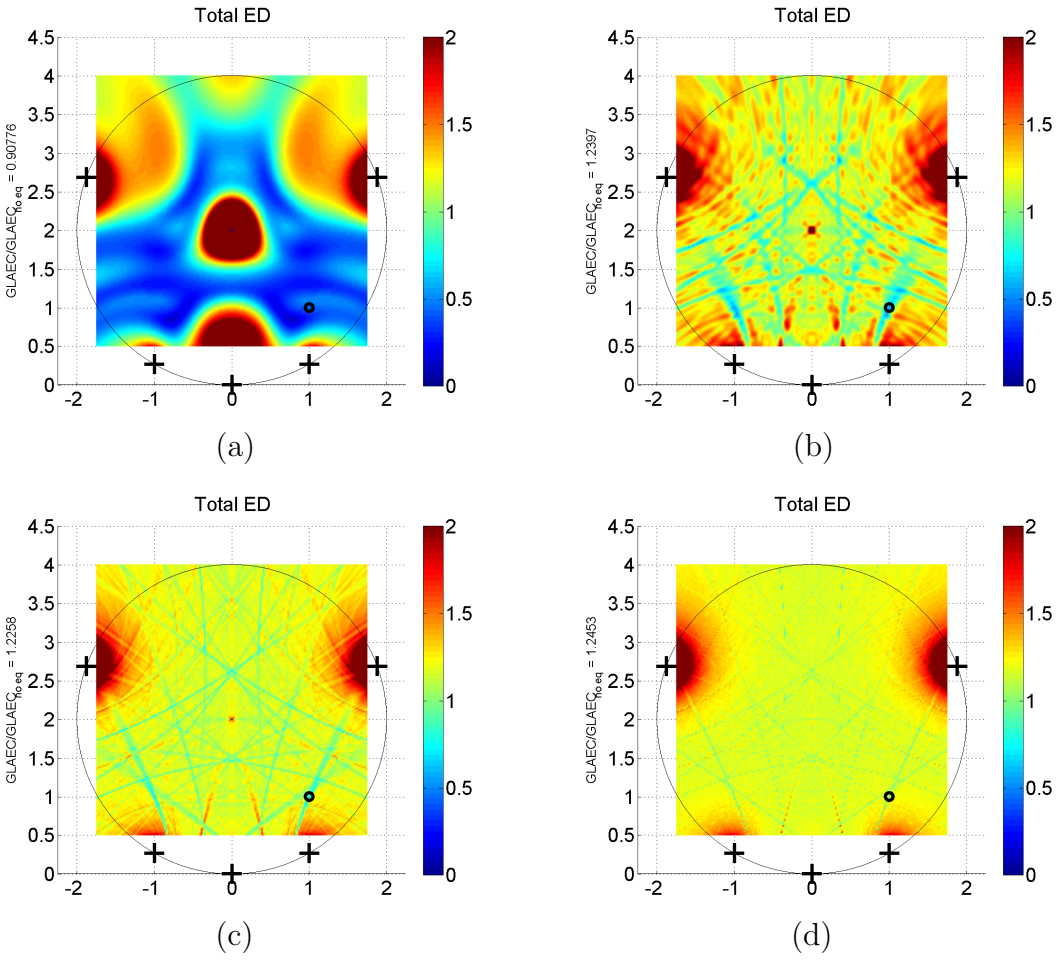

Figure 5.21 The standard deviation of the frequency response equalized using a TED frequency response over a frequency range of (a) 20 Hz to 200 Hz, (b) 20 Hz to 2 kHz, (c) 20 Hz to 6 kHz, and (d) 20 Hz to 20 kHz. The sound sources are marked by + while the sensor is located at the point marked by ∘. The axes are labeled in meters.

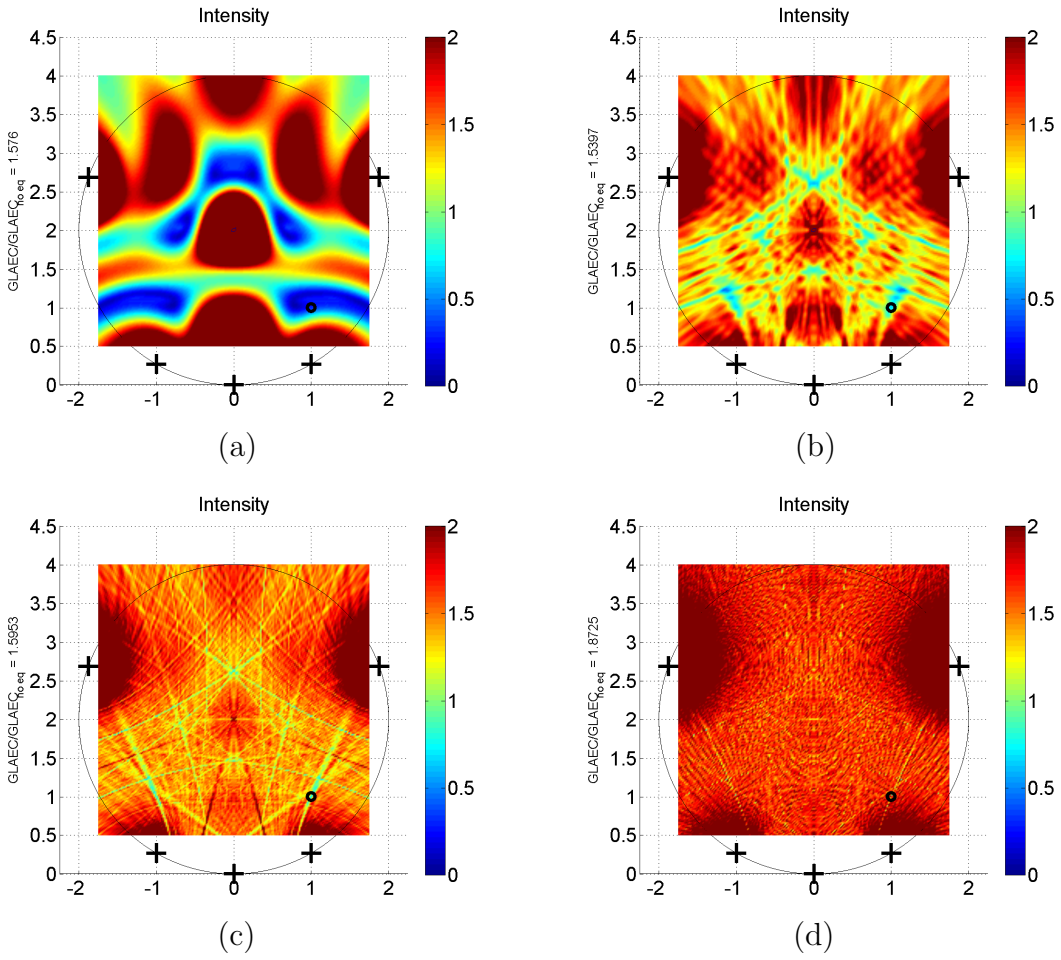

Figure 5.22 The standard deviation of the frequency response equalized using the vector magnitude of intensity frequency response over a frequency range of (a) 20 Hz to 200 Hz, (b) 20 Hz to 2 kHz, (c) 20 Hz to 6 kHz, and (d) 20 Hz to 20 kHz. The sound sources are marked by + while the sensor is located at the point marked by ∘. The axes are labeled in meters.

an enclosure may be modeled using many image sources, suggests that equalization of an enclosed field may be more successful than equalization of a few sources in a free field.

Reinforced Sound Fields

Cases where one or more of the sound sources contributing to a sound field is a reinforcing source introduces interesting complexities for equalization. To examine this situation, Figs. 5.25 and 5.26 have a side by side comparison of sound fields equalized with the filter designed for a point near the equalized source, marked by $+$, to one with a filter designed for a point near the unequalized source, marked by $\times$. Equalization is better globally within the listening area when the sensor is placed near the equalized source. One reason for the improved performance with the sensor placed near the equalized source is that the field near the equalized source benefits more from the filter, while the filter does less to alter the sound field near the unequalized sound source.

An interesting change happens with the symmetry of the system as well. When the sensor is placed near the unequalized source, there is a region near the equalized source where equalization is improved when using a filter designed using TED or intensity. The region where the equalization improves is opisit to the position of the location of the sensor used to design the equalization filter (see Fig. 5.26). With PED and KED, the same symmetry occurs, but the equalization is only degraded less, not improved, in the region away from the sensor (see Fig. 5.25). The same symmetric pattern results with the sensor placed near the equalized source for filters deigned using PED, TED, and the vector magnitude of intensity, but the improvement is much less drastic.

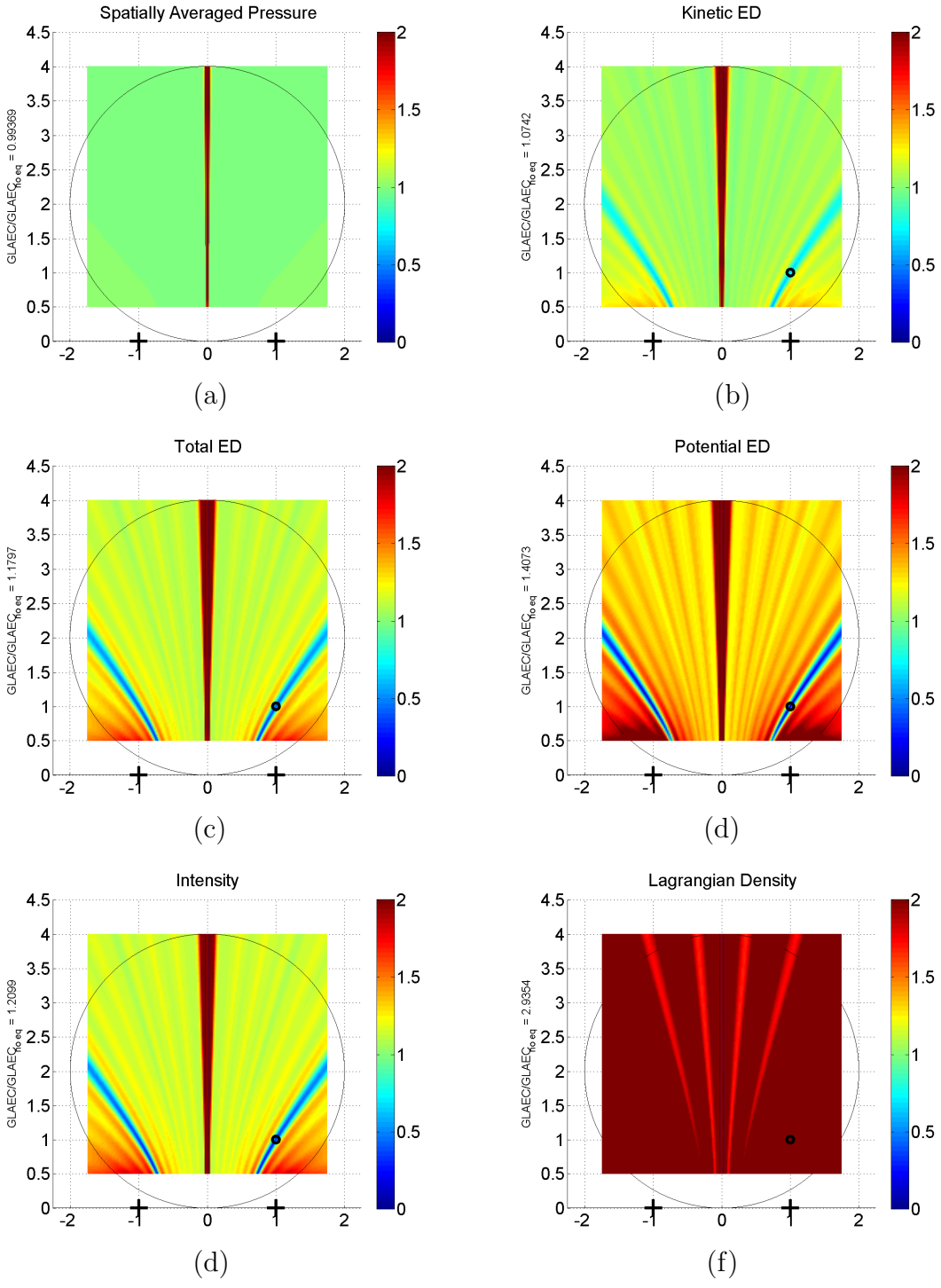

Figure 5.23 Two sound sources equalized with a filter designed for the point marked by ∘ over the frequency range of 20 Hz to 2 kHz.

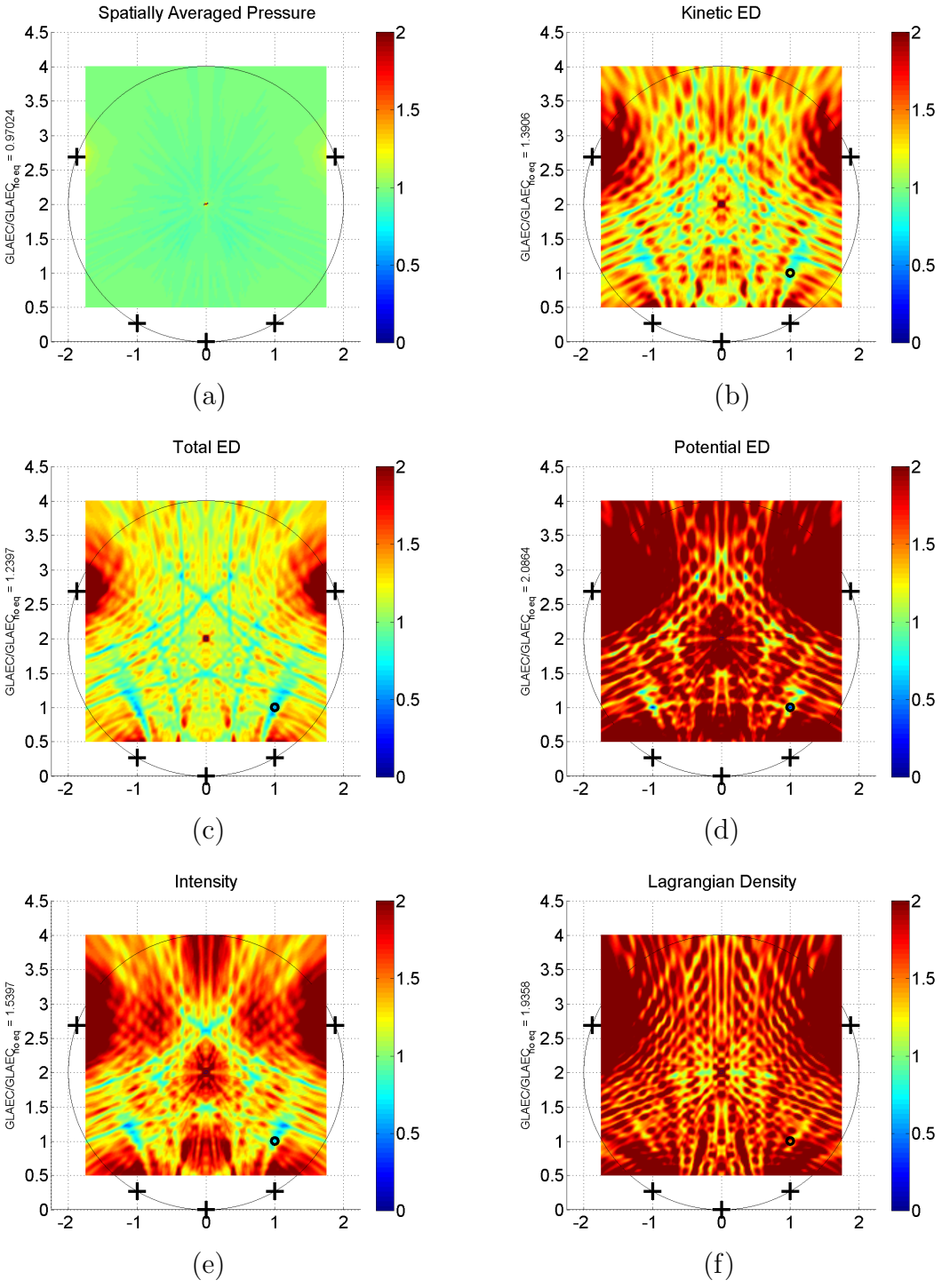

Figure 5.24 Five sound sources equalized with a filter designed for the point marked by ∘ over the frequency range of 20 Hz to 2 kHz.

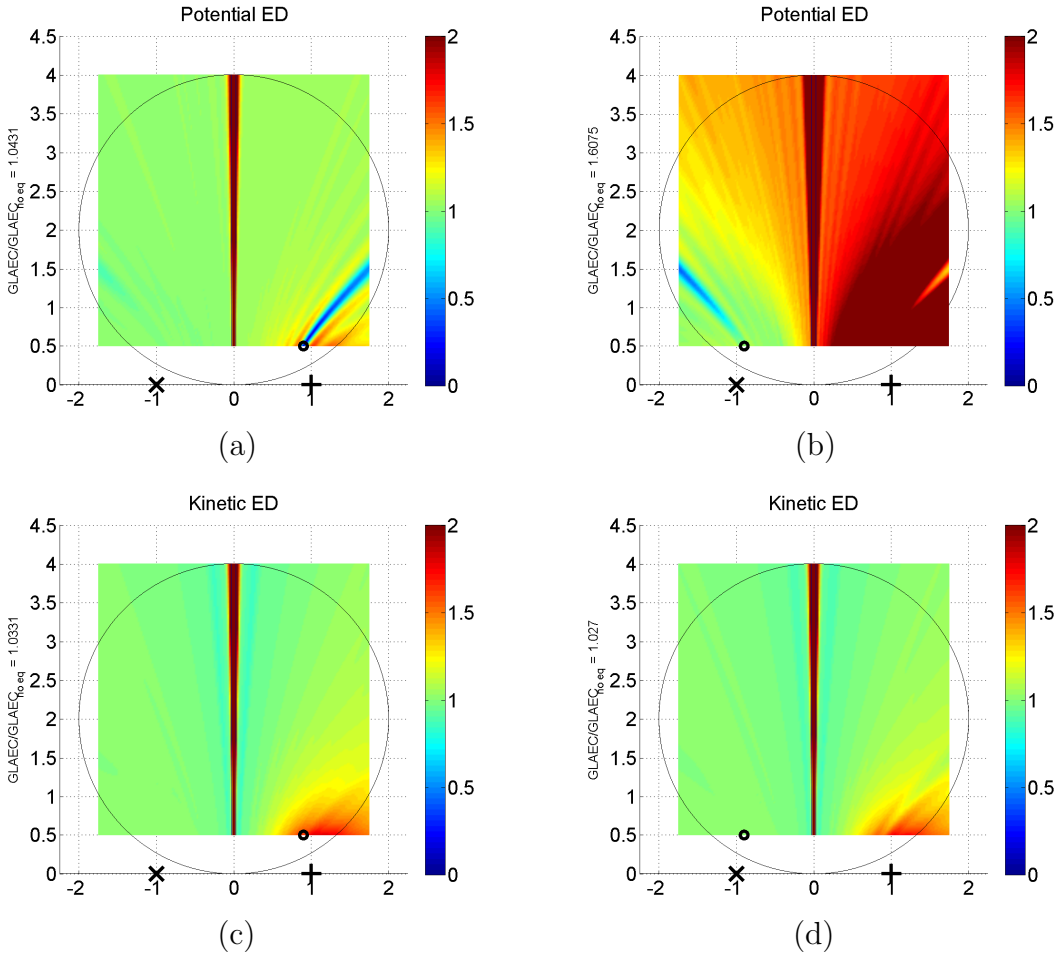

Figure 5.25 Comparison of a sound field equalized for a position near the equalized sound source, (a) and (c), to a sound field equalized with a position near the unequalized sound source, (b) and (d). Figures (a) and (b) show fields equalized using PED, while Figs. (c) and (d) show sound fields equalized using KED. These sound field is equalized from 20 Hz to 2 kHz. The $\times$ indicates the unequalized sound source, $+$ indicates the unequalized sound source and $\circ$ indicates the sensor location.

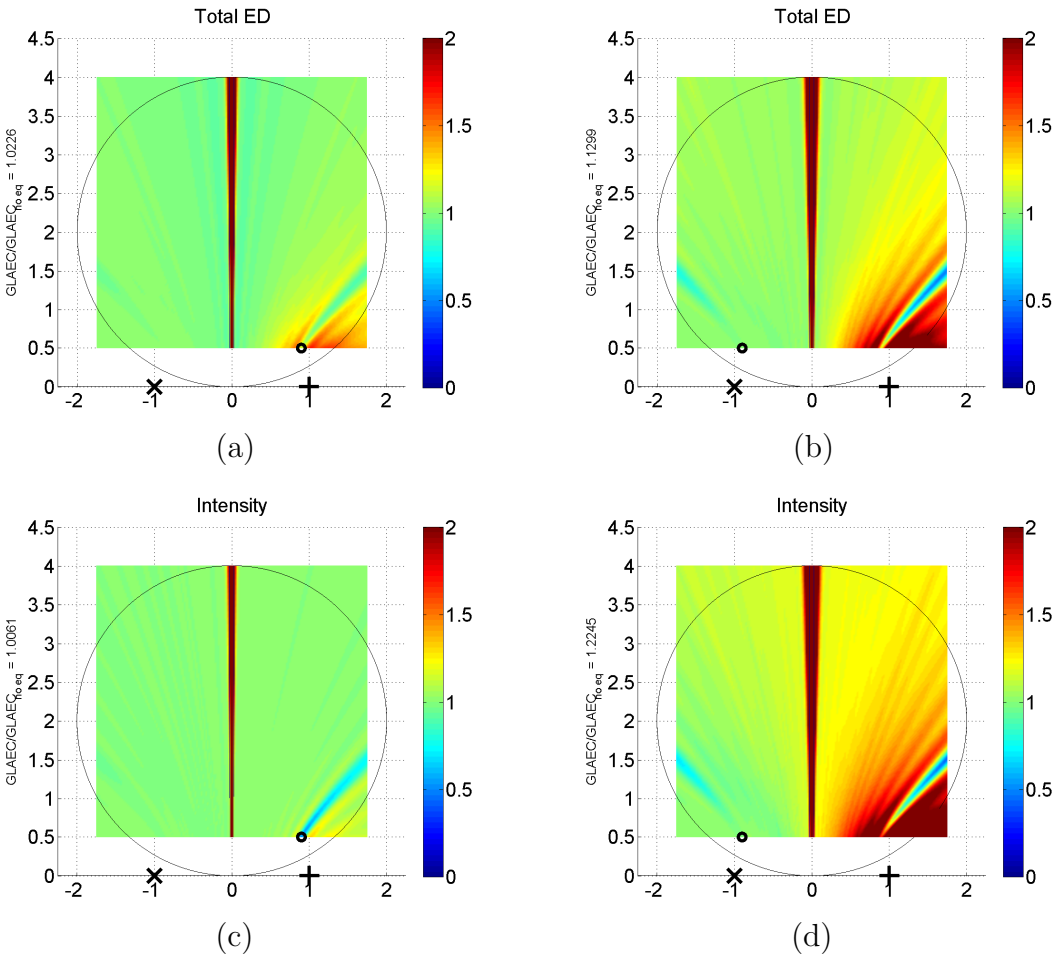

Figure 5.26 Comparison of a sound field equalized for a position near the equalized sound source, (a) and (c), to a sound field equalized with a position near the unequalized sound source, (b) and (d). Figures (a) and (b) show fields equalized using TED, while Figs. (c) and (d) show sound fields equalized using the vector magnitude of intensity. These sound field is equalized from 20 Hz to 2 kHz. The × indicates the unequalized sound source, + indicates the unequalized sound source and ∘ indicates the sensor location.

Symmetry

In the equalization plots throughout this thesis, it is apparent that equalizing symmetrically arranged equal-strength sound sources result in a sound field that is also symetric. This means that equalizing a symmetric sound field at one point will produce a corresponding equalized location on the opposite side of the axis of symmetry. This symmetry brakes down in cases when a source is driven with a different signal than the source that is located on the opposite side of the axis of symmetry. This property of symmetry is expected. An equivalent pattern would be generated using the sources on one side of the axis of symmetry and a reflecting plane placed along the axis of symmetry.

Sensor Position

To examine the effects of sensor location, a method that produces a plot similar to the MEDToPO plots for equalization has been generated. It involves calculating the GLAEC for equalization performed for different measurements at each point of a grid in a listening area. For each of these points the GLAEC is saved to an array of data. The data is used to generate a plot showing the value of the GLAEC as a function of the location of the sensor used to design the equalization filter. Examples of these visualizations are found in Figs. 5.27, 5.28, and 5.29.

Examining Fig. 5.27 reveals that placement of the sensor used to acquire data to design the filter does change the success of global equalization in the listening area. Comparing Fig. 5.27(a), which indicates good sensor locations, to Figs. 5.18(a), 5.19(a), 5.20(a), 5.21(a), and 5.22(a), which plots regions where equalization is improved over the same frequency range, there are some similarities in appearance. The regions where equalization is improved has a similar, but not identical, spatial arrangement to the regions where placing a pressure based sensor improves performance

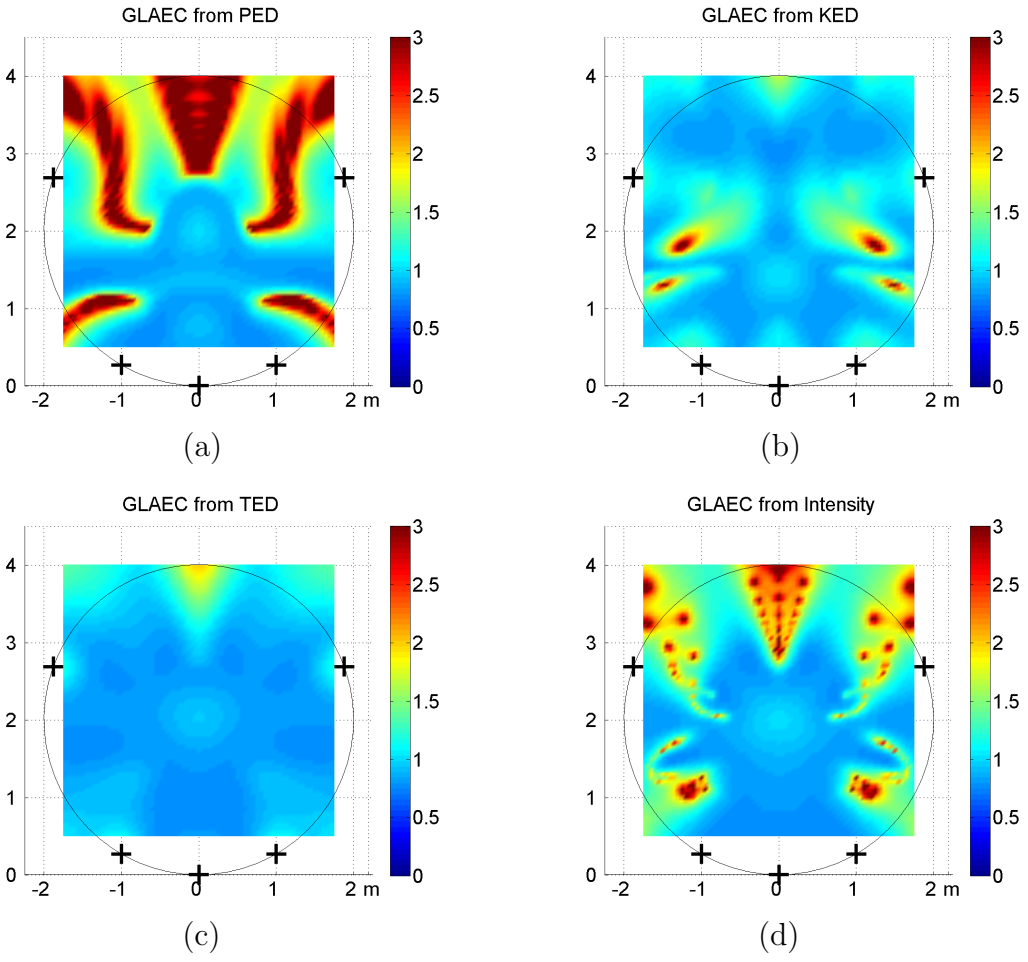

Figure 5.27 The GLAEC normalized by the GLAEC of the unequalized field as a function of sensor location for equalizing over a frequency range of 20 Hz to 200 Hz in 10 Hz increments. The sources are marked by +.

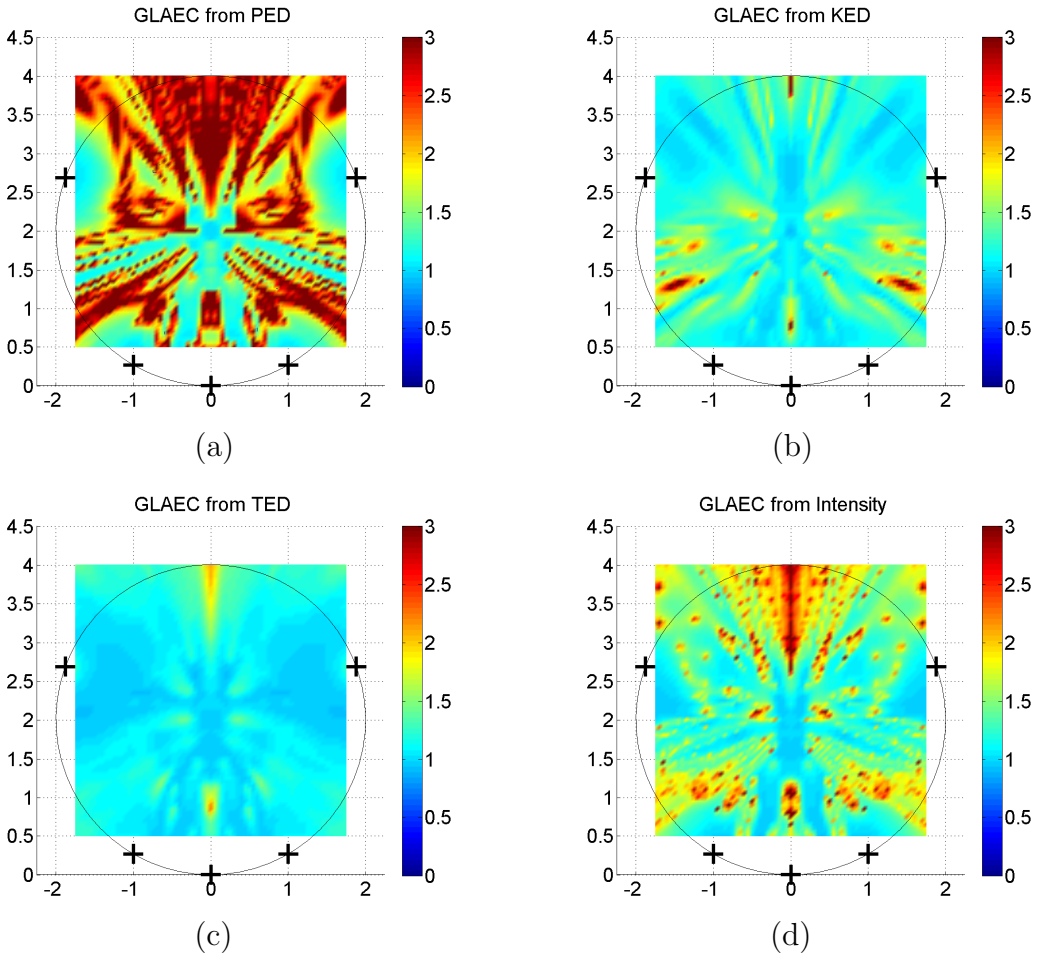

Figure 5.28 The GLAEC normalized by the GLAEC of the unequalized field as a function of sensor location for equalizing over a frequency range of 20 Hz to 800 Hz in 10 Hz increments. The sources are marked by +.

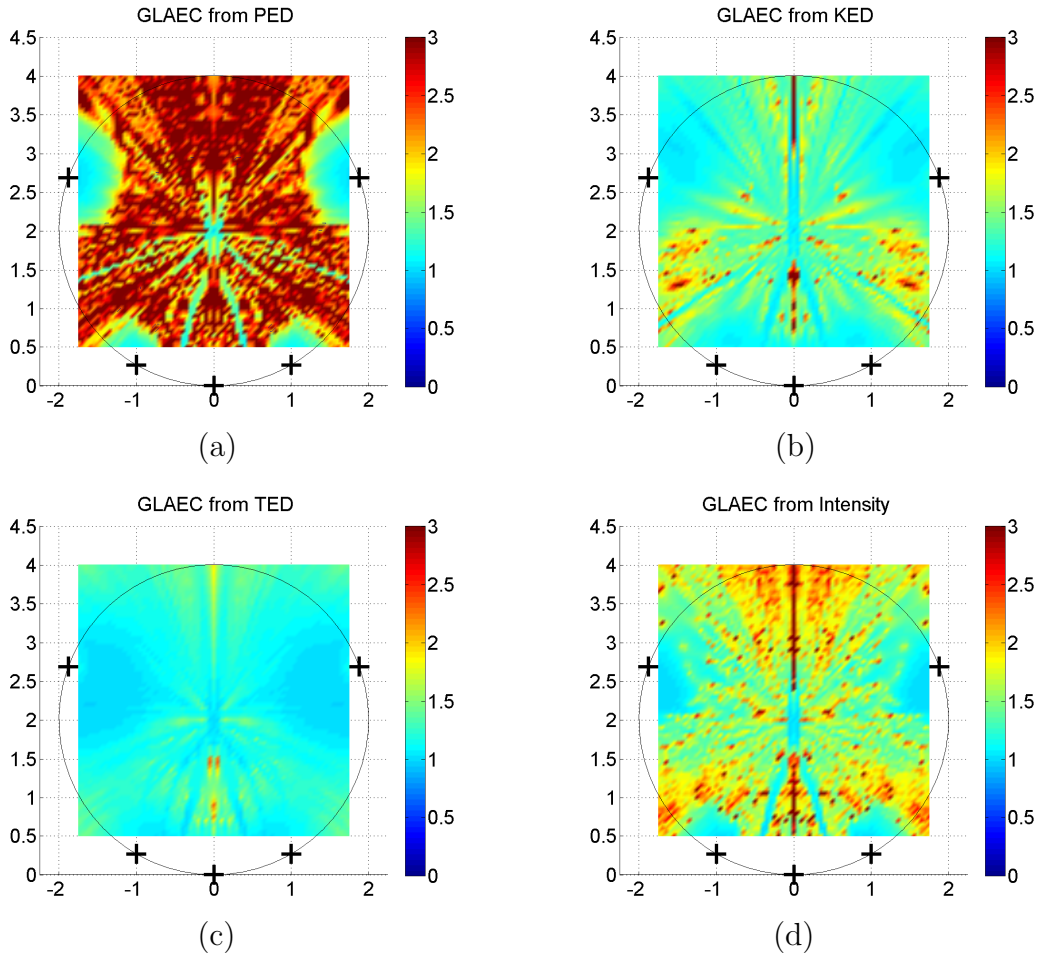

Figure 5.29 The GLAEC normalized by the GLAEC of the unequalized field as a function of sensor location for equalizing over a frequency range of 20 Hz to 2 kHz in 10 Hz increments. The sources are marked by +.

globally in the listening area. Figure 5.27 also reveals that for many locations in the region surrounded by the point sources a TED sensor will produce good global equalization of the listening area. It is relatively insensitive to sensor position. Figure 5.27 also reveals that any of the measurements may be used to improve equalization globally if the placement is chosen carefully to optimize the performance.

Expanding the frequency range, as shown in Fig. 5.28 for 20 Hz to 800 Hz and in Fig. 5.29 for 20 Hz to 2 kHz, decreases the success of the equalization of the sound field. Equalization over a broad band region using a single error sensor does not improve the equalization of the listening environment. For most sensor locations, using single measurement to design an equalization filter actually degrades the global equalization equalization when PED, KED or intensity are used. The best measurement for designing an equalization filter employing a single sensor is TED.

In the cases tested here, a filter designed using the TED measurements with a sensor placed inside the listening area can improve equalization over a limited low-frequency band, for example 20 Hz to 200 Hz, as shown in Fig. 5.27. With the TED sensor, care should still be taken to chose a good sensor location, but randomly placing the sensor within a listening region is less likely to result in degraded performance than the other measurements considered. With a TED sensor, for many sensor locations, the equalization is not degraded when a wider band is equalized, as shown in Fig. 5.28 for 20 Hz to 800 Hz and in Fig. 5.29 for 20 Hz to 2 kHz. For broadband equalization a better strategy may be to equalize the sources individually, rather than applying an identical filter to each source. For equalization, filters designed using TED measurements provide the best opportunity for successful global equalization with the least risk of degraded equalization for the use of a single sensor in a free field. TED also gives the best equalization over an extended region using a single measurement location to define the equalization filter.

5.3.4 Auralization

The method of images, discussed in Sec. 2.1.3, can be used to model an enclosed sound field. The point source model used in this research was used to generate an impulse response to produce auralizations of a recording in a room. Some of these recordings may be heard in the electronic version of Appendix F. These auralizations demonstrate the effects of equalization.

An auralization made using the techniques discussed in Sec. 3.3.1 may be convolved with the impulse response of an equalization filter to demonstrate the results of the equalization techniques. The result will demonstrate the success or failure of the equalization filter. This process may be written,

$$s(t) \otimes r(t) \otimes e(t) = p(t), \tag{5.4}$$

where $\otimes$ denotes convolution, $S(t)$ is the recorded signal, $R(t)$ is the response of the listening area, $E(t)$ is the response of the equalizing filter, and $P(t)$ is the resulting auralization showing the effects of equalization.

The equalization filter may also be convolved with the impulse response of a listening environment to show graphically the effects of equalization. Equation (5.4) may be transformed to the frequency domain to demonstrate this,

$$\hat{S}(f)\hat{R}(f)\hat{E}(f) = \hat{P}(f). \tag{5.5}$$

Dividing Eq. (5.5) by the input signal, $\hat{R}(f)$, yields the ratio of the output signal of the system to the input signal of the system, which is the definition of frequency response. This gives the combined frequency response of the listening environment and the filter, which may be expressed

$$\hat{S}(f)\hat{E}(f) = \frac{\hat{P}(f)}{\hat{R}(f)} = \hat{H}(f). \tag{5.6}$$

The resulting system impulse response may than be written,

$$s(t) \otimes e(t) = h(t). \tag{5.7}$$

The resulting responses may be plotted to visually understand the equalization process. Ideally, equalization will result in an impulse response that is a Dirac delta, $\delta(t)$, function and the the frequency response will be uniform over the spectrum.[4]

Some Example Cases

Using a single measurement point to equalize a sound field results in a more uniform frequency response at the measurement location; at other locations the resulting frequency response is often less uniform. To demonstrate this, equalization filters were designed for a free field sound environment using the computational models in this research. One set of equalization filters was made using measurements at one listening position while another set of equalization filters was deigned at another point. The impulse and frequency response measurements were generated for the equalization at the equalization point and at a point several centimeters away. These filters were convolved with the auralization of the room for a listener at the first location to provide a pair of auralizations. One auralization models what would be heard for a listener at the filter's correct position. The other demonstrates what would be heard by a listener at a position away from the filter's target location. Figures displaying the resulting responses were also made to illustrate the effects of equalization. For comparison, the unequalized responses are provided in Fig. 5.30. The examples in Figs. 5.31 through 5.36 an array of seven sources placed at (0,0,$n/2$) meters where n is the source number was used, expressed in Cartesian coordinates. In these figures,

[4]The following figures are shown a second time in Appendix F.3 along with the corresponding auralizations. This demonstrates how the plots indicate equalization.

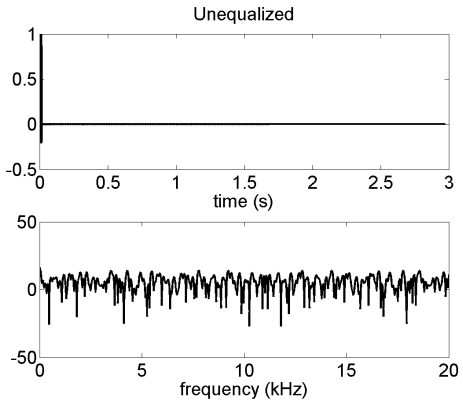

Figure 5.30 The impulse and frequency responses for the unequalized case are presented here.

the plot labeled (a) is for a sensor at (4.2,0,0) meters, and the plot labeled (b) has a sensor at at (4.0,0.2,0) meters.

Typically, the equalization filters designed using complex pressure performed the worst at locations away from the location for which the filter is designed, compared to the other measurements considered in this research. Figure 5.31 shows the equalized frequency responses. The impulse and frequency responses at the location that the filter was designed for match the ideal case. The impulse and responses at locations away from the sound source are much different when compared to the unequalized case. This can be seen by comparing Fig. 5.31 to Fig. 5.30.

Using the minimum phase portion of the pressure measurement to design the equalization filter produces a very similar result to those found using the entire complex pressure measurement. The resulting frequency responses are nearly identical; however, there are some notable differences in the impulse responses, see Figs. 5.31 and 5.32. The impulse response for the minimum-phase filter equalization has the Dirac delta function at time zero, while the complex equalization puts the function at another, delayed, location. The impulse response for the complex pressure equalization displays some pre-ringing suggesting that the modeled filter may not meet

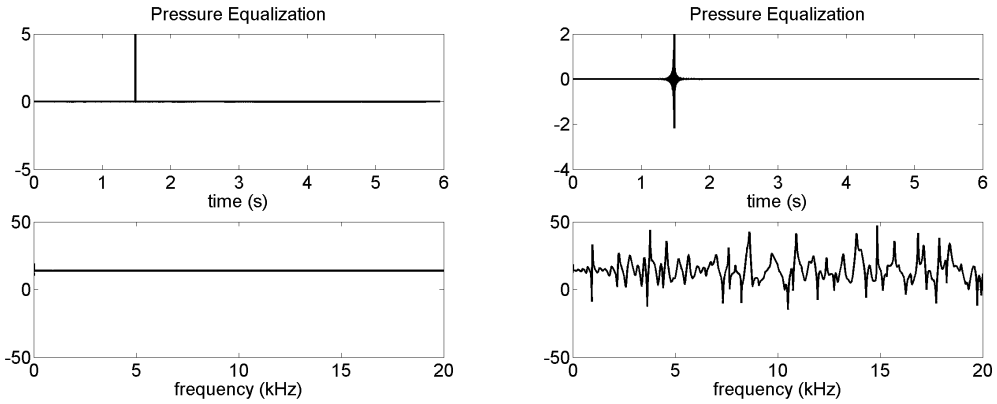

(a)

(b)

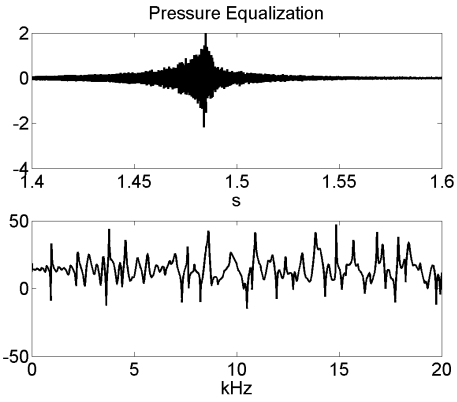

(c)

Figure 5.31 These are responses for a system equalized using (a) a filter designed for the listening position and (b) using a filter designed for a listening position several centimeters away. The equalization filters in this figure were designed using complex pressure. Plot (c) is a zoomed in version of (b).

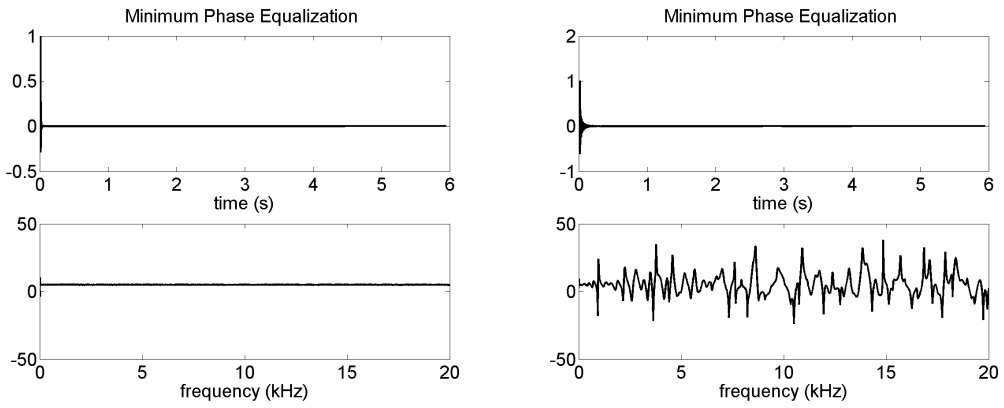

(a) (b)

Figure 5.32 These are responses for a system equalized using (a) a filter designed for the listening position and (b) using a filter designed for a listening position several centimeters away. The equalization filters in this figure were designed using the minimum phase portion of complex pressure.

the causality requirements of a real filter. The pre-ringing does not appear when the minimum phase of the pressure response is used to design a filter. This is shown to be true for both cases. A slight ringing is audible in the auralization representing equalization performed with a minimum phase filter designed for the listening position of the model. This ringing goes away if the impulse response is designed using a much longer impulse response, or if the sources of the frequency response are clustered closer together, thus resulting in a shorter duration of the excited portion of the impulse response.

Filters designed using potential energy density perform differently than those designed using complex pressure. At the location where the response is measured, equalization is less successful than for the equalization performed using complex pressure. When the filter designed for the other location is used, the potential energy density performs better than the filter designed using complex pressure. The equalization is still worse than the system would have been had no equalization been applied. This

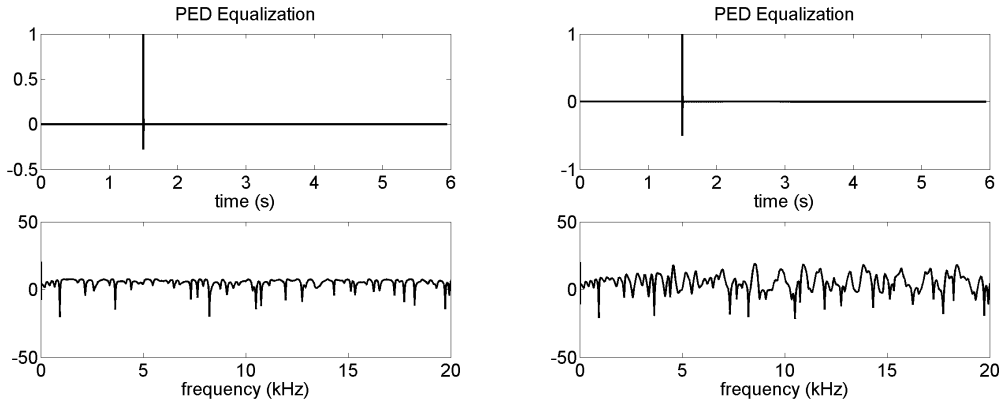

(a) (b)

Figure 5.33 These are responses for a system equalized using (a) a filter designed for the listening position and (b) using a filter designed for a listening position several centimeters away. The equalization filters in this figure were designed using PED.

can be seen comparing the plots of the responses given in Fig. 5.33 to those found in Figs. 5.30 and 5.31. The degradation of equalization at points away from the filters target location occurs because the filters response is finely tuned to the specific location of the source. With complex pressure, the phase information is also included, so a filter designed using the complex pressure is more sensitive to position than one that only deals with the squared magnitude of the sources.

Filters designed using KED measurements typically perform worse than the PED counterparts. Still, in the case where the equalization filter is designed for a position away from the actual listener location, the results are better than those using equalization filters designed using complex pressure. The peaks in the complex pressure frequency response produce strong resonances shown in Fig. 5.31. The majority of the peaks in the frequency response for equalization performed using KED, are not as dominant as those for equalization performed using complex pressure, see Fig. 5.34.

Equalization filters designed using TED perform better than the the KED and

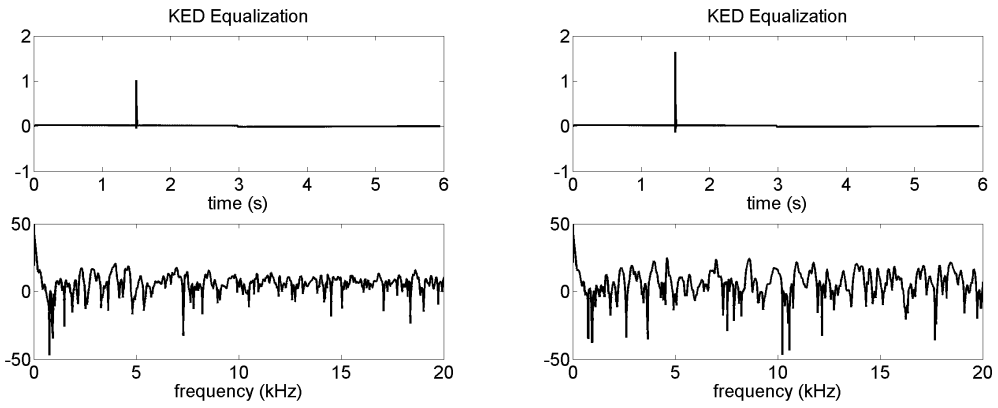

(a) (b)

Figure 5.34 These are responses for a system equalized using (a) a filter designed for the listening position and (b) using a filter designed for a listening position several centimeters away. The equalization filters in this figure were designed using KED.

PED versions of equalization. At the location where the filter is designed, the frequency response can become better than the unequalized sound measurement. The equalized frequency response still deteriorated with the equalization filter designed for the remote location, approximately 28 cm away. However, the filter designed using a TED measurement caused less deterioration at other locations than the other equalization methods discussed here.

In the process of evaluating the performance of the equalizing filters, it became apparent that the the impulse response used to equalize the sound field needs to be much longer than just the time length of the modeled sound source arrangement. The preceding figures were generated from calculations where the sound field and filters were built using responses 2^{17} terms long at a sample frequency of 44.1 kHz. Figure 5.36 shows the same equalization setup as that found in Fig. 5.31, but this time the sound field was modeled using 2^{13} terms. The resulting impulse response has some extra ripples, indicating some residual reverberations. The frequency response

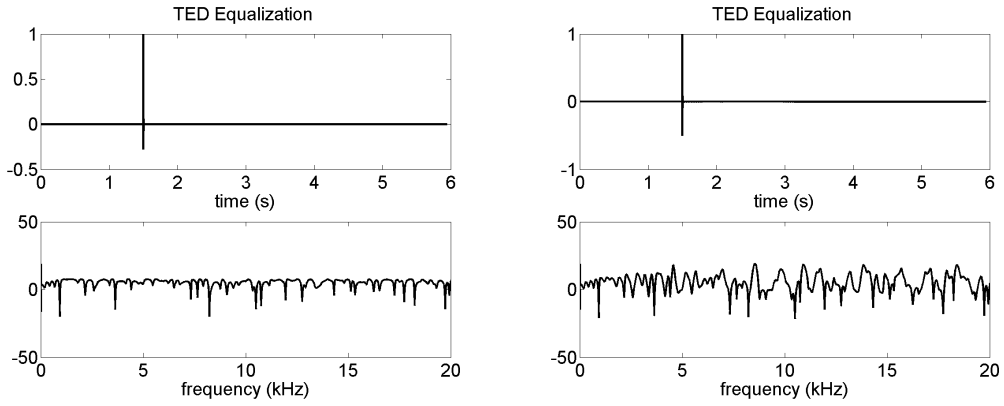

(a) (b)

Figure 5.35 These are responses for a system equalized using (a) a filter designed for the listening position and (b) using a filter designed for a listening position several centimeters away. The equalization filters in this figure were designed using TED.

for the filter designed for the listening location results in a frequency response with some deviations from the ideal case. In the case where the filter was designed for another location, there is more visible modulation in the frequency response. The auralizations demonstrate this degradations as well. The degradation is apparent as a slight echo, which is indicated by additional ripples in the plot of the impulse response.

This example shows the inefficiency of these techniques for designing an equalization filter. The filters designed using the 2^{17} points correspond to a real world measurement on the order of 143 thousand years. The filterers designed using 2^{13} points correspond to a measurement taking 14 years. This method does show a proof of concept that a filter with an inverse frequency response can equalize the frequency response at a point. This also shows that the spatial sensitivity of equalization. Perhaps a better approach to equalization could be to use smoothing or curve fitting technique.

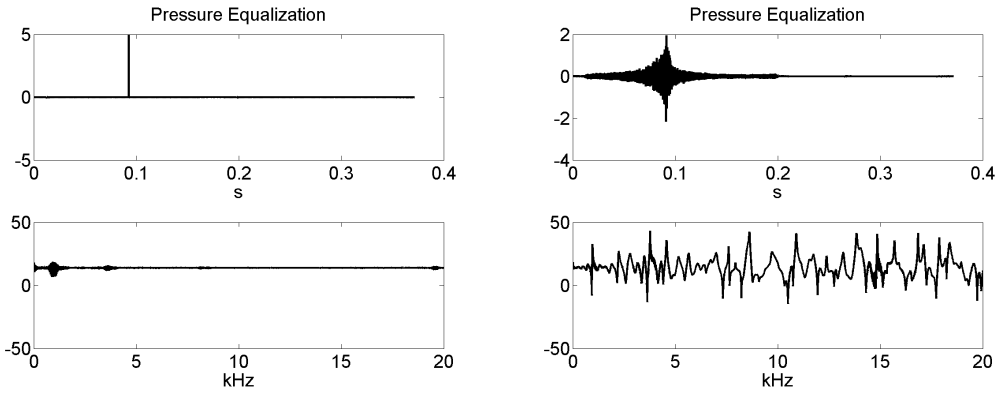

(a) (b)

Figure 5.36 These are responses for a system equalized using (a) a filter designed for the listening position and (b) using a filter designed for a listening position several centimeters away. The equalization filters in this figure were designed using complex pressure. This is similar to Fig. 5.31, the difference is that this model used significantly fewer terms to generate the responses for designing the filter an the model.

5.4 Toward Enclosures

The method of images may be used to model a sound field in an enclosure. This is done by generating many virtual sound sources to model the sound field. This model will produce frequency and impulse responses that represent a sound field that may be used to generate auralizations that simulate the sound field. One big constraint for modeling a sound field using these virtual sources is the time it can take for a single point. Another limitation comes from modeling absorptive absorptive surfaces for multiple reflections in a three dimensional field.

One important thing to note with this model is that it quickly become unreliable for room impulse responses that last more than a few hundred milliseconds. Even with classical air absorption added to the model, the reverberation becomes excessive for long impulse responses. For this reason the auralizations included in this work are generated using limited time length impulse responses. Even though the model used

to verify the model was for a reverberant room with dimensions of 5x6x7 m, which should have a reverberation time on the order of several seconds, it was difficult to model a response longer than a couple of seconds. The longer frequency responses did not sound like a reverberant room in the computer model used.[5] One possible necessity for this model is a practical method for modeling the wall absorption on each reflection. This type of correction is outside of the scope of the research considered here.

[5]Two auralizations showing the sound for the modeled room using different length impulse responses are found in Appendix F.2 in Table F.2.

Chapter 6

Conclusions

The preceding chapters have discussed methods for controlling sound in a free field. Analytical and computational models have been used to evaluate the performance of different error sensors used for active noise control (ANC) and equalization. Minimized energy density total power output (MEDToPO) plots were developed to show the effect of sensor location on the performance of global ANC. The investigation of equalization motivated the exploration of an objective factor for evaluating the performance of equalization in a listening environment. This chapter summarizes the results discussed in the previous chapters, draws conclusions, and suggests further research.

6.1 Near Field Sensor Active Noise Control

The research for ANC indicates that there are limitations on using near field error sensors. The results show that the total energy density (TED) is spatially uniform in the near field, which would allow freedom in choosing the placement of the error sensor. However, this uniformity only exists at higher frequencies for which

active control techniques based on strong acoustic coupling fail to produce satisfactory results. Kinetic energy density (KED) measurements did not improve the success of active sound control either. Potential energy density (PED) was shown to produce better results than TED or KED for controllable lowe frequencys. Regardless, there are still many limitations on the use of error sensors in the near field for active noise control.

The MEDToPO plots presented in the thesis verifiy the assertion made by Hansen and Snyder concerning the placement of error sensors for ANC [2]. They indicated that error sensors should be placed where the detected measurement is attenuated the most when comparing the field generated by the uncontrolled source to the optimally controlled field [2]. Comparing plots that indicated where the error sensors should be placed (according to Hansen and Snyder) to MEDToPO plots reveals excellent agreement for pressure based measurements. For KED and TED, the MEDToPO plots show that the positions suggested for use by Hansen and Snyder are correct, but the MEDToPO shows additional locations where control may also perform well.

Another feature of the MEDToPO is that it indicates the sensitivity of ANC performance to the exact location of error sensors. In some applications an error sensor may be placed a small distance away from the best location for performing ANC, while other applications require very accurate and precise placement of the error sensor. The MEDToPO scheme was used to determine the best measurement cases of free-field ANC. It was useful because it shows the maximum possible attenuation using a given error quantity, as well as indicating the regions where sensors using that error quantity perform the best.

6.2 Equalization

The global listening area equalization coefficient (GLAEC), defined in Sec. 5.3.2, and surface plots of the spectral standard deviation of the equalized sound field divided by the spectral standard deviation of the unequalized field were used to evaluate the success of sensor techniques used to design equalization filters. As expected, equalization with filters designed using a spatial average of the pressure frequency response performed better than any other filter designs. The Lagrangian density filters performed worse than the other measurements considered. The PED and complex pressure consistently performed poorly for global equalization. These two measurements provided filters that successfully equalized at the sensor location, but they performed very poorly in the rest of the listening region. This was noted from the surface plots of the spectral standard deviation of the equalized fields divided by the spectral standard deviation of the unequalized fields and also by looking at the frequency response at the sensor location. Other measurements—KED, TED, and the vector magnitude of intensity—did not improve equalization globally in the free field environment for a wide frequency range when the sensor was not surrounded by sources. The performance of these measurements suggest that, in a free field, equalization filters should be designed using more than one measurement location.

Equalization over a narrower low frequency band performed better for all of the measurements used to design the equalization filters. Because of the long wavelengths, there is less variation in the frequency response over position at these lower frequencies. In fact, filters designed using PED, KED, TED, and intensity had much better success at low frequency over limited ranges than for broad-band ranges. For equalization on these narrow band frequency ranges, global improvement is achievable using PED, KED, TED and intensity. Over the narrow-band frequency ranges, TED

yielded more freedom in the placement of the sensor used for designing the equalization filter, and thus is the recommended measurement for designing an equalization filter in a free field, especially when the listening region is surrounded by sources. Cases where equalization was performed using TED, where the listening region was surrounded by five equal-strength point sources with a limited low-frequency bandwidth, provided freedom in choosing the error-sensor location, while still achieving equalization over an extended region.

Though the chosen single point filters did not successfully improve equalization over a large listening area over a broad-band, they were useful for finding a factor that helps evaluate the performance of equalization in an extended region. This was called the global listening area equalization coefficient (GLAEC). The techniques discussed previously were used to generate plots and calculate potential equalization factors to establish the GLAEC. These plots and equalization factors were compared to one another to find a factor that correctly and consistently evaluates the success of equalization.

The quantity that performed best, $\mu_s(\sigma_f)$, is found by taking the spatial average of the spectral standard deviation from several measurement positions. However, this value did not perform correctly in every case. The primary difficulty for all of the proposed equalization coefficients was their inability to distinguish small differences in global equalization. The factor $\mu_s(\sigma_f)$ performed better than the other coefficients in tests intended to make distinguishing the performance of equalization methods difficult. In order to give this coefficient clear meaning, it is recommended to use it in the form of a ratio

$$GLAEC = \frac{\mu_s(\sigma_f)_{equalized}}{\mu_s(\sigma_f)_{unequalized}}. \tag{5.2}$$

When this value is less than one, the overall equalization of the listening area is improved by the equalization method.

Plots of the GLAEC as a function of space demonstrated that equalization could be performed to find good locations for placing an error sensor to equalize a sound field. These plots showed that over a low-frequncy limited band, TED provided the most freedom for placing an error sensor and achieving an overall improvement of the equalization in a listening region. These plots may also be used to choose optimal locations for the error sensors in an experiment.

6.3 Further Research

Most research involving equalization is focused on improving high fidelity sound systems. However, there are other situations in which equalization may be useful. Equalizing a system can produce some dereverberation of the detected signal in a listening space. Commonly, public address systems are used to make announcements. In some situations, subway stations for example, the reverberation destroys speech intelligibility. In theory, implementing a good equalization filter in line with the existing public address system could reduce the reverberation at a discrete listening position. Further research could determine if dereverberation could work more globally for a defined listening area. The issues at hand are first, determining the appropriate equalization filter, and second, checking whether other options such as installing absorptive materials in these rooms would perform better and be more cost effective. In some cases a combination of passive and active approaches may be prudent.

Equalization using more exotic methods, like ED and intensity, may produce more successful results for other cases. In enclosures, ED measurements can perform better for ANC than they do in the free field. A similar improvement in performance may exist for equalization. Equalization filters designed using an average PED measurement produce better equalization than those designed using one pressure measurement. A

spatial average of several measurements may improve equalization employing filters defined by other measurements. A minimum number of measurements necessary to adequately design an equalization filter should also be investigated if the spatial average of other measurements does indeed improve equalization results. The spacing of the error sensors should also be determined.

The GLAEC relies on a number of randomly located measurements. A limitation on the number of sensors necessary to consistently calculate the GLAEC value could be found. Work could also be done to recommend an appropriate sensor spacing to improve the consistency of the value. Currently, the GLAEC only works well to rank equalization methods. Specific requirements on sample size and sensor spacing may improve the consistency of the GLAEC value. With these requirements, the GLAEC could be used to compare equalization of different listening spaces. Area weighting the effective sample areas of the sensors and methods for appropriately normalizing the data used to compute the GLAEC may improve its consistency.

References

[1] X. Qiu, C. Hansen, and X. Li, "Comparison of near-field acoustic error sensing strategies for the active control of harmonic free field sound radiation," Journal of Sound and Vibration **215,** 81 – 103 (1998).

[2] C. H. Hansen and S. D. Snyder, *Active Control of Noise and Vibration* (Chapman and Hall, London, 1997), p. 696.

[3] O. Kirkeby and P. A. Nelson, "Reproduction of plane wave sound fields," The Journal of the Acoustical Society of America **94,** 2992–3000 (1993).

[4] P.-A. Gauthier, A. Berry, and W. Woszczyk, "Sound-field reproduction in-room using optimal control techniques: Simulations in the frequency domain," The Journal of the Acoustical Society of America **117,** 662–678 (2005).

[5] A. O. Santillan, "Spatially extended sound equalization in rectangular rooms," The Journal of the Acoustical Society of America **110,** 1989–1997 (2001).

[6] P. A. Nelson and S. J. Elliott, *Active Control of Sound* (Academic Press Ltd., San Diego California, 1992), pp. 162–175.

[7] G. Schiffrer and D. Stanzial, "Energetic properties of acoustic fields," The Journal of the Acoustical Society of America **96,** 3645–3653 (1994).

[8] P. A. Nelson, A. R. D. Curtis, S. J. Elliott, and A. J. Bullmore, "Miminum Power Output Of Free Field Point Sources and the Active Control of Sound.," Journal of Sound and Vibration **116,** 397 – 414 (1987).

[9] P. A. Nelson and S. J. Elliott, *Active Control of Sound* (Academic Press Ltd., San Diego California, 1992), pp. 235–237.

[10] P. A. Nelson and S. J. Elliott, *Active Control of Sound* (Academic Press Ltd., San Diego California, 1992), pp. 277–279.

[11] J. Mourjopoulos, "On the Variation and Invertibility of Room Impulse Response Functions.," Journal of Sound and Vibration **102,** 217 – 228 (1985).

[12] S. T. Neely and J. B. Allen, "Invertibility of a room impulse response," The Journal of the Acoustical Society of America **66,** 165–169 (1979).

[13] J. N. Mourjopoulos, "Digital equalization of room acoustics," AES: Journal of the Audio Engineering Society **42,** 884 – 900 (1994).

[14] R. B. Schulein, "In Situ Meqsurement and Equaliztion of Sound Reproduction Systems.," Journal of the Audio Engineering Society **23,** 178 – 186 (1975).

[15] B. McCarthy, *Sound Systems: Design and Optimization* (Focal Press, Oxford UK, 2007), pp. 22–24.

[16] B. McCarthy, *Sound Systems: Design and Optimization* (Focal Press, Oxford UK, 2007), pp. 235–239.

[17] S. J. Elliott and P. A. Nelson, "Multiple-point equalization in a room using adaptive digital filters," Journal of the Audio Engineering Society **37,** 899–907 (1989).

[18] E. Geddes and H. Blind, "Localized Sound Power Method.," Journal of the Audio Engineering Society **34,** 167 – 173 (1986).

[19] B. McCarthy, *Sound Systems: Design and Optimization* (Focal Press, 2007), pp. 384, 385.

[20] A. D. Pierce, *Acoustics: An Introduction to Its Physical Principles and Applications* (Acoustical Society of America, Melville, NY, 1994), p. 72.

[21] A. D. Pierce, *Acoustics: An Introduction to Its Physical Principles and Applications* (Acoustical Society of America, Melville, NY, 1994), pp. 72, 160.

[22] L. E. Kinsler, A. R. Frey, A. B. Coppens, and J. V. Sanders, *Fundamentals of Acoustics*, 4th ed. (Willey, Hoboken New Jersey, 2000), p. 171.

[23] L. L. Beranek, *Acoustics* (Acoustical Society of America, Woodbury New York, 1996), p. 36.

[24] L. E. Kinsler, A. R. Frey, A. B. Coppens, and J. V. Sanders, *Fundamentals of Acoustics*, 4th ed. (Willey, Hoboken New Jersey, 2000), p. 119.

[25] P. M. Morse and K. U. Ingard, *Theoretical Acoustics* (Princeton Unversity Press, Princeton, New Jersey, 1968), pp. 311–317.

[26] L. E. Kinsler, A. R. Frey, A. B. Coppens, and J. V. Sanders, *Fundamentals of Acoustics* (Willey, Hoboken New Jersey, 2000), pp. 127,128.

[27] A. D. Pierce, *Acoustics: An Introduction to Its Physical Principles and Applications* (Acoustical Society of America, 1994), pp. 44,45.

[28] J. Ghan, B. S. Cazzolato, and S. D. Snyder, "Expression for the estimation of time-averaged acoustic energy density using the two-microphone method (L)," The Journal of the Acoustical Society of America **113,** 2404–2407 (2003).

[29] P. M. Morse and K. U. Ingard, *Theoretical Acoustics* (Princeton, Unversity Press, Princeton New Jersey, 1968), p. 258.

[30] L. E. Kinsler, A. R. Frey, A. B. Coppens, and J. V. Sanders, *Fundamentals of Acoustics* (Willey, Hoboken New Jersey, 2000), pp. 124–125.

[31] A. D. Pierce, *Acoustics: An Introduction to Its Physical Principles and Applications* (Willey, Melville, NY, 1994), pp. 38–41.

[32] P. A. Nelson and S. J. Elliott, *Active Control of Sound* (Academic Press Ltd., San Diego California, 1992), pp. 17–19.

[33] G. R. Fowles and G. L. Cassiday, *Analytical Mechanics* (Harcourt, Orlando, Florida, 1999), p. 393.

[34] P. M. Morse and K. U. Ingard, *Theoretical Acoustics* (Princeton Unversity Press, Princeton, New Jersey, 1968), pp. 337–350.

[35] L. E. Kinsler, A. R. Frey, A. B. Coppens, and J. V. Sanders, *Fundamentals of Acoustics* (Willey, Hoboken New Jersey, 2000), p. 513.

[36] H. Kuttruff, *Room Acoustics*, 4th ed. (Taylor and Francis, New York, NY, 2000), Chap. 4.

[37] A. D. Pierce, *Acoustics: An Introduction to Its Physical Principles and Applications* (Acoustical Society of America, Melville, NY, 1994), pp. 105–106,208–211.

[38] P. A. Nelson and S. J. Elliott, *Active Control of Sound* (Academic Press Ltd., San Diego California, 1992), pp. 269–271.

[39] P. A. Nelson and S. J. Elliott, *Active Control of Sound* (Academic Press Ltd., San Diego California, 1992), p. 238.

[40] J. W. Parkins, S. D. Sommerfeldt, and J. Tichy, "Error analysis of a practical energy density sensor," Journal of the Acoustical Society of America **108,** 211 – 222 (2000).

[41] B. S. Cazzolato and J. Ghan, "Frequency domain expressions for the estimation of time-averaged acoustic energy density," The Journal of the Acoustical Society of America **117,** 3750–3756 (2005).

[42] C. D. Kestell, B. S. Cazzolato, and C. H. Hansen, "Active noise control in a free field with virtual sensors," The Journal of the Acoustical Society of America **109,** 232–243 (2001).

[43] P. A. Nelson and S. J. Elliott, *Active Control of Sound* (Academic Press Ltd., San Diego California, 1992), pp. 27–29.

[44] L. L. Beranek, *Acoustics* (Acoustical Society of America, Woodbury New York, 1996), pp. 81–83,109–112.

[45] L. E. Kinsler, A. R. Frey, A. B. Coppens, and J. V. Sanders, *Fundamentals of Acoustics*, 4th ed. (Willey, Hoboken New Jersey, 2000), pp. 130–133.

[46] A. D. Pierce, *Acoustics: An Introduction to Its Physical Principles and Applications* (Acoustical Society of America, 1994), pp. 60–65.

[47] D. B. Nutter, T. W. Leishman, S. D. Sommerfeldt, and J. D. Blotter, "Measurement of sound power and absorption in reverberation chambers using energy density," Journal of the Acoustical Society of America **121,** 2700 – 2710 (2007).

[48] D. B. Nutter, Master's thesis, Brigham Young University, Provo, Utah, 2006.

[49] P. A. Nelson and S. J. Elliott, *Active Control of Sound* (Academic Press Ltd., San Diego California, 1992), p. 240.

[50] A. Santillan, "Spatially extended sound equalization in rectangular rooms," Journal of the Acoustical Society of America **110,** 1989 – 1997 (2001).

[51] S. Elliott, I. Stothers, and P. Nelson, "A multiple error LMS algorithm and its application to the active control of sound and vibration," Acoustics, Speech, and Signal Processing [see also IEEE Transactions on Signal Processing], IEEE Transactions on **35,** 1423–1434 (1987).

[52] F. Asano and D. C. Swanson, "Sound equalization in enclosures using modal construction," Journal of the Acoustical Society of America **98,** 2062 – (1995).

[53] B. D. Radlovic and R. A. Kennedy, "Nonminimum-phase equalization and its subjective importance in room acoustics," Speech and Audio Processing, IEEE Transactions on **8,** 728–737 (2000).

[54] A. V. Oppenheim and R. W. Schafer, *Discrete-Time Signal Processing*, 2nd ed. (Prentice Hall, Upper Saddle River, NJ, 1999), pp. 33,34,248–250.

[55] M. Miyoshi and Y. Kaneda, "Inverse filtering of room acoustics," Acoustics, Speech, and Signal Processing [see also IEEE Transactions on Signal Processing], IEEE Transactions on **36,** 145–152 (1988).

[56] H. F. Silverman and A. E. Pearson, "On Deconvolution Using the Discrete Fourier Transform.," Audio and Electroacoustics, IEEE Transactions on **AU-21,** 112 – 118 (1973).

[57] A. V. Oppenheim and R. W. Schafer, *Discrete-Time Signal Processing*, 2nd ed. (Prentice Hall, 1999), pp. 564–567.

[58] A. V. Oppenheim and R. W. Schafer, *Discrete-Time Signal Processing*, 2nd ed. (Prentice Hall, Upper Saddle River, NJ, 1999), pp. 280–291.

[59] A. V. Oppenheim and R. W. Schafer, *Discrete-Time Signal Processing*, 2nd ed. (Prentice Hall, 1999), pp. 105–111.

[60] M. Tohyama and T. Koike, *Fundamentals of Acoustic Signal Processing* (Academic Press, 1998), Chap. 5, 8.

[61] J. Marple, L., "Computing the discrete-time "analytic" signal via FFT," Signal Processing, IEEE Transactions on [see also Acoustics, Speech, and Signal Processing, IEEE Transactions on] **47,** 2600–2603 (Sep 1999).

[62] L. Meirovitch, *Fundamentals of Vibrations* (McGraw-Hill, New York, NY, 2001), pp. 168–177,719,765,766.

[63] A. V. Oppenheim and R. W. Schafer, *Discrete-Time Signal Processing*, 2nd ed. (Prentice Hall, Upper Saddle River, NJ, 1999), pp. 60–61, 576–588, 659.

[64] H. Kuttruff, *Room Acoustics*, 4th ed. (Taylor and Francis, New York, NY, 2000), pp. 19,305.

[65] H. Irisawa, S. Shimada, H. Hokari, and S. Hosoya, "Study of a fast method to calculate inverse filters," AES: Journal of the Audio Engineering Society **46,** 611 – 620 (1998).

[66] O. Kirkeby and P. A. Nelson, "Digital filter design for inversion problems in sound reproduction," AES: Journal of the Audio Engineering Society **47,** 583 – 595 (1999).

[67] B.-I. Dalenbäck, The excitable file, GratisVolver.exe, was downloaded from http://www.catt.se/ and was still avalable as of November 13, 2007.

[68] J. Lawson and J. Erjavec, *Modern Statistics for Engineering and Quality Improvement* (Duxbury, Pacific Grove, CA, 2001), pp. 109–113.

[69] M. R. Morrise, Senior's thesis, Brigham Young University, 2007.

[70] T. J. Hargreaves, T. J. Cox, Y. W. Lam, and P. D'Antonio, "Surface diffusion coefficients for room acoustics: Free-field measures," The Journal of the Acoustical Society of America **108,** 1710–1720 (2000).

[71] G. Keller, *Applied Statistics with Microsoft Excel* (Duxbury, Pacific Grove, CA, 2001), pp. 182–185, 361–367.

[72] P. A. Nelson and S. J. Elliott, *Active Control of Sound* (Academic Press Ltd., San Diego California, 1992), pp. 271–274.

[73] K. L. Gee and S. D. Sommerfeldt, "Application of theoretical modeling to multichannel active control of cooling fan noise," The Journal of the Acoustical Society of America **115,** 228–236 (2004).

[74] L. L. Beranek, *Acoustics* (Acoustical Society of America, 1996), pp. 91–114.

[75] A. D. Pierce, *Acoustics: An Introduction to Its Physical Principles and Applications* (Acoustical Society of America, Melville, NY, 1994), pp. 157–158, 167–171.

[76] J. W. Worley, P. D. hatziantoniou, and J. N. Mourjopoulos, in *Subjective Assessments of Real-Time Room Dereverberation and Loudspeaker Equalization*, Audio Engineering Society (60 East 42nd St., New York, New York 10165-2520, USA, 2005).

[77] P. D'Antonio, "Performance evaluation of optimized diffusors," The Journal of the Acoustical Society of America **97,** 2937–2941 (1995).

[78] G. Keller, *Applied Statistics with Microsoft Excel* (Duxbury, Pacific Grove, CA, 2001), pp. 361–367, 472–482.

[79] "ISO 354:2003. Acoustics – Measurement of sound absorption in a reverberation room. (International Organization for Standardization, Geneva).,".

[80] D. J. Griffiths, *Introduction to Electrodynamics*, 3rd ed. (Prentice Hall, 1999), pp. 13–16.

[81] G. Keller, *Applied Statistics with Microsoft Excel* (Duxbury, Pacific Grove, CA, 2001), pp. 61–64.

[82] G. Keller, *Applied Statistics with Microsoft Excel* (Academic Press Ltd, Pacific Grove, CA, 2001), pp. 54–58.

[83] P. A. Nelson, *Active Control of Sound* (Academic Press Ltd., San Diego California, 192), pp. 78–89.

[84] L. Meirovitch, *Fundamentals of Vibrations* (McGraw-Hill, New York, NY, 2001), pp. 110–113.

[85] A. V. Oppenheim and R. W. Schafer, *Discrete-Time Signal Processing*, 2nd ed. (Prentice Hall, Upper Saddle River, NJ, 1999), pp. 55–58.

Appendix A

Explicit Derivation of Particle Velocity

Euler's equation relates between the two fundamental measurements in acoustics, acoustic pressure and particle velocity. As mentioned in Sec. 2.1, Eulers equation is

$$-\nabla\hat{p} = j\omega\rho_0\hat{\vec{u}} = jck\rho_0\hat{\vec{u}}. \tag{2.5}$$

Acoustic pressure may be described as it is written in Eq. (2.1), but for the purposes here a frequency domain expression is sufficent. The acoustic pressure in the frequency domain may be expressed by

$$\hat{p} = \frac{\hat{A}}{r}e^{-jkr}. \tag{A.1}$$

The first step to find an expression for particle velocity is to take the gradient of pressure. It is useful to move any terms out in front of the gradient that are not altered, as follows:

$$\nabla\hat{p} = \nabla\frac{\hat{A}}{r}e^{-jkr} = \hat{A}\nabla\frac{e^{-jkr}}{r}. \tag{A.2}$$

For convenience in MATLAB®, the expression for particle velocity derived here will be found in Cartesian coordinates. In Cartesian coordinates, the gradient of the

spatially dependent terms of acoustic pressure is written [80]

$$\hat{A}\nabla\frac{e^{-jkr}}{r} = \hat{A}\Big[\hat{\mathbf{x}}\frac{\partial}{\partial x} + \hat{\mathbf{y}}\frac{\partial}{\partial y} + \hat{\mathbf{z}}\frac{\partial}{\partial z}\Big]\frac{e^{-jkr}}{r}, \tag{A.3}$$

where

$$r = \sqrt{(x-x_1)^2 + (y-y_1)^2 + (z-z_1)^2}. \tag{A.4}$$

Because the derivative function acts identically on each of the three Cartesian coordinates. The Cartesian coordinates each appear in the expression for pressure in the same form, so the following steps are shown only for the x component here. Leaving the amplitude out simplifies Eq. (A.2) to

$$\frac{\partial}{\partial x}\frac{e^{-jkr}}{r} = \frac{1}{r}\frac{\partial}{\partial x}e^{-jkr} + e^{-jkr}\frac{\partial}{\partial x}r^{-1}, \tag{A.5}$$

remembering that r depends on x. Explicitly writing out the coordinate dependence of r further simplifies the expression to

$$\begin{aligned}\frac{\partial}{\partial x}\frac{e^{-jkr}}{r} =& \frac{1}{r}\frac{\partial}{\partial x}e^{-jk\sqrt{(x-x_1)^2+(y-y_1)^2+(z-z_1)^2}} + \\ & e^{-jkr}\frac{\partial}{\partial x}((x-x_1)^2 + (y-y_1)^2 + (z-z_1)^2)^{-\frac{1}{2}}.\end{aligned} \tag{A.6}$$

The next step is to differentiate

$$\begin{aligned}\frac{\partial}{\partial x}\frac{e^{ikr}}{r} =& \frac{1}{r}\frac{(-jk)\frac{1}{2}2(x-x_1)}{\sqrt{(x-x_1)^2+(y-y_1)^2+(z-z_1)^2}}e^{-jk\sqrt{(x-x_1)^2+(y-y_1)^2+(z-z_1)^2}} + \\ & e^{-jkr}\frac{-\frac{1}{2}2(x-x1)}{(x-x_1)^2+(y-y_1)^2+(z-z_1)^2)^{(3/2)}} \\ =& \frac{-jk(x-x_1)}{r^2}e^{-jkr} - e^{-jkr}\frac{(x-x1)}{r^3} \\ =& \frac{-jkr(x-x_1)}{r^3}e^{-jkr} - e^{-jkr}\frac{(x-x1)}{r^3} \\ =& \frac{-(jkr+1)(x-x_1)}{r^3}e^{-jkr}\end{aligned}$$

This result may be substituted in to Eq. (A.2), keeping in mind that an identical derivative is performed for each of the three Cartesian coordinates. This simplifies

Eq. (A.2) to

$$\nabla\hat{p} = -\frac{\hat{A}}{r^3}e^{jkr}(jkr+1)\begin{pmatrix} x-x_1 \\ y-y_1 \\ z-z_1 \end{pmatrix} \tag{A.7}$$

The result of the the gradient includes a term that describes the vector between the source and receiver positions. At this point it is appropriate to substitute the pressure amplitude, Eq. (2.2) [21–23]

$$\hat{A} = \frac{j\rho_0 ck\hat{q}}{4\pi}, \tag{A.8}$$

into the expression for $-\nabla\hat{p}$, yielding

$$-\nabla\hat{p} = \frac{j\rho_0 ck\hat{q}}{4\pi r^3}e^{jkr}(jkr+1)\begin{pmatrix} x-x_1 \\ y-y_1 \\ z-z_1 \end{pmatrix}. \tag{A.9}$$

Now it is useful to begin to consider the right hand side of Eulers equation, Eq. (2.5),

$$\nabla\hat{p} = \frac{j\rho_0 ck\hat{q}}{4\pi r^3}e^{jkr}(jkr+1)\begin{pmatrix} x-x_1 \\ y-y_1 \\ z-z_1 \end{pmatrix} = jck\rho_0\hat{\vec{u}}. \tag{A.10}$$

It is helpful to note that the density ρ_0, wave number k, and wave speed c are on both sides of the equation so they may be removed from the expression, yielding

$$\hat{\vec{u}} = \frac{\hat{q}}{4\pi r^3}e^{jkr}(jkr+1)\begin{pmatrix} x-x_1 \\ y-y_1 \\ z-z_1 \end{pmatrix}. \tag{A.11}$$

which describes the particle velocity of a point source. Placing the source at the origin further simplifies the expression to

$$\hat{u}_r = \frac{\hat{q}}{4\pi r^2}e^{-jk(r-ct)}(jkr+1) \tag{A.12}$$

which agrees with expressions found in the works by Beranek, Morse and Ingard, Kinsler *et al.*, and Pierce and for particle velocity in the r direction [23, 25–27]. Another way to arrive at the expression here would be to use the result in spherical coordinates and convert it to cartesian coordinates. The particle velocity expression can be used for multiple point sources, where the Cartesian components of the particle velocity are summed. This generalizes Eq. (A.11) to

$$\hat{\vec{u}} = \sum_{n=1}^{N} \left(\frac{\hat{q}_n}{4\pi r_n^3} e^{ik(r_n - ct)} (ikr_n - 1) \begin{pmatrix} x - x_n \\ y - y_n \\ z - z_n \end{pmatrix} \right). \tag{A.13}$$

The result is a vector expression for particle velocity caused by a set of point sources.

Appendix B

Statistical Techniques

B.1 Derivation of an Alternate Expression for Standard Deviation

Lawson and Erjavec have an expression for the population standard deviation that functions well without the need of all of the data available simultaneously. This expression is expressed as [68, 81]

$$s^2 = \frac{\sum_{i=1}^{N} (y_i - \bar{y})^2}{N-1} \tag{B.1}$$

or

$$\frac{\sum_{i=1}^{N} y_i^2 - \frac{\left(\sum_{i=1}^{N} y_i\right)^2}{N}}{N-1}. \tag{B.2}$$

Strictly speaking, s^2 is a variance, the square root of which is the standard deviation. Expression (B.2) provides an alternate method that produces an identical result. The two methods described in Eqs. (B.1) and (B.2) both follow standard methods for calculating standard deviation, however they have different situations in which one is more practical than the other. When the mean is already known, Eq. (B.1) is more

convenient; however, this is not always the case. In some of the computer models discussed in this work, the entire set of data in the sample is not available simultaneously. For such cases, Eq. (B.1) requires acquisition of the data twice, once to find the mean and again to calculated the sample standard deviation. Equation (B.2) only requires access to the data once. This helps improve computational efficiency and speed.

In order to verify the equality of these expressions we must show that

$$\sum_{i=1}^{N}(y_i-\bar{y})^2=\sum_{i=1}^{N}y_i^2-\frac{\left(\sum\limits_{i=1}^{N}y_i\right)^2}{N}. \tag{B.3}$$

Working from the left side of the equation, we can expand the expression such that

$$\sum_{i=1}^{N}(y_i-\bar{y})^2=\sum_{i=1}^{N}(y_i^2-2y_i\bar{y}+\bar{y}^2). \tag{B.4}$$

By using the standard definition for the sample mean [68, 82]

$$\bar{y}=\frac{\sum\limits_{i=1}^{N}x_i}{N}, \tag{B.5}$$

the expression may be further expanded to

$$\begin{aligned}
\sum_{i=1}^{N}(y_i-\bar{y})^2 &= \sum_{i=1}^{N}(y_i^2-2y_i\bar{y}+\bar{y}^2)\\
&= \sum_{i=1}^{N}y_i^2-2\bar{y}\sum_{i=1}^{N}y_i+N\bar{y}^2\\
&= \sum_{i=1}^{N}y_i^2-2\frac{\sum\limits_{i=1}^{N}y_i}{N}\sum_{i=1}^{N}y_i+N\left(\frac{\sum\limits_{i=1}^{N}y_i}{N}\right)^2\\
&= \sum_{i=1}^{N}y_i^2-\frac{2}{N}\left(\sum_{i=1}^{N}y_i\right)^2+\frac{\left(\sum\limits_{i=1}^{N}y_i\right)^2}{N}\\
&= \sum_{i=1}^{N}y_i^2+\left(\sum_{i=1}^{N}y_i\right)^2\frac{1-2}{N}\\
&= \sum_{i=1}^{N}y_i^2-\frac{\left(\sum\limits_{i=1}^{N}y_i\right)^2}{N}.
\end{aligned} \tag{B.6}$$

When the denominator is included, this result is exactly the value listed by Lawson and Erjavec as stated in Eq. (B.1). This calculation shows that the equations published by Lawson and Erjavec are truly equal.

The convenience of using Eq. (B.2) to calculat the standard deviation when only partial amounts of data can be found comes at the cost of susceptibility to numerical error. When the standard deviation is very small, calculating the standard deviation from a small sample can result in an estimate of the standard deviation that is negative. It is important to note that by definition standard deviation is a positive-valued number. The negative standard deviation problem disappears with large sample sizes. The error in this calculations of standard deviation tend to be less than 10^{-5}, which is in the realm of numerical error. At this point there is no resolution or clear explanation for the numerical discrepancy. Because of the small size of the error, it will be left for to resolve this issue.

B.2 Statistical Values of Energies

Calculating averages and standard deviations on a dB scale unfairly weights lower values. This is because the equalizations incorporate a summing process, which is invalid because dB measurements inherently do not superpose. Several methods have been proposed to deal with the inherent errors when a statistical evaluation of energy is desired.

It is important to remember when calculating the sound, that it is an energy value that is expressed on a logarithmic scale. For L_p, the sound level is a squared pressure measurement. Sound pressure level may be averaged using the expression [70]

$$\bar{L}_p = 10 \log_{10} \frac{1}{N} \sum_{i=1}^{N} 10^{\frac{SPL_i}{10}}. \tag{B.7}$$

This expression may be simplified by substituting in the expression for L_p found in Eq. 2.45. This results in

$$L_p = 10 \log_{10} \frac{1}{N} \sum_{i=1}^{N} \frac{|\hat{p}|^2}{2p_{ref}^2}, \tag{B.8}$$

which is the same as finding the L_p from the average of squared pressure, which is proportional to energy. This process is an energetic average, which may be performed without multiplying by 10 and taking the $\log_{10}$ of the average. This procedure avoids the mess of averaging a decibel value, and additionally avoids the problems of trying to average a complex valued data set.

Some argue that standard deviation of levels describes the frequency variation that is sensed by human listeners [70]. However, these calculations are weighted in a way that is undesirable. One suggestion has been to replace the average term in the standard deviation with the average level expression from Eq. (B.7), resulting in [70]

$$s^2 = \frac{1}{N} \sum_{i=1}^{N} (L_i - \bar{L})^2. \tag{B.9}$$

The standard deviation may be thought of as an average of the deviation from the mean. Equation (B.9) is actually calculating the deviation from the mean of another measurement. Though these two measurements are related, they are not linearly related and thus produce, a mixed metric. A more appropriate measure would be to look at the standard deviation of energetic quantities. This would correspond nicely with the calculation for averages found in Eq. (B.8). In order to keep the method for calculating the average and standard deviation consistent, the variance may be calculated using

$$s^2 = \frac{\sum_{i=1}^{N} (|\hat{p}|^2 - |\bar{\hat{p}}|^2)^2}{N-1}. \tag{B.10}$$

In order to keep units consistent with conventional sound pressure levels, it is important to calculate s rather than s^2 before taking the $\log_{10}$. Standard deviation has the same units the values in the data set, while the variance has units that are the

square of the units of the data set. This would require a reference value with units of Pa^4. Fortunately, this type of energetic standard deviation works well with the method described in Appendix B.1 which demonstrates how to calculate a standard deviation in a computer model as the field is calculated.

Appendix C

Calculations for MEDToPO

The simplest case for the MEDToPO is the case where one control source is used to minimize the sound radiated by a single primary source. In this appendix the calculations for the minimization of the ED quantities for this specific case are shown in Secs. C.1, C.2 and C.3. The MEDToPO may also be applied to a more general case. The generalization is applied in Secs. C.4, C.5, and C.6 for a case where the primary sources all have the same source strength, as do the control sources. The results are given as a magnitude and phase of the source strength that provide minimization of the ED quantities at a given error sensor location. These results are than used to find the total sound power radiated from the combination of sources and used to produce the MEDToPO plots found in Secs. 3.1.2, 4.2.1, and E.1.

C.1 Minimizing PED for One Primary Source and One Control Source

Minimizing pressure squared or PED result in the same control source strength calculations because they are related to one another by a constant. The calculations

are perfumed here for pressure squared starting with an expression simplified from Eqs. (2.1) and (2.2)

$$\hat{p} = \frac{j\rho_0 ck}{4\pi} \sum_{n=1}^{N} \frac{\hat{q}_n e^{-jkR_n}}{R_n} \tag{C.1}$$

For our simple case, a single primary source $\hat{q}_p$ and single control source $\hat{q}_s$ the pressure becomes

$$\hat{p} = \frac{j\rho_0 ck}{4\pi} \left(\sum_{pn=1}^{N} \frac{\hat{q}_p e^{-jkR_{pn}}}{R_{pn}} + \sum_{sn=1}^{N} \frac{\hat{q}_s e^{-jkR_{sn}}}{R_{sn}} \right). \tag{C.2}$$

The squared magnitude pressure is calculated by multiplying pressure by its complex conjugate,

$$\begin{aligned} |\hat{p}|^2 =& \hat{p}\hat{p}^* \\ =& \left(\frac{\rho_0 ck}{4\pi}\right)^2 \left(\hat{q}_p \frac{e^{-jkR_{pn}}}{R_{pn}} + \hat{q}_s \frac{e^{-jkR_{sn}}}{R_{sn}}\right) \left(\hat{q}_p \frac{e^{-jkR_{pn}}}{R_{pn}} + \hat{q}_s \frac{e^{-jkR_{sn}}}{R_{sn}}\right)^* . \end{aligned} \tag{C.3}$$

This may be simplified to

$$|\hat{p}|^2 = \frac{(\rho_0 ck)^2}{16\pi^2 R_p^2 R_s^2} \begin{pmatrix} |\hat{q}_p|^2 R_s^2 + |\hat{q}_s|^2 R_p^2 + \\ R_p R_s |\hat{q}_p||\hat{q}_s| e^{-j(\phi_p - \phi_s)} e^{-jk(R_p - R_s)} + \\ R_p R_s |\hat{q}_p||\hat{q}_s| e^{j(\phi_p - \phi_s)} e^{jk(R_p - R_s)} \end{pmatrix} \tag{C.4}$$

where

$$\hat{q}_n = |\hat{q}_n| e^{-j\phi_n}. \tag{C.5}$$

At this point it is convenient to express the difference in phase between the control source and the primary source as

$$\phi_p - \phi_s = \gamma. \tag{C.6}$$

The result simplifies to

$$|\hat{p}|^2 = \frac{(\rho_0 ck)^2}{16\pi^2 R_p^2 R_s^2} \begin{pmatrix} |\hat{q}_p|^2 R_s^2 + |\hat{q}_s|^2 R_p^2 + \\ R_p R_s |\hat{q}_s||\hat{q}_p| \left(e^{-j\gamma} e^{-jk(R_p - R_s)} + e^{j\gamma} e^{jk(R_p - R_s)}\right) \end{pmatrix}. \tag{C.7}$$

Using Euler's identity $e^{jx} = \cos x + j \sin x$, this may be further simplified to

$$|\hat{p}|^2 = \frac{(\rho_0 ck)^2}{16\pi^2 R_p^2 R_s^2} \left(\begin{array}{l} |\hat{q}_p|^2 R_s^2 + |\hat{q}_s|^2 R_p^2 + \\ \\ R_p R_s |\hat{q}_s||\hat{q}_p| \left[\begin{array}{l} \cos\gamma \cos\left(k(R_p - R_s)\right) + \\ -\sin\gamma \sin\left(k(R_p - R_s)\right) \end{array} \right] \end{array} \right). \tag{C.8}$$

This form also shows explicitly that the squared pressure magnitude is real, as we would expect. It is helpful to define the ratio

$$B = \frac{|\hat{q}_s|}{|\hat{q}_p|} \tag{C.9}$$

when it comes time to find the source strength that minimizes PED at the field point. Applying this definition to Eq. (C.8) gives

$$|\hat{p}|^2 = \frac{(\rho_0 ck)^2}{16\pi^2 R_p^2 R_s^2} |\hat{q}_p|^2 \left(R_s^2 + B^2 R_p^2 + 2 R_p R_s B \left[\begin{array}{l} \cos\gamma \cos\left(k(R_p - R_s)\right) + \\ -\sin\gamma \sin\left(k(R_p - R_s)\right) \end{array} \right] \right). \tag{C.10}$$

C.1.1 Finding the Phase Difference of the Control Source

To minimize a measured quantity, the appropriate phase and magnitude of the control source must be found. The phase of the control sources are found by differentiating with respect to the phase difference, setting the result equal to zero, and solving for the phase difference. Differentiating the result from Eq. (C.10) yealds

$$\frac{\partial}{\partial\gamma}|\hat{p}|^2 = \frac{-(\rho_0 ck)^2}{16\pi^2 R_p^2 R_s^2} |\hat{q}_p|^2 \left[\sin\gamma \cos\left(k(R_p + R_s)\right) - \cos\gamma \sin\left(k(R_p - R_s)\right)\right] \tag{C.11}$$

The trigonometric identity $\sin\theta\cos\phi + \cos\theta\sin\phi = \sin(\theta+\phi)$ simplifies the expression to

$$\frac{\partial}{\partial\gamma}|\hat{p}|^2 = \frac{-(\rho_0 ck)^2}{16\pi^2 R_p^2 R_s^2} |\hat{q}_p|^2 \sin\left(\gamma + k(R_p - R_s)\right) \tag{C.12}$$

Setting this derivative equal to zero and simplifying the expression gives the relationship

$$\sin\left(\gamma + k(R_p - R_s)\right) = 0. \tag{C.13}$$

Because the sin function is periodic,

$$\gamma + k(R_p - R_s) = n\pi, \tag{C.14}$$

where n is an integer. The optimal value for γ depends on the position of the error sensor and wave number such that

$$\gamma = -k(R_p - R_s). \tag{C.15}$$

C.1.2 Finding the Magnitude of the Control Source

A process similar to that used to find the optimal phase is performed to find the relative source strength, B which in turn reveals the optimal control source strength. Starting by differentiating the result in Eq. (C.10) we find

$$\frac{\partial}{\partial B}|\hat{p}|^2 = \frac{(\rho_0 ck)^2}{16\pi^2 R_p^2 R_s^2}|\hat{q}_p|^2 \left(2BR_p^2 + 2R_p R_s \left[\begin{array}{l} \cos\gamma\cos\left(k(R_p - R_s)\right) + \\ -\sin\gamma\sin\left(k(R_p - R_s)\right) \end{array} \right] \right). \tag{C.16}$$

Setting this equation to zero and solving for B gives the relationship

$$B = -\frac{R_s}{R_p}\left[\cos\gamma\cos\left(k(R_p - R_s)\right) - \sin\gamma\sin\left(k(R_p - R_s)\right)\right]. \tag{C.17}$$

Using the definition for B found in Eq. (C.9). This expression further simplifies to

$$|\hat{q}_s| = -|\hat{q}_p|\frac{R_s}{R_p}\left[\ \cos\gamma\cos\left(k(R_p - R_s)\right) - \sin\gamma\sin\left(k(R_p - R_s)\right)\ \right]. \tag{C.18}$$

Using the trig identity $\cos\theta\cos\phi - \sin\theta\sin\phi = \cos(\theta+\phi)$ the source strength further simplifies to

$$|\hat{q}_s| = -|\hat{q}_p|\frac{R_s}{R_p}\cos\left(\gamma + k(R_p - R_s)\right). \tag{C.19}$$

Now the result for the relative phase γ, found in Eq. (C.15) is substituted in order to find the correct control magnitude,

$$|\hat{q}_s| = -|\hat{q}_p|\frac{R_s}{R_p}. \tag{C.20}$$

C.2 Minimizing KED for One Primary Source and One Control Source

Minimizing the magnitude of particle velocity squared is the same as minimizing KED because they are related to one another by a constant. Derivation of the control source strength starts with Eqs. (2.6) and (2.7).

$$\hat{\vec{u}} = \sum_{n=1}^{N} \frac{\hat{q}_n e^{-jkR_n}}{4\pi R_n^3}(jkR_n + 1)\vec{R}_n \tag{2.6}$$

where

$$\vec{R}_n = \begin{pmatrix} x - x_n \\ y - y_n \\ z - z_n \end{pmatrix}, \tag{2.7}$$

For the special case of a single primary source and a single control source the expression for $\hat{\vec{u}}$ becomes

$$\hat{\vec{u}} = \frac{\hat{q}_p}{4\pi}\frac{e^{-jkR_p}}{R_p^3}(jkR_p + 1)\vec{R}_p + \frac{\hat{q}_s}{4\pi}\frac{e^{-jkR_s}}{4\pi R_s^3}(jkR_s + 1)\vec{R}_s. \tag{C.21}$$

The expression for the squared vector magnitude of the particle velocity is found using

$$|\hat{\vec{u}}|^2 = \hat{\vec{u}} \cdot \hat{\vec{u}}^* = \hat{u}_x \hat{u}_x^* + \hat{u}_y \hat{u}_y^* + \hat{u}_z \hat{u}_z^* = |\hat{u}_x|^2 + |\hat{u}_y|^2 + |\hat{u}_z|^2. \tag{2.52}$$

In Cartesian coordinates, the squared magnitude of each of the components may be found separately than summed in order to find expression for the squared vector magnitude of particle velocity. The calculations for squared particle velocity are identical for each component, so the computations will be performed for the x component, and than applied to the y and z components as in Appendix A.

Calculating the x component multiplied by its complex conjugate results in

$$\begin{aligned}|\hat{u}_x|^2 = &\left(\frac{\hat{q}_p}{4\pi}\frac{e^{-jkR_p}}{R_p^3}(jkR_p+1)(x-x_p) + \frac{\hat{q}_s}{4\pi}\frac{e^{-jkR_s}}{4\pi R_s^3}(jkR_s+1)(x-x_s)\right)\times \\ &\left(\frac{\hat{q}_p}{4\pi}\frac{e^{-jkR_p}}{R_p^3}(jkR_p+1)(x-x_p) + \frac{\hat{q}_s}{4\pi}\frac{e^{-jkR_s}}{4\pi R_s^3}(jkR_s+1)(x-x_s)\right)^*. \end{aligned}\tag{C.22}$$

Simplifying this expression and substituting $|\hat{q}_n|e^{-j\phi_n}$ for $\hat{q}_n$ produces

$$\begin{aligned}|\hat{u}_x|^2 = &\frac{|\hat{q}_p|^2}{16\pi^2 R_p^6}(k^2R_p^2+1)(x-x_p)^2 + \frac{|\hat{q}_s|^2}{16\pi^2 R_s^6}(k^2R_s^2+1)(x-x_s)^2 + \\ &\frac{|\hat{q}_p|e^{-j\phi_p}|\hat{q}_s|e^{j\phi_s}}{16\pi^2 R_p^3 R_s^3}e^{-jk(R_p-R_s)}(jkR_p+1)(-jkR_s+1)(x-x_p)(x-x_s) + \\ &\frac{|\hat{q}_s|e^{-j\phi_s}|\hat{q}_p|e^{j\phi_p}}{16\pi^2 R_p^3 R_s^3}e^{jk(R_p-R_s)}(jkR_s+1)(-jkR_p+1)(x-x_p)(x-x_s). \end{aligned}\tag{C.23}$$

Remembering from Eq. (C.6) that $\phi_p - \phi_s = \gamma$ simplifies the express for the squared magnitude of the x component of particle velocity to

$$|\hat{u}_x|^2 = \frac{|\hat{q}_p|^2}{16\pi^2 R_p^6 R_s^6}\left(\begin{array}{l} R_s^6(k^2R_p^2+1)(x-x_p)^2 + B^2R_p^6(k^2R_s^2+1)(x-x_s)^2 + \\ 2B(x-x_p)(x-x_s)R_p^3R_s^3\left(\begin{array}{l}\left(\begin{array}{l}(\xi)\cos(\chi)+\\ \chi\sin(\chi)\end{array}\right)\cos\gamma + \\ \left(\begin{array}{l}\chi\cos(\chi)-\\ (\xi)\sin(\chi)\end{array}\right)\sin\gamma\end{array}\right)\end{array}\right) \tag{C.24}$$

where $k(R_p - R_s) = \chi$ and $k^2 R_p R_s + 1 = \xi$. Performing the same calculations on the y and z components, and summing the results, as prescribed in Eq. (2.52), gives

$$|\hat{\vec{u}}|^2 = \frac{|\hat{q}_p|^2 \left(\begin{array}{l} R_s^6(k^2R_p^2+1)(x-x_p)^2 + B^2R_p^6(k^2R_s^2+1)(x-x_s)^2 + \\ 2B(x-x_p)(x-x_s)R_p^3R_s^3 \left(\begin{array}{l} \left(\begin{array}{l} (\xi)\cos(\chi) + \\ \chi\sin(\chi) \end{array} \right) \cos\gamma + \\ \left(\begin{array}{l} \chi\cos(\chi) - \\ (\xi)\sin(\chi) \end{array} \right) \sin\gamma \end{array} \right) + \\ R_s^6(k^2R_p^2+1)(y-y_p)^2 + B^2R_p^6(k^2R_s^2+1)(y-y_s)^2 + \\ 2B(y-y_p)(y-y_s)R_p^3R_s^3 \left(\begin{array}{l} \left(\begin{array}{l} (\xi)\cos(\chi) + \\ \chi\sin(\chi) \end{array} \right) \cos\gamma + \\ \left(\begin{array}{l} \chi\cos(\chi) - \\ (\xi)\sin(\chi) \end{array} \right) \sin\gamma \end{array} \right) + \\ R_s^6(k^2R_p^2+1)(z-z_p)^2 + B^2R_p^6(k^2R_s^2+1)(z-z_s)^2 + \\ 2B(z-z_p)(z-z_s)R_p^3R_s^3 \left(\begin{array}{l} \left(\begin{array}{l} (\xi)\cos(\chi) + \\ \chi\sin(\chi) \end{array} \right) \cos\gamma + \\ \left(\begin{array}{l} \chi\cos(\chi) - \\ (\xi)\sin(\chi) \end{array} \right) \sin\gamma \end{array} \right) \end{array} \right)}{16\pi^2 R_p^6 R_s^6}. \quad \text{(C.25)}$$

Further simplification reduces this expression to

$$|\hat{\vec{u}}|^2 = \frac{|\hat{q}_p|^2}{16\pi^2 R_p^4 R_s^4} \left(\begin{array}{l} R_s^4(k^2R_p^2+1) + B^2R_p^4(k^2R_s^2+1) + \\ 2BR_pR_s \left(\begin{array}{l} \left(\begin{array}{l} (\xi)\cos(\chi) + \\ \chi\sin(\chi) \end{array} \right) \cos\gamma + \\ \left(\begin{array}{l} \chi\cos(\chi) - \\ (\xi)\sin(\chi) \end{array} \right) \sin\gamma \end{array} \right) \Delta \end{array} \right), \quad \text{(C.26)}$$

where $\Delta = (x - x_p)(x - x_s) + (y - y_p)(y - y_s) + (z - z_p)(z - z_s)$.

C.2.1 Finding the Phase Difference of the Control Source

To find the appropriate phase difference for the control source to to minimize KED we differentiate $|\hat{\vec{u}}|^2$ with respect to γ, than set the result to zero and solve for γ. Ignoring the constants in front of the expression, the derivative is

$$\frac{\partial}{\partial\gamma}|\hat{\vec{u}}| = \frac{\partial}{\partial\gamma} 2BR_pR_s\Delta \left(\begin{array}{l} \left(\begin{array}{l} (k^2R_pR_s+1)\cos(k(R_p-R_s))+ \\ k(R_p-R_s)\sin(k(R_p-R_s)) \end{array} \right) \cos\gamma + \\ \left(\begin{array}{l} k(R_p-R_s)\cos(k(R_p-R_s))- \\ (k^2R_pR_s+1)\sin(k(R_p-R_s)) \end{array} \right) \sin\gamma \end{array} \right). \quad \text{(C.27)}$$

Setting the derivative equal to zero and simplifying the expression yields

$$\tan\gamma = \frac{k(R_p-R_s)\cos(k(R_p-R_s)) - (k^2R_pR_s+1)\sin(k(R_p-R_s))}{(k^2R_pR_s+1)\cos(k(R_p-R_s)) + k(R_p-R_s)\sin(k(R_p-R_s))}. \quad \text{(C.28)}$$

There is an ambiguity whenever the arctangent is calculated so care must be taken in finding the appropriate phase difference to minimize KED at an error sensor.

C.2.2 Finding the Magnitude of the Control Source

Differentiating Eq. (C.26) with respect to B gives

$$\frac{\partial}{\partial B}|\hat{\vec{u}}|^2 = \frac{|\hat{q}_p|^2}{16\pi^2R_p^4R_s^4} \left(\begin{array}{l} 2BR_p^4(k^2R_s^2+1)+ \\ 2R_pR_s \left(\begin{array}{l} \left(\begin{array}{l} (\xi)\cos(\chi)+ \\ \chi\sin(\chi) \end{array} \right) \cos\gamma + \\ \left(\begin{array}{l} \chi\cos(\chi)- \\ (\xi)\sin(\chi) \end{array} \right) \sin\gamma \end{array} \right) \Delta \end{array} \right). \quad \text{(C.29)}$$

By setting the derivative equal to zero and solving for B we arrive at

$$B = -\frac{R_p R_s}{R_p^4(k^2R_s^2+1)}\left(\begin{array}{l}\left(\begin{array}{l}(k^2R_pR_s+1)\cos(k(R_p-R_s))+\\ k(R_p-R_s)\sin(k(R_p-R_s))\end{array}\right)\cos\gamma+\\ \left(\begin{array}{l}k(R_p-R_s)\cos(k(R_p-R_s))-\\ (k^2R_pR_s+1)\sin(k(R_p-R_s))\end{array}\right)\sin\gamma\end{array}\right)\Delta. \quad \text{(C.30)}$$

Remembering that $B = |\hat{q}_s|/|\hat{q}_p|$ as defined in Eq. (C.9), we find that the magnitude of the source strength is

$$|\hat{q}_s| = -\frac{|\hat{q}_p|R_s}{R_p^3(k^2R_s^2+1)}\left(\begin{array}{l}\left(\begin{array}{l}(k^2R_pR_s+1)\cos(k(R_p-R_s))+\\ k(R_p-R_s)\sin(k(R_p-R_s))\end{array}\right)\cos\gamma+\\ \left(\begin{array}{l}k(R_p-R_s)\cos(k(R_p-R_s))-\\ (k^2R_pR_s+1)\sin(k(R_p-R_s))\end{array}\right)\sin\gamma\end{array}\right)\Delta \quad \text{(C.31)}$$

where $\Delta = (x-x_p)(x-x_s)+(y-y_p)(y-y_s)+(z-z_p)(z-z_s)$.

C.3 Minimizing TED for One Primary Source and One Control Source

As described in Eq. (2.8), TED is calculated by

$$\langle w\rangle_t = \langle w_p\rangle_t + \langle w_k\rangle_t = \frac{|\hat{p}|^2}{4\rho_0 c^2} + \frac{\rho_0}{4}\hat{\vec{u}}\cdot\hat{\vec{u}}^*. \tag{C.32}$$

Using Eq. (C.9)

$$|\hat{p}|^2 = \frac{(\rho_0 ck)^2}{16\pi^2 R_p^2 R_s^2}|\hat{q}_p|^2\left(R_s^2 + B^2R_p^2 + 2R_pR_sB\left[\begin{array}{l}\cos\gamma\cos\left(k(R_p-R_s)\right)+\\ -\sin\gamma\sin\left(k(R_p-R_s)\right)\end{array}\right]\right) \tag{C.33}$$

and Eq. (C.26)

$$|\hat{\vec{u}}|^2 = \frac{|\hat{q}_p|^2}{16\pi^2 R_p^4 R_s^4}\left(\begin{array}{l} R_s^4(k^2R_p^2+1) + B^2R_p^4(k^2R_s^2+1)+\\ 2BR_pR_s\left(\begin{array}{l}\left(\begin{array}{l}(k^2R_pR_s+1)\cos(k(R_p-R_s))+\\ k(R_p-R_s)\sin(k(R_p-R_s))\end{array}\right)\cos\gamma+\\ \left(\begin{array}{l}k(R_p-R_s)\cos(k(R_p-R_s))-\\ (k^2R_pR_s+1)\sin(k(R_p-R_s))\end{array}\right)\sin\gamma\end{array}\right)\Delta\end{array}\right) \tag{C.34}$$

in Eq. (C.32) yields this expression for TED

$$\langle w\rangle_t = \frac{(\rho_0 ck)^2}{16\pi^2 R_p^2 R_s^2}|\hat{q}_p|^2 \frac{\left(R_s^2 + B^2R_p^2 + 2R_pR_sB\left[\begin{array}{l}\cos\gamma\cos\left(k(R_p-R_s)\right)+\\ -\sin\gamma\sin\left(k(R_p-R_s)\right)\end{array}\right]\right)}{4\rho_0 c^2} + \\ + \frac{\rho_0}{4}\frac{|\hat{q}_p|^2}{16\pi^2 R_p^4 R_s^4}\left(\begin{array}{l} R_s^4(k^2R_p^2+1) + B^2R_p^4(k^2R_s^2+1)+ \\ 2BR_pR_s\left(\begin{array}{l}\left(\begin{array}{l}(k^2R_pR_s+1)\cos(k(R_p-R_s))+\\ k(R_p-R_s)\sin(k(R_p-R_s))\end{array}\right)\cos\gamma+\\ \left(\begin{array}{l}k(R_p-R_s)\cos(k(R_p-R_s))-\\ (k^2R_pR_s+1)\sin(k(R_p-R_s))\end{array}\right)\sin\gamma\end{array}\right)\Delta\end{array}\right). \tag{C.35}$$

The expression for TED simplifies to

$$\langle w\rangle_t = \frac{|\hat{q}_p|^2\rho_0}{64\pi^2 R_p^4 R_s^4}\left(\begin{array}{l} 2k^2R_s^4R_p^2 + R_s^4 + B^2(2k^2R_p^4R_s^2 + R_p^4)+ \\ +2k^2R_p^3R_s^3B\left[\begin{array}{l}\cos\gamma\cos\left(k(R_p-R_s)\right)+\\ -\sin\gamma\sin\left(k(R_p-R_s)\right)\end{array}\right]+ \\ +2BR_pR_s\Delta\left(\begin{array}{l}\left(\begin{array}{l}(k^2R_pR_s+1)\cos(k(R_p-R_s))+\\ k(R_p-R_s)\sin(k(R_p-R_s))\end{array}\right)\cos\gamma+\\ \left(\begin{array}{l}k(R_p-R_s)\cos(k(R_p-R_s))-\\ (k^2R_pR_s+1)\sin(k(R_p-R_s))\end{array}\right)\sin\gamma\end{array}\right)\end{array}\right). \tag{C.36}$$

C.3.1 Finding the Phase Difference of the Control Source

Again, to find the ideal phase the field quantity is differentiated with respect to the relative phase of the system. The derivative of TED with respect to the phase

difference γ is

$$\frac{\partial}{\partial\gamma}\langle w\rangle_t = \frac{|\hat{q}_p|^2\rho_0}{64\pi^2 R_p^4 R_s^4}\left(\begin{array}{l} 2k^2R_p^3R_s^3B\left[\begin{array}{l}-\sin\gamma\cos\left(k(R_p-R_s)\right)+\\ -\cos\gamma\sin\left(k(R_p-R_s)\right)\end{array}\right]+\\ +2BR_pR_s\Delta\left(\begin{array}{l}-\left(\begin{array}{l}(k^2R_pR_s+1)\cos(k(R_p-R_s))+\\ k(R_p-R_s)\sin(k(R_p-R_s))\end{array}\right)\sin\gamma+\\ \left(\begin{array}{l}k(R_p-R_s)\cos(k(R_p-R_s))-\\ (k^2R_pR_s+1)\sin(k(R_p-R_s))\end{array}\right)\cos\gamma\end{array}\right)\end{array}\right) \tag{C.37}$$

Setting the derivative equal to zero and isolating γ results in

$$\tan\gamma = \frac{B\left(\begin{array}{l}-k^2R_p^3R_s^3\sin\left(k(R_p-R_s)\right)+\\ \quad R_pR_s\Delta\left(\begin{array}{l}k(R_p-R_s)\cos(k(R_p-R_s))-\\ (k^2R_pR_s+1)\sin(k(R_p-R_s))\end{array}\right)\end{array}\right)}{B\left(\begin{array}{l}k^2R_p^3R_s^3\cos\left(k(R_p-R_s)\right)+\\ +R_pR_s\Delta\left(\begin{array}{l}(k^2R_pR_s+1)\cos(k(R_p-R_s))+\\ k(R_p-R_s)\sin(k(R_p-R_s))\end{array}\right)\end{array}\right)}. \tag{C.38}$$

At this point we do not know the ideal relationship for the magnitudes of the sound sources, represented by B. Assuming that $B \neq 0$, B cancels in the devision, resulting in a phase difference of

$$\gamma = \tan^{-1}\frac{\left(\begin{array}{l}-k^2R_p^3R_s^3\sin\left(k(R_p-R_s)\right)+\\ \quad R_pR_s\Delta\left(\begin{array}{l}k(R_p-R_s)\cos(k(R_p-R_s))-\\ (k^2R_pR_s+1)\sin(k(R_p-R_s))\end{array}\right)\end{array}\right)}{\left(\begin{array}{l}k^2R_p^3R_s^3\cos\left(k(R_p-R_s)\right)+\\ +R_pR_s\Delta\left(\begin{array}{l}(k^2R_pR_s+1)\cos(k(R_p-R_s))+\\ k(R_p-R_s)\sin(k(R_p-R_s))\end{array}\right)\end{array}\right)}. \tag{C.39}$$

Since $B = |\hat{q}_s|/|\hat{q}_p|$, assuming that $B \neq 0$ is true unless the secondary source turned off. Again care must be taken to determine the appropriate quadrant for minimizing sound at the error sensor.

C.3.2 Finding the Magnitude of the Control Source

To find the source strength of the control sources, we differentiate TED by the ratio of the source strength magnitudes B giving

$$\frac{\partial}{\partial B}\langle w\rangle_t = \frac{|\hat{q}_p|^2\rho_0}{64\pi^2 R_p^4 R_s^4}\left(\begin{array}{l} 2B(2k^2R_p^4R_s^2 + R_p^4)+ \\ +2k^2R_p^3R_s^3\left[\begin{array}{l}\cos\gamma\cos\left(k(R_p-R_s)\right)+\\ -\sin\gamma\sin\left(k(R_p-R_s)\right)\end{array}\right]+ \\ +2R_pR_s\Delta\left(\begin{array}{l}\left(\begin{array}{l}(k^2R_pR_s+1)\cos(k(R_p-R_s))+\\ k(R_p-R_s)\sin(k(R_p-R_s))\end{array}\right)\cos\gamma+ \\ \left(\begin{array}{l}k(R_p-R_s)\cos(k(R_p-R_s))-\\ (k^2R_pR_s+1)\sin(k(R_p-R_s))\end{array}\right)\sin\gamma\end{array}\right)\end{array}\right). \tag{C.40}$$

Setting the derivative equal to zero and solving for B gives

$$B = -\frac{R_pR_s\left(\begin{array}{l}k^2R_p^2R_s^2\left[\cos\gamma\cos\left(k(R_p-R_s)\right)-\sin\gamma\sin\left(k(R_p-R_s)\right)\right]+ \\ +\Delta\left(\begin{array}{l}\left(\begin{array}{l}(k^2R_pR_s+1)\cos(k(R_p-R_s))+\\ k(R_p-R_s)\sin(k(R_p-R_s))\end{array}\right)\cos\gamma+ \\ \left(\begin{array}{l}k(R_p-R_s)\cos(k(R_p-R_s))-\\ (k^2R_pR_s+1)\sin(k(R_p-R_s))\end{array}\right)\sin\gamma\end{array}\right)\end{array}\right)}{(2k^2R_p^4R_s^2+R_p^4)}. \tag{C.41}$$

Finally, we use the identity $B = |\hat{q}_s|/|\hat{q}_p|$ found in Eq. (C.9) to arrive at the magnitude of the control source that will minimize TED.

$$|\hat{q}_s| = -\frac{|\hat{q}_p| R_s \left(\begin{array}{l} k^2 R_p^2 R_s^2 \left[\cos\gamma \cos\left(k(R_p - R_s)\right) - \sin\gamma \sin\left(k(R_p - R_s)\right)\right] + \\ +\Delta \left(\begin{array}{l} \left(\begin{array}{l} (k^2 R_p R_s + 1)\cos(k(R_p - R_s)) + \\ k(R_p - R_s)\sin(k(R_p - R_s)) \end{array} \right) \cos\gamma + \\ \left(\begin{array}{l} k(R_p - R_s)\cos(k(R_p - R_s)) - \\ (k^2 R_p R_s + 1)\sin(k(R_p - R_s)) \end{array} \right) \sin\gamma \end{array} \right) \end{array} \right)}{R_p^3 (2k^2 R_s^2 + 1)} \tag{C.42}$$

where $\Delta = (x - x_p)(x - x_s) + (y - y_p)(y - y_s) + (z - z_p)(z - z_s)$.

C.4 Minimizing PED

The process for finding a more general solution to the minimization problem is very similar to that used for finding the specific case of a single control source and a single primary source. First, a general expression that describes the sound field is found. The phase and magnitude that of the control source is found by differentiating with respect to those variables and setting the derivatives equal to zero. The resulting equations are than solved for phase and magnitude respectively.

A minimizing a completely general expression is very complicated. For our purposes, we assume that all of primary sources have identical source strengths as do the control sources. These assumptions turn Eqs. (2.1) and (2.2) into

$$\hat{p} = \frac{j\rho_0 ck}{4\pi} \left(\hat{q}_p \sum_{pn=1}^{N} \frac{e^{-jkR_{pn}}}{R_{pn}} + \hat{q}_s \sum_{sn=1}^{N} \frac{e^{-jkR_{sn}}}{R_{sn}} \right). \tag{C.43}$$

Computing the pressure is very cumbersome, assigning variables to the sums helps

simplify this issue. Here ψ_p and ψ_s are defined as

$$\psi_p = \sum_{pn=1}^{N} \frac{e^{-jkR_{pn}}}{R_{pn}} \tag{C.44}$$

$$\psi_s = \sum_{sn=1}^{N} \frac{e^{-jkR_{sn}}}{R_{sn}} \tag{C.45}$$

which reduces the expression for pressure to

$$\hat{p} = \frac{j\rho_0 ck}{4\pi} \left(\hat{q}_p\psi_p + \hat{q}_s\psi_s\right). \tag{C.46}$$

At this point, the squared pressure magnitude is computed by multiplying the pressure by its complex conjugate

$$|\hat{p}|^2 = \hat{p}\hat{p}^* = \frac{j\rho_0 ck}{4\pi} \left(\hat{q}_p\psi_p + \hat{q}_s\psi_s\right) \frac{-j\rho_0 ck}{4\pi} \left(\hat{q}_p^*\psi_p^* + \hat{q}_s^*\psi_s^*\right). \tag{C.47}$$

After simplification the magnitude of pressure squared is expressed as

$$|\hat{p}|^2 = \left(\frac{\rho_0 ck}{4\pi}\right)^2 \left(|\hat{q}_p|^2|\psi_p|^2 + |\hat{q}_s|^2|\psi_s|^2 + 2|\hat{q}_p||\hat{q}_s| \left(\Re\{\psi_s^*\psi_p\}\cos\gamma + \Im\{\psi_s^*\psi_p\}\sin\gamma\right)\right) \tag{C.48}$$

where $\hat{q}_n = |\hat{q}_n|e^{-j\phi_n}$ and $\gamma = \phi_p - \phi_s$ as defined in Eqs. (C.5) and (C.6) respectively.

C.4.1 Finding the Phase Difference of the Control Source

Differentiating squared pressure magnitude by the phase difference γ yields

$$\frac{\partial}{\partial\gamma}|\hat{p}|^2 = \left(\frac{\rho_0 ck}{4\pi}\right)^2 2|\hat{q}_p||\hat{q}_s| \left(-\Re\{\psi_s^*\psi_p\}\sin\gamma + \Im\{\psi_p\psi_s^*\}\cos\gamma\right). \tag{C.49}$$

Solving this expression for γ produces

$$\gamma = \tan^{-1}\left(\frac{\Im\{\psi_p\psi_s^*\}}{\Re\{\psi_s^*\psi_p\}}\right). \tag{C.50}$$

Care must be taken to assure that the appropriate quadrant is used when γ is found using the arctangent.

C.4.2 Finding the Magnitude of the Control Source

It is useful to again define B as $|\hat{q}_s|/|\hat{q}_p|$ as in Eq. (C.9), which simplifies Eq. (C.48) to

$$|\hat{p}|^2 = \left(\frac{\rho_0 ck}{4\pi}\right)^2 |\hat{q}_p|^2 \left(|\psi_p|^2 + B^2|\psi_s|^2 + 2B\left(\Re\{\psi_s^*\psi_p\}\cos\gamma + \Im\{\psi_p\psi_s^*\}\sin\gamma\right)\right). \tag{C.51}$$

Differentiating with respect to B gives

$$\frac{\partial}{\partial B}|\hat{p}|^2 = \left(\frac{\rho_0 ck}{4\pi}\right)^2 |\hat{q}_p|^2 \left(2B|\psi_s|^2 + 2\left(\Re\{\psi_s^*\psi_p\}\cos\gamma + \Im\{\psi_p\psi_s^*\}\sin\gamma\right)\right). \tag{C.52}$$

Setting the derivative equal to zero and solving for B gives

$$B = -\frac{\left(\Re\{\psi_s^*\psi_p\}\cos\gamma + \Im\{\psi_p\psi_s^*\}\sin\gamma\right)}{|\psi_s|^2} \tag{C.53}$$

which becomes

$$|\hat{q}_s| = -|\hat{q}_p|\frac{\left(\Re\{\psi_s^*\psi_p\}\cos\gamma + \Im\{\psi_p\psi_s^*\}\sin\gamma\right)}{|\psi_s|^2} \tag{C.54}$$

when the definition for B is used.

C.5 Minimizing KED

Again, we address the problem of minimizing KED, this time for a case with identical primary sources and identical control sources. Using these assumptions, Eqs. (2.6) and (2.7) become

$$\hat{\vec{u}} = \frac{\hat{q}_s}{4\pi}\sum_{sn=1}^{N}\frac{e^{-jkR_{sn}}}{R_{sn}^3}(jkR_{sn}+1)\vec{R}_{sn} + \frac{\hat{q}_p}{4\pi}\sum_{pn=1}^{N}\frac{e^{-jkR_{pn}}}{R_{pn}^3}(jkR_{pn}+1)\vec{R}_{pn}. \tag{C.55}$$

To keep the computations for particle velocity from becoming unwieldy, it is useful to find the vector magnitude of the particle velocity component by component. In

Cartesian coordinates, the calculations are performed for one component, and the others follow the same process. To start out we express the x component as

$$\hat{u}_x = \frac{\hat{q}_s}{4\pi}\sum_{sn=1}^{N}\frac{e^{-jkR_{sn}}}{R_{sn}^3}(jkR_{sn}+1)(x-x_{sn}) + \frac{\hat{q}_p}{4\pi}\sum_{pn=1}^{N}\frac{e^{-jkR_{pn}}}{R_{pn}^3}(jkR_{pn}+1)(x-x_{pn}). \tag{C.56}$$

Again it is useful to define the sums in the equation as

$$\xi_{sx} = \sum_{sn=1}^{N}\frac{e^{-jkR_{sn}}}{R_{sn}^3}(jkR_{sn}+1)(x-x_{sn}) \tag{C.57}$$

$$\xi_{px} = \sum_{pn=1}^{N}\frac{e^{-jkR_{pn}}}{R_{pn}^3}(jkR_{pn}+1)(x-x_{pn}). \tag{C.58}$$

Expressions for the y and z components also may be defined in a similar manner. These definitions simplify the expression for $\hat{u}_x$ to

$$\hat{u}_x = \frac{\hat{q}_s}{4\pi}\xi_{sx} + \frac{\hat{q}_p}{4\pi}\xi_{px}. \tag{C.59}$$

Next we multiply the x component of particle velocity by its complex conjugate

$$|\hat{u}_x|^2 = \left(\frac{\hat{q}_s}{4\pi}\xi_{sx} + \frac{\hat{q}_p}{4\pi}\xi_{px}\right)\left(\frac{\hat{q}_s}{4\pi}\xi_{sx} + \frac{\hat{q}_p}{4\pi}\xi_{px}\right)^*. \tag{C.60}$$

This further simplifies to

$$|\hat{u}_x|^2 = \frac{1}{16\pi^2}\left(|\hat{q}_s|^2|\xi_{sx}|^2 + |\hat{q}_p|^2|\xi_{px}|^2 + 2|\hat{q}_s||\hat{q}_p|\left(\Re\{\xi_{sx}^*\xi_{px}\}\cos\gamma + \Im\{\xi_{sx}^*\xi_{px}\}\sin\gamma\right)\right). \tag{C.61}$$

where $\hat{q}_n = |\hat{q}_n|e^{-j\phi_n}$ and $\gamma = \phi_p - \phi_s$ as defined in Eqs. (C.5) and (C.6) respectively. The magnitude of the components may be combined as in Eq. (2.52)

$$|\hat{\vec{u}}|^2 = |\hat{u}_x|^2 + |\hat{u}_y|^2 + |\hat{u}_z|^2, \tag{2.52}$$

which results in

$$
\begin{aligned}
|\hat{\vec{u}}|^2 =& \frac{1}{16\pi^2}\left(|\hat{q}_s|^2|\xi_{sx}|^2 + |\hat{q}_p|^2|\xi_{px}|^2 + 2|\hat{q}_s||\hat{q}_p|\left(\Re\{\xi_{sx}^*\xi_{px}\}\cos\gamma + \Im\{\xi_{sx}^*\xi_{px}\}\sin\gamma\right)\right) + \\
& \frac{1}{16\pi^2}\left(|\hat{q}_s|^2|\xi_{sy}|^2 + |\hat{q}_p|^2|\xi_{py}|^2 + 2|\hat{q}_s||\hat{q}_p|\left(\Re\{\xi_{sy}^*\xi_{py}\}\cos\gamma + \Im\{\xi_{sy}^*\xi_{py}\}\sin\gamma\right)\right) + \\
& \frac{1}{16\pi^2}\left(|\hat{q}_s|^2|\xi_{sz}|^2 + |\hat{q}_p|^2|\xi_{pz}|^2 + 2|\hat{q}_s||\hat{q}_p|\left(\Re\{\xi_{sz}^*\xi_{pz}\}\cos\gamma + \Im\{\xi_{sz}^*\xi_{pz}\}\sin\gamma\right)\right).
\end{aligned}
\tag{C.62}
$$

The vector magnitude of particle velocity simplifies to

$$
|\hat{\vec{u}}|^2 = \frac{1}{16\pi^2}\left(\begin{array}{l}
|\hat{q}_p|^2\left(|\xi_{px}|^2 + |\xi_{py}|^2 + |\xi_{pz}|^2\right) + \\
|\hat{q}_s|^2\left(|\xi_{sx}|^2 + |\xi_{sy}|^2 + |\xi_{sz}|^2\right) + \\
2|\hat{q}_s||\hat{q}_p|\left(\begin{array}{l}
\left(\Re\{\xi_{sx}^*\xi_{px}\} + \Re\{\xi_{sy}^*\xi_{py}\} + \Re\{\xi_{sz}^*\xi_{pz}\}\right)\cos\gamma + \\
\left(\Im\{\xi_{sx}^*\xi_{px}\} + \Im\{\xi_{sy}^*\xi_{py}\} + \Im\{\xi_{sz}^*\xi_{pz}\}\right)\sin\gamma
\end{array}\right)
\end{array}\right).
\tag{C.63}
$$

C.5.1 Finding the Phase Difference of the Control Source

Differentiating Eq. (C.63) with respect to the phase difference γ results in

$$
\frac{\partial}{\partial\gamma}|\hat{\vec{u}}|^2 = \frac{2|\hat{q}_s||\hat{q}_p|}{16\pi^2}\left(\begin{array}{l}
-\left(\Re\{\xi_{sx}^*\xi_{px}\} + \Re\{\xi_{sy}^*\xi_{py}\} + \Re\{\xi_{sz}^*\xi_{pz}\}\right)\sin\gamma + \\
\left(\Im\{\xi_{sx}^*\xi_{px}\} + \Im\{\xi_{sy}^*\xi_{py}\} + \Im\{\xi_{sz}^*\xi_{pz}\}\right)\cos\gamma
\end{array}\right).
\tag{C.64}
$$

Setting the derivative equal to zero and solving for γ simplifies to

$$
\gamma = \tan^{-1}\left(\frac{\Im\{\xi_{sx}^*\xi_{px}\} + \Im\{\xi_{sy}^*\xi_{py}\} + \Im\{\xi_{sz}^*\xi_{pz}\}}{\Re\{\xi_{sx}^*\xi_{px}\} + \Re\{\xi_{sy}^*\xi_{py}\} + \Re\{\xi_{sz}^*\xi_{pz}\}}\right).
\tag{C.65}
$$

As always, care must be taken to assure that the correct quadrant is used for finding the appropriate phase difference.

C.5.2 Finding the Magnitude of the Control Source

Using the identity $B = |\hat{q}_s|/|\hat{q}_p|$ from Eq. (C.9) in Eq. (C.63) produces

$$|\hat{\vec{u}}|^2 = \frac{|\hat{q}_p|^2}{16\pi^2}\left(\begin{array}{l}(|\xi_{px}|^2+|\xi_{py}|^2+|\xi_{pz}|^2)+\\ B^2\left(|\xi_{sx}|^2+|\xi_{sy}|^2+|\xi_{sz}|^2\right)+\\ 2B\left(\begin{array}{l}\left(\Re\{\xi_{sx}^*\xi_{px}\}+\Re\{\xi_{sy}^*\xi_{py}\}+\Re\{\xi_{sz}^*\xi_{pz}\}\right)\cos\gamma+\\ \left(\Im\{\xi_{sx}^*\xi_{px}\}+\Im\{\xi_{sy}^*\xi_{py}\}+\Im\{\xi_{sz}^*\xi_{pz}\}\right)\sin\gamma\end{array}\right)\end{array}\right) \tag{C.66}$$

as an expression for the vector magnitude of particle velocity. Differentiating this result by B gives

$$\frac{\partial}{\partial B}|\hat{\vec{u}}|^2 = \frac{|\hat{q}_p|^2}{16\pi^2}\left(\begin{array}{l}2B\left(|\xi_{sx}|^2+|\xi_{sy}|^2+|\xi_{sz}|^2\right)+\\ 2\left(\begin{array}{l}\left(\Re\{\xi_{sx}^*\xi_{px}\}+\Re\{\xi_{sy}^*\xi_{py}\}+\Re\{\xi_{sz}^*\xi_{pz}\}\right)\cos\gamma+\\ \left(\Im\{\xi_{sx}^*\xi_{px}\}+\Im\{\xi_{sy}^*\xi_{py}\}+\Im\{\xi_{sz}^*\xi_{pz}\}\right)\sin\gamma\end{array}\right)\end{array}\right) \tag{C.67}$$

which we set equal to zero and solve for B. After applying the definition given by Eq. (C.9), we find that the magnitude of the control source strength should be

$$|\hat{q}_s| = -|\hat{q}_p|\frac{\left(\begin{array}{l}\left(\Re\{\xi_{sx}\xi_{px}^*\}+\Re\{\xi_{sy}\xi_{py}^*\}+\Re\{\xi_{sz}\xi_{pz}^*\}\right)\cos\gamma+\\ \left(\Im\{\xi_{sx}^*\xi_{px}\}+\Im\{\xi_{sy}^*\xi_{py}\}+\Im\{\xi_{sz}^*\xi_{pz}\}\right)\sin\gamma\end{array}\right)}{\left(|\xi_{sx}|^2+|\xi_{sy}|^2+|\xi_{sz}|^2\right)}. \tag{C.68}$$

C.6 Minimizing TED

To find the TED we use Eq. (C.48) for squared pressure magnitude and Eq. (C.63) for the squared vector magnitude of particle velocity in

$$\langle w\rangle_t = \frac{|\hat{p}|^2}{4\rho_0 c^2} + \frac{\rho_0}{4}\hat{\vec{u}}\cdot\hat{\vec{u}}^* \tag{C.69}$$

as described in Eq. (2.8). The resulting expression for time averaged TED is

$$\begin{aligned}\langle w\rangle_t =&\frac{1}{4\rho_0 c^2}\left(\frac{\rho_0 ck}{4\pi}\right)^2\left(\begin{array}{l}|\hat{q}_p|^2|\psi_p|^2+|\hat{q}_s|^2|\psi_s|^2+\\ 2|\hat{q}_p||\hat{q}_s|\left(\Re\{\psi_s^*\psi_p\}\cos\gamma+\Im\{\psi_p\psi_s^*\}\sin\gamma\right)\end{array}\right)+\\ &+\frac{\rho_0}{4}\frac{1}{16\pi^2}\left(\begin{array}{l}|\hat{q}_p|^2\left(|\xi_{px}|^2+|\xi_{py}|^2+|\xi_{pz}|^2\right)+\\ |\hat{q}_s|^2\left(|\xi_{sx}|^2+|\xi_{sy}|^2+|\xi_{sz}|^2\right)+\\ 2|\hat{q}_s||\hat{q}_p|\left(\begin{array}{l}\left(\Re\{\xi_{sx}^*\xi_{px}\}+\Re\{\xi_{sy}^*\xi_{py}\}+\Re\{\xi_{sz}^*\xi_{pz}\}\right)\cos\gamma+\\ \left(\Im\{\xi_{sx}^*\xi_{px}\}+\Im\{\xi_{sy}^*\xi_{py}\}+\Im\{\xi_{sz}^*\xi_{pz}\}\right)\sin\gamma\end{array}\right)\end{array}\right).\end{aligned} \tag{C.70}$$

Simplifying TED results in

$$\begin{aligned}\langle w\rangle_t =&\frac{\rho_0}{64\pi^2}\left(\begin{array}{l}|\hat{q}_p|^2\left(|\psi_p|^2k^2+|\xi_{px}|^2+|\xi_{py}|^2+|\xi_{pz}|^2\right)+\\ |\hat{q}_s|^2\left(|\psi_s|^2k^2+|\xi_{sx}|^2+|\xi_{sy}|^2+|\xi_{sz}|^2\right)+\\ 2|\hat{q}_s||\hat{q}_p|\left(\begin{array}{l}\Re\{\psi_s^*\psi_p\}k^2\cos\gamma+\Im\{\psi_p\psi_s^*\}k^2\sin\gamma+\\ \left(\Re\{\xi_{sx}^*\xi_{px}\}+\Re\{\xi_{sy}^*\xi_{py}\}+\Re\{\xi_{sz}^*\xi_{pz}\}\right)\cos\gamma+\\ \left(\Im\{\xi_{sx}^*\xi_{px}\}+\Im\{\xi_{sy}^*\xi_{py}\}+\Im\{\xi_{sz}^*\xi_{pz}\}\right)\sin\gamma\end{array}\right)\end{array}\right).\end{aligned} \tag{C.71}$$

To simplify the expression further, it is useful to make some definitions:

$$\tau_p = |\psi_p|^2k^2+|\xi_{px}|^2+|\xi_{py}|^2+|\xi_{pz}|^2 \tag{C.72}$$

$$\tau_s = |\psi_s|^2k^2+|\xi_{sx}|^2+|\xi_{sy}|^2+|\xi_{sz}|^2 \tag{C.73}$$

$$\chi_\Re = \Re\{\psi_p\psi_s^*\}k^2+\Re\{\xi_{sx}^*\xi_{px}\}+\Re\{\xi_{sy}^*\xi_{py}\}+\Re\{\xi_{sz}^*\xi_{pz}\} \tag{C.74}$$

$$\chi_\Im = \Im\{\psi_p\psi_s^*\}k^2+\Im\{\xi_{sx}^*\xi_{px}\}+\Im\{\xi_{sy}^*\xi_{py}\}+\Im\{\xi_{sz}^*\xi_{pz}\}. \tag{C.75}$$

Using these definitions, TED simplifies to

$$\langle w\rangle_t = \frac{\rho_0}{64\pi^2}\left(|\hat{q}_p|^2\tau_p+|\hat{q}_s|^2\tau_s+2|\hat{q}_s||\hat{q}_p|\left(\chi_\Re\cos\gamma+\chi_\Im\sin\gamma\right)\right). \tag{C.76}$$

This expression for TED is much less cumbersome for the process of finding optimal control source strengths for minimizing TED at the error sensor location.

C.6.1 Finding the Phase Difference of the Control Source

Again, the first step in finding the phase is to differentiate with respect to the phase difference γ. The derivative of time averaged particle velocity with respect to γ is.

$$\frac{\partial}{\partial\gamma}\langle w\rangle_t = \frac{\rho_0}{64\pi^2}2|\hat{q}_s||\hat{q}_p|\left(-\chi_{\Re}\sin\gamma + \chi_{\Im}\cos\gamma\right) = 0 \tag{C.77}$$

Setting the derivative equal to zero and solving for the phase difference γ gives

$$\gamma = \tan^{-1}\left(\frac{\chi_{\Im}}{\chi_{\Re}}\right). \tag{C.78}$$

Using Eqs. (C.74) and (C.75), a more explicit description for phase difference is

$$\gamma = \tan^{-1}\left(\frac{\Im\{\psi_p\psi_s^*\}k^2 + \Im\{\xi_{sx}^*\xi_{px}\} + \Im\{\xi_{sy}^*\xi_{py}\} + \Im\{\xi_{sz}^*\xi_{pz}\}}{\Re\{\psi_p\psi_s^*\}k^2 + \Re\{\xi_{sx}^*\xi_{px}\} + \Re\{\xi_{sy}^*\xi_{py}\} + \Re\{\xi_{sz}^*\xi_{pz}\}}\right). \tag{C.79}$$

Again, care must be taken to assure that γ falls within the correct quadrant.

C.6.2 Finding the Magnitude of the Control Source

Using Eq. (C.9) to change $|\hat{q}_s|/|\hat{q}_p|$ to B to simplify Eq. (C.76) we express TED as

$$\langle w\rangle_t = \frac{\rho_0}{64\pi^2}|\hat{q}_p|^2\left(\tau_p + B^2\tau_s + 2B\left(\chi_{\Re}\cos\gamma + \chi_{\Im}\sin\gamma\right)\right) \tag{C.80}$$

Differentiating with respect to B yields

$$\frac{\partial}{\partial B}\langle w\rangle_t = \frac{\rho_0}{64\pi^2}|\hat{q}_p|^2\left[2B\tau_s + 2(\chi_{\Re}\cos\gamma + \chi_{\Im}\sin\gamma)\right] \tag{C.81}$$

After setting the derivative equal to zero and solving for B we find that the control source strength is

$$|\hat{q}_s| = -|\hat{q}_p|\frac{\chi_{\Re}\cos\gamma + \chi_{\Im}\sin\gamma}{\tau_s}. \tag{C.82}$$

Replacing the definitions from Eqs. (C.73), (C.74), and (C.75) produces

$$|\hat{q}_s| = -|\hat{q}_p| \frac{\left(\begin{array}{l} \left(\Re\{\psi_p \psi_s^*\} k^2 + \Re\{\xi_{sx}^* \xi_{px}\} + \Re\{\xi_{sy}^* \xi_{py}\} + \Re\{\xi_{sz}^* \xi_{pz}\}\right) \cos\gamma + \\ + \left(\Im\{\psi_p \psi_s^*\} k^2 + \Im\{\xi_{sx}^* \xi_{px}\} + \Im\{\xi_{sy}^* \xi_{py}\} + \Im\{\xi_{sz}^* \xi_{pz}\}\right) \sin\gamma \end{array} \right)}{|\psi_s|^2 k^2 + |\xi_{sx}|^2 + |\xi_{sy}|^2 + |\xi_{sz}|^2}, \tag{C.83}$$

a more explicit expression for the magnitude of the control source strengths.

C.7 Issues With Arctangents

Care must be taken when an arctangent is used in calculations in order to assure that the result pertains to the correct quadrant. A very simple method is used in this research to find the correct quadrant. This is done by finding the result of the arctangent for all four quadrants. The result is used to calculate the power output of the system with that phase angle. This results in four values for the total sound power of the system. The smallest of these four values is chosen for the MEDToPO plots. In this way the ambiguity is thoroughly explored to avoid potential errors that may arise in minimizing a field quantity at a chosen field point.

Appendix D

Finding an Impulse Response from a Frequency Response

In this research, the computer model was developed in the frequency domain. However, in order to examen the effect in the time domain, it is useful to have a time domain representation of that system as well as a time domain representation that shows the effect of control on the system. The correcting method needs to be implemented using a time domain description in order to implement it in a practical situation. Fortunately, the impulse response, which is simply the inverse Fourier transform of the frequency response, is the time domain description of an acoustic system.

The frequency spectrum may be calculated using the information discussed in Ch. 2. This spectrum may be divided by the input signal, in general the response of a system may be described by the output divided by the input. In the frequency domain, the response may be written [83, 84]

$$H(f) = \frac{S_{output}(f)}{S_{input}(f)}. \tag{D.1}$$

This may be inverse Fourier transformed to get the impulse response of the system.[1] To find an impulse response using a discrete model, care must be taken when taking the Fourier transform.

One feature of a realistic impulse response is that the it must only be real-valued. Certain features must exist in the frequency response in order to assure that this happens . The real part of the frequency response must be symmetric, while the imaginary portion of the frequency response must be antisymmetric [85]. Also, the first element in the frequency response represents the 0 Hz, or DC, portion of the response, which should be zero. In order to meat this requirement, it is helpful to remember that the DFT assumes a periodic system, and that as a sequence goes from the time domain to the frequency domain through a Fourier transform, the result ends up with negative frequencies. If negative frequencies are not deleted, then an inverse DFT (IDFT) will result in the original time domain signal [85]. These negative frequencies are not generated in the typical model, however they must be generated to arrive at a realistic impulse response using a Fourier transform. The appropriate technique for finding negative frequents depend on the length of the array representing the frequency response. Both techniques involve approximately doubling the length of the array. If the desired length of the resulting array is odd, a zero may be inserted at the start of the remaining terms in the array, and may be built from the known frequency response such that

$$H_r[n] = \begin{cases} 0 & n = 0 \\ H[n-1] & 1 \leq n \leq N \\ H^*[2N-n] & N+1 \leq n \leq 2N \end{cases} \tag{D.2}$$

where N is the length of the original frequency response, n indicates the numbered

[1] There are other forms of the equation for frequency response that are less susceptible to noise in the measurement. These other methods could work equally well for this discussion.

element in the response, * indicates taking the complex conjugate, and $H[n]$ is the original frequency response. The IDFT may be operated on the reflected frequency response, $H_r[n]$, to find an impulse response that is $2N+1$ long. If the desired length of the impulse response is even the expression is slightly different. It may be expressed

$$H_r[n] = \begin{cases} 0 & n = 0 \\ H[n-1] & 1 \leq n \leq N \\ 0 & n = N+1 \\ H^*[2N-n] & N+2 \leq n \leq 2N+1. \end{cases} \tag{D.3}$$

The resulting reflected frequency response will be $2N+2$ long. It is also possible to make the array shorter. It may be convenient to make the array $2N$ long, for example, if the initial array is radix 2 and the chosen fast Fourier transform (FFT) algorithm to be used requires such a data set. To do this the last term in the initial frequency response may be dropped before entering the array into Eq. (D.3). This may also be done by changing Eq. (D.3) to

$$H_r[n] = \begin{cases} 0 & n = 0 \\ H[n-1] & 1 \leq n \leq N-1 \\ 0 & n = N \\ H^*[2N-n] & N+1 \leq n \leq 2N-1. \end{cases} \tag{D.4}$$

This method finds an impulse response that is exactly $2N$ long, however the cost is the destruction of some information already obtained.

One important thing to note is that the sample rate is changed when using this process to find the impulse response. Sampling period, τ, may be expressed by [85]

$$\tau = \frac{1}{f_s} = \frac{1}{f_{max}} \tag{D.5}$$

where f_s is the sample frequency, which is equal to the highest frequency corresponding to the frequency response array. When the reflected arrays are created, the

maximum frequency is extended, but the time spent sampling does not change, the resolution does. This means that if the frequency range, or equivalently array length, is doubled in the sample frequency is doubled so the sample period is halved. The modeled frequency response may be designed such that the final sample frequency matches that of the signal with which it will be convolved. Alternatively, the resultant impulse response may be decimated by a factor of two. To perform this alternating terms in the discrete array are deleted. The resulting array represents an impulse response taken at half the sample frequency.

Appendix E

Animations

In the process of analyzing the sound fields, it became useful to look at four dimensions simultaneously. One way to easily visualize four dimensions simultaneously is to animate a plot over one of the demotions. Because it is not reasonable to include these animations in a paper copy of a thesis, these animations have been reserved for this appendix for use in digital copies of this thesis. A digital copy of this thesis may be found in the back of this thesis.

E.1 MEDToPO Animation

The MEDToPO plot is used to illustrate the minimum sound power possible for a given error sensor location. This can be done because sound power is a global quantity, so it is independent of the location where it is measured. Each point on the plot has a color assigned to it representing the sound power that would be radiated from the combination of sources if the error sensor in an ANC system were placed at that position.

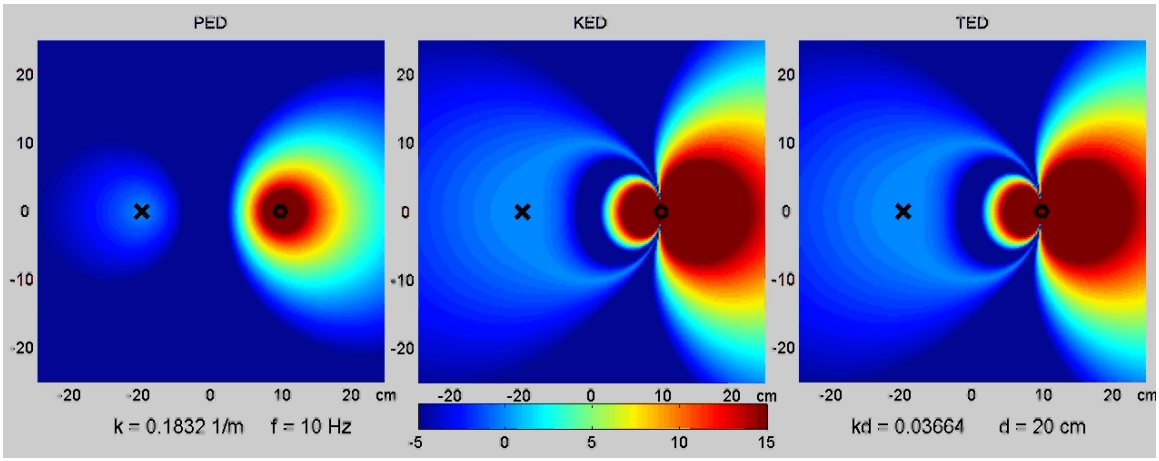

Figure E.1 This is an animated MEDToPO plot for two sound sources where one source is minimizing the given ED quantity, while the other is putting out a predetermined signal. See also Figs. 3.1 and 4.6 and the accompanying discussions found in Secs. 3.1.2 and 4.2.1. The × indicates the control sources while the ∘ indicates the primary source.

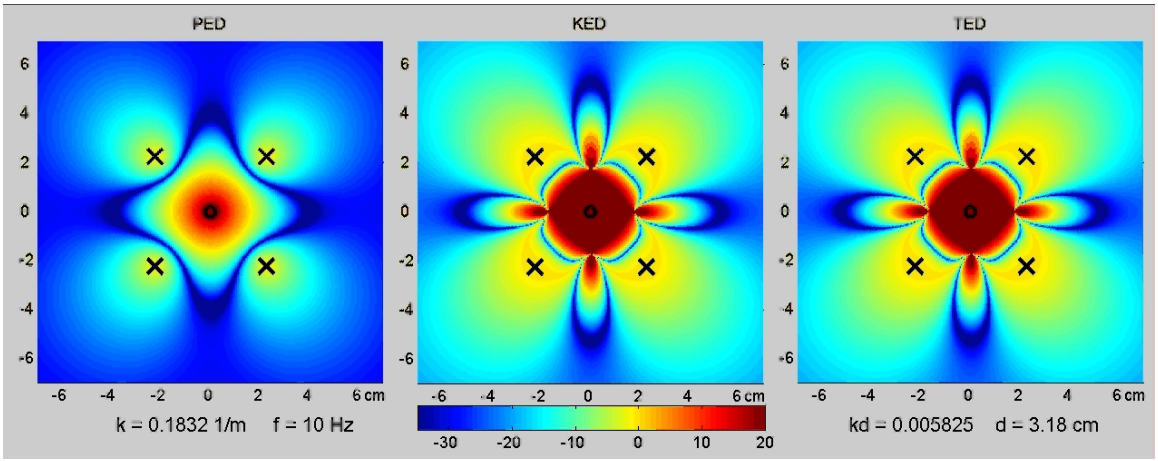

Figure E.2 This is an animated MEDToPO plot for five sound sources where four sources are minimizing the given ED quantity, while the other is putting out a predetermined signal. See also Fig. 4.9 and the accompanying discussions found in Secs. 3.1.2 and 4.2.1. The ×s indicate the control sources while the ∘ indicates the primary source.

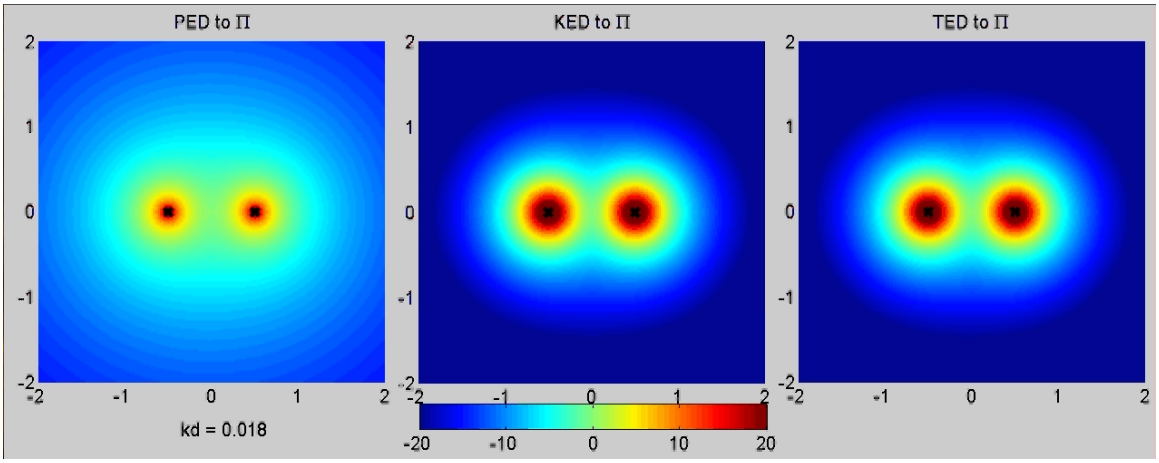

Figure E.3 This animation shows the conversion factor from ED to sound power, discussed in Secs. 2.2.4 and 4.2.2, animated over frequency.

E.2 Relations Between ED and Power

Two important measurements in sound control are ED and Sound Power. Though there are difficulties with ED measurements, it is more convenient to measure ED than sound power in a real system. Unfortunately, if the relationship between ED and power depend on exact knowledge of the positions of the sound sources, sensor locations, and source strengths. In theoretical calculations this is all that is needed to calculate the sound power, and there are methods to approximate sound power that are more efficient for approximating sound power. This means that the relationship investigated here does not simplify computation of sound power. The animation in Fig. E.3 shows the comparison of exact and approximate solutions of the conversion factor discussed in Secs. 2.2.4 and 4.2.2.

E.3 Sound Fields

In Sec. 3.3.5 it is mentioned that some measurements, such as Lagrangian density, may be used to equalize a sound field, but will produce undesirable results. To

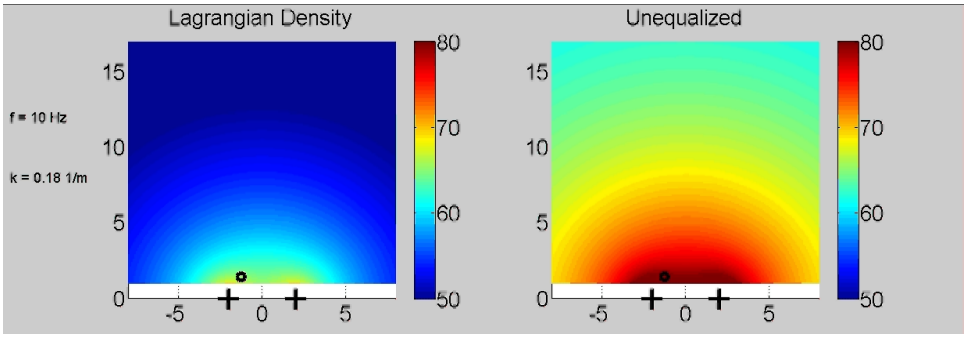

Figure E.4 This is a comparison of equalization using Lagrangian density, on the right and the sound field without equalization on the left. This shows how poorly Lagrangian density performs as a metric for equalizing a sound field.

demonstrate the effects of a bad equalization method, an animation of equalization using Lagrangian density is compared, in Fig. E.4, with an unequalized sound field. The Lagrangian density shows that the L_p of the field increases and decreases wildly at nearly every location in the listening area. Further discussion of this can be found in Sec. 3.3.5.

In order to visualize the effects of equalizing different sound fields it was convenient to animate the sound field over frequency. Equalization performed using PED, or squared pressure, works well at the point where the error sensor is located, this is shown in Fig. E.5 at the point marked by $\circ$. This figure also shows that in locations other than the position of the error sensor experiences degradation to equalization. This Fig. E.5 corresponds to Figs. 5.1 and 5.2.

In Sec. 5.1.2, the effect of amplification of a reinforcing source is examined on a long narrow listening region. Here the effects are animated as a function of the placement of the error sensor. The region around the sensor where equalization is successful increases as the error sensor is moved farther form the sources. The improvement as the sensor moves is not due to better equalization, but due to diminished signal at sensor locations from the sound source. These animations can be seen in Fig. E.6.

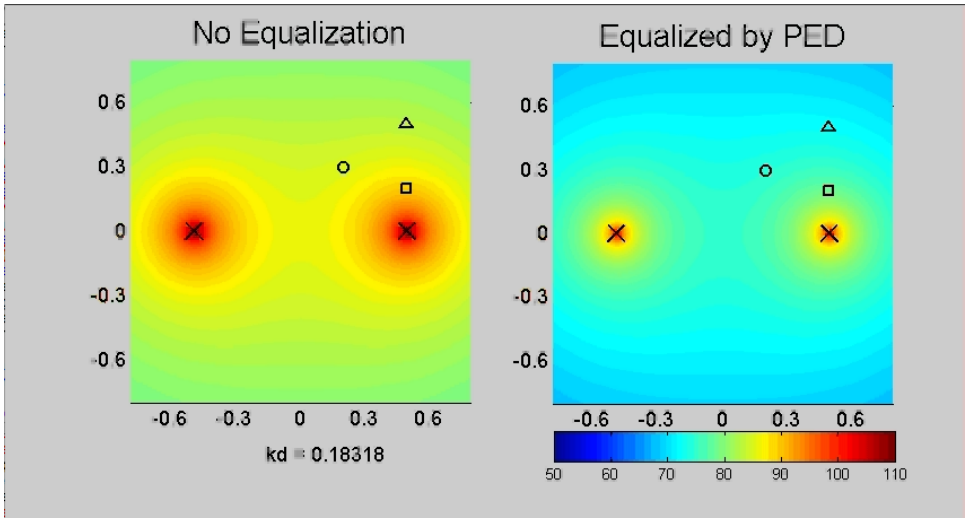

Figure E.5 This animation illustrates how the sound field changes when equalized at a point using PED. Note that the beam pattern is not altered by the equalization, while the sound level adjusts to keep the frequency response constant at the sensor location marked by ∘. This corresponds to Figs. 5.1 and 5.2.

Several movies were made using with MATLAB® to demonstrate the flexibility of the methods used in this research. Two of these animations are shown here. The first animation shows the sound field generated by two arrays consisting of four point sources. The second shows five point sources arranged in a pattern similar to a 5.0 surround sound system. The third shows the sound field generated by two sources modeled by a vibrating cap in a sphere.

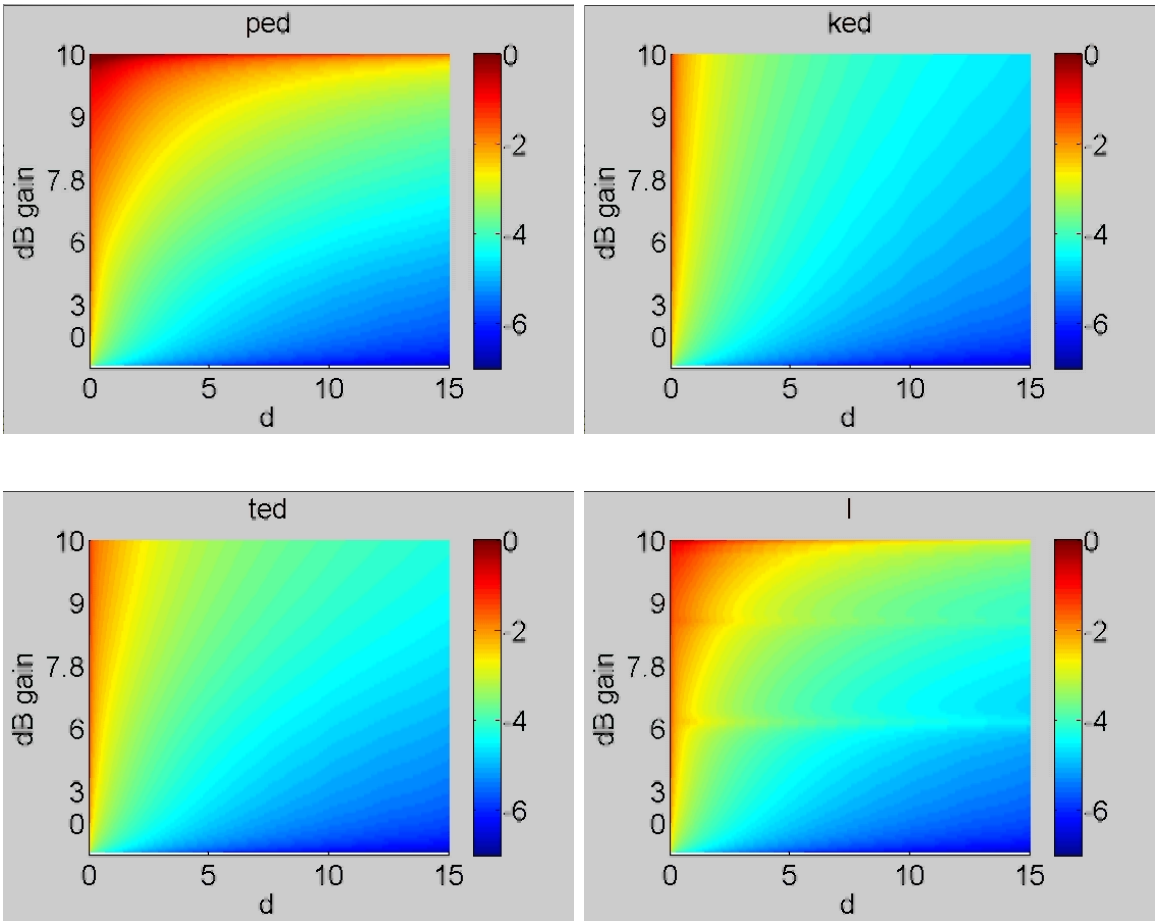

Figure E.6 These movies shows the effect of equalizing a reinforcing loudspeaker as a function of gain and is animated over error sensor location. See Figs. 5.10 and 5.11

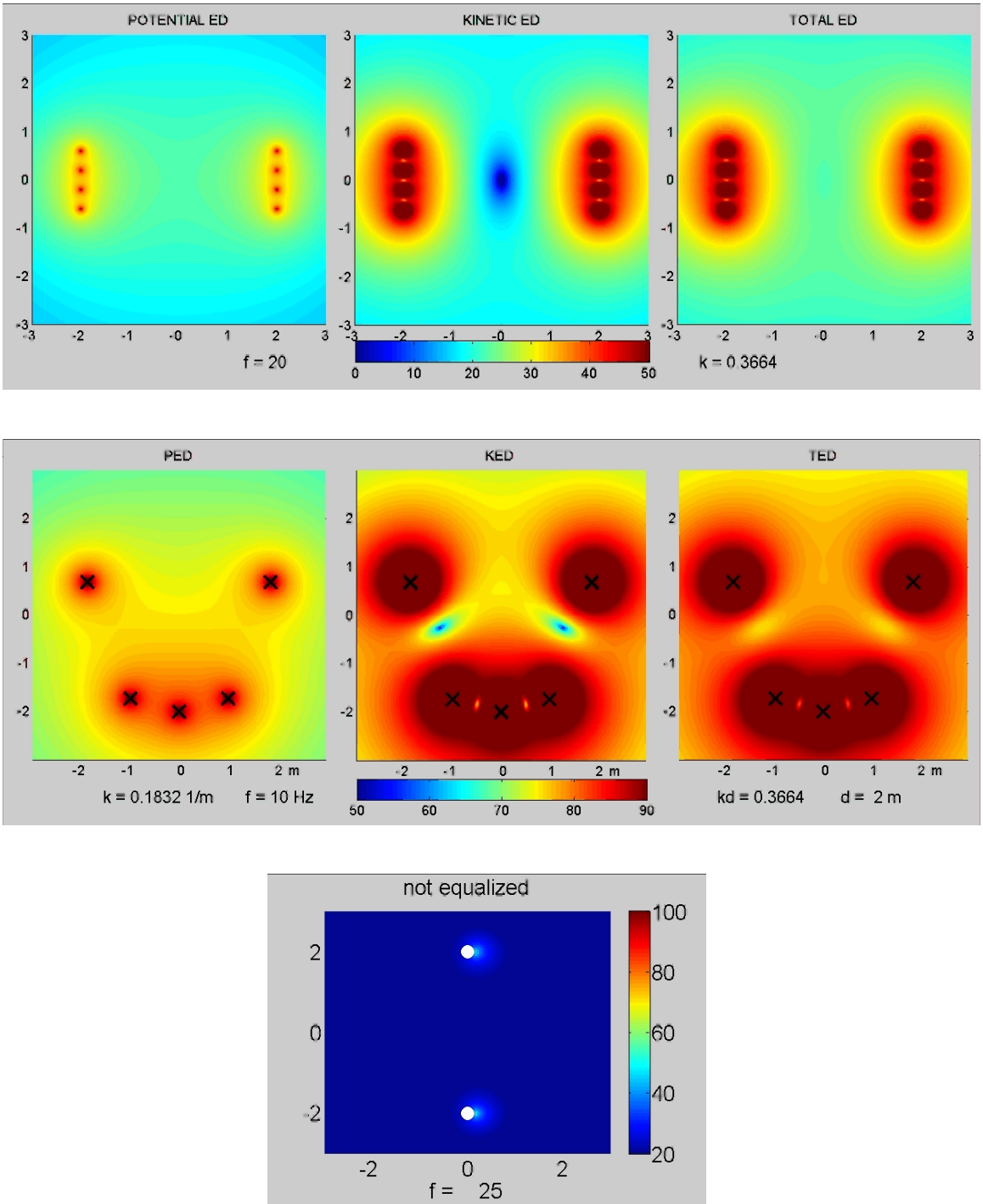

Figure E.7 The above animations demonstrate the flexibility of the methods used in this research. These animations correspond to Figs. 4.3 and 4.4.

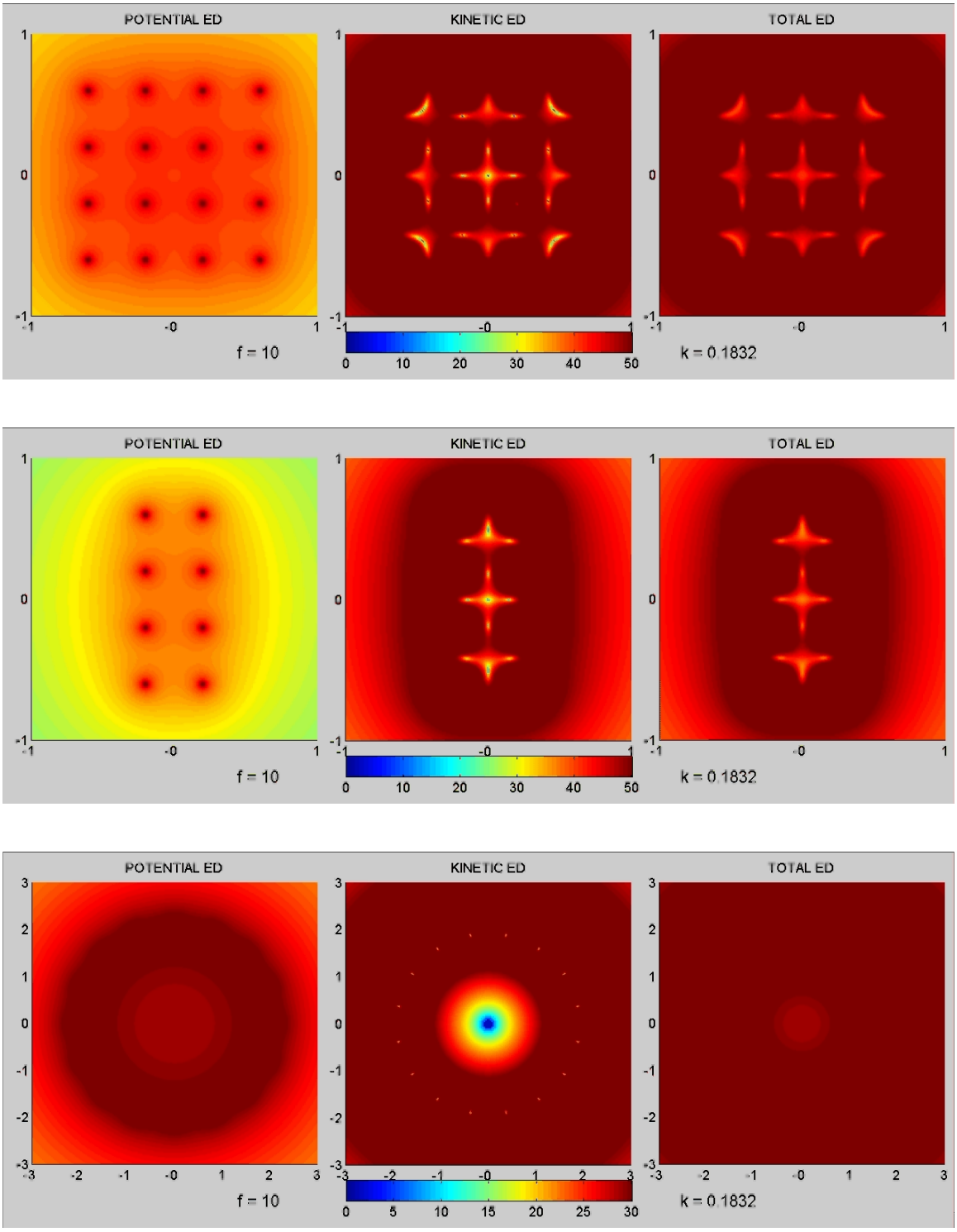

Figure E.8 These are some more animations that were generated to show the power of the computational approach to modeling a sound field. These do not correspond to other figures found in the text.

Appendix F

Auralizations

Auralizations demonstrate what would be heard in a given sound environment. These tools are made by convolving recorded anechoic signal with an impulse response that characterizes the listening situation. This appendix contains several auralizations. A digital copy of this thesis may be found in the back of this thesis.

F.1 Verification of Convolution

Secs. 3.2.2 and 3.3.1 discuss the use of the convolution to produce auralizations. In order to verify that linearconv.m, written in MATLAB®, is correct a convolution using an impulse response of a tube model convolved with prerecorded anechoic speech to produce an auralization. The anechoic speech and impulse response are convolved using GratisVolver™ and MATLAB® producing a pair of auralizations. Figure 3.5 contains plots comparing the resulting auralizations; these auralizations, found in Table F.1, may be listened to in the digital version of this thesis. The code for linearconv.m can be found in Appendix G.

Table F.1 This table compares the results of using the MATLAB® function linearconv.m to produce auralizations to using GratisVolver™ to generate auralizations.

Auralization using GratisVolver.exe to perform the convolution
Auralization using linearconv.m to perform the convolution

F.2 Example of Room Response

The method used in this research to model the response at a point in a sound field has some limitations. The model produces more realistic results when a truncated impulse response is used. Three auralizations are given in Table F.2. The first pressure based auralization is an anechoic recording of speech that is used to produce the other two auralizations. The second auralization was built with an impulse response consisting of 2^{12} terms. The third auralization was created using an impulse response with 2^{16} terms. There is significantly more distortion for the third case compared to the second case.

F.3 Examples of Equalization

Section 5.3.4 describes some equalization results that can be demonstrated using auralizations. Here, the figures from Sec. 5.3.4 are displayed again along with their corresponding auralizations. These auralizations were performed for a simple case consisting of seven sources arranged in a collinear array. The initial auralization

Table F.2 This table compares an auralization of a reverberant room generated using a simulated impulse response 2^{12} terms long to one generated with an impulse response 2^{16} terms long. Both responses are too long for realistic measurements, but provide a proof of concept.

Auralization of anechoic speech.
Auralization generated with 2^{12} term impulse response.
Auralization generated with 2^{16} term impulse response.

was generated at a point near the sound sources. One set of equalization filters were designed at the listening position, while a second set of equalization filters was designed for a point several centimeters away. The auralization of the unequalized sound field was used to show the effect of the equalizing filters at the listening position.

Table F.3 The impulse and frequency responses for the unequalized case are presented here. This is the same figure shown in Fig. 5.30. Below is an auralization of the unequalized case considered in Sec. 5.3.4. Compare with anechoic speech in Table F.2

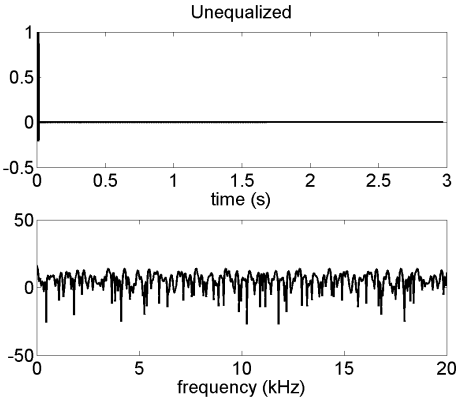

Table F.4 These are responses for a system equalized using a filter designed for the listening position (a) and using a filter designed for a listening position several centimeters away (b). The equalization filters in this figure were designed using complex pressure.

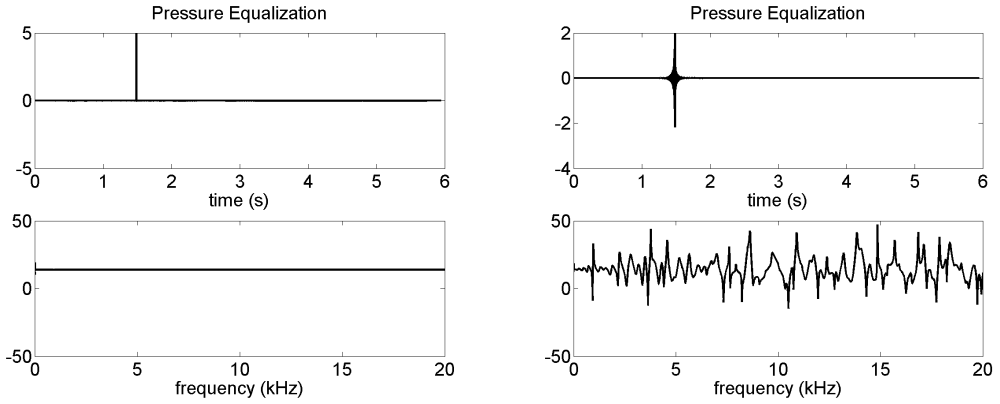

(a) (b)

Equalization defined at sensor location, (a).

Equalization defined away from sensor location, (b).

Table F.5 These are responses for a system equalized using a filter designed for the listening position (a) and using a filter designed for a listening position several centimeters away (b). The equalization filters in this figure were designed using the minimum phase of complex pressure.

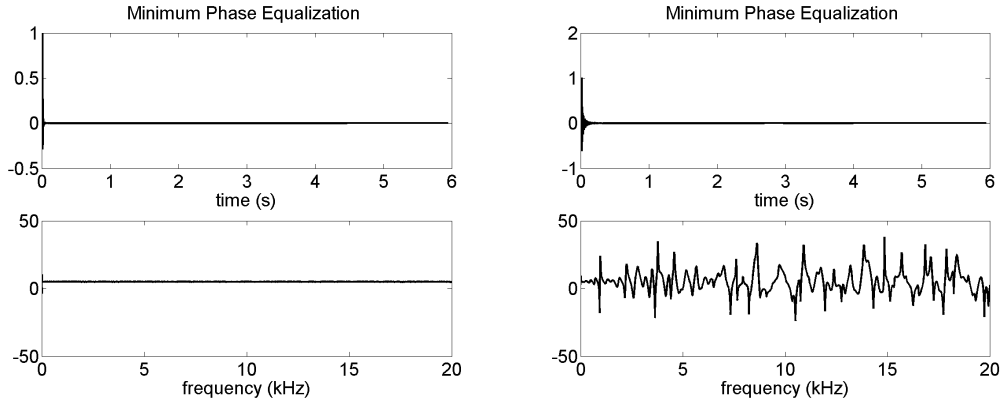

(a) (b)

Equalization defined at sensor location, (a).

Equalization defined away from sensor location, (b).

Table F.6 These are responses for a system equalized using a filter designed for the listening position (a) and using a filter designed for a listening position several centimeters away (b). The equalization filters in this figure were designed using PED.

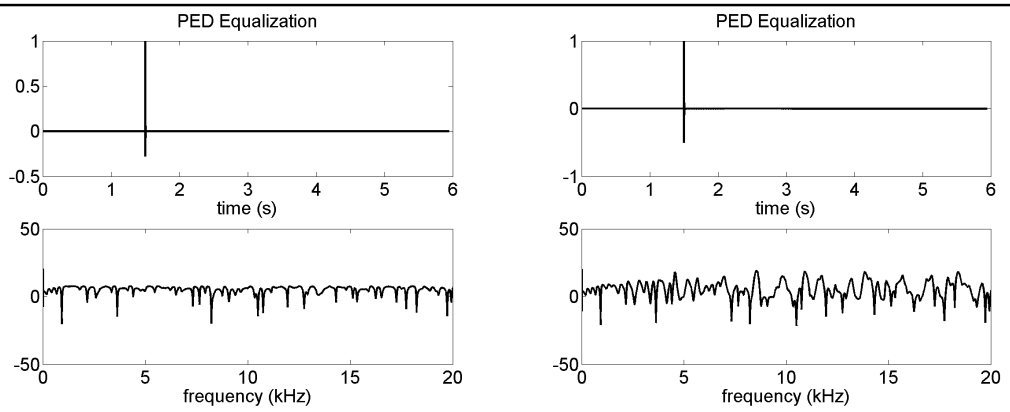

(a) (b)

Equalization defined at sensor location, (a).

Equalization defined away from sensor location, (b).

Table F.7 These are responses for a system equalized using a filter designed for the listening position (a) and using a filter designed for a listening position several centimeters away (b). The equalization filters in this figure were designed using KED.

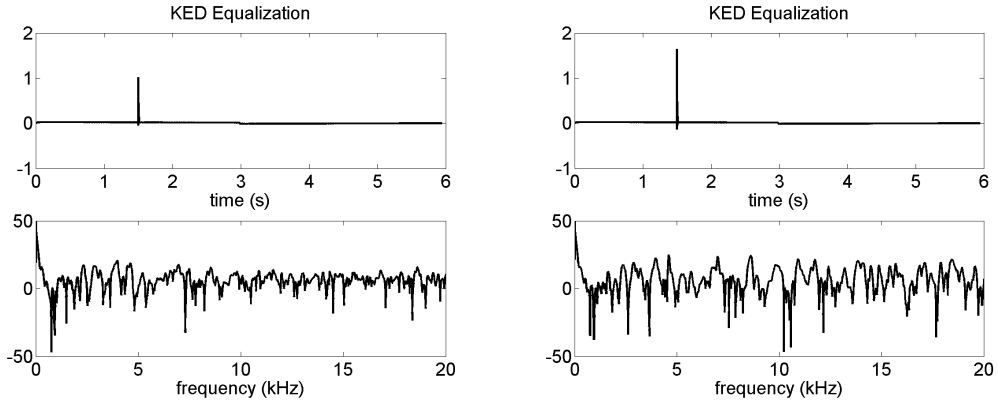

(a) (b)

Equalization defined at sensor location, (a).

Equalization defined away from sensor location, (b).

Table F.8 These are responses for a system equalized using a filter designed for the listening position (a) and using a filter designed for a listening position several centimeters away (b). The equalization filters in this figure were designed using TED.

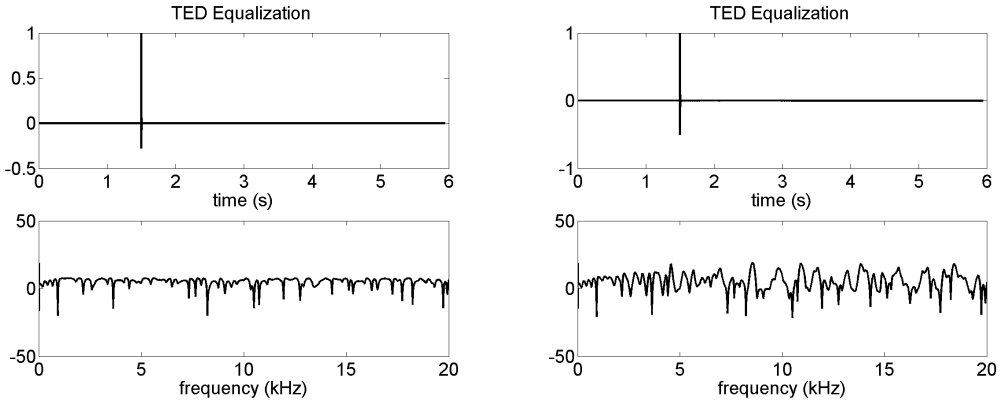

(a) (b)

Equalization defined at sensor location, (a).

Equalization defined away from sensor location, (b).

Table F.9 These are responses for a system equalized using a filter designed for the listening position (a) and using a filter designed for a listening position several centimeters away (b). The equalization filters in this figure were designed using complex pressure. This is similar to Table F.4, the difference is that this model used significantly fewer terms to generate the responses than the one used for Table F.4.

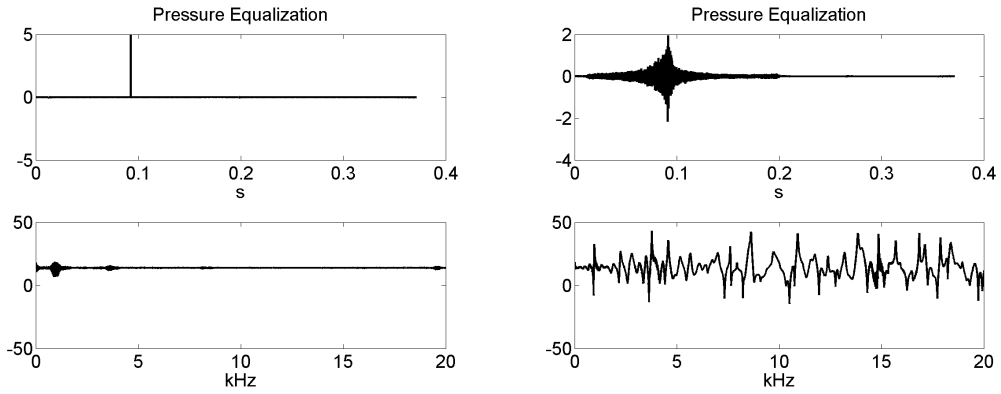

(a) (b)

Equalization defined at sensor location, (a).

Equalization defined away from sensor location, (b).

Appendix G

linearconv.m

```
%  This function determines the linear convolution of signal x with
%  signal y function z=linearconv(x,y)
function z=linearconv(x,y)

lx=length(x);   ly=length(y);
L=lx+ly;

if lx>=ly           %   determines which file is the longer of the two
    sig=x;
    fil=y;
    ls=lx;  lf=ly;
else
    sig=y;
    fil=x;
    ls=ly;  lf=lx;
end

nr=ceil(ls/lf);     %   find how many times to convolve the pieces
sig=[sig,zeros(1,nr*lf-ls)];
                    %   zero pads the system so that the signal has a
                    %   matching length for the last convolution
fif=fft([fil,zeros(1,lf)]);
z=zeros(1,lf+length(sig));

for n=1:nr          %   performing the convolution using the fft and an
                    %   overlap save technique.
    si=fft([sig((n-1)*lf+1:n*lf),zeros(1,lf)]);
```

```
    co=ifft(fif.*si);
    z((n-1)*lf+1:n*lf+lf)=z((n-1)*lf+1:n*lf+lf)+co;
end

z=z(1:L-1);          %   removing the data caused by the extra zeros from
                     %   the zero padding of the signals.
```

Appendix H

MEDToPO.m

H.1 Main File

The following MATLAB® code generates an animated MEDToPO plot. The comments point out portions of the code that may be used to modify the code for use with other source arrangements. This version of the code works with one point source and an arbitrary number of point control sources.

MEDToPO.m

```
%   This porduces a Minimized Energy Density Total Power Output
%   (MEDToPO) plot for cases with a single primary source and
%   multaple control sources.  Notes within the code indicate point
%   where the code may be altered for the desired locations.  This
%   version produces and animation over a range of frequencys.
%   This could easily be altered for dealing  with multiple primary
%   sources.

clear all, close all
tic

fprintf('\n running\n')
global rho c
c=343;  rho=1.21;
```

```
dx=0.0010;
L=0.10;
X=-L:dx:L;
X=X*2.5;
[x,y]=ndgrid(X,X);
z=0;
clear X
N=size(x);

df=10;
f=df:df:5000;   %   This defines the frequency range for the
                %   animation

k=2*pi*f/c;
M=length(f);

d=0.0318;   %   d is the value used for calculating k*d
cd=sqrt(d^2/2);
%   Coord gives the Cartisian coordinates of the sound sources.  The
%   first source is the primary source, the rest are control sources.
coord=[  0,  0,0;
         cd, cd,0;
        -cd, cd,0;
         cd,-cd,0;
        -cd,-cd,0];

Rp= sqrt((x-coord(1,1)).^2+(y-coord(1,2)).^2+(z-coord(1,3)).^2);

qp=.00002./(k);     %   The source strength of the primary source.

[a,b]=size(coord);
save('PowerOutput\Setup4SevralAlt','x','y','k','f','coord','d','a');

%%

for m=1:M
    Pp1=zeros(N);
    Pp2=Pp1;
    Pp3=Pp1;
    Pp4=Pp1;

    Pk1=Pp1;
```

```
Pk2=Pp1;
Pk3=Pp1;
Pk4=Pp1;

Pt1=Pp1;
Pt2=Pp1+1000;
Pt3=Pp1+1000;
Pt4=Pp1+1000;

%   Potential ED
psip=exp(-j.*k(m).*Rp)./Rp;
psis=zeros(N);
for n=2:a
    Rs= sqrt((x-coord(n,1)).^2+(y-coord(n,2)).^2+...
           (z-coord(n,3)).^2);
    psis=psis+exp(-j.*k(m).*Rs)./Rs;
end
psips=psip.*conj(psis);

gp=atan2(imag(psips),real(psips));
qsp1=-abs(qp(m)).*(real(psips).*cos(gp)+imag(psips).*sin(gp))./...
       abs(psis).^2;
gp=atan2(-imag(psips),real(psips));
qsp2=-abs(qp(m)).*(real(psips).*cos(gp)+imag(psips).*sin(gp))./...
       abs(psis).^2;
gp=atan2(imag(psips),-real(psips));
qsp3=-abs(qp(m)).*(real(psips).*cos(gp)+imag(psips).*sin(gp))./...
       abs(psis).^2;
gp=atan2(-imag(psips),-real(psips));
qsp4=-abs(qp(m)).*(real(psips).*cos(gp)+imag(psips).*sin(gp))./...
       abs(psis).^2;

%   Kinetic ED
xipx=(exp(-j.*k(m).*Rp)./Rp.^3).*(j.*k(m).*Rp+1).*(x-coord(1,1));
xipy=(exp(-j.*k(m).*Rp)./Rp.^3).*(j.*k(m).*Rp+1).*(y-coord(1,2));
xipz=(exp(-j.*k(m).*Rp)./Rp.^3).*(j.*k(m).*Rp+1).*(z-coord(1,3));
xisx=zeros(N);
xisy=zeros(N);
xisz=zeros(N);
for n=2:a
    Rs= sqrt((x-coord(n,1)).^2+(y-coord(n,2)).^2+...
       (z-coord(n,3)).^2);
    xisx=xisx+(exp(-j.*k(m).*Rs)./Rs.^3).*(j.*k(m).*Rs+1).*...
```

```
        (x-coord(n,1));
    xisy=xisy+(exp(-j.*k(m).*Rs)./Rs.^3).*(j.*k(m).*Rs+1).*...
        (y-coord(n,2));
    xisz=xisz+(exp(-j.*k(m).*Rs)./Rs.^3).*(j.*k(m).*Rs+1).*...
        (z-coord(n,3));
end

xipsx=xipx.*conj(xisx);
xipsy=xipy.*conj(xisy);
xipsz=xipz.*conj(xisz);

gkn=imag(xipsx)+imag(xipsy)+imag(xipsz);
gkd=real(xipsx)+real(xipsy)+real(xipsz);

gk=atan2(gkn,gkd);
qsk1=-abs(qp(m)).*...
    ((gkd).*cos(gk)+(gkn).*sin(gk))./...
        (xisx.*conj(xisx)+xisy.*conj(xisy)+xisz.*conj(xisz));
gk=atan2(-gkn,gkd);
qsk2=-abs(qp(m)).*...
    ((gkd).*cos(gk)+(gkn).*sin(gk))./...
        (xisx.*conj(xisx)+xisy.*conj(xisy)+xisz.*conj(xisz));
gk=atan2(gkn,-gkd);
qsk3=-abs(qp(m)).*...
    ((gkd).*cos(gk)+(gkn).*sin(gk))./...
        (xisx.*conj(xisx)+xisy.*conj(xisy)+xisz.*conj(xisz));
gk=atan2(-gkn,-gkd);
qsk4=-abs(qp(m)).*...
    ((gkd).*cos(gk)+(gkn).*sin(gk))./...
        (xisx.*conj(xisx)+xisy.*conj(xisy)+xisz.*conj(xisz));

%    Total ED

taus=(psis.*conj(psis)).*k(m).^2+xisx.*conj(xisx)+...
       xisy.*conj(xisy)+xisz.*conj(xisz);
chii=imag(psip.*conj(psis)).*k(m).^2+imag(xipx.*conj(xisx))+...
       imag(xipy.*conj(xisy))+imag(xipz.*conj(xisz));
chir=real(psip.*conj(psis)).*k(m).^2+real(xipx.*conj(xisx))+...
       real(xipy.*conj(xisy))+real(xipz.*conj(xisz));

gt=atan2(chii,chir);
qst1=-abs(qp(m)).*(chir.*cos(gt)+chii.*sin(gt))./taus;
gt=atan2(-chii,chir);
```

```
   qst2=-abs(qp(m)).*(chir.*cos(gt)+chii.*sin(gt))./taus;
   gt=atan2(chii,-chir);
   qst3=-abs(qp(m)).*(chir.*cos(gt)+chii.*sin(gt))./taus;
   gt=atan2(-chii,-chir);
   qst4=-abs(qp(m)).*(chir.*cos(gt)+chii.*sin(gt))./taus;

   % Calculating power from the prescribed control values.
    for nx=1:N(1)
        for ny=1:N(2)
            Pp1(nx,ny)=PowerFun(qp(m),qsp1(nx,ny),coord,k(m));
            Pp2(nx,ny)=PowerFun(qp(m),qsp2(nx,ny),coord,k(m));
            Pp3(nx,ny)=PowerFun(qp(m),qsp3(nx,ny),coord,k(m));
            Pp4(nx,ny)=PowerFun(qp(m),qsp4(nx,ny),coord,k(m));

            Pk1(nx,ny)=PowerFun(qp(m),qsk1(nx,ny),coord,k(m));
            Pk2(nx,ny)=PowerFun(qp(m),qsk2(nx,ny),coord,k(m));
            Pk3(nx,ny)=PowerFun(qp(m),qsk3(nx,ny),coord,k(m));
            Pk4(nx,ny)=PowerFun(qp(m),qsk4(nx,ny),coord,k(m));

            Pt1(nx,ny)=PowerFun(qp(m),qst1(nx,ny),coord,k(m));
            Pt2(nx,ny)=PowerFun(qp(m),qst2(nx,ny),coord,k(m));
            Pt3(nx,ny)=PowerFun(qp(m),qst3(nx,ny),coord,k(m));
            Pt4(nx,ny)=PowerFun(qp(m),qst4(nx,ny),coord,k(m));
        end
    end
    Pp=min(min(Pp1,Pp2),min(Pp3,Pp4));
    Pk=min(min(Pk1,Pk2),min(Pk3,Pk4));
    Pt=min(min(Pt1,Pt2),min(Pt3,Pt4));
    Pref1=k(m).^2.*rho.*c./(8.*pi).*qp(m).*conj(qp(m));

save(['PowerOutput\Power4OneAlt' num2str(m)],'Pp','Pk','Pt','Pref1')
end
toc

%% Refresh the RAM and make plots and animations.
clear all

load 'PowerOutput\Setup4SevralAlt'
x=x*100;    y=y*100;    coord=coord*100;
Xlime=[min(min(x)),max(max(x))];
Ylime=[min(min(y)),max(max(y))];
Pref=10^-12;
cax=[-5,15]; % Set the color range for the plots.
```

```
% Set the plotting space, tick marks and unit labels.
yntics=[-20,-10,0,10,20];
yltics=['-20';'-10';' 0 ';' 10';' 20'];
xntics=[-20,-10,0,10,20,25];
xltics=['-20';'-20';' 0 ';' 10';' 20';' cm'];

M=length(k);

figure
set(gcf,'Position',[6 350 1270 500])
time=clock;
mov=avifile(['MEDToPO_' sprintf('%2.2d%2.2d',time(4),time(5)) ...
           'hours' sprintf('%2.2d',time(3)) 'day' num2str(time(2)) ...
           'month' num2str(time(1)) '.avi'],'compression',...
           'Cinepak','quality',100,'fps',20);
for m=1:M
    load(['PowerOutput\Power4OneAlt' num2str(m)])

    subplot('Position',[.03 .17 .3 .75])
    surf(x,y,10*log10(Pp/Pref1))
    hold on
    plot3(coord(1,1),coord(1,2),11250,'ko','markersize',10,...
          'linewidth',3)
    for n=2:a
        plot3(coord(n,1),coord(n,2),250,'kx','markersize',17,...
              'linewidth',3)
    end
    view(0,90)
    shading interp
    caxis(cax)
    xlim(Xlime);
    ylim(Ylime);
    set(gca,'fontsize',13)
    title('PED','FontSize',13)
    set(gca,'XTick',xntics)
    set(gca,'YTick',yntics)
    set(gca,'XTickLabel',xltics)
    set(gca,'YTickLabel',yltics)
    hold off

    subplot('Position',[.36 .03 .3 .89])
    surf(x,y,10*log10(Pk/Pref1))
```

```
hold on
plot3(coord(1,1),coord(1,2),1250,'ko','markersize',10,...
      'linewidth',3)
for n=2:a
    plot3(coord(n,1),coord(n,2),250,'kx','markersize',17,...
          'linewidth',3)
end
view(0,90)
shading interp
caxis(cax)
xlim(Xlime);
ylim(Ylime);
set(gca,'fontsize',13)
colorbar('horiz'),  set(gca,'fontsize',13)
title('KED','FontSize',13)
set(gca,'XTick',xntics)
set(gca,'YTick',yntics)
set(gca,'XTickLabel',xltics)
set(gca,'YTickLabel',yltics)
hold off

text(max(max(x))*1.5,-max(max(x))*1.25,0,...
     sprintf('kd = %2.4g',k(m)*d),'Rotation',0,'FontSize',16)
text(-max(max(x))*2.75,-max(max(x))*1.25,0,...
     sprintf('k = %2.4g 1/m     f = %2.4g Hz',k(m),f(m)),...
             'Rotation',0,'FontSize',16)
text(max(max(x))*2.35,-max(max(x))*1.25,0,...
     sprintf('d = %2.4g cm',d*100),'FontSize',16)

subplot('Position',[.69 .17 .3 .75])
surf(x,y,10*log10(Pt/Pref1))
hold on
plot3(coord(1,1),coord(1,2),1250,'ko','markersize',10,...
      'linewidth',3)
for n=2:a
    plot3(coord(n,1),coord(n,2),250,'kx','markersize',17,...
          'linewidth',3)
end
view(0,90)
shading interp
caxis(cax)
xlim(Xlime);
ylim(Ylime);
```

```
    set(gca,'fontsize',13)
    title('TED','FontSize',13)
    set(gca,'XTick',xntics)
    set(gca,'YTick',yntics)
    set(gca,'XTickLabel',xltics)
    set(gca,'YTickLabel',yltics)
    hold off

    MEDToPO=getframe(gcf);
    mov=addframe(mov,MEDToPO);

end
mov=close(mov);

toc
```

H.2 Required Function: PowerFun.m

The following code calculates total power output for an array of sound sources. The following code was designed using notes from the work by Nelson and Elliott [38].

PowerFun.m

```
%   This function calculates the radiated sound power output for a system
%   of sources.  To understand how it works look at Nelson and Elliot
%   pages 269 and 270.

function Po=PowerFun(qp,qs,coord,k)

global rho c

[a,b]=size(coord);

q=zeros(a,1)+qs;
q(1)=qp;

d=zeros(a,a);
for n=1:a
    for m=n:a
        d(n,m)=sqrt((coord(n,1)-coord(m,1))^2+...
```

```
                    (coord(n,2)-coord(m,2))^2+...
                    (coord(n,3)-coord(m,3))^2);
    end
end

for n=2:a
    for m=1:n-1
        d(n,m)=d(m,n);
    end
end

                     % this is the impedance for point sources
Z=sinc((k/pi)*d);    % the matlab definition of sinc is
                     % sinc(x)=sin(pi*x)/(pi*x)

Po=rho*c/(8*pi)*k.^2.*(q'*Z*q);
```

Appendix I

STDofEQ.m

This set of MATLAB® m-files was used to generate the plots that indicate the spectral standard deviation as a function of position in a given sound field. Each function should be saved in the same folder as a separate m-files. Plots of the GLAEC value as a function of sensor location can be generated by making a few miner modifications to the function titled STDofEQ.m running it as a MATLAB® function and calling it in a new m-file. An example m-file that uses STDofEQ.m to perform this calculation is fund in Appendix I.3.

I.1 Main File: STDofEQ.m

This file uses three other function files to calculate the spectral standard deviations and generate the plots. In this section of code, there are comments that indicate where things may be changed for use with other source arraignments and sensor locations. There are also some lines of MATLAB® code that are commented out, including these lines and commenting out the lines where `fHigh` and `mic` are defined converts this code to a function. This function may be used in another MATLAB® file,

found in Appendix I.3, to generate a plot that indicates where the spectral standard deviation is minimized.

STDofEQ.m

```
% function STDofEQ(fHigh,mic)

clear all,  close all
tic

global c rho ci
c=343; rho=1.21;    ci=1./c;

%%  frequncy arrays
fLow=0; df=10;       % Define the frequency range
fHigh=200.00;
f=fLow+df+df:df:fHigh;

k=2*pi*f*ci;

%%  source location / sensor location
% Define the location(s) of a source that will not be equalized.
chord=[2*sin(-pi/6),-2*cos(-pi/6)+2,0];
% Define the locations of sources that do get equalized.
chordR=[0,-2+2,0;
        2*sin(pi/6),-2*cos(pi/6)+2,0;
        2*sin(11*pi/18),-2*cos(11*pi/18)+2,0;
        2*sin(-11*pi/18),-2*cos(-11*pi/18)+2,0];

Gain=1;     % This can be set to adjust gain on the equalized
            % sources.  This is just a multiplier.
mic=[1.3,2.2,0];

%%  spatial arrays
% This section defines the grid for the listening space.
dx=.2;
MaxX=1.75;
MinX=-MaxX;
X=(MinX:dx:MaxX);
space=.5;
[x,y]=ndgrid(X,X+MaxX+space);
clear X
```

```
z=mic(3);

%%  source charactaristics
q0=(zeros(size(k))+0.007*(1+j))./k; % Adjust q0 for the source
                                    % strength of the unequalized
                                    % source strength.
A0=j*rho*c*k.*q0/(4*pi);
A0sq=A0.*conj(A0);

%%  useful dsp numbers
N=length(k);
s=size(x);
schord=size(chord);
schR=size(chordR);

%%  fundamental error sensor measurments
[p,ux,uy,uz]=FundamentalAcoustics(q0,k,chord,chordR,Gain,mic);
usq=ux.*conj(ux)+uy.*conj(uy)+uz.*conj(uz);
u=sqrt(usq);

[stdpNoEq,avgfpNoEq,maxpNoEq,stdsNoEq,avgsNoEq] = ...
  pressurefield(q0,q0,k,chord,chordR,Gain,x,y,z,...
                'C:\Temprary\Equalization5b\STDofEQ6\Datum\NoEq');

%%  more exotic error sensor measurments
wkm=usq*rho/4;
wpm=p.*conj(p)/(4*rho*c^2);
wtm=wkm+wpm;
wLm=wkm-wpm;
wIm=sqrt((real(p.*conj(ux))).^2+(real(p.*conj(uy))).^2...
        +(real(p.*conj(uz))).^2)/2;

%%  ploting
figure

subplot(3,1,1)
plot(f/1000,10*log10(p.*conj(p)/(2*(4e-10))),'b','LineWidth',4)
     % Note: (20e-6)^2 = 4e-10
set(gca,'FontSize',20)
title('pressure magnitude')
xlabel('kHz'),ylabel('dB re 20\mu Pa')
ylim([70,100])
```

```
subplot(3,1,2)
plot(f/1000,10*log10(ux.*conj(ux)/(2*25e-16)),'b','LineWidth',4)
% Note: 50 nm/s = 50e-9 m/s = 5e-8 m/s
%       (5e-8 m/s)^2 = 2.5e-15 (m/s)^2 = 25e-16
hold on
plot(f/1000,10*log10(uy.*conj(uy)/(2*25e-16)),'r--','LineWidth',4)
plot(f/1000,10*log10(uz.*conj(uz)/(2*25e-16)),'g-.','LineWidth',4)
plot(f/1000,10*log10(usq/(2*25e-16)),'k-.','LineWidth',4)
set(gca,'FontSize',20)
title('particle velocity magnitude')
legend('u_x','u_y','u_z','|u|',4);
xlabel('kHz'),ylabel('dB re 50 nm/s')
ylim([70,100])

subplot(3,1,3)
plot(f/1000,10*log10(wpm/(3e-15)),'b','LineWidth',4);
hold on
plot(f/1000,10*log10(wkm/(3e-15)),'r--','LineWidth',4);
plot(f/1000,10*log10(wtm/(3e-15)),'k-.','LineWidth',4);
set(gca,'FontSize',20)
title('Energy Density magnitude')
legend('potential','kinetic','total',4);
xlabel('kHz'),ylabel('dB re 3x10^{-15} J/m^3')
ylim([70,100])

%%
figure
subplot(2,1,1)
plot(f/1000,10*log10(wIm/10^-12),'linewidth',2)
set(gca,'FontSize',13)
title('Intensity')
xlabel('kHz'),ylabel('dB re 10^{-12} W/m^2')

% figure
subplot(2,1,2)
plot(f/1000,10*log10((avgsNoEq)/(2*4e-10)),'linewidth',2)
% Note: 1/(2*(2e-5)^2) = 1.25e+9
set(gca,'FontSize',13)
title('Average Pressure Response')
xlabel('kHz'),ylabel('dB re 20\mu Pa')

%%  Design equalizatoin filter      This is 1/H(f)
Eqcp = abs(A0./p);
```

```
Eqcu = abs(A0sq./u);
Eqwp = sqrt(A0sq./(2*wpm));
Eqwk = sqrt(A0sq./(2*wkm));
Eqwt = sqrt(A0sq./(2*wtm));
EqwL = sqrt(A0sq./(2*wLm));
EqwI = sqrt(A0sq./(2*wIm));
Eqavgs=sqrt(A0sq./(2*avgsNoEq));

%%  Setting the appropreate source strengths for equalizatoin
qcp = Eqcp.*q0/mean(abs(Eqcp));
qcu = Eqcu.*q0/mean(abs(Eqcu));
qwp = Eqwp.*q0/mean(abs(Eqwp));
qwk = Eqwk.*q0/mean(abs(Eqwk));
qwt = Eqwt.*q0/mean(abs(Eqwt));
qwL = EqwL.*q0/mean(abs(EqwL));
qwI = EqwI.*q0/mean(abs(EqwI));
qavgs=Eqavgs.*q0/mean(abs(Eqavgs));

%%  Checking on the resulting pressure response
eqcp = pressure(q0,qcp,k,chord,chordR,Gain,mic);
eqcu = pressure(q0,qcu,k,chord,chordR,Gain,mic);
eqwp = pressure(q0,qwp,k,chord,chordR,Gain,mic);
eqwk = pressure(q0,qwk,k,chord,chordR,Gain,mic);
eqwt = pressure(q0,qwt,k,chord,chordR,Gain,mic);
eqwL = pressure(q0,qwL,k,chord,chordR,Gain,mic);
eqwI = pressure(q0,qwI,k,chord,chordR,Gain,mic);
eqavgs = pressure(q0,qavgs,k,chord,chordR,Gain,mic);

%% Plotting the magnitude response of the equalization filters
figure
subplot(2,1,1)
plot(f/1000,abs(eqcp),'b','LineWidth',2)
hold on
plot(f/1000,abs(eqcu),'g','LineWidth',2)
plot(f/1000,abs(eqwp),'r--','LineWidth',2)
plot(f/1000,abs(eqwk),'k--','LineWidth',2)
plot(f/1000,abs(eqwt),'m','LineWidth',2)
plot(f/1000,abs(eqwL),'c','LineWidth',2)
plot(f/1000,abs(eqwI),'color',[.87,.35,0],'LineWidth',2)
plot(f/1000,abs(eqavgs),'y','LineWidth',2)
legend('p','u','ped','ked','ted','Ld','I','avg_s')
xlabel('kHz'),  ylabel('Pa')
title('measured equalized field')
```

```
subplot(2,1,2)
plot(f/1000,10*log10(eqcp.*conj(eqcp)./(A0sq)),'b','LineWidth',2)
hold on
plot(f/1000,10*log10(eqcu.*conj(eqcu)./(A0sq)),'g','LineWidth',2)
plot(f/1000,10*log10(eqwp.*conj(eqwp)./(A0sq)),'r--','LineWidth',2)
plot(f/1000,10*log10(eqwk.*conj(eqwk)./(A0sq)),'k--','LineWidth',2)
plot(f/1000,10*log10(eqwt.*conj(eqwt)./(A0sq)),'m','LineWidth',2)
plot(f/1000,10*log10(eqwL.*conj(eqwL)./(A0sq)),'c','LineWidth',2)
plot(f/1000,10*log10(eqwI.*conj(eqwI)./(A0sq)),'color',[.87,.35,0],...
     'LineWidth',2)
plot(f/1000,10*log10(eqavgs.*conj(eqavgs)./A0sq),'y','LineWidth',2)
legend('p','u','ped','ked','ted','Ld','I','avg_s',4)
xlabel('kHz'),  ylabel('dB')
title('equalized response')

toc

%%  Calculating the standard deviation and pressure field
       [stdpcp,avgfpcp,maxpcp,stdspcp,avgspcp] = ...
           pressurefield(q0,qcp,k,chord,chordR,Gain,x,y,z,...
                     'C:\Temprary\Equalization5b\STDofEQ6\Datum\Eqp');
       [stdpcu,avgfpcu,maxpcu,stdspcu,avgspcu] = ...
           pressurefield(q0,qcu,k,chord,chordR,Gain,x,y,z,...
                     'C:\Temprary\Equalization5b\STDofEQ6\Datum\Equ');
       [stdpwp,avgfpwp,maxpwp,stdspwp,avgspwp] = ...
           pressurefield(q0,qwp,k,chord,chordR,Gain,x,y,z,...
                     'C:\Temprary\Equalization5b\STDofEQ6\Datum\Eqwp');
       [stdpwk,avgfpwk,maxpwk,stdspwk,avgspwk] = ...
           pressurefield(q0,qwk,k,chord,chordR,Gain,x,y,z,...
                     'C:\Temprary\Equalization5b\STDofEQ6\Datum\Eqwk');
       [stdpwt,avgfpwt,maxpwt,stdspwt,avgspwt] = ...
           pressurefield(q0,qwt,k,chord,chordR,Gain,x,y,z,...
                     'C:\Temprary\Equalization5b\STDofEQ6\Datum\Eqwt');
       [stdpwL,avgfpwL,maxpwL,stdspwL,avgspwL] = ...
           pressurefield(q0,qwL,k,chord,chordR,Gain,x,y,z,...
                     'C:\Temprary\Equalization5b\STDofEQ6\Datum\EqwL');
       [stdpwI,avgfpwI,maxpwI,stdspwI,avgspwI] = ...
           pressurefield(q0,qwI,k,chord,chordR,Gain,x,y,z,...
                     'C:\Temprary\Equalization5b\STDofEQ6\Datum\EqwI');
[stdpavgs,avgfpavgs,maxavgs,stdsavgs,avgsavgs] = ...
           pressurefield(q0,qavgs,k,chord,chordR,Gain,x,y,z,...
                   'C:\Temprary\Equalization5b\STDofEQ6\Datum\Eqavgs');
```

```
save('Fields\Data','mic','chord','chordR','q0','N','x','y','z')

toc

cax=[0.0,2]; % Set the color scale of the plots.
PI=-pi:pi/720:pi;

%%
[AA,BB]=find(stdpNoEq==0);
aa=size(AA);
for n=1:aa(1);
    stdpNoEq(AA,BB)=1e-7;
end

%%  difference from NoEq in standard deviatoin and wp
figure
ratwp=(stdpwp./stdpNoEq);

surf([x(1,1),x(1,end);x(end,1),x(end,end)],...
     [y(1,1),y(1,end);y(end,1),y(end,end)],cax(1)+zeros(2,2))
hold on
surf(x,y,(ratwp));

for n=1:schord(1)
    plot3(chord(n,1),chord(n,2),2,'kx','LineWidth',3,'MarkerSize',20)
end
for n=1:schR(1)
    plot3(chordR(n,1),chordR(n,2),2,'k+','LineWidth',3,...
          'MarkerSize',20)
end
plot3(mic(1),mic(2),20,'ko','LineWidth',3,'MarkerSize',8)
plot3(2*sin(PI),2*cos(PI)+2,0*PI+2,'k-')
ylabel(['GLAEC/GLAEC_{no eq} = ' num2str(mean2(stdpwp)/...
         mean2(stdpNoEq))],'fontsize',13)
axis equal
shading interp
caxis(cax)
colorbar
view([0,90])
set(gca,'FontSize',20)

xlim([x(1,1)-space x(end,1)+space])
```

```
ylim([y(1,1)-space y(1,end)+space])
title('Potential ED')

saveas(gcf,['post\STDEV_wp_rat' num2str(mic(1)*100) '_' ...
            num2str(mic(2)*100) '_' num2str(fHigh)],'fig')
saveas(gcf,['post\STDEV_wp_rat' num2str(mic(1)*100) '_' ...
            num2str(mic(2)*100) '_' num2str(fHigh)],'png')
colormap gray
saveas(gcf,['post\STDEV_wp_rat_gray' num2str(mic(1)*100) '_' ...
            num2str(mic(2)*100) '_' num2str(fHigh)],'png')
colormap jet

%%  difference from NoEq in standard deviatoin and wk
figure
ratwk=(stdpwk./stdpNoEq);

surf([x(1,1),x(1,end);x(end,1),x(end,end)],...
     [y(1,1),y(1,end);y(end,1),y(end,end)],cax(1)+zeros(2,2))
hold on
surf(x,y,(ratwk));

for n=1:schord(1)
    plot3(chord(n,1),chord(n,2),2,'kx','LineWidth',3,'MarkerSize',20)
end
for n=1:schR(1)
    plot3(chordR(n,1),chordR(n,2),2,'k+','LineWidth',3,...
          'MarkerSize',20)
end
plot3(mic(1),mic(2),20,'ko','LineWidth',3,'MarkerSize',8)
plot3(2*sin(PI),2*cos(PI)+2,0*PI+2,'k-')
ylabel(['GLAEC/GLAEC_{no eq} = ' num2str(mean2(stdpwk)/...
         mean2(stdpNoEq))],'fontsize',13)
axis equal
shading interp
caxis(cax)
colorbar
view([0,90])
set(gca,'FontSize',20)

xlim([x(1,1)-space x(end,1)+space])
ylim([y(1,1)-space y(1,end)+space])
title('Kinetic ED')
```

```
saveas(gcf,['post\STDEV_wk_rat' num2str(mic(1)*100) '_' ...
            num2str(mic(2)*100) '_' num2str(fHigh)],'fig')
saveas(gcf,['post\STDEV_wk_rat' num2str(mic(1)*100) '_' ...
            num2str(mic(2)*100) '_' num2str(fHigh)],'png')
colormap gray
saveas(gcf,['post\STDEV_wk_rat_gray' num2str(mic(1)*100) '_' ...
            num2str(mic(2)*100) '_' num2str(fHigh)],'png')
colormap jet

%%  difference from NoEq in standard deviatoin and wt
figure
ratwt=(stdpwt./stdpNoEq);

surf([x(1,1),x(1,end);x(end,1),x(end,end)],...
     [y(1,1),y(1,end);y(end,1),y(end,end)],cax(1)+zeros(2,2))
hold on
surf(x,y,(ratwt));

for n=1:schord(1)
    plot3(chord(n,1),chord(n,2),2,'kx','LineWidth',3,'MarkerSize',20)
end
for n=1:schR(1)
    plot3(chordR(n,1),chordR(n,2),2,'k+','LineWidth',3,...
          'MarkerSize',20)
end
plot3(mic(1),mic(2),20,'ko','LineWidth',3,'MarkerSize',8)
plot3(2*sin(PI),2*cos(PI)+2,0*PI+2,'k-')
ylabel(['GLAEC/GLAEC_{no eq} = ' num2str(mean2(stdpwt)/...
         mean2(stdpNoEq))],'fontsize',13)
axis equal
shading interp
caxis(cax)
colorbar
view([0,90])
set(gca,'FontSize',20)
axis equal
xlim([x(1,1)-space x(end,1)+space])
ylim([y(1,1)-space y(1,end)+space])
title('Total ED')


saveas(gcf,['post\STDEV_wt_rat' num2str(mic(1)*100) '_' ...
            num2str(mic(2)*100) '_' num2str(fHigh)],'fig')
```

```
saveas(gcf,['post\STDEV_wt_rat' num2str(mic(1)*100) '_' ...
            num2str(mic(2)*100) '_' num2str(fHigh)],'png')
colormap gray
saveas(gcf,['post\STDEV_wt_rat_gray' num2str(mic(1)*100) '_' ...
            num2str(mic(2)*100) '_' num2str(fHigh)],'png')
colormap jet

%%  difference from NoEq in standard deviatoin and wL
figure
ratwL=(stdpwL./stdpNoEq);

surf([x(1,1),x(1,end);x(end,1),x(end,end)],...
       [y(1,1),y(1,end);y(end,1),y(end,end)],cax(1)+zeros(2,2))
hold on
surf(x,y,(ratwL));

for n=1:schord(1)
    plot3(chord(n,1),chord(n,2),2,'kx','LineWidth',3,'MarkerSize',20)
end
for n=1:schR(1)
    plot3(chordR(n,1),chordR(n,2),2,'k+','LineWidth',3,...
          'MarkerSize',20)
end
plot3(mic(1),mic(2),20,'ko','LineWidth',3,'MarkerSize',8)
plot3(2*sin(PI),2*cos(PI)+2,0*PI+2,'k-')
ylabel(['GLAEC/GLAEC_{no eq} = ' num2str(mean2(stdpwL)/...
         mean2(stdpNoEq))],'fontsize',13)
axis equal
shading interp
caxis(cax);
colorbar
view([0,90])
set(gca,'FontSize',20)

xlim([x(1,1)-space x(end,1)+space])
ylim([y(1,1)-space y(1,end)+space])
title('Lagrangian Density')

saveas(gcf,['post\STDEV_wL_rat' num2str(mic(1)*100) '_' ...
            num2str(mic(2)*100) '_' num2str(fHigh)],'fig')
saveas(gcf,['post\STDEV_wL_rat' num2str(mic(1)*100) '_' ...
            num2str(mic(2)*100) '_' num2str(fHigh)],'png')
colormap gray
```

```
saveas(gcf,['post\STDEV_wL_rat_gray' num2str(mic(1)*100) '_' ...
            num2str(mic(2)*100) '_' num2str(fHigh)],'png')
colormap jet

%%  difference from NoEq in standard deviatoin and wI
figure
ratwI=(stdpwI./stdpNoEq);

surf([x(1,1),x(1,end);x(end,1),x(end,end)],...
     [y(1,1),y(1,end);y(end,1),y(end,end)],cax(1)+zeros(2,2))
hold on
surf(x,y,(ratwI));

for n=1:schord(1)
    plot3(chord(n,1),chord(n,2),2,'kx','LineWidth',3,'MarkerSize',20)
end
for n=1:schR(1)
    plot3(chordR(n,1),chordR(n,2),2,'k+','LineWidth',3,...
          'MarkerSize',20)
end
plot3(mic(1),mic(2),20,'ko','LineWidth',3,'MarkerSize',8)
plot3(2*sin(PI),2*cos(PI)+2,0*PI+2,'k-')
ylabel(['GLAEC/GLAEC_{no eq} = ' num2str(mean2(stdpwI)/...
         mean2(stdpNoEq))],'fontsize',13)
axis equal
shading interp
caxis(cax)
colorbar
view([0,90])
set(gca,'FontSize',20)

xlim([x(1,1)-space x(end,1)+space])
ylim([y(1,1)-space y(1,end)+space])
title('Intensity')

saveas(gcf,['post\STDEV_wI_rat' num2str(mic(1)*100) '_' ...
            num2str(mic(2)*100) '_' num2str(fHigh)],'fig')
saveas(gcf,['post\STDEV_wI_rat' num2str(mic(1)*100) '_' ...
            num2str(mic(2)*100) '_' num2str(fHigh)],'png')
colormap gray
saveas(gcf,['post\STDEV_wI_rat_gray' num2str(mic(1)*100) '_' ...
            num2str(mic(2)*100) '_' num2str(fHigh)],'png')
colormap jet
```

```
%%  difference from NoEq in standard deviatoin and avgs
figure
ratpavgs=(stdpavgs./stdpNoEq);

surf([x(1,1),x(1,end);x(end,1),x(end,end)],...
     [y(1,1),y(1,end);y(end,1),y(end,end)],cax(1)+zeros(2,2))
hold on
surf(x,y,(ratpavgs));

for n=1:schord(1)
    plot3(chord(n,1),chord(n,2),2,'kx','LineWidth',3,'MarkerSize',20)
end
for n=1:schR(1)
    plot3(chordR(n,1),chordR(n,2),2,'k+','LineWidth',3,...
          'MarkerSize',20)
end
plot3(2*sin(PI),2*cos(PI)+2,0*PI+2,'k-')
ylabel(['GLAEC/GLAEC_{no eq} = ' num2str(mean2(stdpavgs)/...
         mean2(stdpNoEq))],'fontsize',13)
axis equal

shading interp
caxis(cax)
colorbar
view([0,90])
set(gca,'FontSize',20)
xlim([x(1,1)-space x(end,1)+space])
ylim([y(1,1)-space y(1,end)+space])
title('Spatially Averaged Pressure')

saveas(gcf,['post\STDEV_avgp_rat' num2str(mic(1)*100) '_' ...
             num2str(mic(2)*100) '_' num2str(fHigh)],'fig')
saveas(gcf,['post\STDEV_avgp_rat' num2str(mic(1)*100) '_' ...
             num2str(mic(2)*100) '_' num2str(fHigh)],'png')
colormap gray
saveas(gcf,['post\STDEV_avgp_rat_gray' num2str(mic(1)*100) '_' ...
             num2str(mic(2)*100) '_' num2str(fHigh)],'png')
colormap jet

%% Making a time stamp (prevents overwriting previous calculations)
time=clock;
save(['post\dataB' num2str(mic(1)*100) '_' ...
```

```
       num2str(mic(2)*100) '_' num2str(fHigh)]);

%%  Saveing/Exporting Statistical Data
% The important data.
statdat={'','avg(std_f)','std(avg_f)','avg(std_f)/noeq',...
             'std(avg_f)/noeq';
         'NoEq',mean2(stdpNoEq),std2(avgfpNoEq),1,1;
         'complex p',mean2(stdpcp),std2(avgfpcp),mean2(stdpcp)/...
             mean2(stdpNoEq),std2(avgfpcp)/std2(avgfpNoEq);
         'complex u',mean2(stdpcu),std2(avgfpcu),mean2(stdpcp)/...
             mean2(stdpNoEq),std2(avgfpcu)/std2(avgfpNoEq);
         'ped',mean2(stdpwp),std2(avgfpwp),mean2(stdpwp)/...
             mean2(stdpNoEq),std2(avgfpwp)/std2(avgfpNoEq);
         'ked',mean2(stdpwk),std2(avgfpwk),mean2(stdpwk)/...
             mean2(stdpNoEq),std2(avgfpwk)/std2(avgfpNoEq);
         'ted',mean2(stdpwt),std2(avgfpwt),mean2(stdpwt)/...
             mean2(stdpNoEq),std2(avgfpwt)/std2(avgfpNoEq);
         'Ld',mean2(stdpwL),std2(avgfpwL),mean2(stdpwL)/...
             mean2(stdpNoEq),std2(avgfpwL)/std2(avgfpNoEq);
         'spatial avg p',mean2(stdpavgs),std2(avgfpavgs),...
             mean2(stdpavgs)/mean2(stdpNoEq),...
             std2(avgfpavgs)/std2(avgfpNoEq);
         'I',mean2(stdpwI),std2(avgfpwI),mean2(stdpwI)/...
             mean2(stdpNoEq),std2(avgfpwI)/std2(avgfpNoEq);
         };

warning off MATLAB:xlswrite:AddSheet

file=['F:\post\GLAEC_' num2str(mic(1)*100) '_' num2str(mic(2)*100) ...
      '_' num2str(fHigh)];
xlswrite(file,statdat,'measured')

%  This time the full data set.
statdat={'','avg(std_f)','std(std_f)','avg(std_f)+std(std_f)',...
            'avg(avg_f)','std(avg_f)','avg(std_s)','std(std_s)',...
            'avg(std_s)+std(std_s)','stdev(avg_s)','avg(avg_s)',...
            'std(sqrt(avg_s))';
         'NoEq',mean2(stdpNoEq),std2(stdpNoEq),mean2(stdpNoEq)+...
             std2(stdpNoEq),mean2(avgfpNoEq),std2(avgfpNoEq),...
             mean(stdsNoEq),std(stdsNoEq),mean(stdsNoEq)+...
             std(stdsNoEq),std(avgsNoEq),mean(avgsNoEq),...
             std(sqrt(avgsNoEq));
         'complex p',mean2(stdpcp),std2(stdpcp),mean2(stdpcp)+...
```

```
            std2(stdpcp),mean2(avgfpcp),std2(avgfpcp),...
            mean(stdspcp),std(stdspcp),mean(stdspcp)+std(stdspcp),...
            std(avgspcp),mean(avgspcp),std(sqrt(avgspcp));
        'complex u',mean2(stdpcu),std2(stdpcu),mean2(stdpcu)+...
            std2(stdpcu),mean2(avgfpcu),std2(avgfpcu),...
            mean(stdspcu),std(stdspcu),mean(stdspcu)+std(stdspcu),...
            std(avgspcu),mean(avgspcu),std(sqrt(avgspcu));
        'ped',mean2(stdpwp),std2(stdpwp),mean2(stdpwp)+...
            std2(stdpwp),mean2(avgfpwp),std2(avgfpwp),...
            mean(stdspwp),std(stdspwp),mean(stdspwp)+std(stdspwp),...
            std(avgspwp),mean(avgspwp),std(sqrt(avgspwp));
        'ked',mean2(stdpwk),std2(stdpwk),mean2(stdpwk)+...
            std2(stdpwk),mean2(avgfpwk),std2(avgfpwk),...
            mean(stdspwk),std(stdspwk),mean(stdspwk)+...
            std(stdspwk),std(avgspwk),mean(avgspwk),...
            std(sqrt(avgspwk));
        'ted',mean2(stdpwt),std2(stdpwt),mean2(stdpwt)+...
            std2(stdpwt),mean2(avgfpwt),std2(avgfpwt),...
            mean(stdspwt),std(stdspwt),mean(stdspwt)+...
            std(stdspwt),std(avgspwt),mean(avgspwt),...
            std(sqrt(avgspwt));
        'Ld',mean2(stdpwL),std2(stdpwL),mean2(stdpwL)+...
            std2(stdpwL),mean2(avgfpwL),std2(avgfpwL),...
            mean(stdspwL),std(stdspwL),mean(stdspwL)+std(stdspwL)...
            ,std(avgspwL),mean(avgspwL),std(sqrt(avgspwL));
        'spatial avg p',mean2(stdpavgs),std2(stdpavgs),...
            mean2(stdpavgs)+std2(stdpavgs),mean2(avgfpavgs),...
            std2(avgfpavgs),mean(stdsavgs),std(stdsavgs),...
            mean(stdsavgs)+std(stdsavgs),std(avgsavgs),...
            mean(avgsavgs),std(sqrt(avgsavgs));
        'I',mean2(stdpwI),std2(stdpwI),mean2(stdpwI)+std2(stdpwI),...
            mean2(avgfpwI),std2(avgfpwI),mean(stdspwI),...
            std(stdspwI),mean(stdspwI)+std(stdspwI),std(avgspwI),...
            mean(avgspwI),std(sqrt(avgspwI));
        };

warning off MATLAB:xlswrite:AddSheet
xlswrite(file,statdat,'More Measured')
toc
```

The following files are functions required for the preceding MATLAB® code to run.

I.2 Required Functions

I.2.1 Required Function: FundamentalAcoustics.m

FundamentalAcoustics.m

```
function [p,ux,uy,uz]=FundamentalAcoustics(q,k,chord,chordR,Gain,mic)

global rho c
A=j*rho*c*k.*q/(4*pi);
s=size(chord);
sR=size(chordR);

p=zeros(size(k));
ux=zeros(size(k));
uy=zeros(size(k));
uz=zeros(size(k));
for n=1:s(1)
    dx=chord(n,1)-mic(1);
    dy=chord(n,2)-mic(2);
    dz=chord(n,3)-mic(3);
    r=sqrt(dx.^2+dy.^2+dz.^2);
    p=p+A.*exp(-j*k*r)/r;
    dk=exp(-j.*r.*k).*(j.*k.*r+1).*q;
    ux=ux+dk.*(dx)./r.^3;
    uy=uy+dk.*(dy)./r.^3;
    uz=uz+dk.*(dz)./r.^3;
end
for n=1:sR(1)
    dx=chordR(n,1)-mic(1);
    dy=chordR(n,2)-mic(2);
    dz=chordR(n,3)-mic(3);
    r=sqrt(dx.^2+dy.^2+dz.^2);
    p=p+Gain*A.*exp(-j*k*r)/r;
    dk=Gain*exp(-j.*r.*k).*(j.*k.*r+1).*q;
    ux=ux+dk.*(dx)./r.^3;
    uy=uy+dk.*(dy)./r.^3;
    uz=uz+dk.*(dz)./r.^3;
end
ux=ux/(4*pi);
uy=uy/(4*pi);
uz=uz/(4*pi);
```

I.2.2 Required Function: pressurefield.m

pressurefield.m

```
function [stdevf,avgf,maxpf,stds,avgs,stdevfL,avgfL,stdsL,avgsL]=...
          pressurefield7(q0,q,k,chord,chordR,Gain,x,y,z,name)
global c rho
A=j*rho*c*k.*q/(4*pi);
A0=j*rho*c*k.*q0/(4*pi);
sch=size(chord);
schR=size(chordR);
sx=size(x);
N=length(k);
avgs=zeros(size(k));
stds=zeros(size(k));
Bsq=zeros(sx);  B=zeros(sx);
avgsL=zeros(size(k));
stdsL=zeros(size(k));
BsqL=zeros(sx);  BL=zeros(sx);
maxpf=zeros(sx);
for n=1:N
    K=k(n);
    p=zeros(sx);
    for m=1:sch(1)
        r=sqrt((chord(m,1)-x).^2+(chord(m,2)-y).^2+...
               (chord(m,3)-z).^2);
        [xx,yy]=find(r==0);
        t=size(xx);
        if t(1)~=0;
            if xx>=0 || xx<=0
                r(xx,yy)=0.000001;
            end
        end
        p=p+A0(n).*exp(-j*r*K)./r;
    end
    for m=1:schR(1)
        r=sqrt((chordR(m,1)-x).^2+(chordR(m,2)-y).^2+...
               (chordR(m,3)-z).^2);
        [xx,yy]=find(r==0);
        t=size(xx);
        if t(1)~=0;
            if xx>=0 || xx<=0
                r(xx,yy)=0.000001;
```

```
            end
        end
        p=p+Gain*A(n).*exp(-j*r*K)./r;
    end
    psq=sqrt(p.*conj(p));%;(abs(p).^2)
    Bsq=Bsq+psq.^2;
    B=B+psq;
    maxpf=max(maxpf,abs(p));
    avgs(n)=sum(sum(psq))/(sx(1)*sx(2));
    stds(n)=sum(sum((psq-avgs(n)).^2))/(sx(1).*sx(2)-1);

    psqL=log10(p.*conj(p));%;(abs(p).^2)
    BsqL=BsqL+psqL.^2;
    BL=BL+psqL;
    avgsL(n)=sum(sum(psqL))/(sx(1)*sx(2));
    stdsL(n)=sum(sum((psqL-avgsL(n)).^2))/(sx(1).*sx(2)-1);

    save([name num2str(n)],'p','K')
end
var=(Bsq-((B.*conj(B))/N))/(N-1);
varL=(BsqL-((BL.*conj(BL))/N))/(N-1);
if min(min(var))>=-10e-6
    var=abs(var);
else
    fprintf('Error in Standard deviation of Unequalized\n')
    min(min(var))
end
if min(min(varL))>=-10e-6
    varL=abs(varL);
else
    fprintf('Error in Standard deviation of Unequalized\n')
    min(min(varL))
end
stdevf=sqrt(var);
avgf=B/N;

stdevfL=sqrt(varL);
avgfL=BL/N;
```

I.2.3 Required Function: pressure.m

pressure.m

```
function p=pressure(q0,q,k,chord,chordR,Gain,mic)
global c rho
A0=j*rho*c*k.*q0/(4*pi);
A=j*rho*c*k.*q/(4*pi);
s=size(chord);
sR=size(chordR);

p=zeros(size(k));
for n=1:s(1)
    r=sqrt((chord(n,1)-mic(1)).^2+(chord(n,2)-mic(2)).^2+...
           (chord(n,3)-mic(3)).^2);
    p=p+A0.*exp(-j*k.*r)./r;
end
for n=1:sR(1)
    r=sqrt((chordR(n,1)-mic(1)).^2+(chordR(n,2)-mic(2)).^2+...
           (chordR(n,3)-mic(3)).^2);
    p=p+Gain*A.*exp(-j*k.*r)./r;
end
```

I.3 Optional Controlling m-file: SpatialGLAEC.m

This function can be used to call a slightly modified version of STDofEQ.m to generate plots of the GLAEC as a function of the sensor location. The STDofEQ.m file must be made into a function and the lines indicating the fHigh and mic values must be commented out. It is also very highly recommended to remove all of the plotting procedures from STDofEQ.m to make the process run faster.

SpatialGLAEC.m

```
clear all;  close all;

fhigh=[200,800,2000,20000,6000];
en=3;
tic
```

```
dx=.05;
MaxX=1.75;
MinX=-MaxX;
X=(MinX:dx:MaxX);
space=.5;
[x,y]=ndgrid(X,X+MaxX+space);
Xs=length(X);
xs=size(x);

chord=[];
schord=size(chord);
chordR=[0,-2+2,0;
        2*sin(pi/6),-2*cos(pi/6)+2,0;
        2*sin(-pi/6),-2*cos(-pi/6)+2,0;
        2*sin(11*pi/18),-2*cos(11*pi/18)+2,0;
        2*sin(-11*pi/18),-2*cos(-11*pi/18)+2,0];
schR=size(chordR);

PI=-pi:.1:pi;

for en=3
    Gwp=zeros(xs);
    Gwk=zeros(xs);
    Gwt=zeros(xs);
    Gi=zeros(xs);
    for n=1:Xs
        for m=1:Xs
            [Gwp(n,m),Gwk(n,m),Gwt(n,m),Gi(n,m)]=STDofEQ7_3Feb16GLAECspace(fhigh(e
        end
    end


save(['GLAEC\PsicoticMessOfData2' num2str(fhigh(en))])
toc

%%  PED
figure
surf([x(1,1),x(1,end);x(end,1),x(end,end)],[y(1,1),y(1,end);y(end,1),y(end,end)],z
hold on
surf(x,y,Gwp)
for n=1:schord(1)
    plot3(chord(n,1),chord(n,2),20,'kx','LineWidth',3,'MarkerSize',20)
```

```
end
for n=1:schR(1)
    plot3(chordR(n,1),chordR(n,2),20,'k+','LineWidth',3,'MarkerSize',20)
end
plot3(2*sin(PI),2*cos(PI)+2,0*PI+20,'k-')
axis equal
shading interp
colorbar
view([0,90])
set(gca,'FontSize',20)
xlim([x(1,1)-space x(end,1)+space])
ylim([y(1,1)-space y(1,end)+space])
title('GLAEC from PED')
toc

saveas(gcf,['GLAEC\GLAEC_PED' num2str(fhigh(en))],'fig')
saveas(gcf,['GLAEC\GLAEC_PED' num2str(fhigh(en))],'png')
colormap gray
saveas(gcf,['GLAEC\GLAEC_PED_gray' num2str(fhigh(en))],'png')
colormap jet

%%  KED
figure
surf([x(1,1),x(1,end);x(end,1),x(end,end)],[y(1,1),y(1,end);y(end,1),y(end,end)],zeros(2
hold on
surf(x,y,Gwk)
for n=1:schord(1)
    plot3(chord(n,1),chord(n,2),20,'kx','LineWidth',3,'MarkerSize',20)
end
for n=1:schR(1)
    plot3(chordR(n,1),chordR(n,2),20,'k+','LineWidth',3,'MarkerSize',20)
end
plot3(2*sin(PI),2*cos(PI)+2,0*PI+20,'k-')
axis equal
shading interp
colorbar
view([0,90])
set(gca,'FontSize',20)
xlim([x(1,1)-space x(end,1)+space])
ylim([y(1,1)-space y(1,end)+space])
title('GLAEC from KED')
toc
```

```
saveas(gcf,['GLAEC\GLAEC_KED' num2str(fhigh(en))],'fig')
saveas(gcf,['GLAEC\GLAEC_KED' num2str(fhigh(en))],'png')
colormap gray
saveas(gcf,['GLAEC\GLAEC_KED_gray' num2str(fhigh(en))],'png')
colormap jet

%%  TED
figure
surf([x(1,1),x(1,end);x(end,1),x(end,end)],[y(1,1),y(1,end);y(end,1),y(end,end)],z
hold on
surf(x,y,Gwt)
for n=1:schord(1)
    plot3(chord(n,1),chord(n,2),20,'kx','LineWidth',3,'MarkerSize',20)
end
for n=1:schR(1)
    plot3(chordR(n,1),chordR(n,2),20,'k+','LineWidth',3,'MarkerSize',20)
end
plot3(2*sin(PI),2*cos(PI)+2,0*PI+20,'k-')
axis equal
shading interp
colorbar
view([0,90])
set(gca,'FontSize',20)
xlim([x(1,1)-space x(end,1)+space])
ylim([y(1,1)-space y(1,end)+space])
title('GLAEC from TED')
toc

saveas(gcf,['GLAEC\GLAEC_TED' num2str(fhigh(en))],'fig')
saveas(gcf,['GLAEC\GLAEC_TED' num2str(fhigh(en))],'png')
colormap gray
saveas(gcf,['GLAEC\GLAEC_TED_gray' num2str(fhigh(en))],'png')
colormap jet

%%  intensity
figure

surf([x(1,1),x(1,end);x(end,1),x(end,end)],[y(1,1),y(1,end);y(end,1),y(end,end)],z
hold on
surf(x,y,Gi)
for n=1:schord(1)
    plot3(chord(n,1),chord(n,2),20,'kx','LineWidth',3,'MarkerSize',20)
end
```

```
for n=1:schR(1)
    plot3(chordR(n,1),chordR(n,2),20,'k+','LineWidth',3,'MarkerSize',20)
end
plot3(2*sin(PI),2*cos(PI)+2,0*PI+20,'k-')
axis equal
shading interp
colorbar
view([0,90])
set(gca,'FontSize',20)
xlim([x(1,1)-space x(end,1)+space])
ylim([y(1,1)-space y(1,end)+space])
title('GLAEC from Intensity')
toc

saveas(gcf,['GLAEC\GLAEC_intensity' num2str(fhigh(en))],'fig')
saveas(gcf,['GLAEC\GLAEC_intensity' num2str(fhigh(en))],'png')
colormap gray
saveas(gcf,['GLAEC\GLAEC_intensity_gray' num2str(fhigh(en))],'png')
colormap jet

%%
end
```

Appendix J

EDfields.m

This MATLAB® script produces an animation over frequency of PED, KED and TED fields. This code can be modified for different source arrangements. The progam can be further modified to have different source strengths on each source. This file makes plots and animations like those found in Figs. 4.1, 4.3, E.7(a) and (b), and E.8.

EDfields.m

```
clear all, close all
tic

%%   Define universal constants
global c rho
c=343;  rho=1.21;

%%   Define frequency arrays
fLow=0; df=10.00; fHigh=10000;
f=fLow+df:df:fHigh;
w=2*pi*f;
k=w/c;
N=length(f);

d=2;
dx=0.0050;
```

```
L=1;
X=-L:dx:L;
X=X*0.25;
[x,y]=ndgrid(X,X);
z=0;
clear X
sx=size(x);

%%   Define source
coord=[-0.1,0,0;0.1,0,0];

scoord=size(coord);
r=zeros(sx(1),sx(2),scoord(1));
dx=r;   dy=r;   dz=r;
for n=1:scoord(1)
    rtemp=sqrt((coord(n,1)-x).^2+(coord(n,2)-y).^2+(coord(n,3)-z).^2);
    [xx,yy]=find(rtemp==0);
    if min(size(xx))~=0
        if xx >= 0 || xx <= 0
            rtemp(xx,yy) = 0.000001;
        end
    end
    r(:,:,n)=rtemp;
    dx(:,:,n)=(coord(n,1)-x)./rtemp.^3;
    dy(:,:,n)=(coord(n,2)-y)./rtemp.^3;
    dz(:,:,n)=(coord(n,3)-z)./rtemp.^3;
end
clear rtemp xx yy

%%   Define source strengths (volume velocity)
q=(.0005+.00025*j)./k;  %   The source strength.
%   The code may be modified for different valuse of q for each source
%   loacation.
A=j*rho*c*k.*q/(4*pi);

%%   Build the sound fields as measured by ED
w=zeros(size(x));
v=zeros(size(x));
for n=1:N
    p=zeros(size(x));
    ux=p;   uy=p;   uz=p;
    for m=1:scoord(1)
        p=p+A(n).*exp(-j*k(n)*r(:,:,m))./r(:,:,m);
```

```
        dq=q(n).*(j*k(n)*r(:,:,m)+1).*exp(-j*k(n)*r(:,:,m));
        ux=ux+dq.*dx(:,:,m);
        uy=uy+dq.*dy(:,:,m);
        uz=uz+dq.*dz(:,:,m);
    end
    wp=p.*conj(p)./(4*rho*c^2);
    usq=(ux.*conj(ux)+uy.*conj(uy)+uz.*conj(uz));
    wk=rho*usq/(64*pi^2);

    wt=wp+wk;
    wL=wk-wp;

    cop=conj(p);
    Ix=cop.*ux;
    Iy=cop.*uy;
    Iz=cop.*uz;

    X=sqrt(imag(Ix*.5).^2+imag(Iy*.5).^2+imag(Iz*.5).^2);
    I=sqrt(real(Ix*.5).^2+real(Iy*.5).^2+real(Iz*.5).^2);

    w=w+abs(p);
    v=max(v,abs(p));

    save(['Fields\Data' num2str(n)],'p','wp','wk','wt','wL','X',...
           'I','ux','uy','uz','d')
end
w=w/N;

save('Fields\info','x','y','f','k','N','scoord','coord','w','v')
toc

%%  Generate surfac plot and animation
clear all

load Fields\info
cax=[50,90];
figure
set(gcf,'Position',[6 350 1270 500])
MinX=min(min(x));
MaxX=max(max(x));
MinY=min(min(y));
MaxY=max(max(y));
```

```
yntics=[-.2,-.1,0,.1,.2];
yltics=['-20';'-10';'  0';' 10';' 20'];
xntics=[-.2,-.1,0,.1,.2,.24];
xltics=['-20';'-10';'  0';' 10';' 20';'cm '];

time=clock;
mov=avifile(['Field_' sprintf('%2.2d%2.2d',time(4),time(5)) ...
             'hours' sprintf('%2.2d',time(3)) 'day' ...
              num2str(time(2)) 'month' num2str(time(1)) '.avi'],...
             'compression','Cinepak','quality',100,'fps',20);
for n=1:N
    load(['Fields\Data' num2str(n)])

    subplot('Position',[.03 .17 .3 .75])
    surf(x,y,10*log10(wp./3e-15))
    hold on
    surf(x,y,50+zeros(size(x)))
    for m=1:scoord(1)
        plot3(coord(m,1),coord(m,2),250,'kx','markersize',...
              17,'linewidth',3)
    end
    hold off
    view(0,90)
    set(gca,'fontsize',13)
    axis equal
    xlim([MinX,MaxX])
    ylim([MinY,MaxY])
    title('PED','fontsize',13)
    shading interp
    set(gca,'XTick',xntics)
    set(gca,'YTick',yntics)
    set(gca,'XTickLabel',xltics)
    set(gca,'YTickLabel',yltics)
    caxis(cax)


    subplot('Position',[.36 .03 .3 .89])
    surf(x,y,10*log10(wk./3e-15))
    hold on
    surf(x,y,50+zeros(size(x)))
    for m=1:scoord(1)
        plot3(coord(m,1),coord(m,2),250,'kx','markersize',17,...
              'linewidth',3)
```

```
end
hold off
view(0,90)
set(gca,'fontsize',13)
axis equal
xlim([MinX,MaxX])
ylim([MinY,MaxY])
title('KED','fontsize',13)
shading interp
caxis(cax)
colorbar('horiz')
shading interp
set(gca,'XTick',xntics)
set(gca,'YTick',yntics)
set(gca,'XTickLabel',xltics)
set(gca,'YTickLabel',yltics)
set(gca,'fontsize',13)

text(max(max(x))*1.5,-max(max(x))*1.25,0,sprintf('kd = %2.4g',...
     k(n)*d),'Rotation',0,'FontSize',16)
text(-max(max(x))*2.75,-max(max(x))*1.25,0,sprintf('k = %2.4g ...
     1/m     f = %2.4g Hz',k(n),f(n)),'Rotation',0,'FontSize',16)
text(max(max(x))*2.35,-max(max(x))*1.25,0,sprintf('d = %2.4g ...
      m',d),'FontSize',16)

subplot('Position',[.69 .17 .3 .75])
surf(x,y,10*log10(wt./3e-15))
hold on
surf(x,y,50+zeros(size(x)))
for m=1:scoord(1)
    plot3(coord(m,1),coord(m,2),250,'kx','markersize',17,...
          'linewidth',3)
end
hold off
view(0,90)
set(gca,'fontsize',13)
axis equal
xlim([MinX,MaxX])
ylim([MinY,MaxY])
title('TED','fontsize',13)
shading interp
shading interp
set(gca,'XTick',xntics)
```

```
    set(gca,'YTick',yntics)
    set(gca,'XTickLabel',xltics)
    set(gca,'YTickLabel',yltics)
    caxis(cax)

    EdField=getframe(gcf);
    mov=addframe(mov,EdField);
end
mov=close(mov);

saveas(gcf,'Field','fig')
saveas(gcf,'Field','png')
```

Appendix K

HandS.m

This MATLAB® script produces an animated plot that follows the method described by Hansen and Snyder [2]. They point out that the error sensors used for ANC should be placed at locations where attenuation is the greatest when the the control sources are acting optimally. The results of this can be seen in Figs. 4.8.

HandS.m

```
clear all, close all
tic

%%   Define universal constants
global c rho chord d
c=343;  rho=1.21;

%%   Define frequency arrays
fLow=0; df=10; fHigh=5000;
f=fLow+df:df:fHigh;

w=2*pi*f;
k=w/c;
N=length(f);

%%   Build grid for maping fields
dx=0.001;
```

```
MaxX=.10;
MinX=-.10;
X=MinX:dx:MaxX;
MaxY=.10;
MinY=-.10;
Y=MinY:dx:MaxY;
sizing=.7;
X=X*sizing;  Y=Y*sizing;
MinX=min(X);    MaxX=max(X);
MinY=min(Y);    MaxY=max(Y);
[x,y]=ndgrid(X,Y);
z=0;
sx=size(x);
scl=(-3:.4:3)*.25;


%%   Define source / recever loctions
%   This array chord has the first source as the primary source and the
%   following sources are the control sources.  Sorry, it is just easyer to
%   do it this way.
de=0.0318;
cd=sqrt(de^2/2);
chord=[0, 0, 0;
       cd, cd, 0;
      -cd, cd, 0;
      -cd,-cd, 0;
       cd,-cd, 0];
schord=size(chord);

%%  Finding distances between the control source and the primary sources.
%   This is for finding the appropreate source strengths to minimize the
%   sound field.
d=zeros(schord(1),schord(1));
for n=1:schord(1)
    for m=n:schord(1)
        d(n,m)=sqrt((chord(n,1)-chord(m,1)).^2+(chord(n,2)-chord(m,2)).^2+(chord(n,3)-ch
        d(m,n)=d(n,m);
    end
end

%%   Define source strengths (volume velocity)
%   In this step, I need to find the appropreate source strengths to
%   minimize the sound power.  To do this will use an altered version of
```

```
%   Homework 3 from Dr. Sommerfeldt's phys. 566 course.

sizek=size(k);
qp=(.001+.001*j)*1e-1./k;
q=zeros(schord(1),sizek(2));
q(1,:)=qp;

zscal=rho*c/(4*pi);
kk=k.^2;
Pi=zeros(sizek);
A=zeros(schord(1),sizek(2));
for nf=1:sizek(2)
    Z=kk(nf).*sinc((k(nf)/pi)*d)*zscal;
    Zss=Z(2:end,2:end);
    Zpp=Z(1,1);
    Zps=Z(2:end,1);

    Aa=real(Zss)*.5;
    B=qp(nf)*real(Zps)*.5;
    C=qp(nf)'*real(Zpp)*qp/2;

    Ainv=inv(Aa);
    q(2:end,nf)=-(Ainv)*B;
    Pi(nf)=C(nf)-(B'*Ainv*B);

    A(:,nf)=k(nf)*q(:,nf);
end
Pi_monopole=kk*rho*c.*qp.*conj(qp)/(8*pi);
clear kk zscal Aa B C Ainv
save('F:\MinimumPower','f','Pi','Pi_monopole','d','chord')

A=j*rho*c*A/(4*pi);

%%  Define the relationship between field points and sources
r=zeros(sx(1),sx(2),schord(1));
dx=r;   dy=r;   dz=r;
for n=1:schord(1)
    rtemp=sqrt((chord(n,1)-x).^2+(chord(n,2)-y).^2+(chord(n,3)-z).^2);
    [xx,yy]=find(rtemp==0);
    if min(size(xx))~=0
        if xx >= 0 || xx <= 0
            rtemp(xx,yy) = 0.000001;
        end
```

```
    end
    r(:,:,n)=rtemp;
    dx(:,:,n)=(chord(n,1)-x)./rtemp.^3;
    dy(:,:,n)=(chord(n,2)-y)./rtemp.^3;
    dz(:,:,n)=(chord(n,3)-z)./rtemp.^3;
end
clear rtemp xx yy

%%   Build the sound fields as measured by ED
wLma=zeros(size(k));
for n=1:N
    p=zeros(size(x));
    ux=p;   uy=p;   uz=p;
    for m=1:schord(1)
        p=p+A(m,n).*exp(-j*k(n)*r(:,:,m))./r(:,:,m);
        dq=q(m,n).*(j*k(n)*r(:,:,m)+1).*exp(-j*k(n)*r(:,:,m));
        ux=ux+dq.*dx(:,:,m);
        uy=uy+dq.*dy(:,:,m);
        uz=uz+dq.*dz(:,:,m);
        if m==1
            PED1=p.*conj(p)./(4*rho*c^2);
            KED1=(ux.*conj(ux)+uy.*conj(uy)+uz.*conj(uz))*rho/(64*pi^2);
            TED1=PED1+KED1;
        end
    end
    wp=p.*conj(p)./(4*rho*c^2);
    usq=(ux.*conj(ux)+uy.*conj(uy)+uz.*conj(uz));
    wk=rho*usq/(64*pi^2);

    wt=wp+wk;
    wL=wk-wp;
    save(['F:\Fields\Data' num2str(n)],'wp','wk','wt','wL','PED1','KED1','TED1')
wLma(n)=min(min(wL));
end
D=max(max(d));
wLm=min(wLma);
save('F:\info','x','y','f','k','MinX','MinY','MaxX','MaxY','N','scl','schord','chord','D
toc


%%  surfice plots
clear all
```

```
load F:\info
[a,b]=size(chord);

cax=[-35,20];

MinX=MinX*100;
MaxX=MaxX*100;
x=x*100;
MinY=MinY*100;
MaxY=MaxY*100;
y=y*100;

yntics=[-6,-4,-2,0,2,4,6];
yltics=['-6';'-4';'-2';'0 ';'2 ';'4 ';'6 '];
xntics=[-6,-4,-2,0,2,4,6,6.6];
xltics=['-6';'-4';'-2';'0 ';'2 ';'4 ';'6 ';'cm'];

chord=chord*100;

d=D/2;
mov=avifile('ANC4control2008Feb16_2.avi','compression','Cinepak','quality',100,'fp
for m=1:N
    figure
set(gcf,'Position',[6 350 1270 500])
    load(['F:\Fields\Data' num2str(m)])

    subplot('Position',[.03 .17 .3 .75])
%     surf(x,y,10*log10(wp./min(min(wp))))
    surf(x,y,10*log10(wp./PED1))
    hold on
    plot3(chord(1,1),chord(1,2),250,'ko','markersize',10,'linewidth',3)
    for n=2:a
        plot3(chord(n,1),chord(n,2),250,'kx','markersize',17,'linewidth',3)
    end
    view(0,90)
    shading interp
    xlim([MinX,MaxX])
    ylim([MinY,MaxY])
    caxis(cax)
    set(gca,'fontsize',13)
    set(gca,'XTick',xntics)
    set(gca,'YTick',yntics)
    set(gca,'XTickLabel',xltics)
```

```
    set(gca,'YTickLabel',yltics)
    title('POTENTIAL ED','FontSize',13)
    hold off

    subplot('Position',[.36 .03 .3 .89])
%     surf(x,y,10*log10(wk./min(min(wk(102:201,102:201)))))
    surf(x,y,10*log10(wk./KED1))
    hold on
    plot3(chord(1,1),chord(1,2),250,'ko','markersize',10,'linewidth',3)
    for n=2:a
        plot3(chord(n,1),chord(n,2),250,'kx','markersize',17,'linewidth',3)
    end
    view(0,90)
    shading interp
    xlim([MinX,MaxX])
    ylim([MinY,MaxY])
    caxis(cax)
    set(gca,'fontsize',13)
    set(gca,'XTick',xntics)
    set(gca,'YTick',yntics)
    set(gca,'XTickLabel',xltics)
    set(gca,'YTickLabel',yltics)
    colorbar('horiz')
    set(gca,'fontsize',13)
    title('KINETIC ED','FontSize',13)
    hold off

    text(max(max(x))*1.5,-max(max(x))*1.25,0,sprintf('kd = %2.4g',k(m)*d),'Rotation',0,'
    text(-max(max(x))*2.75,-max(max(x))*1.25,0,sprintf('k = %2.4g 1/m       f = %2.4g Hz
    text(max(max(x))*2.35,-max(max(x))*1.25,0,sprintf('d = %2.4g cm',d*100),'FontSize',1

    subplot('Position',[.69 .17 .3 .75])
%     surf(x,y,10*log10(wt./min(min(wt))))
    surf(x,y,10*log10(wt./TED1))
    hold on
    plot3(chord(1,1),chord(1,2),250,'ko','markersize',10,'linewidth',3)
    for n=2:a
        plot3(chord(n,1),chord(n,2),250,'kx','markersize',17,'linewidth',3)
    end
    view(0,90)
    shading interp
    caxis(cax)
    xlim([MinX,MaxX])
```

```
    ylim([MinY,MaxY])
    set(gca,'fontsize',13)
    set(gca,'XTick',xntics)
    set(gca,'YTick',yntics)
    set(gca,'XTickLabel',xltics)
    set(gca,'YTickLabel',yltics)
    title('TOTAL ED','FontSize',13)
    hold off

    EdField=getframe(gcf);
    mov=addframe(mov,EdField);
end
mov=close(mov);

toc
```